



Durham E-Theses

Tee failure of carbon fibre reinforced plastic laminated plates under biaxial stresses

Mottram, J.T.

How to cite:

Mottram, J.T. (1984) *Tee failure of carbon fibre reinforced plastic laminated plates under biaxial stresses*, Durham theses, Durham University. Available at Durham E-Theses Online: <http://etheses.dur.ac.uk/7152/>

Use policy

The full-text may be used and/or reproduced, and given to third parties in any format or medium, without prior permission or charge, for personal research or study, educational, or not-for-profit purposes provided that:

- a full bibliographic reference is made to the original source
- a [link](#) is made to the metadata record in Durham E-Theses
- the full-text is not changed in any way

The full-text must not be sold in any format or medium without the formal permission of the copyright holders.

Please consult the [full Durham E-Theses policy](#) for further details.

THE FAILURE OF CARBON FIBRE REINFORCED PLASTIC
LAMINATED PLATES UNDER BIAXIAL STRESSES

by
J.T. MOTTRAM

A thesis presented for the degree of

DOCTOR OF PHILOSOPHY

in the

UNIVERSITY OF DURHAM

May 1984

The copyright of this thesis rests with the author.
No quotation from it should be published without
his prior written consent and information derived
from it should be acknowledged.

Department of Engineering
Faculty of Science
University of Durham



17 11 1984

ABSTRACT

A new biaxial test procedure, known as the 'plate bending method' is investigated for thin multilayered generally orthotropic laminated plate structures. The method is evaluated with reference to the four criteria for a satisfactory biaxial test. A number of experiments have been performed to determine the applicability of the criteria to the new method. Surface strains, transverse displacements and visual observations have been recorded, from which the bending behaviour and failure mechanisms in the experiments are examined.

A classical 2-dimensional thin plate finite element analysis has been developed to predict the stresses generated in the small (linear) and large (non-linear) deformation domains. To minimise computing effort in the analyse of non-linear bending, the formulation omitted the effects of shear deformation, shear stresses, material non-linearities and the exact position of the neutral axis. The omission of these factors has been examined and it is shown that the individual errors are small. Analytical solutions for simple isotropic, and, where available, laminated plate bending examples, have been used to establish the limitations of the finite element analysis. Numerical results have been compared with the measured surface strains and transverse displacements. From the comparison it is shown that the plate bending method can be accurately modelled by the linear analysis. However, the non-linear analysis is shown to be inaccurate when predicting the measured bending for reasons which are discussed.

ACKNOWLEDGEMENTS

The author would like to thank Professor Braiden for his helpful comments on the presentation of this thesis and his encouragement throughout the progress of this work. I would also like to thank the other members of the staff in the Engineering Department at Durham who gave support to the development of the finite element analysis.

The author is indebted to Mr Fray (British Aerospace, Woodford) for the provision of specimens and information concerning the properties of the material..

CONTENTS

	Page
Title page	
Abstract	
Acknowledgements	
Contents	
Symbols	
Chapter 1 INTRODUCTION	1
Chapter 2 BIAXIAL TEST METHODS	5
2.0 Introduction	5
2.1 Previous Biaxial Test Methods	6
2.1.1 Tubular	6
2.1.2 Off-Axis Coupon	7
2.1.3 Crossbeam	8
2.1.4 Bulge Plate	10
2.2 Plate Bending Method - Rationale and Development	10
Chapter 3 FINITE ELEMENT ANALYSIS	15
3.0 Introduction	15
3.1 Literature survey	22
3.1.1 Small (Linear) Deformation - Isotropic	22
3.1.2 Small (Linear) Deformation - Laminated	26
3.1.3 Large (Non-Linear) Deformation - Isotropic	27
3.1.4 Large (Non-Linear) Deformation - Laminated	36
3.2 Finite Element Formulation	42
3.2.1 Principle of minimum Potential Energy	42
3.2.2 Geometric Non-Linear Plate Bending	44
3.2.2.1 Iterative Solution	45
3.2.2.2 Geometric Non-Linear Finite Element Plate Bending	47
Representation For Generally Symmetrical Orthotropic Laminates	
3.3 Linear Comparison	57
3.3.1 Isotropic Examples - ACM - With Several Other Rectangular And Triangular Elements	57
3.3.2 Isotropic Examples Approximating To The Experiment - ACM	61

3.3.3	Orthotropic Example - ACM - PAFEC 75	64
3.3.3.1	Test Example	64
3.3.3.2	Analytical Solution	65
3.3.3.3	Finite Element Modelling	67
3.3.3.4	Results	67
3.3.4	Laminated Plates - ACM	69
3.4	Non-Linear (ACMBC) Comparison	74
3.4.1	Isotropic Examples - ACMBC	76
3.4.2	Isotropic Examples - Modifying ACMBC	81
Chapter 4	EXPERIMENTS	86
4.0	Introduction	86
4.1	Specimens For The Plate Bending Experiment	86
4.1.1	Material Properties And Physical Parameters of the Specimens	87
4.2	Shear Deformation And Shear Stresses	90
4.2.1	Shear Deformation	91
4.2.2	Comparison Of Classical Linear Finite Element Analysis (ACM) With Shear Flexible Elements	97
4.2.3	High Order Plate Deformation Theory For Laminated Plates	100
4.2.3.1	Numerical Procedure - Stress-Strain Relations	102
4.2.3.2	Equilibrium Equations	104
4.2.4	Shear Stresses	107
4.3	Experiment Procedure	113
4.3.1	Apparatus	113
4.3.2	Specimen Preparation	114
4.3.3	Experimental Arrangement	118
4.3.4	Test Procedure	119
4.4	Experimental Results (Fig. 4.11 - 4.53)	120
4.5	Discussion of Results	123
4.5.1	Plate Bending	124
4.5.2	Failure Mechanisms	129

Chapter 5	COMPARISON OF EXPERIMENT AND COMPUTER ANALYSIS	137
5.0	Introduction	
5.1	Linear Displacement : Experimental - Numerical Comparison (ACM)	138
5.1.1	Standard Definitions For The Material Properties	138
5.1.2	Plate Modelling Of Experiments 1 And 2	140
5.1.3	Overall Modelling Of Experiments 1 And 2	142
5.1.4	Central Biaxial Stresses	143
5.1.5	Plate Modelling	145
5.1.6	Overall Modelling Of Experiment 7	147
5.2	Large Displacement : Experimental - Computation Comparison (ACMBC - Modified)	148
5.3	Numerical Assumptions	150
5.3.1	Material Non-Linearities - Assumption 9	150
5.3.2	Position of The Neutral Axis - Assumption 11	152
Chapter 6	CONCLUSIONS	154
6.1	The Feasibility Of The 'Plate Bending Method'	154
6.2	Observed Failure Mechanisms	155
6.3	The Validity Of The Finite Element Analysis To Model The Plate Bending Method	156
6.3.1	Linear Analysis, ACM	156
6.3.2	Non-Linear Analysis, ACMBC	157
Chapter 7	FURTHER WORK	159
References		161
Appendix I		172
Appendix II		174

SYMBOLS

Numerical techniques

- a finite element side length in X-direction m
b finite element side length in Y-direction m
c centre of plate
h plate thickness m
i }
j } index counters
k }
m }
n }
- nl number of layers in half the plate
q uniform pressure load N/m^2
q_o maximum uniform pressure load N/m^2
 \bar{q} normalised uniform pressure load N/m^2
t lamina thickness
u in-plane displacement in X-direction, $u(x,y)$, u_o weighed average
v in-plane displacement in Y-direction, $v(x,y)$, v_o weighed average
w transverse displacement in -ve Z-direction, $w(x,y)$, w_o weighed average
x in the global X-direction
y in the global Y-direction
z in the global Z-direction
A plate side length in X-direction m
B plate side length in Y-direction m
D isotropic stiffness coefficient Nm
E isotropic Young's modulus N/m^2
E₁₁, E_{11t}, E_{11c} longitudinal Young's modulus, tensile, compressive N/m^2
E₂₂, E_{22t}, E_{22c} transverse Young's modulus, tensile, compressive N/m^2
E₃₃ equal to E₂₂ N/m^2
G₁₂, G₁₃, G₂₃ shear modulus N/m^2
K_w, K_x, K_y summation terms . transverse displacement , stress in X-direction,
stress in Y-direction
K_i constants in High Order analytical plate bending analysis
M_{xx} , M_{yy} finite element moment loading about Y-axis, X-axis Nm
P transverse load N
S $\left[\frac{A \text{ or } B}{h} \right]$ span to thickness ratio

S.S simply supported edge

CL. clamped edge

U strain energy J

W, W_p potential energy J

X, Y, Z plate global axis system

1, 2, 3 lamina principal axis system

α_i, β_i finite element D.O.F.

α non-dimensional central displacement for a uniform loaded isotropic plate

β factor $0 \leq \beta \leq 1$ for assumed displacements in determining the finite element displacement corrections

$\epsilon, \epsilon_{pl}, \epsilon_{rot}, \epsilon_w$ error quantity, in-plane, rotational, transverse displacement

θ° orientation of principal directions of a lamina with respect to the global axis system

Π total potential energy

ν, ν_{12} Poissons ratio, principal

$\frac{dw}{dx}, \psi_x$ slope about the X-axis

$\frac{dw}{dy}, \psi_y$ slope about the Y-axis

$\xi_x, \xi_y, \xi_z, \psi_x, \psi_y, \psi_z, u_o, v_o, w_o, \phi_x, \phi_y$ High Order generalised co-ordinates specifying the plate configuration

$\eta = \frac{x}{A}, \xi = \frac{y}{B}$, normalised distances in X-direction, Y-direction

$\epsilon, \bar{\epsilon}, \gamma$ strain, normalised, shear

$\sigma, \bar{\sigma}$ stress, normalised N/m^2

$\tau, \bar{\tau}$ shear stress, normalised N/m^2

Matrices for the finite element formulation

[A], [Q] defined by $[B] = [Q][A]^{-1}$ with [A] defined in terms of the element side lengths, and [Q] relating the displacement functions to the strains

[D] plate stiffness coefficients

[G] matrix defined in terms of the co-ordinates of the element

[H] = $[w^{\#}]$ matrix defining non-linear displacements

[K] stiffness matrix

$\left[\frac{Qdw}{dx} \right], \left[\frac{Qdw}{dy} \right]$ matrices relating the bending displacement function to the rotational terms in matrix [H]

$\{Q^\theta\}$ transformed stiffnesses of a lamina at orientation θ°
 $\{\phi\}$ vector relating rotations and displacements
 $\{\epsilon\}$ vector of strains
 $\{\sigma\}$ vector of stresses
 $\{R\}$ vector of external forces
 $\{U\}$ vector sum of the internal and external forces
 $\{d\}$ vector of nodal displacements

Subscripts for the above matrices

b bending
pl in-plane
o linear
L non-linear
T tangential
 σ initial stress
- large displacements
k k^{th} layer in laminate

Further matrices for other numerical techniques

[A],[D],[H],[L] High Order theory plate stiffnesses
[B] plate stiffness coefficients relating bending to stretching

Experiments

A_S span distance in X-direction m
 A_P patch load side length in X-direction m
 B_S span distance in Y-direction m
 B_P patch load side length in Y-direction m
A axial strain measurement
B bending strain measurement
L lower plate surface
T upper plate surface

CHAPTER 1 INTRODUCTION

The development of advanced fibre reinforced materials having high specific strength and stiffness has provided the designer with considerable potential for weight saving. The advent of these composites has also allowed greater flexibility in the design of such light weight structures (1,2). No longer is it necessary to commence with a known material of specific properties. By the selection of fibre and matrix in appropriate proportions the properties of a material can be controlled. Combining laminae of such material at differing orientations then allows the production of laminates having the desired strength, stiffness and degree of anisotropy .

A necessary precursor to the effective design of composite structures is reliable knowledge of the strength properties of the laminated material. At present, only uniaxial loading conditions have been investigated in depth. Little relevant data has been collected for biaxial or more complex forms of loading.

The aim of this work is to present a biaxial test method which will enable accurate strength data to be obtained from laminated specimens representing, say, a section of an aeroplane wing or fuselage. British Aerospace have proposed that such structures be manufactured from generally symmetrical orthotropic laminated composite thin plates, with the composite consisting of carbon fibres embedded in an epoxy resin. Hence the test method was chosen to handle thin laminated plate specimens. For a review of the terminology used in the work refer to the 'Primer on Composite Materials : Analysis', by Ashton et al (3).



A typical section of a specimen is illustrated in Fig. 1.1. Following from the sign convention applied in the Primer, the figure indicates the definitions for the global axes, the lamina principal axes and the lamina material properties. When lay-up arrangements are stated, the 0° direction means that direction in which the principal load was to be imposed.

When choosing the test procedure it was also required that strength data could be obtained after the specimen had been subjected to low energy impact producing damage. This implied that the specimen had to have sufficient dimensions so that impact damage did not subsequently alter the inherent edge effects. In addition, the method should enable strength data to be acquired when the material has suffered deterioration due to prolonged environmental exposure. Hence, if loaded specimens are to be exposed to an active environment most of the surface area should be free from external contact.

Several contrasting biaxial test methods have been used with laminated specimens, but none were deemed suitable when the above test requirements were considered. A new test procedure has been proposed to determine the biaxial strength of generally symmetrical laminated plates. In this thesis it will be referred to as the 'Plate Bending Method'. In the method a thin rectangular plate is symmetrically supported at four points, not the corners, and subjected to a centrally placed transverse rectangular patch load. The test section is a small area directly below the centre and first fibre failure should start in an outer layer subjected to biaxial tensile stresses.

The required strength has been taken as the maximum stresses experienced in the lamina where first fibre failure occurs. The design and rationale behind such a procedure is discussed in the thesis.

Four criteria have been presented (by Pipes and Coles (4)), concerning the feasibility of a biaxial test method. These are:-

- (a) The state of stress throughout the test section should be uniform and determinate.
- (b) Failure of the specimen should initiate in the test section so that static strength will be obtained.
- (c) The test section over which the stress will be uniform should provide a volume of material large enough to eliminate the effects of point defects, and hence make the data significant.
- (d) The test should be capable of providing a varied combination of stress states in the material.

The limitations of these criteria pertaining to the plate bending method have been examined by the application of experimental and numerical techniques. A classical two-dimensional (2-D) thin plate bending finite element analysis has been developed to solve both the small (linear) and large (non-linear) deformation of laminates in the plate bending method. To keep the computing effort at a minimum the formulation omits the effects of shear deformation, shear stresses, material nonlinearities and the exact position of the neutral axis. Hence, care has been taken in choosing sensible experimental parameters to minimise the inherent shear effects in the tests.

It should be noted that the laminated specimens were fabricated some time prior to testing and may have incurred some environmental degradation. As a result, the data shown is not necessarily representative of that which can be obtained with good quality T300/Code 69 carbon epoxy material.

To establish the limitations of criteria (a) and (d) relevant numerical models, together with experimental measurements, have been investigated. As a consequence of the comparison between the numerical and experimental results the assumptions applied in the finite element approach have been studied. To test the applicability of the other two criteria it was only necessary to study the experimental results.

CHAPTER 2 BIAXIAL TEST METHODS

2.0 Introduction

Composite structures are often subjected to biaxial stress or combined stress or complex stress loadings. At present a substantial amount of data is available for uniaxial conditions, but little reliable data is available for biaxial or more complex forms of loading. Biaxial strength predictions for laminates are commonly based on classical lamination theory and a ply wise application of various failure criteria (5,6). A multitude of interaction curves (30+) based on such analytic predictions are available, but to date few experimental programmes have tried to verify the information (4,7). Simply put, the biaxial characteristics of composites have not yet been defined and investigated to a sufficient depth to allow the same confidence level in design as is possible with metals. The lack of confidence in design is a major factor preventing more widespread use of composite hardware today.

To provide a valid assessment of the biaxial strength and elastic properties, it is necessary that an appropriate test specimen should meet the four criteria presented in Chapter 1. In the choice of the test specimen used in this research it was required that the specimen should represent a section of an aircraft wing or fuselage which was subjected to damage, this damage being in the form of an area of low energy impact damage (8), or the study of the effects of altering the environment surrounding the plate (9). A simple test was sought so that experiments could be repeated readily.

To date the deficiency in biaxial data is partly due to the lack in

understanding biaxial test technology, and of the four previously explored techniques, only the tubular and off-axis specimens have been found suitable when applied to laminated composites (4). Specimen geometry and loading of these methods are shown in Fig. 2.1.

It is relevant to describe these four tests, to indicate their relative merits, and then explain why none of them are suitable for the aims of this work.

2.1 Previous Biaxial Test Methods

2.1.1 Tubular

The tubular (filament wound) method has been found to fit all the above criteria for an acceptable biaxial test, and is better than other previous methods in respect of criteria (c) and (d). Cylindrical specimens are subjected to the combination of axial compression, torque, and surface pressures to induce a uniform state of biaxial stress in the test section, Fig. 2.1.1. To maintain a constant ratio of principal stresses fine control on the increase in loads is imperative. Several researchers (4,10,11,12) have shown that a wide range of biaxial stress ratios can be obtained and that information recorded can be verified utilising numerical techniques.

The primary problem with the method is that unwanted stress concentrations are induced by the introduction of axial force through end grips. These nonhomogeneous stress fields often result in premature failure. Sophisticated loading rigs were developed by Pipes and Coles (4) and later by Nahas (10) which in theory should totally eliminate the end restraints. In Pipes and Coles' arrangement the axial and

circumferential stresses were applied to the specimen solely through the use of hydraulic pressure. Torsion was applied mechanically through an end spline arrangement which allows independent expansion or contraction of the end tabs.

However, even with the advances in the technology of tubular specimens several disadvantages make the test method unsuitable for this research:-

- (i) Fabrication of the tubes restricts the number of lay-up arrangements, and it is difficult to obtain filament wound laminates which are characteristic of plate material.
- (ii) Specimens are required to have both uniform and precise geometry to help prevent the occurrence of premature induced fracture. Manufacturing costs are therefore high.
- (iii) Since the loads are imposed through a combination of compression, torque and wall pressure, the rig for experiments is both complicated and expensive.
- (iv) The introduction of the pressure of fluid to the surfaces prevents the inclusion of a typical environment.
- (v) The addition of low energy impact damage will not be characteristic of the same impact damage in a plate specimen due to the inherent material differences between filament wound and flat plate construction.

For the other three biaxial test methods point (v) is of less significance since they are based on a plate construction.

2.1.2 Off-Axis Coupon

The off-axis coupon test as shown in Fig. 2.1.2 can provide valid

strength properties when properly designed (4,13). A long thin plate is axially loaded through end tabs made usually of glass fibre or aluminium. The plate can be unidirectional or laminated with the principal direction of the fibres aligned at some angle to the vertical. The uniaxial loading induces a biaxial strain state within the test section due to the anisotropic nature of composite materials.

The coupon test satisfied criteria (a) and (c), but can only provide a limited combination of stress conditions. Criterion (b) causes severe handicaps and, as has already been mentioned in the previous section, rigid grips create edge constraints and hence a nonhomogeneous stress field. To initiate failure in the test section and remote from the end regions the design of the coupon requires special attention. It has been shown that a length/width ratio greater than 25 is necessary (4). The geometry of the specimen may cause edge delamination when low energy impact damage is applied. Some lamination arrangements induce high shear coupling in the test region which may create delamination at the free edges prior to ultimate failure and invalidate the data.

Due to the limited variation in biaxial stress states, (4:1:1) the restriction on test geometry, and the difficulties in transferring the load to the sample, this type of test is not acceptable.

2.1.3. Crossbeam

Test specimens of a cruciform geometry, consisting of a sandwich of two laminated beams with a honeycomb centre, have been investigated by Kamanski (14), Bert (15) and Coles and Pipes (4). The object

of the test is to produce a known state of biaxial stress in the specimen at a point of intersection of the centre lines of the beams, Fig. 2.1.3.

The beams are subjected to four point bending which induces pure bending in the test section. Simple beam theory and elastic material behaviour means that the stress state at the centre is readily soluble. However, the stress at the intersection is not truly statically determinate since the principal axes of stress are not parallel to the beam axes throughout the intersection region even when the beam axes of the material orthotropy coincide. Furthermore, the sharp corner sections produce indeterminate stress concentrations which then cause first fibre failure under most test conditions.

Several modifications to the specimen geometry have been tried to overcome the inherent stress concentration problems. Curved corners were included, but finite element results showed that this was not adequate, while the stresses in the test region were still indeterminate and failure still started in the corners (4).

To force fibre failure in the test section Bert et al (15) created an elliptical area of reduced thickness in the test section, but the stress state is again uncertain. Other configurations were tried by Pipes and Coles (4), who came to the final conclusion that the crossbeam showed less promise than either of the tubular or off-axis specimen.

The above reasons (the complex nature of the test sample, and the formidable task of maintaining uniform loads across the specimen width),

suggest that this type of biaxial stress test is not suitable for this research.

2.1.4 Bulge Plate

The last method is called the bulge plate test. The specimen utilises an elliptic sample which has the edge clamped to prevent displacement and rotations, and is then subjected to a uniform lateral pressure on one surface Fig. 2.14(4). The biaxial tension due to high membrane strains is varied by altering the aspect ratio of the ellipse, giving results with $\tau_{xy}=0$ (with unidirectional laminates aligned relative to the axes of the ellipse), or by using off-axis laminate alignment relative to the axes of the ellipse, biaxial tension and shear τ_{xy} .

A major handicap with this test is that first fibre failure usually occurs remote from the test section, around the periphery of the plate, making the results invalid.

Creation of a uniform strain is difficult and elastic theory can show that an enormous major diameter/thickness ratio is required (≈ 300), i.e. the bending strains are insignificant to the membrane strain. Difficulties in describing the true stress condition in the test region have been noted by Chow et al (16), where tests on brass plates have indicated that the biaxial ratio tends to change with deformation. For these reasons the method has been rejected as a possible biaxial test for laminates.

2.2 Plate Bending Method - Rationale and Development

The review of the previously developed biaxial test methods indicate that a new procedure is desirable so that strength data for laminated plates containing externally induced degradation can be analysed. Any method accepted must be found not to deviate from the criteria stated earlier, must utilise a plate 'structural' specimen, and has to be suitable for a loading machine available. An Instron 1195 (tension + compression) screw thread machine was available and would provide the expected load range and speed of cross head movement that would be required. The test method and apparatus were therefore developed to be compatible with this machine.

To eliminate the obstacles in transferring load to the material through rigid grips, (found to be a major disadvantage of other methods), the following plate bending procedure was investigated. Simply supported, rectangular plate specimens were subjected to patch transverse loads. Deformation induces bending and a unique biaxial stress state, ($\tau_{xy}=0$) at the centre.

Fig. 2.2 shows the arrangement of the test. In designing the experiment, symmetry about the axes $O-O$ and $O'-O'$ was maintained. The plate is supported on four 'corner' points (some distance in from the corners), in preference to edge supports (e.g. totally simply supported) so as to prevent lift-off (17). This sustains a uniform distribution of reactions, while, at the same time, permitting relative motion without the plate slipping off the support system. The latter will aid longitudinal relaxation as deformation grows and helps suppress the inherent axial strain. Transverse loads are employed through a rectangular patch area, being centred about the centre of the plate and

having sufficient dimensions to ensure that the surface pressure does not exceed that required to punch a hole.

Special attention has been spent on evaluating the correct geometry of the plate to minimise the detrimental effects of shear deformation and shear stresses, as these effects have not been quantified in the numerical modelling. Careful design should also mean that as the deformation increases bending dominates the axial component so that support restraints are minimised. Small axial components and a linear variation of bending strains with deformation will help to maintain a constant biaxial stress ratio within the test section.

Bending which is characteristic in most plate structures (e.g. aircraft wings and fuselages) does however violate criteria (a) by not providing a uniform state of strain through the thickness.

First fibre failure will occur in the test section (under the loading area) as the strain experienced within the plate diminishes dramatically away from the centre, and as long as shear coupling does not induce excessive shear and tensile transverse normal stresses, edge delamination should not exist prior to fibre failure. The actual test section is minute, theoretically the centre of the plate, but due to the distribution in strains surrounding the test area, it is taken to be that on which the load is applied.

This test method produces two combinations of stress states in every case, tension-tension in the lower half and compression-compression in

the upper section. The magnitude of the biaxial stress ratios depends on both the experimental geometry and plate lay-up arrangement. From the analytical work of Timoshenko and Woinowsky-Kreiger (18) the sort of range of biaxial stresses possible becomes apparent. Taking the example of a simply supported isotropic rectangular plate with a central rectangular patch load the change in stress ratio $\frac{\sigma_x}{\sigma_y}$ with alteration in A/B (for constant A_p/B_p and then A_p/B_p (constant A/B)) are evident in Fig. 2.3, 2.4. These results are for small displacements and take no account of any further variation as the deformation becomes large.

For the laminated plate bending method four parameters can be altered which can contribute to varying the magnitude of the biaxial stress ratio, Fig. 2.2. These are:-

- 1) the plate aspect ratio A/B
- 2) the point support aspect ratio A_s/B_s
- 3) the central patch load aspect ratio A_p/B_p , and
- 4) since all laminates have changing directional properties, then the orientation of the principal direction of the plate to that of the apparatus has a profound outcome on the biaxial stress state experienced, even with the other three parameters constant.

It is not expensive or complex to study this method as no further technical equipment is required other than the compression machine, with controlled displacement to apply the load. Unlike the previous biaxial test methods no problem is incurred with the introduction of the surface

damage . Specimens having sufficient dimension when subjected with low energy impact will produce internal damage remote from the free edges. This test also allows most of the material, except under the patch load, to be exposed to any environment for which strength data is required.

CHAPTER 3 FINITE ELEMENT ANALYSIS

3.0 Introduction

From the discussion on the techniques of biaxial stress testing with composite materials, it was imperative that the test method chosen has a test section within which the true state of the stress could be evaluated. For this work a plate bending method, as introduced in section 2.2, was studied.

For any particular experimental arrangement a numerical procedure was required to give some insight into the range of central biaxial stress ratios possible, the ratio being varied as the result of geometric changes. Also, unlike isotropic materials, a numerical prediction was required to determine the distribution of stress through the thickness of the plate, since under certain conditions first fibre failure can occur within the body of the plate. The most suitable numerical method to evaluate the small (linear) and large (geometric nonlinear) deformation in the plate bending test is the Finite Element Method (F.E.M.) It has proved a convenient and powerful technique for the analysis of problems in all types of continuum mechanics. Since its original development in the early 50s, the method has been applied to a wide range of problems with noteworthy success. One of the great virtues of the method is its versatility. The same general techniques are employed in analysing the stresses and deflections in any type of elastic continuum with arbitrary loading and boundary conditions. The general features of the finite element analysis are well known, and so will not be presented here in detail (19,20).

This thesis is concerned with the development of a displacement finite element analysis for the non-linear bending of generally symmetrical orthotropic laminated thin structures. It is worth noting at this point that the bending is deemed non-linear once the maximum transverse deflection is greater than 0.4 of the plate thickness (21), and that the linear analysis is the initial part of the non-linear solution.

An overall picture of the deformation was obtained from this displacement finite element analysis through the displacements and rotations at discrete nodal points. Strains and stresses were then computed at the nodes. The following factors were taken into account in choosing an appropriate method of solution.

A primary object of the work was to compare the displacements and strains from the experimental and the numerical analyses in the linear and non-linear regions. Hence it was necessary to establish the limitations of the constructed F.E.M., in modelling the plate bending experiment. If the method was found to be accurate the results could then be used in understanding the observed failure.

Finite element procedures obviously have inherent numerical errors, (e.g. lack of exact displacement representation and round off errors), which must be minimised if an acceptable comparison is to be made. Thus, to prevent further errors due to excessive element distortion (aspect ratio $\leq 3:1$) in modelling the experiment and at the same time providing nodes at corresponding positions where strains were measured experimentally, it was found that one quarter of the plate required at

least 36 elements.

The non-linear finite element analysis was limited by the computing resources available (IBM 370/167). The programme was limited to a maximum array storage per COMMON block of 1 megabyte and a maximum single job run time of 1000 C.P.U. seconds (Central Processing Unit Time).

The plates used in the experiments were composed of orthotropic laminae of carbon fibre reinforced plastic arranged in generally symmetrical manner about the mid-plane. Although a plate can be represented with a mesh consisting of 36 elements the number of layers in half the plate could be as high as 20. Therefore the element stiffness matrices are the sum of several ply contributions. The time taken to compute all the stiffness matrices could thus become important, especially when a non-linear analysis requires several iterations.

Most of the computing effort in all analyses will be used by the routine solving the finite element set of equations. If an efficient storage method is applied then the time limitation will not be a problem for the linear analysis. Basically, if sufficient storage space is available then very refined meshes can be employed. Although the time to solve the equations will be proportional to the square of the stiffness matrix size (total number of degrees of freedom, D.O.F.), the process is performed only once. However, in the non-linear analysis (total number of D.O.F. have increased by 1.6) several matrix solutions are required. The total time then required to solve the non-linear equations can easily exceed the 1000 second limit. A very efficient and

fast solution routine is thus required. The above points suggest the following conditions for the finite element analysis.

Since at least 36 elements are needed the number of nodes should be a minimum. A minimum of 5 D.O.F. are required to define the non-linear response (three bending $w, \frac{dw}{dx}, \frac{dw}{dy}$ and two inplane u, v), as long as the effect of shear deformation is neglected. To ensure that the total number of D.O.F. are minimised a rectangular element with corner nodes only must be used. The element then has a total of 20 D.O.F. making the governing non-linear stiffness matrix of the 36 element mesh 245×245 , (which underlines the importance of time considerations).

Next, to avoid the utilisation of numerical integration for the evaluation of the element stiffness matrices, the element should have simple displacement functions to describe both the bending and in-plane deformations. These together with several assumptions concerning the non-linear behaviour enable all element stiffness matrices to be determined explicitly.

With the above restrictions on the finite element analysis the computing limitations make it quite obvious that a 3-D model (to include shear stresses) was totally impractical. Section 4.2 illustrates that for the test under scrutiny the omission of shear stresses from the numerical analysis does not seriously detract from an accurate prediction of overall response. Fortunately existing methods allowed the plates to be represented as a lumped system, (in the 2-D X-Y plane) positioned at its mid-plane with a fundamental assumption defining the variation of displacement in the Z-direction. A further simplification may be

made by imposing a state of plane stress.

A geometric non-linear finite element set of equilibrium equations for the general case of plate bending are developed in section 3.2. With these equations the following enabled a solution.

First, the deformation shape about the mid-plane is defined by the most simple approximation (22)

$$\begin{aligned}U &= U^{\circ} + z \psi_x \\V &= V^{\circ} + z \psi_y \\W &= W^{\circ}\end{aligned}\tag{3.1}$$

where $U^{\circ}, V^{\circ}, W^{\circ}$ are weighted averages. ψ_x, ψ_y are the two rotational terms and, since classical thin plate theory (C.P.T.) is applied, they are equated to the ^{surface} curvatures $\frac{dw}{dx}, \frac{dw}{dy}$ respectively, (this being a statement of Kirchoffs fundamental assumption, that normals remain straight and normal (23)).

The limitations of Kirchoffs assumption will be examined in section 4.2 for laminates, where it will be shown that shear deformation (where $\psi_x \neq \frac{dw}{dx}$ and $\psi_y \neq \frac{dw}{dy}$) does not have to be incorporated in the analysis providing the span to thickness ratio S is greater than 30.

A linear solution then follows, providing all C.P.T. assumptions and specific assumptions pertaining to the laminate material are applied.

For a geometric non-linear analysis, one further fundamental assumption is necessary. The large displacement behaviour will be defined as follows. Following Von-Karman (2 4) it is assumed that

although the deflections, w from the initial X-Y plane are sufficient to induce sizeable membrane stresses (therefore invalidating linear plate theory), the slopes $\frac{dw}{dx}$, $\frac{dw}{dy}$ remain much less than unity. This leads to the formulation of the Von-Karman strain equations.

Finally the iterative procedure must be carefully chosen. If the time taken to construct and solve the non-linear equations is large, the number of times that this must be performed should be restricted.

The element used will now be briefly described. Fig. 3.1.1 shows the four noded rectangular element and Fig. 3.1.2 indicates the transverse loadings which can be applied to each node. In-plane loading has been omitted in the formulation since the experiment experiences vertical loads only.

The in-plane deformation requires eight D.O.F., Fig. 3.1.3, which can be represented by the following two simple polynomial expressions:

In-plane displacement function

$$\begin{aligned} U &= \alpha_1 + \alpha_2 x + \alpha_3 y + \alpha_4 xy \\ V &= \alpha_5 + \alpha_6 x + \alpha_7 y + \alpha_8 xy \end{aligned} \quad (3.2)$$

The element is known as the constant strain element (25). The corresponding bending element has twelve D.O.F., Fig. 3.1.4, and the simple polynomial expression representing the displacement were formulated independently by Adini and Clough (26) and Melosh (27).

The bending displacement function is:

$$\begin{aligned}
 W = & \alpha_9 + \alpha_{10}x + \alpha_{11}y + \alpha_{12}x^2 + \alpha_{13}xy + \alpha_{14}y^2 + \alpha_{15}x^3 \\
 & + \alpha_{16}x^2y + \alpha_{17}xy^2 + \alpha_{18}y^3 + \alpha_{19}x^3y + \alpha_{20}xy^3
 \end{aligned}
 \tag{3.3}$$

This linear 'pure' bending element, describing the linear response, will be known as the ACM element.

Inter-element compatibility is satisfied by the function but the inter element normal slope is not continuous, (the element is non-conformal, [0]) (28). However, it does not exhibit all the rigid body displacements and constant strain terms.

Combining the bending and the in-plane element provides an element capable of modelling the non-linear response of plates (29,30). The element will be referred to as ACMBC (20 D.O.F.), after Brebbia and Connor who first applied it to the geometric non-linear finite element analysis of isotropic structures.

3.1 LITERATURE SURVEY

3.1.1. Small (Linear) Deformation-Isotropic

Here the term small or linear implies that the maximum transverse displacement for which the analyses hold is 0.4 of the plate thickness, and that, at no time do in-plane displacements exist. We are therefore concerned with pure bending. Unless specified, the methods do not incorporate the effects of shear deformation and shear stresses and so the plates can be termed as 'thin'. The plates are always represented as 2-D lumped systems, and, because of symmetry, (and providing correct boundary conditions are applied) only one quarter of the plate needs to be modelled.

In the early Sixties the first rectangular and triangular elements used had simple non-conforming polynomials (T,ACM)(31,26). Even though the elements were non-conforming convergence to the exact solution occurred (32), providing sufficient elements were used. Both elements used in the non-linear programme are members from the simple family.

For all the element types the examples used to characterise the accuracy of the elements were simply or clamped supported square plates having either a uniform pressure or a concentrated load. In general only the central displacement was compared to its analytical solution. Occasionally stresses were also involved.

Since the simple triangular element T appeared to be limited due to its lack of compatibility a refined triangular element HCT was formulated from three of these simple elements. This element was reviewed in a

report by Clough and Tocher (33) and found to be much more accurate than the simple elements. Taking four of these refined triangular elements (ECT) (Clough and Fellipa (34) developed a conformal quadrilateral element (Q-19) which gave quicker convergence than previous elements. Improved convergence was measured by how few elements were needed to attain a correct solution. Later in 1968, Bell (35) proposed a further conformal triangular element (B) using a full quintic polynomial and, like Clough, a condensation method to remove unwanted D.O.F. from the formulation of the stiffness matrix. The basic element has a central and mid-side nodes which introduce the unnecessary D.O.F. Convergence again was quicker than with the simple elements.

Quadrilateral elements with full compatibility were also derived. Several improved families of elements were produced to provide compatibility and most of these elements possess more D.O.F. than the simple counterpart. The benefit of compatibility meant that as often as not convergence was possible with coarser meshes. The expense for this was that the displacement functions were more involved and a solution required numerical integration to evaluate the stiffness matrix.

Schmit et al (36) developed a series of rectangular elements (S) based on Hermitian (linear) interpolation polynomials. These elements were found to be very accurate and converged quickly; but the algebraic complexity means that the method is extremely difficult to apply.

Another group of elements was formulated around the assumed stress-hybrid method. Pian and Tong (37,38) derived this method for a series

of quadrilateral elements due to its versatility and ease of operation. Their base element has 20 D.O.F.

Two further types of elements have been very popular, the Lagrangian and Serendipity families (28). These two types of displacement functions have been applied to both triangular and rectangular elements (39). Serendipity elements have functions derived by inspection whereas Lagrangian were formed from generating displacement shapes of any order from simple products of appropriate polynomials in the 2-D co-ordinate system. All shape functions were normalised so that translation into actual co-ordinates, or transformation of the various expressions occurring for instance in stiffness derivation, were trivial.

The Lagrange family was found to be limited not only due to the large number of internal nodes needed but also due to the poor curvature-fitting properties of the higher order polynomials. On the basis of computational efficiency Serendipity elements should be preferred because of fewer total D.O.F., but because of locking (40), Lagrangian elements have been the preferred family. Together, these interpolation elements are known as iso-parametric and have been exclusively used in the general purpose finite element package, PAFEC 75, which is available on the NUMAC systems. Elements from both families can be formed as linear, quadratic, cubic and, for extreme refinement, quartic.

The accumulation of results obtained from applying the above elements in the modelling of isotropic plate problems were presented by Spilker and Munir in 1980 (41). Since Lagrangian elements contained spurious zero energy modes not associated with rigid body movement and Serendipity

elements caused locking when representing certain thin plate examples they developed a new element type, referred to as Heterosis. The element is based on an 8-noded Serendipity element with a shear deformation hybrid-stress method of solution. Numerical studies indicated that this new element had 'safe' characteristics with comparable accuracy to its earlier counterparts.

When increasing the complexity of the element to provide compatibility the question should be asked as to whether any economic or other advantage was actually being gained. An answer here is not simple, although it can be stated as a general rule that as the order of an element increases so the total number of unknowns in a problem can be reduced for a given accuracy of representation. The only proviso is that the elements do not become too distorted. Economic advantage requires a reduction of total computation and data preparation effort. This does not follow automatically for a reduced number of total variables as, although equation solving time may be reduced, the time required for element formulation increases. For this work the most important factor was that at least 36 elements were necessary in a quarter plate model of the experiment.

Thus, with the knowledge that the simple element ACM gives accurate results, providing sufficient elements are used, and that for identical models with all higher order elements more computing effort will be needed, the choice of ACM for the non-linear analysis was practical. ACM along with the following bending elements, Spilker and Munir (SM), Schmit et al (S), Bell (B), Tocher (T) and Clough and Tocher (HCT) is compared with exact solutions for several isotropic examples in Section 3.4.1.

From this comparison further reasons for the choice of ACM instead of a compatible element will become apparent.

3.1.2. Small (Linear) Deformation=Laminated

Progress with analytical solutions for laminated plates during the Seventies suggested that shear deformation effects on the behaviour of the plates were much more pronounced than for isotropic plates (42, 43). Hence, it was not surprising that the majority of F.E.M. used a refined element in a shear deformation analysis. They were therefore concerned with pure bending of 'thick' laminated plates. A review and discussion on the accuracy of these shear flexible elements is made in Section 4.2.

Reddy (44) in 1980 gave a full appraisal of the development in linear F.E.M. for laminates. The overall picture showed that the refined elements only gave improved accuracy when shear deformation was important. Contributions to the art were made by Pryor and Barker (45), Mau, Tong and Pian (38), Mawenya and Davies (46), Panda and Natarajan (47), Noor et al (48, 49) and finally Reddy. In all procedures time consuming numerical integration schemes were needed for the evaluation of the stiffness terms.

From the previous approaches element ACM has been used by Pryor and Barker. It was combined with the constant strain and shear rotation elements to enable the determination of shear deformation. The element has a total number of 28 D.O.F. and like ACM is only accurate when the mesh has a lot of elements. By ignoring shear deformation in ACMBC the number of D.O.F. per node were reduced by 2, so greatly reducing the effort

in formulating the governing stiffness matrix.

Section 4.2 explains why it was acceptable for the finite element analysis of the plate bending method not to include shear deformation. The investigation shows that providing the span to thickness ratio, $S > 30$ the shear deformation in multilayered generally symmetrical orthotropic laminates can be assumed small compared to the bending response. With this proposal in mind, the element ACM in a linear thin plate theory has been taken as suitable for analysing the experiments.

3.1.3. Large (Non-Linear) Deformation-Isotropic

Geometric non-linearity will be considered only to the extent required to account for effects of membrane forces on effective flexural stiffness. For an introduction to the ideology of non-linear problems the paper by Gallagher (50) is very informative.

The introduction to the review states that at the time a disproportionate amount of attention had been given to non-linear analyses, involving both geometric and material non-linearities. There were two reasons for this statement. First, not all the fundamental concepts and theoretical aspects had been explained or agreed upon. Second, in those portions of the problem where the theory was in good agreement (e.g. the procedure developed in this work) the cost of numerical solution was vastly greater than for the equivalent linear solution. The latter point has ensured that a great deal of effort has been devoted on the minimization of computing cost, while at the same time preventing significant loss in accuracy.

Several successful geometric non-linear analyses applying the elements already discussed will now be introduced. In all cases the accuracy of these methods was measured against analytical reported solutions on simple isotropic plate problems. Notable contributions were made by Levy (51), Wang (52), Berger (53) and Rushton (54).

Since the analytical problems were relatively simple (e.g. a simply supported square isotropic thin plate with a uniform pressure load and constrained with Levy's in-plane boundary conditions), only a few elements 16, were required in a quarter plate mesh for accurate modelling. It is open to question whether any of the methods presented would be capable of coping with a 36 element mesh when implemented on the most powerful computer.

This does not mean that these analyses are misleading since they achieve their objectives. From the numerical techniques used in these F.E.M. several time saving operations have been extracted and involved in the non-linear programme (ACMBC). Without these techniques the solution of the geometric non-linear displacement F.E.M. of the experiment would have been more difficult.

Before embarking on the discussion of previous procedures, it is worthwhile introducing the methods for solving the potential energy expressions. No one algorithm has gained universal preference, mainly because each is suited for particular situations, but becomes inefficient or invalid for different situations. The solution procedure will generally be the most expensive, both in terms of computing time and storage. This is the reason why so much attention has been spent on

improving this area.

Methods attacking the solution of the simultaneous algebraic equations directly are overwhelmingly the most popular. Many different basic forms are possible, including the direct iteration (55), Newton-Raphson (56), incremental (57), and initial value methods (58). Several of these techniques will be mentioned in this section. It must be remembered that these techniques trace a load displacement response through a significant range of non-linear behaviour. Essentially they operate with intervals of loading, the solution for one being the starting data for the next. Numerical experience has indicated that it is generally impractical to proceed from the initial to the final state in a single step due to numerical instabilities.

Earlier work on the non-linear response of structures by Turner et al (59), Oden and Sato (60), and Martin (61), paved the way for the finite element plate bending methods. To reduce the very complicated approaches required, certain assumptions had to be made, and some restrictions were placed on the displacement field. Fortunately no significant loss in accuracy was incurred. Simplification of this type lead for instance to the Von-Karman strain expressions for plates.

Incorporating these strain equations with the C.P.T. assumptions has proved to yield excellent analytical results for large deflection plate problems, Levy (51), and successfully applied in a displacement F.E.M. by Brebbia and Connor (29). They developed a consistent formulation for arbitrary plates and shallow shell elements. Strains and products of rotations were negligible with respect to unity, and this restriction

could only be removed at great computational expense (62,63). To make a linear buckling analysis possible (64,61) the governing equations for Newton-Raphson iterative procedure were followed.

In this thesis Brebbia and Connor's basic finite element isotropic formulation has been developed to analyse plates consisting of generally orthotropic laminae in a symmetrical arrangement. The element ACMBC has been retained and, whereas the original analysis terminated after the evaluation of nodal displacements, the new programme also evaluates nodal strains and stresses.

However, there is one major difference between the two approaches. To eliminate the need for numerical integration schemes in ACMBC, the substitution of the full bending displacement polynomial, (Equ. 3.3) into matrix $[H]^e$ (Equ. 3.44) $\{ [w^*] \text{ Brebbia and Connor, Equ. 27c} \}$ was dropped. Instead the rotational terms in matrix $[H]^e$ have been assigned values using a new technique, section 3.4. Consequently, when results from programme ACMBC are studied in section 3.4 a thorough examination for a new definition of $[H]^e$ will be made.

Unless otherwise stated, the following methods are based on thin plate theory, i.e. no shear deformation, with Von-Karman strain equations for flat plates and Marguerre (65) theory for shallow shells.

In 1971 element ACMBC was built into an analysis by Roberts and Ashwell (30) to solve structural post buckling. They applied a method of incrementing displacement with a linearised mid-increment stiffness matrix for each increment of displacement. To aid convergence they

employed sparingly the Newton-Raphson iterative method. As in Brebbia and Connor's work all the element stiffness matrices were evaluated by numerical integration, (Gaussian quadrature formulae (28)) with the full bending displacement function.

In 1967, Schmit et al (63) tackled finite deflection structural analysis with their family of plate and cylindrical shell discrete elements. They applied an oscillatory Hermitian linear interpolation bending element with 4 nodes and 48 D.O.F. in a new plate formulation and solutions were obtained by direct minimization of the potential energy formulation. Without the application of complicated boundary conditions the total number of D.O.F. would have been unwieldy for an accurate solution of even a simple problem. This method cannot be used to model structures requiring a lot of elements since it is one of the most involved procedures.

Two years later, Kawia and Yoshimura (66) presented an accurate analysis with the Lagrangian bending displacement function proposed by Greene (67). This rectangular element possesses 4 nodes and 3 bending D.O.F. each, and was combined with the constant strain element (Equ. 3.2) in the non-linear analysis. The element stiffness matrices were large and required evaluation by a numerical integration scheme. Solution of the equilibrium equations was made possible by the procedure devised by Yoshiki, Kawia and Yoshimura (68). However, they demonstrated that the iterative method was often unstable. If $\{d\}_n$ was calculated using only $\{d\}_{n-1}$ (Equ. 3.31), the solution sometimes failed to converge. To avoid such a difficulty they introduced the numerical technique with which Fujino and Ohsaka (69) analysed the large displacement of suspension

bridges. The technique will be outlined since it was included in ACMBC.

When choosing the assumed displacement values to be substituted into the expression of additional nodal forces to calculate the corrections $\Delta\{d\}_n$ not only $\{d\}_{n-1}$ but also $\{d\}_{n-2}$ were considered. The following weighted mean of the two approximated displacement values $\{d\}_{(n-1)}$ and $\{d\}_{(n-2)}$ were used as the assumed displacement values

$$\{d\}_{(n-1)} = (1 - \beta)\{d\}_{(n-2)} + \beta\{d\}_{(n-1)} \quad (3.4)$$

in which $0 \leq \beta \leq 1$.

In Kawia's work, $\beta=0.3$ for large deflection problems, and a larger value, say $\beta=0.5$ was found permissible when a system was linear. In section 3.4 the relevant value for β used in ACMBC will be given for the problems investigated.

Bergan and Clough (70) developed a large displacement analysis for thin plates and shallow shells and placed a great deal of emphasis on a specific matrix formulation, thereby producing a highly efficient method that was suited to modern electronic computers. The bending element was a doubly curved quadrilateral based on the Q-19 expression of Clough and Fellipa (34). The element was formed from four HCT elements and has 19 D.O.F. When combined with the inplane Zienkiewicz-Irons isoparametric element (28) with 2 D.O.F. per corner node, the non-linear element has 29 D.O.F. The 9 internal nodes were eliminated by static condensation leaving a 4 noded element with 20 D.O.F. Initial deformation was provided for in the analysis by using the rectangular linear element of Bogner, Schmit and Fox (S)(36).

Accurate modelling was also obtained after the bending displacement polynomial was shortened in the evaluation of the non-linear stiffness terms (matrix [H]). The coefficients were evaluated by a 2x2 or a 3x3 Gaussian quadrature numerical integration scheme. The equilibrium equations were formed by the 'direct stiffness method' and the direct solution called for a form of numerical iteration. Since the object of a non-linear analysis was to determine more than just a single point on the load deformation curve acceptable results were found by the combination of the Newton-Raphson method and load incrementation.

One feature of the analysis has been implemented in ACMBC. This procedure reduces the number of iterations when establishing convergent non-linear displacements. In order to determine convergence, the following vector was defined,

$$\epsilon_n = \left(\frac{\Delta d_1}{d_{1ref}}, \frac{\Delta d_2}{d_{2ref}}, \frac{\Delta d_{DOF}}{d_{DOFref}} \right)_n^T \quad (3.5)$$

where Δd_{kn} is the change of displacement component k during the iteration cycle n. Every component was then scaled by a reference displacement. For the plate problems all in-plane displacements were scaled by the largest in-plane component, all transverse deflections were scaled by the largest transverse deflection and similarly for rotations. A non-dimensional measure of the change of the displacement vector during a cycle was obtained using the maximum norm.

$$\epsilon = \max_k \left| \frac{\Delta d_k}{\Delta d_{ref}} \right|$$

The following convergence criterion could then be used

$$|\epsilon| < \epsilon$$

The range of $|\epsilon|$ used by Bergan + Clough was approximately 10^{-2} to 10^{-5} depending on the problem. For ACMBC relevant values for $|\epsilon|$ will be given in section 3.4.

During the Seventies more programmes (including the large general packages) started to solve non-linear deformation of structures. These analyses involved some of the techniques already outlined, but generally tended to be much more intricate.

Thomas and Gallagher (71) formulated a geometric non-linear (small strain, finite displacements) analysis with a consistent triangular element, (Lagrangian, 30 D.O.F., 4-noded (one centre)). The procedure was numerically sound but the cost of evaluating the non-linear stiffness coefficients by numerical integration with the full cubic displacement polynomial meant that models were very limited. To combat this, an inconsistent quadrilateral element comprising 4 triangles was constructed. Internal D.O.Fs were eliminated in the usual manner and the introduction of a special matrix took account of the lack in compatibility between adjoining sides.

A large amount of effort was then spent minimising solution time. The approach finally chosen combined two schemes, the Newton-Raphson and incremental methods. The algorithm was termed the 'modified incremental method', and can be thought of as a single cycle of the Newton-Raphson procedure. Hence, by the application of this method only one inversion per load was necessary.

Further notable contributions, which were later developed for generally orthotropic layers were made by Moor (72,73) and Reddy (74,75). These finite element packages solved non-linear bending using an analysis based on Von-Karman strain equations and a shear deformation plate formulation.

The latest analysis used a Mindlin plate formulation. Pica, Wood and Hinton, (76), centred their investigation around the Heterosis element, (Spilker (SM)), to discover if it was still superior to its Serendipity and Lagrangian counterparts. They used the geometric non-linear formulation developed by Noor, Mathers and Anderson (77) which has identical matrix notation to that of ACMBC. The stiffness coefficients were evaluated by several orders of Gaussian quadrature numerical integration. Examination of simple bending problems were performed with a 4-noded linear Serendipity element, a 8-noded quadratic Serendipity, a 9-noded Lagrangian and the 9-noded Heterosis element. A Newton-Raphson procedure was the primary algorithm solving the equilibrium equations, but to save computing effort another modified Newton-Raphson method was later introduced. In this latter method the tangential stiffness matrix was constructed once only during the second iteration of each load increment. Results were presented for standard isotropic square plate examples, together with a skew, a circular and an elliptic plate example. All cases were modelled with a 16 element quarter plate representation and both transverse displacements and stresses were determined.

A thorough comparison was made between the four elements and those of Schmit, Bogner and Fox (63) and Iron-Razzaque (78). They had hoped to find a discernable pattern of element behaviour emerging from the investigation, but this proved not to be the case. The study demonstrated that it was advisable to use the Heterosis element in rectangular meshes due to its safe characteristics. However, the presence of curved boundaries in the models led to inconsistent behaviour of all elements, especially with respect to stresses.

The analyses outlined substantiate the uncertainty already stated concerning the best choice of algorithm to solve the non-linear equilibrium equations. Gallagher (50) and then with Thomas (70) reviewed the problem and suggested that the most appropriate method seemed to be a 'modified' Newton-Raphson. The word 'modified' means that the basic Newton-Raphson was altered (i.e. compare Gallagher and Thomas (70) with Picaet al (76)). This observation made the choice of an algorithm for ACMBC difficult. The programme was formulated with the basic Newton-Raphson procedure for ease of computation. If this was then to be found inaccurate and/or time consuming, a modification could be included providing time allowed.

3.1.4 Large (Non-Linear) Deformation Laminated

The first geometric non-linear F.E.M. for laminated materials was presented by Noor and co-workers (72,73,79,80) in 1975. Over several years the team had developed a wide ranging plate bending package, including the non-linear analysis of generally orthotropic laminated (symmetric and antisymmetric) plates and shells. The formulation was a form of the geometric non-linear Von-Karman type plate theory with the effects of transverse shear deformation, anisotropic material behaviour and bending extension coupling. The general nature of the programme allowed for modelling with Serendipity, Lagrangian and Hermitian rectangular and triangular elements.

To demonstrate the power of their F.E.M., normalised results, published in 1975 for a 16 noded rectangular Lagrangian bending element (80 D.O.F.), were used to study the effects of geometry, lamination

parameters and boundary conditions on the significance of transverse shear deformation and the degree of anisotropy (non-orthotropy) of statically loaded composite plates. Square plates were considered having both symmetric and antisymmetric laminations with respect to the mid-plane. These examples were subjected to uniform transverse loading, and were either simply or clamped supported. Results demonstrating the effect of shear deformation and anisotropy were presented as non-dimensional energy parameters. A full grid contained 36 elements making a total number of bending D.O.F. of 1805. A considerable reduction in unknowns was possible by the utilisation of symmetry (49).

On the basis of the numerical study it was shown that C.P.T. was adequate for the non-linear analysis of uniformly loaded square plates when $S > 20$ and that orthotropic plate theory (when anisotropic terms D_{16} , D_{26} are neglected) was acceptable if angle-ply plates consisted of more than 4 layers. In general if the effect of transverse shear deformation and/or anisotropy on the linear response was not significant, they were not important in the non-linear analysis. This conclusion is very encouraging when the nature of the formulation of ACMBC is scrutinised.

The introduction by Reddy and Chao (74) gave a review to the present standing on non-linear laminated plate analysis. Nearly all previous approximate solutions of the large deflection theory (in Von-Karman sense, and without shear deformation) were analytical and solved either the vibration behaviour (81,82) or the evaluation of central displacement in unsymmetric laminates (83,84). Noor et al's F.E.M. was the only one of its type to date. Unfortunately this analysis involved a very complex

bending element (80 D.O.F.) which limited its application. Reddy stated that the use of such an element inevitably lead to an enormous storage requirement and computational cost.

Reddy and Chao presented a large deflection and large amplitude free vibration analysis for composite plates. The F.E.M. was based on an extended Yang-Norris-Stavsky (YNS) theory (85), which is the transverse shear deformation principle of Mindlin for laminates, that includes the effects of large deflections, in the Von-Karman sense. Two Serendipity rectangular elements with 5 D.O.F. per node (3 displacements u, v and w plus 2 shear rotations ψ_x and ψ_y) resulted in a 20×20 element stiffness matrix for the linear element and a 40×40 matrix quadrature element. Their new algorithm solved the equilibrium equations by a penalty function method and involved the use of the so called 'reduced' integration technique to evaluate the stiffness coefficients. In the reduced integration technique, the 4-noded element required the 1×1 Gaussian rule instead of the standard 2×2 . The technique enabled some saving of computational effort.

Accurate results were presented for deflections, stresses and natural frequencies (74) for rectangular plates with several loading and edge conditions. As expected the results were more accurate with the 8-noded element, than for the 4-noded element. Unfortunately other than a little relevant information on element and mesh sizes, no mention of the actual computing effort was given. It has therefore been impossible to say how large a saving in storage and computing time was gained over that necessary with Noor's F.E.M., and further to compare with that found with ACMBC.

At the same time as Reddy and Chao, Chang and Savamiphakdi (86) reported their non-linear analysis for laminated shells. The object of the work was to extend the application of a degenerated 3-D solid element family to the large displacement analysis of laminated shells. This isoparametric group of solid elements has independent rotations and translational D.O.F. and was originally proposed by Ahmad, Irons and Zienkiewcz (87). After some assessment an 8-noded Serendipity and a 9-noded Lagrangian rectangular element (5 D.O.F. per node) were selected for the present work.

The approach was based on an up to date Lagrangian formulation by McMeeking and Rice (88) following on from Hill's (89) virtual work equation. From the study of the numerical characteristics (Programme NFAP (90)) the 8-noded element showed locking (too stiff) when modelling thin plate structures. The element was too stiff due to the presence of unnecessary shear stresses. This locking phenomenon was probably not seen by Reddy since thin plates were not studied in his work.

Accuracy of the elements was determined through the use of the analytical solutions of standard isotropic examples. To display the modelling of laminated systems, the following flat plate example was examined. A square sandwich plate, consisting of two identical aluminium facings and an aluminium honeycomb core, was subjected to a uniform load and had all its edges damped. Excellent agreement was obtained between the F.E.M. with a 4 element quarter plate mesh and the central displacement from the analysis by Schmit and Monforton (91). As usual, this example did not stretch the limits of the method, since the problem required only a few elements in the model, and the plate consisted of a few layers

in an orthotropic arrangement. A more realistic test would have involved more elements and generally orthotropic plies.

Chang and Sawamiphakdi concluded that the Lagrangian element provided a much better numerical behaviour than the Serendipity element.

It is interesting to find that none of the previous non-linear deformation finite element analyses for laminated plates applied the element ACMBC. It is worth noting also that the formulations and solution techniques differ considerably, with the Von-Karman strain equations and the shear deformation assumption of Mindlin being most generally used (Section 3.1.3). The solution procedure was often centred on the Newton-Raphson iterative technique.

In every method the full bending displacement function was applied in the definition of matrix $[H]^e$ and numerical integration evaluated the stiffness coefficients. The methods all involved elements from the Serendipity and Lagrangian families, since their refined elements were known to be very accurate (especially for coarse meshes) and the polynomial representations lend themselves to numerical integration.

Taking the above observations together, it appears that none of the F.E.Ms to date would be capable of dealing with large mesh problems since the requirement for storage space and computing time would be too high for modern electronic computers. An upper limit on the number of elements each procedure can handle was obviously not ascertainable due to the fact that the following factors differ. First, the programming

techniques for storage and solution are not reported. Second, the power of the computers on which they were built is not given. Third, the time taken to formulate the stiffness matrix, and then to solve the equilibrium equation are not presented, and fourth, the number of iterations for a particular type of solution are also unavailable.

If the cautionary words in the papers concerning their individual difficulties in computation are also noted, it appears extremely likely that none of the previous F.E.Ms could be used to model our plate bending experiment. Not only does the model of our experiment require at least 36 elements in a quarter plate, but the number of individual element stiffness matrices is large, since a plate can consist of up to 40 layers. This latter consideration means that the time to construct the stiffness terms can be high (even comparable with that to solve the equilibrium equations).

Taking all the factors outlined in this section it was reasonable to apply element ACMBC in a non-linear displacement finite element formulation based on Von-Karman's strain equations and the classical thin plate theory to analyse the plate bending experiment. To reduce computational effort further several material assumptions were introduced and numerical integration was eliminated by the new definition of the terms in matrix $[H]^e$. After the equilibrium equations had been evaluated the Newton-Raphson method solved the flexural problem.

3.2 FINITE ELEMENT FORMULATION

The precise details of the FORTRAN IV programmes have been omitted from the thesis. However, flow diagrams explaining the analysis are presented in Appendix I.

3.2.1 Principle of Minimum Potential Energy

The total potential, or potential energy, of an elastic body is defined as (92)

$$\Pi = U + W_p \quad (36)$$

where U is the strain energy, and W_p is the potential of the applied loads. Because the forces are assumed to remain constant during a variation of the displacements, one can relate the variations of the work done by the loads, W , and the potential of the loads as follows (93).

$$\delta W = \delta W_p \quad (37)$$

The variation in $W = W(x)$ is defined as an infinitesimal arbitrary change in W for a fixed value of the independent variable x , that is for $dx=0$.

The principle of Minimum Potential Energy is

$$\delta \Pi = \delta U + \delta W = \delta U - \delta W = 0 \quad (38)$$

The principle and its accompanying conditions can be states as follows:

Of all possible displacement configurations a body can assume, which satisfy compatibility and the constraints or kinematic boundary conditions, the configuration satisfying equilibrium makes the potential energy assume a minimum.

Here it is important to note that variations of displacement are

taken while forces and stresses are assumed constant. Moreover, the resulting equations are equilibrium equations.

The potential energy for a linear elastic body which has no distributed loads acting within the material, or along the boundary, and has no initial stresses or strains is obtained by the sum of the internal work (the strain energy due to internal stresses) and the potential of the external forces. Following the terminology used by Zienkiewicz(20) the potential energy functional is

$$\int_V \{\epsilon\}^T \{\sigma\} d(\text{vol}) - \{d\}^T \{R\} = \pi \quad (3.9)$$

Thus equ. 3.8 can be written as

$$\int_V d\{\epsilon\}^T \{\sigma\} d(\text{vol}) - d\{d\}^T \{R\} = 0 \quad (3.10)$$

The above statement means that for equilibrium to be ensured the total potential energy must be stationary for variations of admissible displacements. A finite element method is simply the statement of this variation with respect to displacements constrained to a number of parameters $\{d\}$ and can be written as

$$\frac{d\pi}{d\{d\}} \left\{ \begin{array}{c} \frac{d\pi}{d d_1} \\ \frac{d\pi}{d d_2} \\ \vdots \\ \frac{d\pi}{d d_{DOF}} \end{array} \right\} = 0 \quad (3.11)$$

It can be shown that in elastic situations the total potential energy is not only stationary but is a minimum. Thus the displacement finite element process seeks a minimum within the constraint of an assumed displacement pattern.

In the finite displacement method the plate is subdivided into a

number of discrete elements which are interconnected at specific nodal points, a solution to the complex numerical problem being made by the use of matrix algebra. The greater the number of D.O.F. the more closely will the solution approximate to the true one, providing the true displacement can in the limit be approximated.

3.2.2 Geometric Non-Linear Plate Bending

Whether the displacements (or strains) are large or small equilibrium conditions between internal and external forces have to be satisfied. If $\{\psi\}$ represents the vector sum of the internal and external forces, equ. 3.10 becomes

$$d\{d\}^T \{\psi\} = \int_V d\{\epsilon\}^T \{\sigma\} d(\text{vol}) - d\{d\}^T \{R\} = 0 \quad (3.12)$$

where $\{R\}$ represents all the external forces due to imposed loads.

Using the displacement method the variation of strains can be written as

$$d\{\epsilon\} = [\bar{B}] d\{d\} \quad (3.13)$$

The bar suffix indicates that as displacements are large, the strains depend on non-linearity in the induced displacement, and the matrix $[\bar{B}]$ is therefore dependent on $\{d\}$. Equ. 3.12, the governing equilibrium equation for the body becomes

$$\{\psi\}(\{d\}) = \int_V [\bar{B}]^T \{\sigma\} dV - \{R\} = 0 \quad (3.14)$$

The actual stresses $\{\sigma\}$ are dependent on the strain level obtained.

As $\{\sigma\}$ is dependent on strain and hence on displacements one has, therefore, to solve the non-linear equation

$$\{\psi\}(\{d\}) = 0 \quad (3.15)$$

This then summarises the basic problem.

Matrix $[\bar{B}]$ can always be conveniently written as

$$[\bar{B}] = [B_0] + [B_L(\{d\})] \quad (3-16)$$

in which $[B_0]$ is that governing linear infinitesimal strain analysis and only $[B_L]$ depends on the displacements. For the displacement model constructed $[B_L]$ is a linear function of the displacements. If the strains are reasonably small (in elastic range) the general elastic relation, with no initial stresses or strains, is

$$\{\sigma\} = [D]\{\epsilon\} \quad (3-17)$$

in which $[D]$ is the usual set of elastic constants. In equ. 3.12, the stress components are those corresponding to the strain components used. In some gross displacement problems such strain components are subjected to considerable change of direction from the global axes.

3.2.2.1 Iterative Solution

Clearly the solution of equ. 3.14 will be approached iteratively. The Newton-Raphson (94) process is adopted here, to establish the relationship between $d\{d\}$ and $d\{\psi\}$.

Thus by taking the appropriate variations of equ. 3.14 with respect to $d\{d\}$

$$d\{\psi\} = \int_V d[\bar{B}]^T \{\sigma\} dV + \int_V [\bar{B}]^T d\{\sigma\} dV \quad (3-18)$$

and applying equ. 3.17 and equ. 3.13,

$$d\{\sigma\} = [D]d\{\epsilon\} = [D][\bar{B}]d\{d\} \quad (3-19)$$

From equ. 3.16

$$d[\bar{B}] = d[B_L] \quad (3-20)$$

due to the non-linear effects.

Therefore

$$d\{\psi\} = \int_V d[B_L]^T \{\sigma\} dV + [\bar{K}] d\{d\} \quad (3-21)$$

where

$$[\bar{K}] = \int_V [\bar{B}]^T [D] [\bar{B}] dV = [K_0] + [K_L] \quad (3-22)$$

in which $[K_0]$ represents the linear stiffness matrix. This is the governing matrix from which the linear programme was based.

$$[K_0] = \int_V [B_0]^T [D] [B_0] dV \quad (3-23)$$

The matrix $[K_L]$ is due to the large displacements and is

$$[K_L] = \int_V \left([B_0]^T [D] [B_L] + [B_L]^T [D] [B_L] + [B_L]^T [D] [B_0] \right) dV \quad (3-24)$$

and is known as the large displacement matrix. It can also be shown that this matrix can be derived by using an infinitesimal strain approach by adjusting element co-ordinates in the computation of the stiffness.

The first term in equ. 3.21 generally becomes

$$\int_V d[B_L]^T \{\sigma\} dV = [K_\sigma] d\{d\} \quad (3-25)$$

where $[K_\sigma]$ is a symmetric matrix dependent on the stress level, and known as the initial stress matrix or geometric matrix (95).

Thus

$$d\{\psi\} = ([K_0] + [K_L] + [K_\sigma]) d\{d\} = [K_T] d\{d\} \quad (3-26)$$

with $[K_T]$ the total, tangential stiffness matrix governing the non-linear response.

The Newton type iterative procedure can be applied in the manner summarised.

(a) The elastic linear solution is determined as a first approximation

$$[K_0] \{d\}_1 = \{R\} \quad (3-27)$$

(b) $\psi \{d\}_1$ is obtained from equ. 3.14, with approximate definition of

$[\bar{B}]$ and the stresses,

$$\psi\{d\}_1 = \int_V [\bar{B}]^T \{\sigma\}_1 dV - \{R\} \quad (3.28)$$

with

$$\{\sigma\}_1 = [D]\{\epsilon\} = [D][\bar{B}]\{d\}_1 \quad (3.29)$$

which gives

$$\psi\{d\}_1 = \int [\bar{B}]^T [D][\bar{B}]\{d\}_1 dV - \{R\} \quad (3.30)$$

and reduces to

$$\psi\{d\}_1 = [\bar{K}]\{d\}_1 - \{R\} \quad (3.31)$$

where the large displacement stiffness matrix has been defined as above.

(c) Matrix $[K_T] = [\bar{K}] + [K_\sigma]$ (3.32)

is established, and

(d) The correction is calculated as

$$\Delta\{d\}_1 = -[K_T]^{-1} \psi\{d\}_1 \quad (3.33)$$

making the new displacements equal to

$$\{d\}_n = \{d\}_{(n-1)} + \Delta\{d\}_{(n-1)} \quad (3.34)$$

This process is then repeated until $\psi\{d\}_n$ becomes sufficiently small.

3.2.2.2 Geometric Non-Linear Finite Element Plate Bending Representation For Generally Symmetrical Orthotropic Laminates

Having formulated a general set of equilibrium equations, with a Newton-Raphson iterative solution procedure, plate bending assumptions must be specified so that the finite element representation can be solved.

For the non-linear behaviour under consideration Von-Karman's

assumption is applicable (24). As has already been mentioned a 3-D was impractical, so a lumped 2-D representation (Equ. 3.1) has been chosen, being based on the classical thin plate assumption attributed to Kirchoff, (normals remain straight and normal) (23).

In most practical applications of thin plates the magnitude of the stresses acting on the surface parallel to the middle plane are small compared to the bending the membrane stresses. Since the plate is thin, this implies that the traction on any surface parallel to the mid-plane is relatively small. In particular, an approximate state of plane stress exists.

A standard X, Y, Z co-ordinate system, Fig. 3.1.1., has been taken. The displacements in the X, Y and Z directions are denoted by $u(x, y)$, $v(x, y)$ and $w(x, y)$ respectively. A list of the plate bending and material assumptions follows.

- 1) The plate is constructed of an arbitrary number of layers of orthotropic sheets bonded together, with the restriction that the configuration must be symmetrical about the mid-plane. However, the orthotropic axes of material symmetry need not coincide with the X, Y axes of the plate.
- 2) Perfect bonding exists between the fibres and surrounding matrix, and between each lamination. The fibres are assumed continuous along the length of a lamina and all aligned in the principal direction.
- 3) There are no initial displacements, the plate is flat, and no initial stresses are present.
- 4) The plate is thin, i.e. the thickness, h , is smaller than the

other physical dimensions.

- 5) The in-plane strains ϵ_x, ϵ_y and ϵ_{xy} are small compared to unity, and zero for the linear solution.
- 6) The displacements u and v due to plate curvatures are linear functions of the z direction, equ. 3.1, i.e. they are zero along the mid-plane.
- 7) Transverse shear strains ϵ_{xz} and ϵ_{yz} are negligible and the corresponding shear stresses τ_{xz}, τ_{yz} ignored.
- 8) The transverse normal stress is negligible. σ_z
- 9) Each ply obeys Hookes law; all the material properties being linearly dependent on the respective strain up to failure.
- 10) The plate has uniform thickness.
- 11) The location of the neutral axis coincides with the mid-plane in the linear deformation.
- 12) Rotary inertia terms are assumed very small.
- 13) There are no body forces.

It is noted that assumption 7 is a direct consequence of plane stress. Together, assumptions 6 and 7 constitute Kirchoffs assumption, and, with assumption 8, allows, the problem to be simplified to the 2-D about the mid-plane.

The 2-D representation of the displacement F.E.M. can now be constructed. Formulation of the stiffness matrices will now follow by applying the basic rectangular element, Fig. 3.1 and its simple displacement functions, Equ. 3.2 and 3.3.

The plates in the experiments will be subjected to transverse loading only so the analysis does not include in-plane loading.

For the non-linear solution the displacements are not minute, but also not excessively large. It is well known that in such situations the lateral displacements will be responsible for developing membrane strains and the two problems of in-plane and lateral deformation can no longer be dealt with separately, but are coupled.

In Fig. 3.2.1, plate strains are defined in terms of the mid-plane displacements, i.e. if the X-Y global plane coincides with the mid-plane, then

$$\{\epsilon\} = \begin{Bmatrix} \epsilon_x \\ \epsilon_y \\ \epsilon_{xy} \\ -z \frac{d^2 w}{dx^2} \\ -z \frac{d^2 w}{dy^2} \\ -2z \frac{d^2 w}{dxdy} \end{Bmatrix} = \begin{Bmatrix} \epsilon_{pl} \\ \epsilon_b \end{Bmatrix} \quad (3-35)$$

If the deformed shape is considered as in Fig. 3.2.2., then applying Von-Karmans assumption the lateral deformation, w , induces some additional extension in the X and Y directions of the mid-surface and the length dx stretches to

$$dx = \sqrt{1 + \left(\frac{dw}{dx}\right)^2} = dx \left\{ 1 + \frac{1}{2} \left(\frac{dw}{dx}\right)^2 + \dots \right\} \quad (3-36)$$

i.e. defining the x elongation to the second approximation

$$\epsilon_x = \frac{du}{dx} + \frac{1}{2} \left(\frac{dw}{dx}\right)^2 \quad (3-37)$$

Considering in a similar way the other components, the strains are

defined by Greene's strain vector, (96).

$$\{E\} = \left\{ \begin{array}{c} \frac{du}{dx} \\ \frac{dv}{dy} \\ \frac{du}{dy} + \frac{dv}{dx} \\ -z \frac{d^2w}{dx^2} \\ -z \frac{d^2w}{dy^2} \\ -2z \frac{d^2w}{dxdy} \end{array} \right\} + \left\{ \begin{array}{c} \frac{1}{2} \left(\frac{dw}{dx} \right)^2 \\ \frac{1}{2} \left(\frac{dw}{dy} \right)^2 \\ \frac{1}{2} \left(\frac{dw}{dx} \frac{dw}{dy} \right) \end{array} \right\} = \left\{ \begin{array}{c} \epsilon_{Pl}^0 \\ \epsilon_b^0 \end{array} \right\} + \left\{ \begin{array}{c} \epsilon_{Pl}^L \\ 0 \end{array} \right\} \quad (3-38)$$

in which the first term is the linear expression and the second is the non-linear components. In the above expression u , v and w stand for appropriate displacements of the middle surface.

As the behaviour is considered linear elastic, the $[D]$ matrix is composed of a plane stress and a bending component

$$[D] = \begin{bmatrix} [D^{Pl}] & 0 \\ 0 & [D^b] \end{bmatrix} \quad (3-39)$$

Finally the displacements are defined in terms of nodal parameters using the appropriate shape functions, Equ. 3.2 and 3.3.

$$\text{Thus for instance } \begin{Bmatrix} u \\ v \\ w \end{Bmatrix}^e = [N] \{d\}^e \quad (3-40)$$

where a typical set of nodal parameters is conveniently divided into those which influence in-plane and bending deformation, respectively.

$$\{d_i\} = \begin{Bmatrix} d_i^{pl} \\ d_i^b \end{Bmatrix} \quad (3.41)$$

with $\{d_i^{pl}\} = \begin{Bmatrix} u_i \\ v_i \end{Bmatrix}$ and $\{d_i^b\} = \begin{Bmatrix} w_i \\ \frac{dw}{dx_i} \\ \frac{dw}{dy_i} \end{Bmatrix}$

and i is the node number. The node possesses 5 D.O.F. to describe the deformation at the location. Thus the shape function can also be subdivided as

$$[N_i] = \begin{bmatrix} [N_i]^{pl} & 0 \\ 0 & [N_i]^b \end{bmatrix} \quad (3.42)$$

and indeed the assumption that the final assembled displacement vector is also subdivided in the same way as Equ. 3.41, will be used.

To continue the formulation it will be necessary to form expressions for $[\bar{B}]^e$ and $[K_T]^e$ From Equ. 3.16

$$[\bar{B}]^e = [B_0]^e + [B_L]^e \quad (3.43)$$

and the subdivision gives

$$[B_0]^e = \begin{bmatrix} [B_0^{pl}]^e & 0 \\ 0 & [B_0^b]^e \end{bmatrix}; [B_L]^e = \begin{bmatrix} 0 & [B_L^b]^e \\ 0 & 0 \end{bmatrix}$$

where $[B_0^{pl}]^e = [Q_0^{pl}]^e [A^{pl}]_e^{-1}$ and $[B_0^b]^e = z [Q_0^b]^e [A^b]_e^{-1}$

are the well defined, standard matrices for the linear in-plane and bending elements. $[B_L^b]^e$ is obtained by taking a variation of $\{\epsilon_{pl}^L\}^e$ with respect to the parameters $\{d^b\}^e$.

Thus the non-linear, strain components of Equ. 3.38 can be written conveniently as,

$$\{\epsilon_L^{Pl}\}^e = \frac{1}{2} \begin{bmatrix} \frac{dw}{dx} & 0 \\ 0 & \frac{dw}{dy} \\ \frac{dw}{dy} & \frac{dw}{dx} \end{bmatrix}^e \begin{Bmatrix} \frac{dw}{dx} \\ \frac{dw}{dy} \end{Bmatrix}^e = \frac{1}{2} [H]^e \{\phi\}^e \quad (3.44)$$

where the derivatives (slopes) of w can be related to the nodal parameters as,

$$\{\phi\}^e = [G]^e \{d^b\}^e \quad (3.45)$$

with

$$[G]^e = [Q_{Pl}^L]^e [A^b]_e^{-1}$$

Thus $[G]^e$ is a matrix defined purely in terms of the co-ordinates of the element. Taking the variation of Equ. 3.44.

$$\begin{aligned} d\{\epsilon_L^{Pl}\}^e &= \frac{1}{2} d[H]^e \{\phi\}^e + \frac{1}{2} [H]^e d\{\phi\}^e = [H]^e d\{\phi\}^e \\ &= [H]^e [G]^e d\{d^b\}^e \end{aligned} \quad (3.46)$$

and hence immediately by definition

$$[B_L^b]^e = [H]^e [G]^e \quad (3.47)$$

With all the necessary components the element matrix $[K_T]^e$ can be evaluated. The linear small deformation matrices are written as

$$[K_0]^e = \begin{bmatrix} [K_0^{Pl}]^e & 0 \\ 0 & [K_0^b]^e \end{bmatrix} = \begin{bmatrix} \int_V [B_0^{Pl}]^T [D^{Pl}] [B_0^{Pl}] dV & 0 \\ 0 & \int_V [B_0^b]^T [D^b] [B_0^b] dV \end{bmatrix}^e \quad (3.48)$$

From which the following expression solves the linear displacements.

$$\{R\} = \sum_e \left[[A^b]_e^{-T} \int_V [Q_0^b]^T [D^b] [Q_0^b] dV [A^b]_e^{-1} \right]^e \{d\} = [K_0^b] \{d\} \quad (3.49)$$

This is the matrix representation of Equ. 3.28 and the matrix $[K_0^b]$ is the total contribution due to all the elements.

Taking Equ. 3.24 the large element displacement matrix can be defined

on substituting Equ. 3.39 and 3.43. Thus after some manipulation,

$$[K_L]^e = \begin{bmatrix} 0 & \int_V [B_L^p]^T [D^p] [B_L^b] dV \\ \text{SYMMETRICAL} & \int_V [B_L^b]^T [D^b] [B_L^b] dV \end{bmatrix}^e \quad (3-50)$$

Finally, $[K_\sigma]^e$ has to be constructed using the definition of Equ. 3.25. From Equ. 3.16 on taking a variation

$$d[B_L]^T{}^e = \begin{bmatrix} 0 & 0 \\ d[B_L^b]^T & 0 \end{bmatrix}^e \quad (3-51)$$

the substitution into 3.25 and 4.47 gives,

$$[K_\sigma]^e d\{\delta\} = \int_V \begin{bmatrix} 0 & 0 \\ [G]^T d[H] & 0 \end{bmatrix}^e \begin{Bmatrix} \sigma_{xp|} \\ \sigma_{yp|} \\ \sigma_{xyp|} \\ \sigma_{xb} \\ \sigma_{yb} \\ \sigma_{xyb} \end{Bmatrix}^e dV \quad (3-52)$$

wherein the x -direction $\sigma_{xp|}$ is average membrane stress in the element.

By a special property of matrix manipulation, (28).

$$[K_\sigma]^e = \begin{bmatrix} 0 & 0 \\ 0 & [K_\sigma^b] \end{bmatrix}^e \quad (3-53)$$

with

$$[K_\sigma^b]^e = \int_V [G]^T{}^e \begin{bmatrix} \sigma_{xp|} & \sigma_{xyp|} \\ \sigma_{xyp|} & \sigma_{yp|} \end{bmatrix}^e [G]^e dV$$

which is the symmetrical element geometric stress plate matrix. Putting all the element stiffness matrices together the element tangential matrix is

$$[K_T]^e = \left[\begin{array}{c}
 [A^{Pl}]^T \int_V [Q_0^{Pl}]^T [D^{Pl}] [Q_0^{Pl}] dV [A^{Pl}]^{-1} \quad [A^{Pl}]^T \int_V [Q_0^{Pl}]^T [D^{Pl}] [Q_{Pl}^L] dV [H] [A^b]^{-1} \\
 \\
 [A^{Pl}]^T \int_V [Q_0^{Pl}]^T [D^{Pl}] [Q_{Pl}^L] dV [H] [A^b]^{-1} \quad [A^b]^{-1} \int_V [Q_0^b]^T [D^b] [Q_0^b] dV [A^b]^{-1} \\
 + [A^b]^{-1} [H] \int_V [Q_{Pl}^L]^T [D^b] [Q_{Pl}^L] dV [H] [A^b]^{-1} \\
 + [A^b]^{-1} \int_V [Q_{Pl}^L]^T \begin{bmatrix} \sigma_{xPl} & \sigma_{xyPl} \\ -\sigma_{xyPl} & \sigma_{yPl} \end{bmatrix} [Q_{Pl}^L] dV [A^b]^{-1}
 \end{array} \right]^T$$

It is then only a matter of correctly summing up the appropriate element stiffness terms and placing the values into the specific locations within the governing plate stiffness matrix, for a solution. After the stiffness matrix has been evaluated the boundary conditions are imposed and the nodal displacements are determined following the solution technique Equ. 3.27 - 3.34.

After the nodal displacements have been calculated at each load increment a further programme evaluates the nodal strains and stresses. The following equations define the formulation of the stress programme.

Taking the nodal displacements (D.O.F.) for each element in turn

the strains are given by Equ. 3.38, and with appropriate substitutions

$$\begin{aligned} \{\epsilon_{pl}^o\}^e &= [Q_{pl}^o] [A^{pl}]_e^{-1} \{d\}^e \\ \{\epsilon_{pl}^L\}^e &= \frac{1}{2} [H] [Q_{pl}^L] [A^b]_e^{-1} \{d\}^e \end{aligned} \quad (3.55)$$

$$\{\epsilon_b\}^e = -z [Q_b^o] [A^b]_e^{-1} \{d\}^e$$

and

$$\{\epsilon_{pl}\}^e = \{\epsilon_{pl}^o\}^e + \{\epsilon_{pl}^L\}^e$$

Stresses are then evaluated from Equ. 3.17 by taking the definition for the stiffness matrix $[D]$ Equ. 3.39

$$\begin{Bmatrix} \sigma_{pl} \\ \sigma_b \end{Bmatrix}_k^e = \begin{bmatrix} [Q^{pl}] & 0 \\ 0 & [Q^b] \end{bmatrix}_k^e \begin{Bmatrix} \epsilon_{pl} \\ \epsilon_b \end{Bmatrix}_k^e \quad (3.56)$$

For nodes surrounded by several elements the strains and stresses at that node are determined by that number of elements. To calculate a representative value the average was determined.

3.3 LINEAR COMPARISON

The modelling ability of the linear finite element analysis ACM will now be compared against several analytical solutions and further finite element approximations. The various mesh constructions used are presented in Table 3.1. Plate symmetry in the isotropic and orthotropic examples meant that an accurate model was obtained with only a quarter plate mesh, and Fig. 3.81 shows a typical mesh construction.

Results for displacements and stresses are studied for isotropic, orthotropic and laminated examples. Where possible all the values are presented normalised. The exception being the stresses for problems with a central point load. When uniform loading is being considered the load vector can either be constructed as vertical loads only (V.L.O.) or as a consistent nature (C.L.V.) (28).

3.3.1 Isotropic examples - ACM - With Several Other Rectangular And Triangular Elements

The ability of six elements to provide convergent results to the exact solutions of three thin plate bending problems are now examined. The elements comprise three rectangular (including ACM) and three triangular. Table 3.2 gives the definitions for the type of element approximation and the procedure to a solution. Also given are the important factors which should be taken into consideration if any of the elements were to be chosen for a non-linear analysis. It must be remembered that if a non-linear analysis was considered there must exist an in-plane element compatible with the bending element.

All elements, except SM, have been employed in programmes applying classical thin plate theory. SM has been built in an analysis based on the shear deformation theory of Mindlin.

Exact solutions for the central displacement in the three examples have been reported by Timoshenko (18). In addition he presented the value for the central stresses in the uniform loaded examples. In the case of a point load the theoretical stress is infinite due to a singularity, so no exact solution is available.

Figures 3.3 and 3.4 present the non-dimensional central displacement α , β or stress $\bar{\sigma}$ for the six elements, against the total number of D.O.F. The number of D.O.F. modelling one quarter of the plate being given on a Logarithmic scale. Table 3.1 defines the square meshes and Figure 3.8.2 shows the boundary conditions imposed. The test cases were:

Fig 3.3 Square simply supported isotropic plate with a uniform distributed load (V.L.O.)

Fig 3.3.1 α is the non-dimensional central displacement

$$\alpha = \frac{w_c D}{q A^2} \quad (3.57)$$

with $D = \frac{E h^3}{(1 - \nu^2)}$

and

Fig 3.3.2 $\bar{\sigma}$ is the non-dimensional central stress.

$$\bar{\sigma} = \frac{\sigma_c}{q} \quad q = \frac{P}{A^2} \quad (3.58)$$

The value for the central stress σ_c (i.e. σ_x since by symmetry $\sigma_x = \sigma_y$) was taken to be that experienced on the tensile surface.

Fig 3.4.1 Square simply supported isotropic plate, with a concentrated central load.

Fig. 3.4.2 Square clamped isotropic plate, with a concentrated central load.

β is the non-dimensional central displacement

$$\beta = \frac{w_c D}{P A^4} \quad (3.59)$$

The exact values attributed to Timoshenko are presented as solid straight lines on the figures.

Referring to the figures the following observations were made.

For the three problems the element ACM is found to converge to the exact solution as long as sufficient elements, ≥ 36 , are applied. The errors are in the order of 1% and the trends suggest that the exact values will be reached. The largest errors are found for the point load examples, which are known to impose severe limitations on the accuracy of the displacement method (28).

Compared with the results of the equivalent triangular element T, ACM is seen to be far superior. Accuracy of the same order was established when modifications were made to T, but there is no advantage since the element HCT needs a more involved procedure for solution than ACM.

Accuracy is improved with sparse meshes when the elements were more refined with ACM. Elements S, SM and B are compatible, require numerical integration for evaluation of stiffness matrices and possess 24, 24 and 18 D.O.F./element respectively. The latter element B is triangular which obviously requires two elements to produce a rectangular element, and hence the equivalent number of D.O.F. is 24. Hence for the improvement in modelling the stiffness matrix is larger than with element

ACM. This would be detrimental to an analysis since computing time is approximately proportional to the square of the size of the governing stiffness matrix. It has previously been stated that a model of the plate bending method requires at least 36 elements (with this number of element accuracy is comparable), and so none of the more refined elements appear practical for the non-linear analysis.

3.3.2 Isotropic Examples Approximating to the Experiment; ACM.

Examined now are two isotropic examples to observe the modelling ability of the element ACM for more stringent problems approximating to the experiment. It has already been mentioned that point loads provide a severe limitation on accuracy, and was one of the reasons for the choice of a patch loading in the experiment. However, the reactions are taken through four symmetrical located point supports, since this prevents lift off. It is possible that these point supports will contribute to limiting the accuracy of the numerical analysis. This will now be investigated using the examples.

An identical procedure to the previous subsection was followed. Where possible approximate known solutions are given. Both test cases have a uniform pressure loading so a nondimensional expression can be used.

$$\alpha = \frac{w_c D}{q A^4} \quad \text{with} \quad D = \frac{E h^3}{12(1-\nu^2)} \quad (3.60)$$

and
$$\sigma = \frac{\sigma_c}{q}$$

with $q = \frac{P}{A_p \times B_p}$ for the patch loading. P is the total load.

The first example was a square thin isotropic plate with corner supports and a uniformly distributed load, (V.L.O.), Fig. 3.5. Approximate analytical solutions for the problem were separately presented by Marcus (97) and Lee and Ballesteros (98). These have been shown as solid straight lines on the diagrams.

In Fig. 3.5.1 the results for α using ACM are about 13% on the

analytical low side, and do not approach the average of the two analytical values as the meshes become finer, (6SQU and 7SQU). Central stress $\bar{\sigma}$, Fig. 3.5.2, results are all within 4% of the analytical and the trend suggests that the final value will be on the high side. A very reasonable agreement for both displacement and stresses has been obtained if account is taken of the nature of the approximate formulation and that the corner supports will cause numerical difficulties.

To involve nearly all the experimental parameter and at the same time have an analytical solution, the second case was a square thin isotropic plate with corner supports and a central square patch load (V.L.O.). The results are given in Fig. 3.6 for a patch area having sides 0.1 of the respective plate sides. Unfortunately there is no exact solution to the central displacement, but Marcus (97) reported an approximate value for the central stress.

When modelling this example it was possible to employ a different number of elements in the patch loading while maintaining the same number of elements in the mesh. In the investigation one mesh had 4 nodes, (3SQG(A)) and one had 9 nodes, (3SQG(B)) for the loading, with the same number of D.O.F.

Fig. 3.6 shows that for all meshes with more D.O.F. than mesh 1SQG the central displacement α and stress $\bar{\sigma}$ deviate by no more than 5%. It can also be observed that the two numerical trends due to the different patch models do not suggest identical final results. Fortunately, the central stress calculated by all models is within 3% of the analysis which is certainly acceptable.

The two examples demonstrate that element ACM is a suitable choice for modelling the experiment with further improvement expected once the point supports are no longer at the corners.

3.3.3. Orthotropic Example - ACM - PAFEC 75.

Available on the IBM 370/167 NUMAC system is a general finite element package known as PAFEC 75. Since one of its options can solve generally orthotropic laminated thin plates (no shear deformation) it was appropriate to compare with ACM.

3.3.3.1. Test Example

A numerical comparison was performed using a square, simply supported, four layered orthotropic cross-ply plate with a central concentrated load, Fig. 3.7.1. Fig. 3.7.2 shows the symmetrical lamination configuration ($0^\circ, 90^\circ, 90^\circ, 0^\circ$) of the laminate.

It was possible for this example to derive analytical values for transverse displacements and stresses, (except for the stresses at the centre). The actual calculations are presented since the stresses for point load problems cannot be non-dimensionalised.

The material properties chosen are those for the carbon fibre/epoxy resin combination T300/Code 69.

Fig. 3.7.1 defines the test parameters and symbols

$$A = 0.2 \text{ m}$$

$$P = 500 \text{ N}$$

$$t = 0.508 \text{ E-03 m}$$

$$h_2 = 2h_1 = 2t$$

$$E_{11} = 0.1351 \text{ E+12 N/m}^2$$

$$E_{22} = 0.1096 \text{ E+11 N/m}^2$$

$$G_{12} = 0.5771 \text{ E+10 N/m}^2$$

$$\nu_{12} = 0.3$$

3.3.3.2. Analytical Solution

The standard solution to the governing equation for the deflection (3) of an orthotropic, cross-ply, square thin plate, simply supported along all its free edges, and vertically loaded only, is given in the form of a Fourier series by Lekhnitskii (99)

$$w(x,y) = \frac{A^4}{\pi^4} \sum_{m=1}^{\infty} \sum_{n=1}^{\infty} a_{mn} \frac{\sin \frac{m\pi x}{A}}{A} \frac{\sin \frac{n\pi y}{A}}{A} \frac{1}{D_{11}m^4 + 2(D_{12} + 2D_{66})m^2n^2 + D_{22}n^4} \quad (3-61)$$

where a_{mn} for a single point load is

$$a_{mn} = \frac{4P}{A^2} \frac{\sin \frac{m\pi \eta}{A}}{A} \frac{\sin \frac{n\pi \xi}{A}}{A} \quad (3-62)$$

and

$$D_{ij} = \frac{2}{3} \sum_{k=1}^{nl} \bar{Q}_{ij}^0 (h_{(k)}^3 - h_{(k-1)}^3)$$

\bar{Q}_{ij}^0 are the transformed stiffnesses

nl the number of layers in half the plate, and

h_{k^s} are the distances of the under surface of the k^{th} lamina from the mid-plane.

For the example under consideration there is a single central point load, i.e. $\eta = \xi = \frac{A}{2}$, Fig. 3.7.1, and the solution for the displacements in the problem becomes

$$w(x,y) = \frac{4PA^4}{\pi^4} \sum_{m=1}^{\infty} \sum_{n=1}^{\infty} \frac{\sin \frac{m\pi x}{A} \sin \frac{n\pi y}{A} \sin \frac{m\pi x}{A} \sin \frac{n\pi y}{A}}{D_{11}m^4 + 2(D_{12} + 2D_{66})m^2n^2 + D_{22}n^4} \quad (3-63)$$

i.e.

$$w(x,y) = \frac{4PA^4}{\pi^4} K_w$$

where K_w is the summation expression. A FORTRAN programme was developed to determine K_w at any position on the plate, with relevant combination of values for D_{11}, D_{12}, D_{66} and D_{22} . It was found that the value for K_w converged rapidly with increasing number of summations, a very accurate result being obtained with all the terms up to $m=n=1,2,3$ (odd) ie 144.

The stresses in each layer are given by the expressions

$$\begin{aligned} \sigma_x(x,y) &= +z Q_{ij}^{\theta} \left[\frac{d^2 w}{dx^2} + \nu_{21} \frac{d^2 w}{dy^2} \right] \\ \sigma_y(x,y) &= +z Q_{ij}^{\theta} \left[\frac{d^2 w}{dy^2} + \nu_{12} \frac{d^2 w}{dx^2} \right] \end{aligned} \quad (3.64)$$

where z is the distance from the mid-plane to the plane of stress calculation, (Kirchoff's assumption and displacement functions, Equ. 3.1) in the lamina with the orientation θ° .

From the Fourier solution of the displacements, Equ. 3.63 ,

$$\begin{aligned} \frac{d^2 w}{dx^2} &= \frac{-4P}{\pi^2} \sum_{m=1}^{\infty} \sum_{n=1}^{\infty} \frac{m^2}{n^2} \text{ or } \frac{\sin \frac{m\pi x}{A} \sin \frac{n\pi y}{A} \sin \frac{m\pi x}{A} \sin \frac{n\pi y}{A}}{D_{11}m^4 + 2(D_{12} + 2D_{66})m^2n^2 + D_{22}n^4} \end{aligned} \quad (3.65)$$

substituting these expressions into the bracket terms of the stress equations produce two more summations.

$$K_x = \frac{d^2 w}{dx^2} + \nu_{21} \frac{d^2 w}{dy^2} \quad \text{and} \quad (3.66)$$

$$K_y = \frac{d^2 w}{dy^2} + \nu_{12} \frac{d^2 w}{dx^2}$$

A further programme was constructed to calculate K_x and K_y . The

convergence of K_x and K_y was much slower than K_w and for locations other than the centre, terms up to $M=N=1,201$ (odd), 40000 were required. At the centre, where the stress is theoretically infinite, the summations did not converge and so for a comparison, values with $M=N=1,801$ (odd), 64000 were taken.

3.3.3.3. Finite Element Modelling

The two finite element programmes were run to predict the bending displacements and stresses for the orthotropic example. Initially the comparison was made with the 49 element graded mesh, 3SQG(A)(Fig. 3.8.1.), using ACM and the PAFEC 75 isoparametric Lagrangian 4 node (44205) element. Programme ACM is a pure small displacement bending analysis, whereas PAFEC 75 includes in-plane components, but not coupled for symmetrical laminates. To improve accuracy with ACM a 100 element mesh, 5SQG, was also studied, and, because of its wide options, an 8 (44215) and a 12 noded (44220) element, with the 49 element mesh in PAFEC 75. These latter two elements possess mid-side nodes and so have refined displacement functions to define their deformation behaviour. The refinement should mean improved accuracy.

3.3.3.4. Results

A selection of typical nodal values, displacements (Table 3.3), and stresses (Table 3.4) for the following models are given.

- (i) ACM - 49 element mesh
- (ii) ACM - 100 element mesh
- (iii) PAFEC 75 - 4 noded, 49 element mesh

(iv) PAFEC 75 - 8 noded, 49 element mesh
with relevant analytical values.

The 49 element mesh as displayed in Fig. 3.8.1 marks the nodal positions used in the comparison. Boundary conditions for the ACM models are shown in Fig. 3.8.2(A) and for the PAFEC 75 models in Fig. 3.8.2(B).

The analytical values for stresses were made along the mid-plane of the outer lamina (0°) under tension, Fig. 3.7.2. The stresses have been presented as an average of the values determined from the elements surrounding the node under consideration, together with the percentage variation between the highest and lowest of these values. The latter was not necessary for the models using ACM since the calculated difference in stresses were never more than $\pm 1\%$.

From the results presented the following observations were made: Table 3.3 demonstrates that the models with ACM provided deflections to within 1% of those determined analytically. Whereas, those deflections evaluated by PAFEC 75 exceed the analytical by 20% , in the case of the 4 noded element, and 6% for the 8 noded element, with all other parameters identical to those applied in the ACM models.

The evaluation of stresses derived from the nodal displacements and rotations are found to have larger deviations from the approximate analytical values than was anticipated. PAFEC 75 gives comparable results to ACM when the 8 noded element was used, but then, like its 4 noded element, the variation in the stress calculated by the surrounding elements is large. Results from PAFEC 75 with the 8 noded element should

have been more accurate than ACM because the displacement function is more refined. In fact the two models gave same order of accuracy. For all models the greatest errors are encountered in the vicinity of the point load. It is known that point loadings do induce a singularity so this observation was to be expected.

The computing time (C.P.U.) for the various models are shown in Table 3.5. It is immediately obvious that the time taken for a similar problem with PAFEC 75 far exceeds that of ACM.

The time difference between ACM and PAFEC 75 is partly due to increase in the total number of D.O.F. with PAFEC 75, but mostly because of the excessive amount of housekeeping in this programme. From the comparisons it appears reasonable to utilise ACM in favour of the more elaborate PAFEC 75 for the work undertaken here.

3.3.4. Laminated Plates - ACM.

Up to now examples concerned with isotropic and orthotropic plates have all been shown to be modelled accurately with element ACM. Results were however required for laminated plates, which may contain some fraction of plies orientated at θ° to the global axes. These plates are referred to as generally orthotropic laminates. In these laminates the twisting stiffness D_{12} and D_{26} (3) are non-zero for the orientated plies, providing θ° is not 0° or 90° . Plates which were investigated in this work consist of laminae at the four orientations 0° , $+45^{\circ}$, -45° and 90° , being multilayered and arranged symmetrically. As an example of the type of lay-up, an eight layered quasi-isotropic

laminate could have the construction $(0^\circ; +45^\circ; 90^\circ; -45^\circ; 45^\circ; 90^\circ; +45^\circ; 0^\circ)$.

If these generally symmetric orthotropic laminated plates are placed into pure bending the coupling stiffnesses induce warping into the response. Fortunately the behaviour is not further complicated since, if the lay-up is symmetrical, there will be no coupling between the bending and stretching components. The extent of the warping will depend on the relative magnitude of the plate coupling stiffnesses (D_{16}, D_{26}) to the principal stiffnesses (D_{11}, D_{22}, D_{12}). A test example will display that if the twisting is prevented, by imposing non-existent moments through incorrectly fixing nodal D.O.F., then very large discrepancies between what appear similar models will be found. Noor et al (49) are the only researchers who have examined symmetry in laminated plates with the view of reducing the size of the finite element model. Their finite element package allowed for more complex boundary conditions than ACM thus reducing the size of meshes but increasing the complexity of the programme.

Results from previous work were first necessary to demonstrate the modelling ability of the element ACM for generally symmetrical orthotropic laminates. Unfortunately, it has been difficult to uncover appropriate examples. In fact, no plots displaying convergence, like those discussed in 3.4.1 and 3.4.2 are available.

The only example discovered that can be applied to evaluate ACM was presented by Webber (100). He firstly measured the transverse displacements for a four layered symmetrical angle-ply $(+45^\circ; -45^\circ)_s$ rectangular cantilever with a concentrated load on the free edge. Then

he achieved an excellent agreement with a finite element analysis using element ACM, so it only remained a matter of producing an exact correlation with Webber to show that the linear programme was operating correctly. The mesh utilised by Webber, 1RFU is shown in Fig. 3.9.1. It has 16 uniformly sized rectangular elements, and a total of 75 D.O.F (25 nodes). Nodes 1-5 were clamped, the remainder being free. Given are all dimensions, material properties, the lay-up and the magnitude of the point load. All units have been changed from Imperial to Metric to be consistent with the rest of the work. Fig. 3.9.2 shows the displacements for nodes 11-25 from ACM and the corresponding experimental measurements when a concentrated load had been applied at node 25. Together with Webber the fit is very good, especially when experimental and numerical errors are taken into account. This example confirms that our linear programme is identical to Webber's. Webber did not extend the analysis to involve stresses and did no work concerning improvement in accuracy by refining the mesh, so further comparisons were not possible.

Attention now returns to the problem of imposing correct boundary condition when representing laminated plates. Four distinct models of the plate are feasible with programme ACM and Fig. 3.10 shows these models for the plate bending experiment. Due to symmetry the perpendicular rotations along the quarter plate boundaries are zero for isotropic and orthotropic plates, Section 3.3.1-3, so a quarter plate mesh was sufficient to represent the whole structure. But in the case of generally orthotropic laminates the twisting D_{16} and D_{26} induce warping into the response which shifts the location of zero perpendicular rotation away from the quarter plate boundaries.

In Sections 3.1 and 3.0, when discussing the limiting factors for the success of the non-linear analysis, it was explained that a minimum number of elements was necessary because of the restrictions imposed on storage space and central processing time. Therefore, some knowledge of the effect of twisting on the results for the various meshes will be of interest, since it might be shown that a laminate containing a large proportion of $\pm 45^\circ$ plies will only be correctly modelled with a full plate, Fig. 3.10.4. If this is the case then the mesh will have four times the number of elements as the equivalent quarter plate model and the overall size of the stiffness matrix will be much greater. Simply, if it is demonstrated that a full plate model is the only correct representation, a non-linear analysis is impractical on the NUMAC system.

To demonstrate the limitations on modelling due to warping, the following severe case was examined. A pure $+45^\circ$ square laminated plate, arranged as in the plate bending experiment, was represented by the four meshes. All parameters are presented in Table 3.6 together with the central displacements and strains (as determined on the tensile surface) from each model. Fig. 3.10.5 illustrates the shift in position of the perpendicular zero rotations away from the quarter plate boundaries as determined with mesh 1SFGE114.

For this problem the unrestrained full plate model is the only correct representation. A tremendous difference in the values of central displacement and strains is found between the four mesh types. As an example, the imposition of quarter plate boundary conditions on the full plate mesh produces a reduction of $\approx 12\%$ in the central displacement, and over 350% in the central strain.

By taking the ply orientation as $+45^\circ$ or -45° in the programme no resultant effect on the results with the full and half plate models is obtained. However, considerable difference is found with the quarter plate model.

Fig. 3.10.5 illustrates that the shift of the zero perpendicular rotations away from quarter plate boundaries is large. The maximum distance for the example is $\cdot 025M(x')$. The shift reduces as the observer proceeds from the free edge to the centre, where it becomes zero.

The above points indicate that there is a severe restriction on employing quarter or half plate meshes when plates are generally orthotropic, depending on the lamination configuration. Examining the pure $+45^\circ$ laminate was the worse case, so the extent to which commercial laminates are affected will be less.

A measure of the degree of the twisting contribution in general orthotropic laminates can be gained through the size of the ratios D_{11}/D_{16} and D_{22}/D_{26} . For the example just studied $D_{11} = D_{22}$ and the ratios equal 1.17 (being the minimum for the lamina material properties). By calculating the values of D_{11}/D_{16} and D_{22}/D_{26} for a laminate ratios higher than the minimum might indicate that all meshes will model the problem. Later the ratios for the plates tested will be given and used to try and give a rough guide line to when all mesh types are acceptable. If all models are found to be accurate with certain D_{11}/D_{16} and D_{22}/D_{26} ratios, then providing the material properties remain the same calculating the ratios for further laminations will indicate if the warping can be ignored or not.

3.4 NON-LINEAR (ACMBC) - COMPARISON

There now follows a similar investigation on the non-linear thin plate bending programme ACMBC as was performed with ACM. Of special interest is the procedure in ACMBC by which it was made possible to evaluate all the stiffness terms explicitly, through the new definition of the rotations in matrix $[H]^e$, Equ. 3.44. To date, all previous non-linear analyses have defined the two rotation terms with the bending displacement function, in either a truncated form, Gallagher et al (101), Bergan and Clough (70), or more usually in its full form (29,68). With this procedure the explicit formulation of the element non-linear stiffness matrices were impractical and required numerical integration schemes.

For this work the two terms $\frac{dW}{dx_e}$ and $\frac{dW}{dy_e}$ in matrix $[H]^e$ have been thought of as the respective average rotations in the element (at the present deformation) in the X and Y global directions. New definitions have been given to the rotation terms enabling all the stiffness terms to be determined explicitly. Two expressions defining the terms have been formulated which, when incorporated into the programme, give only 1% variation in results.

Taking the basic element as defined in Fig. 3.1, the first equalities are:

$$\frac{dW}{dx_e} = \frac{1}{4} \sum_{i=1}^4 \frac{dW}{dx_{ie}} \qquad \frac{dW}{dy_e} = \frac{1}{4} \sum_{i=1}^4 \frac{dW}{dy_{ie}} \qquad (667)$$

where i is the nodal position and $\frac{dW}{dx_{ie}}$ is the rotation in the X-direction at the nodal position i , in element e .

Mathematically the above is not very sound, so the terms have also been defined as the weighted means over the area of the element.

$$\frac{dw}{dx_e} = \frac{1}{a \times b} \int_0^a \int_0^b \frac{dw}{dx} dx dy \quad (6.68)$$

$$\frac{dw}{dy_e} = \frac{1}{a \times b} \int_0^a \int_0^b \frac{dw}{dy} dx dy$$

where $\frac{dw}{dx}$ $\frac{dw}{dy}$ are given in terms of the bending displacement function and the present element D.O.F, $\{d\}_e$. The above simplifies to the following matrix notation

$$\frac{dw}{dx_e} = \left[Q \frac{dw}{dx} \right] \{d\}_e [A^b]^{-1} \quad (6.69)$$

$$\frac{dw}{dy_e} = \left[Q \frac{dw}{dy} \right] \{d\}_e [A^b]^{-1}$$

Since only a small difference was found between the two sets of definitions the latter were chosen, because they are mathematically more sound.

The modelling ability of ACMBC was studied with two simple isotropic examples. The plate was square with uniform (C.L.V.) loading and the bending boundary conditions were either all edges simply supported or clamped. The inplane boundary conditions could also take two forms, but only Levy's (51) restraints were treated. In this case, the parallel nodal inplane displacement to the direction of the edges are free, whilst the corresponding perpendicular D.O.F. to the edges are fixed. Wang (52) is attributed with the second type, where all the inplane D.O.F. along the edges are fixed. These latter boundary conditions make the non-linear behaviour stiffer than Levy's and the size of the central transverse displacement is lower.

Analytical solutions were readily available for the examples. The results given by Levy (who solved Von-Karman's equations using a double Fourier series) have been quoted as having a possible error of less than 2%.

All results will be presented normalised and for clarity the following parameters in ACMBC are given.

Load increment \bar{q} and the number of iteration steps to convergence at each load increment.

The value of β Equ. 3.4, which was used to establish the next displacement set in the Newton-Raphson iterative procedure.

The value taken for the reference errors $|\epsilon|$ used to determine convergence with Equ. 3.5. It can be noted that for ACMBC the inplane $|\epsilon|_{pl}$, the rotational $|\epsilon|_{rot}$ and transverse displacement $|\epsilon|_w$ terms have been defined separately. $|\epsilon|_w$ was taken to be the smallest, followed by $|\epsilon|_{rot}$ and lastly $|\epsilon|_{pl}$. The reason for this was that a small change in $|\epsilon|_{pl}$ caused a greater change in the number of iterations than if $|\epsilon|_w$ or $|\epsilon|_{rot}$ were changed, with no consequential improvement in accuracy.

3.4.1. Isotropic Examples - ACMBC

The two examples which were modelled are:

A square simply supported isotropic plate, Levy's in-plane restraints, uniform pressure load (C.L.V.), and

A square clamped supported isotropic plate, Levy's inplane restraints, uniform pressure load (C.L.V.), (which in this case was equivalent to the V.L.O.).

A study was made in the flexural response as the pressure increased in increments. Results for the central transverse displacement, central surface tensile stresses (bending and inplane) and mid-side edge surface stresses have been noted. The two cases were modelled with the quarter plate mesh 4SQU which has 16 elements (125 D.O.F.), being the standard mesh with all previous finite element analyses. To possibly improve accuracy a refiner mesh 6SQU containing 36 elements (245 D.O.F.) was used for the simply supported example.

The normalised values are:

$$\text{transverse displacement} \quad \bar{w} = \frac{w}{h} \quad (370)$$

$$\text{surface stress} \quad \bar{\sigma} = \frac{\sigma A^2}{E h^2}$$

which were evaluated at the load increments given by the load factor

$$\bar{q} = \frac{q A^4}{E h^4}$$

N.B. Results from the finite element work of Brebbia and Connor (29)

Thomas and Gallagher (71), plus the analytical analysis of Berger (53) were given for the load factor

$$D \quad \bar{q} = \frac{q A^4}{E h} \quad \text{where} \quad D = \frac{E h^3}{12(1-\nu^2)} \quad (371)$$

and A is half the plate length.

This means that there is a load factor difference of 1.48 between ACMBC and these analyses.

In both examples the following parameters were applied:

$$\beta = 0.5$$

$$|\epsilon|_{pl} = 0.05$$

$$|\epsilon|_{rot} = 0.025$$

$$|\epsilon|_w = 0.01$$

Convergence was only accepted once all the appropriate displacements provided error quantities lower than those stated above.

Table 3.7 gives the load increments \bar{q} , the number of iterations at each load level and the total C.P.U. time for the solution.

Numerical trends with ACMBC are displayed as dotted lines in Fig. 3.11 and 3.12. The solid lines show the analytical solutions of Levy (51). Table 3.8 summarises the values which were available for the comparison. The subscripts are:

$$\begin{aligned} B &= \text{bending} & pl &= \text{inplane} \\ x &= X\text{-direction} & y &= Y\text{-direction} \end{aligned}$$

The locations A to D are shown in Fig. 3.13.1 together with the boundary conditions.

To compare with further finite element procedures the percentage errors at the load factor $\bar{q} = 200$ have been presented for the simply supported and clamped examples in Table 3.9 and 3.10, respectively.

Percentage errors were determined by:

$$\frac{\text{Analytical value} - \text{Finite element value}}{\text{Analytical value}} \times 100\%$$

The subscript (L) means that the value was lower than the analytical and (H) higher.

The following observations were made:

ACMBC gives similar characteristics for both simple isotropic examples as illustrated in Fig. 3.11, 3.12 and Table 3.9, 3.10.

The value of \bar{w}_0 is always less than the corresponding analytical and the deviation increased with load, Fig. 3.11.1, 3.12.1.

The values for the extreme tensile surface stress at the centre,

$\bar{\sigma}_{Dx} = \bar{\sigma}_{RDx} + \bar{\sigma}_{BDx}$ and at the mid-side of the edges $\bar{\sigma}_{Cx}$ are within 1% of the analytical, Fig. 3.11.2, 3.12.2.

The inplane stress at the centre, $\bar{\sigma}_{RDx}$ is always greater than the analytical, Fig. 3.11.3, 3.12.3, and vice versa for the bending component,

$\bar{\sigma}_{BDx}$ Fig. 3.11.4, 3.12.4. Again, as the load increases so does the error.

The inplane stresses at the mid-side nodes for the simply supported case, Fig. 3.11.3, are found to be much lower than the analytical.

The warping stress in the corner $\bar{\sigma}_{B Axy}$ Fig. 3.11.4, is below its analytical for $q < 120$, above which it diverges away at greater value.

Comparing ACMBC with the selection of results from other analyses, Table 3.9 and 3.10, it can be seen that the new analysis is the most inaccurate. The greatest difference from the analytical are found with the 4 noded element meshes. A large reduction in the error is obtained with higher order elements, but at a much higher computing cost.

The major cost is the inversion needed to solve the finite element equilibrium equations. It is known that the time to perform the inversion approximates to the square of the tangential stiffness matrix size. Hence, assuming all the D.O.F. were required the ratio of time needed for the various elements with mesh 4SQU were:

4 node ACMBC	8 node (Serendipity)	9 node (Lagrangian)
1	6.76	11.53

Few publications gave the total C.P.U. time, and even when reported the computers were different so a comparison was not practical.

It has also not been possible to establish if any of the other analyses provide the correct stress distribution. Only Bergan and Clough (70) separated $\bar{\sigma}_x$ into its components, but did not report them. Looking at the results with the refined elements, it does not look likely that the components $\bar{\sigma}_x^{Dx}$ and $\bar{\sigma}_x^{Dy}$ behaved as observed with ACMBC, since \bar{w}_b and $\bar{\sigma}_x^{Dx}$ are near to the analytical.

The results have demonstrated that the non-linear finite element formulation applied in ACMBC does not represent the response of isotropic plates. However, the Principle of Minimum Potential Energy may still hold since the total stress is correct. It is therefore probable that, throughout the plate, the true stress exists but that the distribution between the components is wrong. Values from ACMBC suggest that the bending component is too stiff relative to the inplane component at the centre, and that the situation reverses near the free edges. This implies that the overall deformation for the examples determined by ACMBC is as shown in Fig. 3.13.2. The true deformation is shown as a solid line.

The results also indicate that reasonable accuracy will only be achieved with the high order elements. This means that a 4 x 4 element model contains a lot of D.O.F., and for a precise comparison an equivalent number of D.O.F. should have been used. ACMBC displays little improvement when the finer mesh was applied, (65QU 36 elements, 245 D.O.F.). Brebbia

and Connor (29), Bergen and Clough (70) and Reddy and Chao (74) did not examine further meshes so the difference between the two orders of elements on similar terms could not be ascertained.

Obviously, the computing effort with 8 and 9 noded element meshes was much higher than for 4 noded element meshes. Since it takes >50 C.P.U.s for ACMBC to solve the simply supported example, the time with high order elements must have been enormous. If accurate results can only be obtained with high order elements, computing restrictions will ensure that only simple problems can be solved. This may mean that it will be extremely difficult to use a finite element geometric non-linear procedure to model the plate bending experiment.

3.4.2. Isotropic Examples - Modifying ACMBC

To proceed with the investigation the work of Brebbia and Connor (29) (who used element ACMBC) will be involved. They reported \bar{w}_D for the clamped example, which was always greater than the analytical. The difference between ACMBC and their analysis is very large, and at $\bar{q} = 200$ is $\approx 23\%$ of the analytical, Table 3.10. Now the most drastic change between the two procedures was through the definition of the rotation terms in $[H]^e$, (cf $[w]^*$, Brebbia and Connor). Therefore this area of the analysis must be the most likely source for the differences.

The choice of $\frac{dw}{dx_e}$ and $\frac{dw}{dy_e}$ in ACMBC were only approximate and it will be reasonable to employ any fraction of these values in the programme. Fig. 3.14 displays the change in the trends for the simply supported example observed by equally altering $\frac{dw}{dx_e}$ and $\frac{dw}{dy_e}$ between

$\frac{3}{4}$ and $\frac{5}{6}$ of that given by Equ. 6.69.

At each load increment, the values have been marked and an arrowed line shows the change as the scale factor increased. Comparing with Fig. 3.11 shows the changes from the basic analysis. From the results in Fig. 3.14 the following observations were made.

By decreasing the size of the rotation terms for all elements in the evaluation of the stiffness matrices the ensuing displacements and stresses are increased. This increase grows with load, showing that the plate is now less stiff than calculated with the initial ACMBC. The extent to which the values increase is dependent on the location in the plate, compare $\bar{\sigma}_{pLDx}$ with $\bar{\sigma}_{pLCx}$ in Fig. 3.14.3.

The value of $\bar{\sigma}_{Dx}$, which was originally within 1% of the analytical now diverges away on the high side, being a result of the increase in both σ_{pLDx} and σ_{pLDx} .

Accurate modelling has not been attained by just altering the two rotation terms equally and, in the case of $\bar{\sigma}_{Dx}$, $\bar{\sigma}_{pLCx}$ and $\bar{\sigma}_{pLDx}$ the reduction makes matters worse. It is therefore proposed that two further approaches may result in acceptable modelling.

Instead of reducing $\frac{dw}{dx_e}$ and $\frac{dw}{dy_e}$ by equal amounts on each iteration, a variation over the mesh (i.e. from element to element) may produce the correct flexural response. To accomplish this a lengthy trial and error technique would be needed and time has prevented this.

Altering the two rotation terms has emphasized the original deformation behaviour, that the combination of the bending and in-plane stiffnesses are not in the correct ratio for an accurate model. In all examples, the magnitude of $\bar{\sigma}_{pDx}$ has always exceeded its analytical, while $\bar{\sigma}_{bDx}$ has always been below. Therefore, if either of the linear stiffness coefficients are scaled, a correction to the mismatch might be made.

Fig. 3.15 displays the effect on the simply supported example due to increasing the linear inplane stiffness coefficients by a factor from 1.3 to 1.5.

From the results in Fig. 3.15 the following observations were made.

The overall effect on the results is smaller than that due to changing the rotation terms in $[H]^e$. In fact, for both \bar{w} and $\bar{\sigma}_{Dx}$ the changes were not easily recorded.

Of most relevance is that the value of $\bar{\sigma}_{Dx}$ is below the analytical and that the difference increases with load. This occurs because $\bar{\sigma}_{pDx}$ has greatly decreased (c.f. 3.15.3 with 3.11.3) and $\bar{\sigma}_{bDx}$ has only slightly increased (c.f. 3.15.4 with 3.11.4).

Obviously the results show that an accurate model will never be achieved by just altering the size of the linear inplane stiffness coefficients.

However, the combination of particular non-linear responses due to lowering the rotation terms and increasing the inplane stiffness terms

does suggest that a good model will result. By application of a trial and error procedure a good model was obtained when $\frac{dW}{dx_e}$ and $\frac{dW}{dy_e}$ were scaled by $\frac{3}{4}$ and the inplane stiffnesses were scaled by 1.3. Fig. 3.16 and 3.17 illustrate the improvement for the two isotropic examples. Comparing with the results presented in Table 3.9 and 3.10, at $\bar{q}=200$ it can be seen that a similar level of accuracy has now been obtained to that with the high order elements.

The new model does pose certain questions which should be answered. Does the two scale factors in the modified ACMBC make the formulation mathematically incorrect?

To start with there was nothing wrong in altering the values of $\frac{dW}{dx_e}$ and $\frac{dW}{dy_e}$ since the original definitions are known to be approximate. However, the original definitions, Equ. 6.69, could be misleading and the only correct definition for the terms will be when the full (or truncated) bending displacement is employed in $[H]^e$.

Increasing the inplane stiffness would appear to destroy the consistent formulation of the analysis. It may have been better to have introduced a reduction in the integration of the linear bending stiffnesses as has been used elsewhere.

Does the two scale factors giving the good models here remain constant for all types of problems, especially when the plates are thin generally symmetrical orthotropic laminates?

This question could not be assessed, since of the three available

laminate analyses which provide results no generally symmetrical orthotropic laminated thin plate examples were reported. Chang and Sawamiphakdi (86) only studied a single cross-ply problem, while both Reddy et al. (74) and Noor et al. (73) favoured cross-ply and antisymmetrical problems.

Noor did study two quasi-isotropic laminates but was concerned with shear deformation in thick specimens and so omitted a thin plate analysis. Because of the lack of suitable test cases to establish if the scale factors were universal or not, further development of ACMBC was halted.

CHAPTER 4 EXPERIMENTS

4.0 Introduction

Having proposed a new technique for evaluating the behaviour of carbon fibre reinforced plastic plates under biaxial stresses, several preliminary experiments were necessary to determine whether the test would provide relevant data. If relevant, the information will enable researchers to analyse the complicated modes of composite failure, and provide biaxial strength data.

The aim of the experiments was to verify (or otherwise) the four criteria as laid down in Chapter 1. Since no similar experiments have been performed elsewhere, certain parameters were unavailable before the tests. These included the extent of deformation, the position of the supports on the plates at failure, the maximum load and strains, and the mechanism of failure. Hence collectively, the experiments presented here are just fact finding for the future refinement of the plate bending method. Discussion of the small displacement measurements will be made in Chapter 5 where a thorough numerical comparison will help to establish the limits of criteria (a) and (d).

4.1 Specimens For The Plate Bending Experiment

The specimens tested were multilayered generally symmetrical orthotropic laminated composite thin plates. They consisted of 16 or more laminae, of the material T300/Code 69 at the orientations 0° , 90° , $+45^\circ$ and -45° to the global X-Y directions, Fig. 1.1. The sample was fairly random since the

plates came from excess material at British Aerospace (Woodford).

4.1.1 Material Properties And Physical Parameters Of The Specimens

Table 4.1 gives the material properties used by British Aerospace in design and those typically measured for the unidirectional cured composite material T300/Code 69. The symbols given to the properties appear throughout the text.

The values were measured for a constant lamina thickness of 0.127E-03 M and a fibre volume fraction of 60%. T300 is a Toray high tensile strength fibre produced in Japan, and Code 69 is an epoxy resin manufactured by Fothergill and Harvey.

The dashed lines indicate which typically measured strains were not reported. This was probably due to a very wide variance in their measurements.

It has been known for a long time that the shear modulus, G_{12} , is dependent on both temperature and strain. All experiments were performed at room temperature, (15-20 °C) and hence only strain would have had an effect. Fig. 4.1 illustrates the secant shear modulus against the warping stress, T_{12} (which is itself a function of the shear strain δ_{12}). The transverse modulus, E_{22} , is also dependent on strain. Correspondence has suggested that the dependence is small but noticeable.

These two properties are also found to change when the individual lamina are placed together in the manufacture of generally orthotropic

plates. Large thermal strains develop in the plates when they are cooled down at the end of the curing process, due to the enormous difference in the principal coefficients of thermal expansion, Table. 4.1. The size of the thermal strains varies from layer to layer depending on the relative orientations of the facing plies. Internal plies may then experience strain in their transverse direction in excess of the matrix tensile failure strain ($\approx 0.7\%$) so inducing moderate crazing. The cracking will be parallel to the fibre direction and causes a reduction in the transverse and shear moduli. To allow for this in the numerical work the most realistic assumption to date has been taken.

Resin cracking is ignored - a reduction in the transverse moduli of elasticity of the unidirectional material is taken, and the non-linear stress/strain curve in shear is used.

All specimens contained some entrapped gases, known as voids, whose presence also reduce the shear modulus. From the work of Hancox (102) a 1% void content causes a 10% drop in shear modulus. For the plates tested little background information was available concerning void content so this reduction in shear modulus could not be taken into account.

In the manufacture of the laminates, the pressure subjected during curing tends to squeeze out some of the resin, with the outcome that ply thickness is often below the norm. This inturn causes an increase in fibre volume fraction and hence an increase in the longitudinal modulus, E_{11} . The following relationship allows for the increase in numerical analyses,

$$(E_{11})_{lam} = E_{11} \times \frac{0.127 E_{03}}{(f)_{lam}} \quad (4.1)$$

Material properties examined so far have been for 'freshly' cured material which has not yet been exposed to the degradation of the environment. A lot of research has shown that all resins are attacked to a varying extent by long periods of high humidity and/or high temperature. Again the result shows up as a reduction in the transverse and shear moduli (103).

Specimens had not been kept in a controlled environment, and had spent a varying length of time in ambient room conditions. For this reason the effect on the material could not be assessed and it has been assumed that there has been minimal degradation.

Several laminates were tested to determine the feasibility of the proposed plate bending experiment. Table 4.2 gives the physical parameters and remarks for each experiment. Symbols for the physical parameters are defined in Fig. 2.2.

It should be noted that the sample had been manufactured over a period in excess of three years. The exact dates of manufacture for the specimens used in Experiments 1, 3 and 4 are unknown. Unlike the rest, these two laminates possessed a single protective layer comprising of another soft epoxy resin. This layer had been applied to the upper surface and was nominally two standard plies thick. Symmetry had therefore been lost, but to maintain simplicity of the numerical analyses the layer was ignored, but not forgotten.

From correspondence with British Aerospace it was established that all the specimens had been subjected to the same curing cycles.

4.2 Shear Deformation And Shear Stresses

In the previous chapter the plate bending finite element analysis was introduced. Due to the allocation of storage space and the C.P.U. time allowed, restrictions had to be imposed on the complexity of the model. For the purpose of keeping these two quantities within limits, several thin plate bending assumptions were preserved.

Because of the relatively low interlaminar shear modulus G_{12} in fibre composites, classical laminated plate theory (C.P.T.) becomes inaccurate in determining gross plate response and internal stresses in 'thick' plates. Under these conditions several characteristics of C.P.T. limit its generality in the description of laminated behaviour (104). These are:

- (i) the assumption that uniform inplane displacements through the thickness,
- (ii) the presence of only two boundary conditions per free edge in the classical bending theory precludes the precise calculation of boundary layer effects, such as stress concentration factors,
- (iii) the neglect of shear deformation, implied by the hypothesis (normals remain straight and normal),
- (iv) the assumption of a state of plane stress in the constructive relations, which eliminates the possibility of exact calculation of interlaminar stresses.

Classical theory is merely a special case of the shear deformation theory, where the shear modulus in terms associated with the transverse shear deformation is taken to be very large, such that shear deformation

can be neglected. The finite element method developed ignores shear deformation and shear stresses in both the large and small displacement analyses. It would be of value to be able to predict the extent of shear deformation and shear stresses in our plates. Steps can then be taken in the design of the experiment to minimise these inherent responses.

The remainder of this section is divided into two; shear deformation being studied first, followed by shear stresses. Each study indicates that certain limits on experimental parameters must be made to reduce the unwanted responses to an acceptable level.

4.2.1 Shear Deformation

The treatment of transverse shear deformation effects in plates made of isotropic materials stems from the classical papers of Reissner (105) and Mindlin (106). Both of these theories were based on the displacement form

$$\begin{aligned}u &= u_0 + z \psi_x \\v &= v_0 + z \psi_y \\w &= w_0\end{aligned}\tag{3.1}$$

where u_0 , v_0 and w_0 are weighted averages. The classical theory assumes the same displacement field but with the two rotation terms ψ_x and ψ_y equal to $\frac{dw}{dx}$ and $\frac{dw}{dy}$ respectively. In Reissner's approximate method a special variational theorem was used to determine both the equations of equilibrium in terms of resultants and the stress-strain relations involving Equ. 3.1. The stress fields, along with the displacements, are assumed to vary as a function of z . Reissner's method was extended to orthotropic plates by Girkman and Beer (107) and later to symmetrical

cross-ply plates by Ambartsumyan (108). Whitney (109) then broadened this latter analysis to generally symmetrical laminated plates with orthotropic laminae of arbitrary orientations.

Mindlin employed kinematic assumptions of the form Equ. 3.1 and without introducing corresponding stress distribution assumptions, obtained the governing equations from a direct method. A correction factor was introduced to account for the fact that the displacement relations predict a uniform shear stress through the thickness of the plate, which was incorrect and in general would violate surface conditions. This factor was evaluated by comparison with an exact elasticity solution. A generalisation of Mindlin's theory was developed by Yang, Norris and Stavsky (110) including shear deformation and rotary inertia to obtain frequency responses for arbitrary laminated composites. A review of further papers was given by Bert (111) from which other researchers have stated that the YNS theory is adequate in predicting the behaviour of laminated plates. Although all these procedures are approximate, the algebra is complex and comprehensive results for multilayered generally symmetric laminated plates are very involved.

In parallel with the approximate methods, Pagano and his associates (104,112,113,114) were solving exact solutions of certain cylindrical bending examples. The manipulation of the ensuing theory is intricate and was developed to cope with simple composites containing arbitrarily orientated laminae. From the examples reported, the overall response of the specimen as the span to thickness ratio S is altered was demonstrated.

Fig. 4.2 shows the behaviour found in a symmetrical 3-ply

(equal thickness), cross-ply strip, which is simply supported at each end and has a transverse sinusoidal load (104). With low span to thickness ratios, the figures emphasise that the deviation of the exact solution from the approximate C.P.T. is quite substantial.

Fig. 4.2.2 shows the normalised transverse central displacement, \bar{w}_c plotted versus S and even at $S=20$ where C.P.T. would be accurate for isotropic materials, the deviation is about 20%. The normalised stress $\bar{\sigma}_x$ is plotted through the thickness for values of S of 4 and 10, Fig. 4.2.3, 4.2.4 respectively. Deviation of the classical lamination solution from Pagano's exact elasticity solution is drastic for $S=4$ but not over large when $S=10$. Transverse shear stress, $\bar{\tau}_{xz}$ for $S=4,10$ are shown in Fig. 4.2.5, 4.2.6 and the theories are not significantly different. Inplane normalised displacement, \bar{u}_x , is plotted through the thickness for $S=4$ and $S=10$, Fig. 4.2.7, 4.2.8. Obviously, the displacement varies almost linearly in each layer, but definitely not through the laminate when $S=4$; when $S=10$ the deviation is not as great. Thus the Kirchoff hypothesis of non-deformable normals is not appropriate for low values of S .

For a particular value of S the C.P.T. stresses converge to the exact solution of Pagano much more rapidly than do the displacements. With $S=20$ stresses are in the order of 10% in error.

Displacements are severely underestimated for S less than 25 in this example. If this set-up was tested experimentally, and S was less than 25, then the effects of shear deformation must be included in the numerical analysis.

The theories for shear deformation described above and the classical theory use the same order of approximation, Equ. 3.1, in a power series expansion in z . There have been several theories proposed which are of higher order than those of Reissner and Mindlin. These sophisticated models of plate behaviour are more applicable to laminated plates than isotropic, because strain transverse to the plane of the laminate strongly influences the behaviour. High-order theories were derived to solve the full elastic problems, to provide description of transverse normal strain, shear stresses, and vibration responses, rather than just shear deformation.

The next high-order theory from that embodied in Equ. 3.1 involves displacement forms of the type:

$$\begin{aligned} u &= u^0 + z\psi_x \\ v &= v^0 + z\psi_y \\ w &= w^0 + z\psi_z + z^2\xi_z \end{aligned} \tag{4.2}$$

which includes the effect of transverse normal strain. Whitney and Sun (115) developed Equ. 4.2 for laminated cylindrical shells. The approach was incorrect, a shear-correction factor was employed to derive stress resultants. Whereas a factor was appropriate to Mindlin's derivation since it assumed uniform shear stress across the thickness, the above displacement terms imply a non-uniform shear stress, so the correction factor was not required.

A step-up from Equ. 4.2 is the assumed displacement forms

$$\begin{aligned} u &= u^0 + z\psi_x + z^2\xi_x \\ v &= v^0 + z\psi_y + z^2\xi_y \\ w &= w^0 + z\psi_z + z^2\xi_z \end{aligned} \tag{4.3}$$

Nelson and Lorch (116) applied Equ. 4.3 to laminates, but made the mistake of still operating with a shear correction factor. Hildebrand, Reissner and Thomas (117) briefly examine the theory for the level of Equ. 4.3 and concluded that the inclusion of the quadratic terms in the inplane displacements did not provide extra advantages over low level theory, for problems which were of interest to them.

Reissner (118) has presented a theory which involves

$$\begin{aligned} u &= z\psi_x + z^3\phi_x \\ v &= z\psi_y + z^3\phi_y \\ w &= w^0 + z^2\xi_z \end{aligned} \quad (4.4)$$

He showed that the plate theory corresponding to Equ. 4.4 gave excellent results with the corresponding elasticity solution for the bending of a plate with a circular hole. Though the results obtained were impressive Equ. 4.4 represents the lowest order correction for out-of-plane deformation and inplane deformation was neglected, which was acceptable for the problem studied.

Lo, Christensen and Wu (119) formulated most of the up to date studies in high-order theories. Their 3-dimensional solution was based on the displacement forms

$$\begin{aligned} u &= u^0 + z\psi_x + z^2\xi_x + z^3\phi_x \\ v &= v^0 + z\psi_y + z^2\xi_y + z^3\phi_y \\ w &= w^0 + z\psi_z + z^2\xi_z \end{aligned} \quad (4.5)$$

which are on the same level as the Reissner theory but now take account of both in- and out- plane modes. Displacements and stresses were obtained by substituting Fourier series approximations (for displacement forms and loading) into the governing equilibrium equation which has

been derived from the principle of stationary potential energy. Finding a favourable comparison with isotropic plate test examples the theory was extended to cover laminated strips (120).

Further development of this method is discussed in Section 4.2.3 with special attention to its applicability to the behaviour of our generally symmetric orthotropic laminated plates.

However, the solutions obtained from the above theories are limited to simple geometry, load and boundary conditions. The finite element method of analysis can be adopted for difficult but practical structural configuration, as a general model. With the ever increasing development of elegant finite element procedures considerable effort from the early Seventies has been spent on investigating shear deformation in laminated plates. These finite element methods were generally based on the simple displacement form of Equ. 3.1. The first of the 2-dimensional, small displacement finite element methods to analyse 'thick' plates utilised the conventional displacement procedure. Pryor and Barker's (45) element has 7 D.O.F. (three displacement, two rotations and two shear rotations) per node, Subsection 3.1.2, but unless the mesh was very fine little success with the results was found. Mau, Tong and Pian (38) have employed the so-called hybrid stress FE method to analyse composite plates including shear deformation. Normals are assumed linear within each layer, but can vary from lamina to lamina. Mawenya and Davies (46) applied the same assumption as Mau et al, with a refined element and utilised the displacement method of solution. More recently, Panda and Natarajan (47) used, following Mawenya and Davies, the quadratic Serendipity shell element of Ahmad, Irons and Zienkiewicz (87) with the same normal rotation through

the thickness to claim improved accuracy. The thickness concept mentioned in these methods is essentially the same as that in the YNS theory.

Noor and Colleagues (48,49) developed a package of programmes to solve bending in laminated plates, which incorporates several shear flexible models. The analytic formulation was based on Reissner's theory with the effect of anisotropic material behaviour included. A 16 node Lagrangian element was the most successful, with 80 D.O.F.

The most recent study by Reddy (44) used the YNS theory with the inclusion of a penalty function concept to take account of the shear deformation. As already mentioned in Subsection 3.1.4. large displacement analysis is a facility included in the latter two programmes (72,79,74,75).

4.2.2 Comparison Of Classical Linear Finite Element Analysis (ACM) With Shear Flexible Elements

Considering the present understanding the magnitude of shear deformation in 'thick' laminated composite plates, it might be thought advisable to include shear deformation in the Finite Element Analysis (ACMBC).

Table 4.3 presented here, briefly describes four shear flexible elements which have been developed and verified against Pagano's exact solutions. Pagano employed the full 3-D stress-strain relations in the examples, whereas all the 2-D shear flexible elements account for the assumption $\sigma_z=0$ by altering the appropriate 3-D stress-strain terms. This means that each ply has slightly lower stiffness coefficients than the corresponding 2-D classical plate theory (which totally neglects any

effects in the z direction), and considerably lower than those of the exact solution.

With the shear flexible elements, quarter plate representations were applied to derive results for the cross-ply examples. All meshes, except Mau et al. (38) have an equal number of uniformly sized elements per side. Together with the linear FE analysis (ACM), as described in Chapter 3, the accuracy of the shear flexible elements are measured against the third test case considered in Pagano's paper, 'Exact Solution for Rectangular Bi-directional Composites and Sandwich Plates' (112). Test parameters for this 3 layered symmetrical cross-ply example are defined in Fig. 4.3. Two plots, Fig. 4.4,4.5 show the non-dimensional central transverse displacement, \bar{w}_c , and the non-dimensional maximum stress, $\bar{\sigma}_x$, in the X -direction, for increasing span to thickness ratio, S . Labels on the finite elements indicate the dimensions of the quarter plate meshes and their total number of D.O.F.

From the results the following observations were made for the particular example chosen:

1. Shear flexible models are only required in determining displacements when the value of S is less than 40.
2. Shear flexible elements do not provide an improvement in the prediction of stresses, over the whole range of S , and, in fact, the stresses deviate further from the exact solution than the element ACM.
3. It is to be recalled that the major reason for the adoption of the finite element approach was to evaluate the strains and stresses, and hence explain the behaviour found in the

plate bending experiments. The number of D.O.F. is a measure of the computing time required. It is evident that the solution using the element ACM takes a similar time as the shear flexible elements, and generally gives superior results. This being specially so providing $S > 30$

A shear flexible element was also rejected for the following reasons:

- (i) to represent the experiment, Section 3.0, at least 36 elements are necessary. If one of the shear flexible models was now used in the non-linear analysis, the total number of degrees of freedom would make the size of the governing stiffness matrix too large for the capacity of the computer
- (ii) and the extra complexity to account for a shear flexible model in the programming would inevitably increase the computing time.

Hence no further progress as to the magnitude of shear deformation effects in the tested generally symmetrical orthotropic laminated plates has been made. Two further pieces of information present more factors which will effect the size of shear deformation in the experiment. Whitney (121) reported that the higher the ratio E_{11}/E_{22} of the material, the more drastic was the deviation of the C.P.T. solution at low values of S from his approximate results. The carbon fibre reinforced plastic ply material used in this work has a E_{11}/E_{22} ratio of about 13 which is less than the material employed in Pagano's exact solutions, 25. However, when the plies are distributed in a laminated plate, with orientations of $0^\circ, 90^\circ, \pm 45^\circ$, thermal strains produced in the curing process reduce the transverse modulus considerably. From a private communication the value can decrease to 25% of its original value. Therefore it is possible that

the ratio E_{11}/E_{22} could be about 40 for our laminated plates, and this implies that shear deformation will be higher than found in Pagano's examples.

The second point was given by Pagano and Hatfield (114), who found that the exact solution converges to the C.P.T. solution at lower values of S as the number of layers in the cross-ply example were increased. Their analysis concerned specimens with 3 to 9 layers, so a substantial gain should be found in the plates to be tested, which consist of 16 to 40 layers.

4.2.3 High Order Plate Deformation Theory For Laminated Plates

The distinct methods forecasting the size of shear deformation (see previous Section) all suggest that, providing $S > 30$ there will be a close agreement between the exact solution and classical theory for laminated composite plates. However, as has already been pointed out, there is no idea of the extent of shear deformation in the plates tested, so the value of S stated above could be significantly different. If the magnitude of shear deformation was known progress in developing the plate bending biaxial test method could be made. It would allow a value of S to be fixed for each plate construction, below which incorporation of shear deformation into a numerical method is imperative. The experimenter would then have at his disposal a minimum span to thickness ratio for the design of the experiment parameters.

From the wide range of analytical solutions discussed, the high order plate deformation theory developed by Lo, Christensen and Wu (119,120,122)

appeared suitable for numerical programming. Construction of a 3-D small displacement analysis would predict shear deformation, and then possibly shear stresses in our laminated plates.

The high order displacement assumptions are given by Equ. 4.5. In (120), Lo et al. outlined the equations and relationships required to solve the displacement fields in general laminated plates. Governing equations pertinent to this theory were derived using the principle of stationary potential energy. Eleven second order equilibrium equations {4} were obtained for the determination of the 11 generalised displacement coefficients in Equ. 4.5. Terms in the equilibrium along with the boundary conditions necessary were defined in Equ. {5-7}. These relationships were independent of the properties of the material of the plate and hence hold true for homogeneous isotropic as well as laminated plates. Expressions for the equilibrium equations were given next in terms of the eleven displacement coefficients, using equations 4.5, {5-7} and the strain displacement relations. The coefficients in the relations were defined by {10}.

Formulation of certain classes of problems could then progress, providing the displacement coefficients, and distribution of load could be described by Fourier series. The ensuing displacement forms must then satisfy the boundary conditions. The high order method is now developed to solve the standard cross-ply example of Pagano, which has been compared with shear flexible elements in the last Section. It will be shown that the high-order theory is accurate for this test case, allowing further

{ } brackets indicate that the equation number refers to paper under discussion.



development to include laminates with arbitrary oriented plies. An important restriction was imposed, in that the analysis was only applicable to generally symmetrical orthotropic laminated plates. However, the introduction of the coupling compliances 16, 26 and 36 causes matrix equation to be dependent on the X-Y co-ordinates. This in turn meant that the problem was indeterminate.

4.2.3.1 Numerical Procedure - Stress-Strain Relations

The composite material has 3 mutual elastic axes which means that the governing 3-D principal stress-strain relations for layer K are:

$$\begin{Bmatrix} \sigma_1 \\ \sigma_2 \\ \sigma_3 \\ \sigma_6 \end{Bmatrix}_k = \begin{bmatrix} Q_{11} & Q_{12} & Q_{13} & 0 \\ Q_{21} & Q_{22} & Q_{23} & 0 \\ Q_{31} & Q_{32} & Q_{33} & 0 \\ 0 & 0 & 0 & Q_{66} \end{bmatrix}_k \begin{Bmatrix} \epsilon_1 \\ \epsilon_2 \\ \epsilon_3 \\ \epsilon_6 \end{Bmatrix}_k \quad (4.6)$$

$$\begin{Bmatrix} \sigma_4 \\ \sigma_5 \end{Bmatrix}_k = \begin{bmatrix} Q_{44} & 0 \\ 0 & Q_{55} \end{bmatrix}_k \begin{Bmatrix} \epsilon_4 \\ \epsilon_5 \end{Bmatrix}_k$$

where

$$\sigma_4 = \tau_{23} \quad , \quad \sigma_5 = \tau_{13} \quad , \quad \sigma_6 = \tau_{12} \quad \text{and} \quad \epsilon_4 = \delta_{23} \quad \text{etc.}$$

The material properties imply that the Poissons ratios ν_{13} and ν_{23} (which assume that the 2-3 plane is basically all matrix) are equal to the major Poissons ratio ν_{12} ie $\nu_{12} = \nu_{13} = \nu_{23} = \nu$

Fig. 4.6 below displays the principal axis system related to the unidirectional ply. A further material property relationship is seen to exist. $E_{22} = E_{33}$.

Figure 4.6 3-D Composite Properties

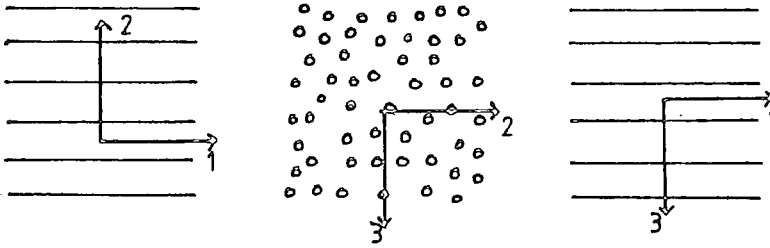


Table 4.4 indicates the 3-D stiffness terms with the corresponding 2-D stiffness coefficients .

Table 4.4

STIFFNESS COEFFICIENTS	3-D	2-D
Q11	$\left[\frac{(1-\nu^2) E_{11}^2}{K'} \right]$	$\frac{E_{11}}{(1-\nu^2) E_{22}/E_{11}}$
Q12 = Q21 = Q13 = Q31	$\left[\frac{\nu(1+\nu)E_{22} E_{11}}{K'} \right]$	$\frac{\nu E_{22}}{(1-\nu^2) E_{22}/E_{11}}$
Q22 = Q33	$\left[\frac{(E_{11}-E_{22}\nu^2) E_{22}}{K'} \right]$	$\frac{E_{22}}{(1-\nu^2) E_{22}/E_{11}}$
Q44	G23	—
Q55	G12	—
Q23 = Q32	$\left[\frac{(E_{11}+E_{22}) \nu}{K'} \right]$	—
Q66	G12	—
where $K' = E_{11}(1 - \nu^2) - 2E_{22}\nu^2(1 + \nu)$		

Stress-strain relations in the X-Y directions at the angle θ° to the principal axes of the ply are given by:

$$\begin{aligned} \{\sigma_i\}_k &= [T]^{-1} [Q_{ij}] [T]_k \{\epsilon_i\}_k \quad ij = 1+6 \quad (4.7) \\ \text{ie} \quad [\hat{Q}_{ij}]_k &= [T]^{-1} [Q_{ij}] [T]_k \end{aligned}$$

The 3-D transformation matrix [T] for fibre reinforced composites with the principal direction 1 being parallel to the direction of the fibres,

making the angle θ° with the x-axis, and with direction 3 remaining parallel to the z-axis is:

$$[T] = \begin{bmatrix} \cos^2\theta^\circ & \sin^2\theta^\circ & 0 & 0 & 0 & 2\sin\theta^\circ\cos\theta^\circ \\ \sin^2\theta^\circ & \cos^2\theta^\circ & 0 & 0 & 0 & -2\cos\theta^\circ\sin\theta^\circ \\ 0 & 0 & 1 & 0 & 0 & 0 \\ 0 & 0 & 0 & 0 & \cos\theta^\circ & -\sin\theta^\circ \\ 0 & 0 & 0 & 0 & -\sin\theta^\circ & \cos\theta^\circ \\ -\sin\theta^\circ\cos\theta^\circ & \cos\theta^\circ\sin\theta^\circ & 0 & 0 & 0 & \cos^2\theta^\circ - \sin^2\theta^\circ \end{bmatrix} \quad (4.8)$$

4.2.3.2 Equilibrium Equations

The governing set of relations $\{\epsilon\}$ are greatly simplified as the laminated plates under investigation are all symmetrical. Therefore the coefficients which are functions of $\int (z, z^3, z^5) \hat{Q}_{ij} dz$ become zero and the governing 11 equilibrium equations can be separated into a set of five second order differential equations describing the inplane displacement components and a set of six second order differential equations governing flexural displacement components of the laminates. Symmetry splits the displacement assumptions into the inplane and flexural components

$$\begin{aligned} \text{Flexural} \\ u &= z\psi_x + z^3\phi_x \\ v &= z\psi_y + z^3\phi_y \\ w &= w^0 + z^2\xi_z \end{aligned} \quad (4.9)$$

In-plane

$$u = u^0 + z^2 \xi_x$$

$$v = v^0 + z^2 \xi_y$$

$$w = z \psi_z$$

The right hand side of {8} is also simplified as the problems studied have only transverse load distribution on the upper surface of the specimen.

With the reduction in complexity the two sets of differential equations are shown in Appendix II . Parameters for Pagano's exact cross-ply solution are shown in Fig. 4.3. The following assumed displacement forms are the simplest:

Flexural

$$u = (zK_1 + z^3K_2) \frac{\cos \frac{\pi x}{A}}{A} \frac{\sin \frac{\pi y}{B}}{B}$$

$$v = (zK_3 + z^3K_4) \frac{\sin \frac{\pi x}{A}}{A} \frac{\cos \frac{\pi y}{B}}{B}$$

$$w = (K_5 + z^2K_6) \frac{\sin \frac{\pi x}{A}}{A} \frac{\cos \frac{\pi y}{B}}{B}$$

In-plane

$$u = (K_7 + z^2K_8) \frac{\cos \frac{\pi x}{A}}{A} \frac{\sin \frac{\pi y}{B}}{B}$$

$$v = (K_9 + z^2K_{10}) \frac{\sin \frac{\pi x}{A}}{A} \frac{\cos \frac{\pi y}{B}}{B}$$

$$w = K_{11} \frac{\sin \frac{\pi x}{A}}{A} \frac{\sin \frac{\pi y}{B}}{B}$$

(4-10)

where $K_i; i = 1, 11$ are constants. Loading distribution is described by a similar Fourier approximation as

$$q = q_0 \frac{\sin \frac{\pi x}{A}}{A} \frac{\sin \frac{\pi y}{B}}{B} \quad (4-11)$$

where q_0 is the maximum pressure imposed.

To determine the K'_s the assumed displacement fields were substituted into the governing relationships, which on rearrangement for the flexural response are shown in Appendix II.

For the 2-D example case, having similar displacement forms as in the

exact solution (112), the values of the K's are independent of the co-ordinates. A solution for the cross-ply example was readily available as all the coupling terms (12,26 and 36) are zero, which eliminates these Fourier products. However, symmetrically laminated plates with arbitrary orientations do not possess a general solution because these coupling terms are present. If the particular values of x and y chosen make either $\cos \theta^\circ$ or $\sin \theta^\circ$ zero, then the determinant of the matrix is also zero, and a solution is impossible.

When the set of equations are solved the K constants can be substituted into the displacement forms describing the behaviour of the plate. Substitution of the displacement forms into the strain-displacement relation, and then the strains into the stress-strain relations, allows the magnitude of the displacements, strains and stresses to be evaluated at any x,y,z position in the specimen.

Although the high order theory is unable to aid in the prediction of shear deformation and possibly shear stresses in our laminated plates, it does produce a fairly accurate picture for the exact solution attributed to Pagano, Table 4.5.

Table 4.5 shows that the high order theory, contrary to the finite element analysis, is weaker in establishing the displacements than the stresses. The fit between these analyses should be better than the finite elements as they both rely on the same 3-D stiffness coefficients. Further information is obtained because the flexural and in-plane components are separate, and a comparison for a range of S are shown in Table 4.6.

For all values of S the inplane components can be neglected unless S is small and σ_z is required. However, transverse stresses are found to be more accurate when the stress equilibrium equations are applied rather than the displacement forms are substituted into the strain displacement relations (122). Doubt is therefore, cast on the validity of the transverse normal stress calculated. The magnitude of σ_z for this example suggests that as long as $S > 10$ then it will be in the order of 100 times less than the maximum normal stress and transverse normal failure will not precipitate prior to fibre failure.

In this Section a very thorough attempt was made to predict the effect of shear deformation in the bending response of generally symmetrical orthotropic laminate plates. Obviously for the plates in question, a solution is complex and an approximate representation, even with a shear flexible finite element, would be difficult. It was also shown that a promising high order plate theory had its limitations. Together the observations suggest that shear deformation effects can be assumed insignificant in the laminated plates tested, being ignored in the finite element analysis providing the span to thickness ratio $S > 30$.

4.2.4 Shear Stresses

In classical lamination theory, no account is taken of interlaminar stresses, and so it is incapable of providing predictions of some of the stresses that actually cause failure of a laminated material. Since the plies in a general orthotropic laminate have different stiffnesses in any given direction, they tend to slide over one another during extension. If the laminae are connected at their interface, interlaminar shear

stresses will develop because of this tendency. Moreover, classical lamination theory implies values of τ_{xy} where it cannot possibly exist, namely at the edge of a laminate. Physical grounds have shown that:

- (a) At the free edges of a laminate, the interlaminar shearing stress is very high (even singular) and would therefore cause the delamination observed in such regions (123),
- (b) the alteration in the layer sequence in a laminate can produce differences in the tensile strength, even though the proportion of each type of oriented plies do not change (124). This sequence alteration changes the interlaminar normal stress, σ_z , near the boundaries and is believed to provide the answer to such strength differences (125).

The problems associated with interlaminar stresses near free edges have been recognised for some time and the literature contains voluminous results of stress calculation for a 2-D section of a laminate in either uniform extension or cylindrical bending. The earliest investigations of the interlaminar stress problem was apparently carried out in Japan by Hayashi (126) and Hayashi and Sando (127) who reported that the maximum interlaminar shear stress occurred at the free edge of a laminate in tension. Hayashi used a plane stress model for the layers and approximated the interlaminar shears by a strain averaging technique. Using a similar model, Puppo and Eversen (128) similarly discovered a sharp rise in the interlaminar stresses near a free edge. Notably, the use of the above models ignored the interlaminar normal stress. This was addressed by Pipes and Pagano (123) who presented a finite difference solution to the exact elasticity equations for a laminate in uniaxial tension. In their development, the stresses were assumed independent of the axial co-ordinate

and include all six components. The results for the example of a $(+45^\circ, -45^\circ)_S$ laminate are shown in Fig. 4.7.1, a sharp rise occurs in both the interlaminar shear stresses and, to a lesser extent, the normal stress near the free edge. These discoveries were later to serve in making strength predictions of laminates based upon the layer stacking sequence (124) and then as a comparison with experimental observations (129). Pipes and Pagano's finite difference procedure is known to be only approximate and requires a vast amount of computing time to be of general application. To analyse multilayered laminates (125) they developed the high order method with the approximation of Whitney and Sun (115) but it was only suitable for symmetrical $\pm\theta^\circ$ composites. Oplinger (130) also carried out an analysis of angle ply laminates in tension similar to Puppo and Eversen. The approach allowed a large number of layers to be considered and, like Pipes and Pagano (123,125) demonstrated that a singularity in the interlaminar shear occurred at the free edge of a laminate for one particular type of layer construction.

An alternative approach to the above was employed by Rybicki (131) and Wang (132) who studied a 3-D finite element formulation. Computing time limits the degree of modelling possible with this numerical approach. Taking advantage of the stress independence in the length direction, Wang and Crossman (133) developed a 2-D finite element solution. The limitation of this numerical solution was that, in order to achieve a realistic prediction of the stress field, sixteen elements in the thickness direction were required within each layer in the region of steep strain gradient. A total of 196 elements per layer were employed. Hence, like Pipes and Pagano (123) the computing time was enormous to achieve a satisfactory solution for a two layer free edge boundary value problem.

Recently Pagano (134), who was extremely critical of the above numerical approximations for the solution of the uniaxial extension example, cited three criteria by which a self consistent theory must be based. He stated that the assumed displacement forms used in most of the above methods leads to a lack of credibility. The paper described the simplest theory based upon the variational theorem derived by Reissner (135) which permits the treatment of discontinuous interfaces. Assumptions for the stress fields were the same as the shear deformation analysis attributed to Reissner. The ensuing numerical values compared favourably with Wang and Crossman for simple laminates. For the most satisfactory correlation, each layer was subdivided into several sections. Computing time was again large as the solution had $13N$ field equations and $7N$ edge conditions (where N is the total number of sublayers).

Free edge effects in laminates under bending have received least attention. Tang (136) reported for a uniformly loaded rectangular plate (4 layers, $(+\theta^\circ, -\theta^\circ)_s$) that 'the interlaminar shear and normal stresses may be as high as 30% and 5% respectively of the maximum bending stress in the laminate'. An assumed displacement field was used in the analytical solution which separated the interior of the plate from the free edge and solved the interior by the classical theory while the boundary layer region was studied by a combination of a modified torsion problem and a modified plane strain problem. Salamon (137) looked at the same laminates as Tang, solving the governing displacement equations by finite difference. These bending cases along with the inplane solutions provide the same picture for the distribution and magnitude of the shear components. The following observations were drawn from the literature:

There are three classes of interlaminar stress problem -

- (a) $\pm\theta^\circ$ laminates exhibit only shear coupling (no Poisson mismatch between layers), so τ_{xz} is the only non-zero interlaminar stress, Fig. 4.7.1
- (b) $0^\circ, 90^\circ$ laminates exhibit only a Poisson mismatch between layers (no shear coupling) so τ_{yz} and σ_z are the only non-zero interlaminar stresses, Fig. 4.7.2
- (c) a combination of the above, for example $\pm\theta_1^\circ, \pm\theta_2^\circ$ laminates, exhibit both shear coupling and Poisson's mismatch between layers, so have τ_{xz} , τ_{yz} and σ_z interlaminar stresses.

Looking at the example of the $(+45^\circ-45^\circ)_s$ laminate in uniaxial strain, with $b=8t$ (width four times the thickness), the inplane stresses σ_x , τ_{xy} the shear stresses τ_{xz} , τ_{yz} and the normal stress σ_z at the interface between layers ($z = t$) are shown in Fig. 4.7.1. The stresses predicted with classical lamination theory were obtained in the centre of the cross-section by the method including shear. However as the free edge is approached, σ_x decreases, τ_{xy} goes to zero, and most significantly, τ_{xz} increases from zero to infinity (a singularity exists at $y = \pm b$). The presence of a singularity was the main reason for the more thorough analyses. The dotted line, Fig. 4.7.1, shows the prediction of τ_{xz} as obtained by Pagano's most recent solution (134). The singularity is still in evidence and grows with increasing subdivision of the two layers and the final limit that would be obtained is questionable. By changing the laminate geometry, the configuration, the total number of laminae, the width of the region in which the stresses differ from those of classical lamination theory has been shown to be about the thickness of the laminate. Thus the deviation from classical lamination theory can be regarded as a boundary layer or edge effect one laminate thickness away

from the edge and, in the rest of the specimen, expected to be valid. As stated at the beginning of this section, layer stacking sequence can change the tensile strength of a laminate. Observing the distribution of σ_z along the centre line and the interface ($z = 0$), Fig. 4.7.2, 4.7.3, of the two examples $(0^\circ, 90^\circ)_s$ and $(90^\circ, 0^\circ)_s$ it can be seen that if the 0° layer is outermost then σ_z is tensile and can induce debonding between the layers. When the 0° layer is innermost σ_z is compressive. This is probably the answer to strength variations found between specimens comprising of twolay-up arrangements. Similar influence, due to the stacking sequence, was found by Pagano and Pipes (124) with $(\pm 15^\circ, \pm 45^\circ)_s$ laminates and Reifsnider et al. (138) with quasi-isotropic $(90^\circ, 0^\circ, -45^\circ, 45^\circ)_s$ and $(0^\circ, 45^\circ, 45^\circ, 90^\circ)_s$ laminates.

In the laminates tested all types of layer sequence exist, i.e. rotating the specimen through 90° changes the lay-up observed. When these generally symmetrical orthotropic laminated plates were tested the distribution and magnitude of shear stress τ_{xz}, τ_{yz} and the transverse normal stress σ_z were unknown. Obviously, none of the analytical solutions discussed could possibly model these multilayered laminates which were subjected to complex strain distributions near the free edges. To minimise the inherent shear strains, the experiment must induce, relative to the test section, small strains in the free boundary regions. This will ensure that the delamination stresses τ_{xz} and σ_z will not cause premature damage. To achieve this, the preferential bending about a centreline must not be excessive. Basically, the combination of the global plate bending stiffness D_{11}, D_{22} and the aspect ratio A_s, E_s must not enable the specimen to behave as a pure beam. It is still possible that, even if preferential bending is minimised, shear stresses become

large. To defuse their detrimental effects the geometry of the plate, with $S > 30$ means that the free edges are remote from the central test section. If delamination is induced during the experiment to failure, it will be hoped that this area of delamination will not have spread far enough into the body of the plate to effect the test section, in which ultimate fibre failure is to occur.

4.3 Experiment Procedure

4.3.1 Apparatus

The apparatus for the plate bending test was designed to fit the specifications of an Instron 1195 machine. The rig had to fit onto the .144m diameter loading platform of a 25KN compression load cell. A base plate was therefore needed to support the specimens. Onto this plate four support columns had to be positioned to provide the various support distances. These positions had to be centred about the centre of the base plate, which was to be placed directly in line with the centre of the load cell. Fig. 4.8.1 illustrates the design for the mild steel base plate and Fig. 4.8.2 shows one of the four identical mild steel supporting columns. To support the specimens ball bearings were placed into the sloped recess of the columns. Two sizes were used, 0.3175E-01 and 0.4445E-01 m diameter.

Columns were introduced to increase the distance from the laminates to the base plate, so that when loading commenced the centre of the specimens did not touch the base plate before fibre failure. The columns were designed to be extremely robust, and fit tightly into the holes machined on the base plate. This ensured that when the supports were

subjected to loading negligible sideways deformation resulted.

For the following reasons the larger of the ball bearings were generally used:

- i) To add extra distance between the specimen and base plate
- ii) To provide a large enough area of contact preventing local yielding. (The area was, however, small enough to be classified as a point when compared to the surface area of a specimen. If local yielding had been allowed, it could have caused unwanted bending deformation and made the numerical comparison more difficult).
- iii) To provide a continuous curved surface which the specimen could easily slide over. The benefit of this was that the sliding reduced inherent axial strains.

Plate 4.1 shows a typical specimen supported by the larger ball bearing awaiting testing. Plate 4.2 shows one of the two loading heads (.02 x .02)m and the observed gross deformation of Experiment 5. Fig. 4.8.3 gives the dimensions for the loading heads. Care had been taken when machining the indenters, since if the ends had not been squared the load would have been unevenly applied.

4.3.2 Specimen Preparation

Before the experiments could be set-up several parameters had to be defined and a choice made for the locations of strain and dial gauges. Table 4.7 contains the distances of the supports A_s and B_s and the patch loading A_p and B_p chosen for the nine experiments. It can be noted with

reference to Fig. 2.2 that the distances 'A' are measured in the global X-direction.

The choice for the supports were made by taking the largest sensible length above the limiting values. A limiting value was equal to that length which made the span to thickness ratio, S , equal to 30. Providing this value of S was exceeded, the effects of shear deformation and shear stresses could be neglected. The values of S for each experiment are given in Table 4.7.

The value of the principal bending stiffnesses force a maximum limit on the relative lengths of A_s and B_s , for the following reason. If, for example, A_s is greater than B_s and the corresponding stiffness D_{11} is smaller than D_{22} , considerable preferential bending will occur about the Y-axis, ($O-O'$ in Fig. 2.2) when the plate is loaded. This makes the response of the specimen approach a 'pure' beam. Large strains will then be induced near free edges providing high shear stresses which may cause delamination and invalidate the results. Because of this condition the practical range of supporting distances will be limited.

Patch load dimensions A_p and B_p were then chosen to be reasonably large and equal, but not greater than 0.1 of the plates minimum length. This ensured that the distribution of load was uniform over sufficient area alleviating spots of high concentration. With this choice of parameters the two indenters, Fig. 4.8.3, were designed.

The positions and orientations for the strain gauges were then chosen. The principal orientations depended on the orientations of the two outer

laminae and the positions were taken to match nodal points in finite element meshes. The majority of the gauges were located in the proximity of the plates' centre, with just the occasional one near an edge. These latter gauges were used to give some insight into the strains inducing shear stresses.

3mm cross-ply and single-ply gauges were used throughout. These were the smallest available which would not overheat when excited with the minimum supply voltage of 1.5 V. Measurements were always made individually so a heat sink problem with the cross-ply gauges was averted. The centre of each gauge was positioned at the nodal points. It has been assumed that a linear variation in strain existed over the entire length of the gauge. With this assumption the strain measured could be directly taken as that which acted at the nodal point.

Gauges were generally placed in pairs on the upper and lower surfaces, except directly below the loading head, and were

Cross-ply	FCA-3-11	3mm	}	TOKYO SUKKI
Single-ply	FLA-3-11	3mm		KENKYUJO Co Ltd.

The gauges had a resistance of $120 \pm 5 \Omega$, a gauge factor of 2.10 and a yield strain of approximately 2.0%. The adhesive was M-Bond 200 (Welwyn) which has a shelf life of only 6 months. This short shelf life was the reason for the difficulties experienced in Experiment 2. Gauges were attached to specimens by following the procedure laid down in the Instruction Bulletin B-276 M-line Accessories, "Strain gauge installation with M-Bond 200 adhesive".

After gauging the plates, the type of strain to be measured was chosen.

It was a simple matter to change the wiring connections of a pair of opposing gauges to enable either the bending, or the axial, or simply a surface strain, to be recorded. Fig. 4.9.1 illustrates the exaggerated bending stretching behaviour expected in laminates due to classical thin plate theory, and Fig. 4.9.2 shows the wiring connections for the various strain measurements. Twice the actual reading was recorded when measuring the axial and bending component since a pair of gauges were employed. The true values are given by the following expressions:

$$\epsilon_b = \pm \left| \frac{\epsilon_{top} + \epsilon_{bottom}}{2} \right| \quad (4.12)$$

where +ve lower surface
-ve upper surface

$$\epsilon_{pl} = \frac{\epsilon_{top} - \epsilon_{bottom}}{2}$$

For the axial strains dummy gauges were required in the full bridge. Experiments were always performed at room temperature, so temperature compensation was not important. Therefore it did not matter that the dummy gauges were attached to aluminium.

After several experiments had been analysed it became apparent that further information was obtainable if all the gauges were separately recorded. Then by the application of the two simple relationships above, the bending and axial components could be determined. Unfortunately the relationships only hold for classical thin plate bending and so, once large deformation has been introduced, they become invalid.

Finally, two points were chosen where dial gauges could be located for a comparison with the calculated finite element transverse displacements. A diagram showing the arrangement of strain gauges, the dimensions of the supports and patch loading for each experiment is presented with the results.

4.3.3 Experimental Arrangement

After the specimen had been prepared the rig was arranged on the compression load cell, as depicted in Plate 4.2. The cell has a maximum capacity of 25KN, and is electrically calibrated. Loads were accurately recorded on a variable speed pen chart recorder.

Connections were then made from the strain gauges to appropriate instrumentation. To cope with up to 25 individual strain measurements several units were needed, as shown in Fig. 4.10. Since the only available instruments were static balance devices all measurements were made with constant central displacement. Strains were measured with two Peekel devices, a B105 battery operated, minimum excitation voltage 1.25V, and a 581DHN mains operated minimum excitation voltage of 1.5V. Both instruments tended to slightly drift with time and accuracy was dependent on the full scale taken. For all experiments full scale deflection was $300\mu\epsilon$ providing an inherent error to the measurements of $\pm 2\mu\epsilon$.

After the strain gauges were connected a simple check discovered if a gap existed between specimen and any of the ball bearing. The existence of a gap was due entirely to the laminate not being exactly flat. The gap was removed by placing shims under the base of the lowest column. When this had been accomplished further inspection generally showed that the specimen was not horizontal. Fortunately, further checks revealed that the load cells platform and the crosshead were also on a slight slant, and that as a complete unit all components were within reason parallel to each other.

4.3.4 Test Procedure

The following procedure was carried out with each experiment to gather as much relevant information as possible. With the specimen unloaded all strain gauges were electrically balanced. On occasions a balance was unobtainable due to poor electrical contact. Remaking the suspect connection was the usual course of action necessary to produce the balance.

To discover if any of the gauges were insecure the plate was then subjected to a simple load cycle. The maximum load for the cycle was taken so that either the greatest surface strain did not exceed $1000\mu\epsilon$ (0.1%) or that the central transverse displacement did not exceed the plates' thickness, whichever came sooner. Table 4.8 gives the embedding cycles for the nine experiments and the time period at which the load increments were maintained. The cycle was repeated three times to make absolutely sure that all gauges were correctly attached.

By noting the strain at the maximum load, a quick comparison with a finite element model, (ACM), showed up the faulty gauges. Providing that these gauges were not in the test section they were ignored in subsequent loadings.

Measurements had to be made with a constant crosshead position since the Instron does not have a constant load facility. This meant that with up to 25 separate strain measurements, the operation of balancing and recording took about 5 minutes. During this period of time a small amount of load relaxation was generally inherent. Therefore, it was standard

practice to start the measurements at the centre of the plate and record any changes in these gauges at the end. This enabled any changes due to load relaxation and material deterioration to be noted.

A set of measurements were then taken for the evaluation of the linear bending by the finite element method, ACM. Load was imposed in several equal increments up to the maximum of the embedding cycle, by making the central transverse displacement increase at a uniform rate. After each load level was reached crosshead movement was stopped and the readings taken. Once readings were taken at the maximum load, the specimen was unloaded by the same increments and the measurements remade. It soon became apparent from Experiments 1 and 5 that there was virtually no difference between the two sets of values, and so a good approximation to the linear strains in the remaining experiments was found by the results during the embedding load range in the test to failure.

Applying the same procedure as for linear evaluation the specimen was finally loaded to first fibre failure. Unfortunately this was not the case with Experiments 3 and 5 because of unforeseen difficulties, and meant that these specimens were retested. Table 4.9 gives the load increments applied in each experiment, the speed of the crosshead and the final load. The strains and transverse displacements and any visual observations were recorded at each load increment.

4.4 Experimental Results Fig. 4.11 - 4.53

Selected strains and transverse displacements have been presented in graphical form. To make the presentation comprehensive the following

information has also been given. Prior to each set of results there is a section entitled 'Notes and Observations'. All features specific to the experiment which affect its behaviour and the visual observations made during loading were recorded here. Also noted are the final strains measured, (generally at the load increment below failure) for those gauges not shown in the graphs.

Before the graphs displaying the measurements a diagram shows the plan for the experiment indicating the locations and orientations of the strain gauges.

There are several reasons why measured strains, and not the stresses have been presented.

The stresses were in fact indeterminate, since the strain field at most locations was not fully recorded. Even if it had been, (i.e. centre where $\tau_{xy} = 0$) a prediction of the stresses would have meant applying the principle of linear elasticity and the material moduli are not precisely known. To complicate the problem further, if the lamina's transverse strain exceeds 0.7% the matrix will fail and prevent stress transfer in that direction. It was found impractical to determine the area suffering matrix failure.

All the measurements have been presented from Experiment 2 since it was chosen as representative. Its load/displacement trace, recorded on the Instron chart recorder, can be found between the linear and failure strain plots, and is characteristic of the remaining experiments. For this reason no further load/displacement traces have been given.

A diagram to illustrate surface fibre failure has been placed after the results of Experiments 1,2 and 4. It was not necessary to provide such diagrams for Experiments 6 and 7 since there was only a small amount of visible damage. Instead the surface damage characteristics were included in the 'Notes and Observations'. Since no visible damage occurred in Experiments 3,5,8 and 9 no such diagram was necessary.

To aid examination of the results presented, the format employed will now be explained. The plots were formed using the measurements at each load increment. The curves created by these points were not joined, since individual measurements would have been obscured, making inspection (especially in the linear load range) difficult.

At the top of each set of values a label indicates the measurement and its position on the plate. Directly beneath the label the final value has been noted. The labels take the following notation:

$1\ 0^\circ\ L\ B+A$ means gauge 1, orientation 0° (tensile unless stated negative) lower surface and the strain consists of the components due to bending and axial.

If subscript L happens to be T then the gauge was on the top surface (compressive).

To enable a quick comparison between a pair of gauges on the top and lower surfaces, i.e. $6\ 0^\circ\ L$ and $6\ 0^\circ\ T\ B+A$ both were presented as positive. It will therefore be important to remember that, where subscript T appears, the strain recorded was compressive. $2\ 90^\circ\ B$ or A means gauge 2, orientation 90° , and the strain was either the bending or axial

component.

4.5 Discussion On Results

It will be found convenient when discussing the results for the various aspects to be split into two parts. The bending of the laminates throughout loading will be discussed first, followed by an examination of the failure mechanisms. The latter section will also be concerned with the problem of determining the governing biaxial stresses.

It was stated in the introduction to this Chapter that certain experimental parameters were unknown before the tests. These parameters included the magnitude of deformation, maximum load and strains and the failure mechanisms. The analysis of the results reveals some of the parameters for the lamination configurations tested, which can be used at a later date for further development.

Measurements taken in the embedding load range will be analysed in Section 5.1, where numerical comparisons will be made. All that needs to be noted now is that the results from Experiment 2 (Fig. 4.16 - 4.19) are typical. Errors inherent in the measurements are also discussed in Section 5.1, since they are more relevant to the numerical comparison. In fact, since the total error in the measurements cannot be assessed, it has been assumed small in comparison with the measurements at high loads.

It has been assumed that loading was uniform over the patch area and that the reactions at the supports remained identical. To state categorically that all the plates were loaded uniformly would be incorrect,

since observations made in Experiments 2 and 5 suggest otherwise. The reactions were not always identical too, since the twisting stiffnesses caused warping. Only Experiment 9 (Fig. 4.50 - 4.53) showed considerable twisting so the variation in reactions for the remaining experiments has been assumed small.

4.5.1 Plate Bending

The load/displacement trace for Experiment 2 (Fig. 4.20) shows typical behaviour, with a virtually linear increase in load with transverse displacement. Small flutters can be seen which were most likely caused by spontaneous movement between the specimen and supports. The trace also shows a small amount of load relaxation at each increment during the time interval needed to take the measurements. It was thought that the relaxation was a result of the laminate settling to a state of equilibrium. However, this is not substantiated since the central strains did not change (except at high loads) during the time interval.

The plots of transverse displacement are always continuous and the trends generally indicate that there was a slight increase in central displacement for load, (Experiment 2, Fig. 4.21, Experiment 3 and 4, Fig. 4.29, Experiment 7, Fig. 4.42 and Experiment 8, Fig. 4.47). The exception to the above were Experiments 5 (Fig. 4.33) and 9 (Fig. 4.51) because of the experimental difficulties experienced.

Generally the plots for the strains are smooth, continuous and of similar trends up to catastrophic fibre failure. The lack of any sudden change indicates that little or no local delamination damage occurred

until fibre failure. Experiments 5 and 9 did produce a variation in the trends, but this was due to uncharacteristic deformation.

The other gauges which also recorded a different trend were the central gauges in Experiment 7 (Fig. 4.43) and 8 (Fig. 4.48), and, to a much lesser extent, in Experiment 2 (Fig. 4.22) and 4 (Fig. 4.30). These gauges recorded a strain increase at high loads during the time to take measurements. It can be seen that the gauges measuring transverse to the fibre direction in Experiments 7 and 8 recorded massive increases. In fact, growth became so rapid that just prior to fibre failure it was not measurable. This behaviour has been termed strain runaway. When strain runaway became prominent the surrounding gauges kept constant readings, showing that the effect was localised. The behaviour will be examined further in the Section concerning failure mechanisms.

Strain measurements and visual observations show that the laminates stiffened with load, as predicted by geometric non-linear considerations. When the geometric non-linear behaviour, as defined in programme ACMBC, is no longer valid could not be established for the reasons given in Section 3.4. This was quite disappointing since it would have been valuable to the understanding of the test to know when Kirchoffs and Von-Karmans assumptions and material non-linearity no longer existed.

Except in Experiment 6 (Fig. 4.37 - 4.40), (the specimen had previously been tested in Experiment 5 (Fig. 4.33 - 4.36)) the maximum strain measured was at the centre, but not necessarily in the direction of the fibres. Taking this a step further, the largest strain in all the major directions ($0^\circ, 90^\circ, \pm 45^\circ$) probably existed at the centre. This cannot be proven

since not all strain components were recorded.

Where convenient a pair of gauges, which were recorded separately, have been presented on the same diagram (i.e. Experiment 2, $60^\circ T$ and $60^\circ L$ (Fig. 4.23)). It is noted that the trends show that the bending strain was usually much greater than the axial and that the axial was tensile.

In terms of the expected deformation a desirable distribution of strain in all the experiments but 5, was measured. It is of particular interest that the maximum inplane strains were at the centre, and that they decreased rapidly towards the free edge. This is a necessary condition for the plate bending method since small inplane strains near the free edges mean negligible edge effects. Section 4.2 has shown that if shear stresses are allowed to become large then edge delamination may start before fibre failure. This would be extremely undesirable since it could invalidate the data and break criterion (b), Chapter 1, for reliable biaxial strength and elastic properties assessment.

Experiments 5 (Fig. 4.33 - 4.37) and 7 (Fig. 4.41 - 4.45) on the same lamination, can be taken to illustrate the above point; even though delamination in Experiment 5 did not occur before the load was removed. The deformation in Experiment 5 at high loads can be likened to a pure beam where the strain near the edge $120^\circ L_{B+A}$ was nearly equal to that at the centre $190^\circ L_{B+A}$ (Fig. 4.35). Experiment 7 illustrates a desirable response with relatively low edge strains (gauges 9,10,11 (Fig. 4.44 and 4.45)) and a bending response which did not dominate about an axis. The largest measured edge strain, $110^\circ L_{B+A}$, always remained below 50% of that

measured by 5°L B+A (Fig. 4.43). This comparison of the bending in the two experiments suggests that, providing geometric parameters are carefully chosen to prevent the response found in Experiment 5, shear stresses will remain low enough for edge delamination to be neglected.

The measurements plotted in Fig. 4.13 from Experiment 1, indicate that the supports provided no restraints to the complicated free bending deformation. The two gauge pairs, 13+45° B and 14-45° A which were placed on the diagonals near the supports, also show that the axial strain became proportionally less than the bending (response stiffened) as the transverse deformation increased. The exact opposite would have been expected had the supports restrained the deformation. Although not checked, this conclusion has been assumed to hold for all remaining experiments.

The most interesting discovery concerning the bending is that each plate not only stiffened, but exhibited preferential bending about a centreline. The dominating deformation was found to increase with load at expense of bending about the other centreline. Table 4.10 was constructed to collate the extent of preferential bending in the nine experiments.

The behaviour was even apparent with the symmetrical experiment arrangements. The deformation in Experiments 1 and 2 was dominated by the difference between the principal stiffnesses D11 and D22. In this lamination D22 is much smaller than D11 so the plates deformed in the less stiff direction, i.e. about the X-axis. The only plate to show a small amount of preferential bending was tested in Experiments 3 and 4 which has similar principal stiffnesses.

From this it can be seen that, by altering the spans A_s and B_s with or without changing the plate dimensions A and B , the magnitude and axis of the preferential bending is controllable. Experiments 5 and 6 are good examples to illustrate this point. In Experiment 5 poor choice of span distances caused excessive bending about a centreline making the experiment unsuccessful.

In those laminations which produced considerable preferential bending it can be noted that the strains measured parallel to the axis of dominant bending attained a maximum at a load below failure, and decreased gradually thereafter (Experiments 1,2 and almost in 6, 7).

It would broaden the understanding of the method to know why preferential bending increased at the expense of unbending about the other centreline. Especially, since as deformation increased the points of contact moved down the ball bearings, Fig. 4.54.1, making bending about the preferential axis stiffer. This should have in principle reduced the dominant deformation.

The most probable reason to date to explain the behaviour is that the response is anticlastic. Unfortunately, little relevant information concerning anticlastic bending is available, and Timoshenko (18) only discussed the problem for isotropic plates. In fact, there are no solutions for the anticlastic bending in generally orthotropic laminates. It had been hoped that the non-linear analysis ACMBC would have provided the necessary information to dispel or otherwise the proposed cause of the bending behaviour.

Another possible factor which may contribute to the deformation comes from work by British Aerospace. They found that as composites deformed the nonlinearity of the material caused the twisting stiffnesses D16 and D26 to increase in importance. For the experiments here it is felt that the change to these stiffnesses was small, except near the centre at high loads. It is therefore concluded that this was only a minor contributor to the bending behaviour.

It should have become apparent that the central biaxial stresses were not constant due to the nature of specimen deformation. In all experiments the change in central stress ratio was gradual (only becoming prominent at large loads due to material nonlinearities), suggesting that the stress state remained constant in the linear load range.

4.5.2 Failure Mechanisms

Visible edge delamination was found in Experiments 1 and 2 (Fig. 4.14 and 4.26) as a result of central fibre failure and not because of edge effects. Together with several other experiments they provided considerable delamination in the central region as a result of central fibre failure, Fig. 4.32. This central area of delamination was not present prior to catastrophic failure since the measurements about the centre were continuous. Hence, the experiments show that delamination will not present a problem in the collection of data and that the method satisfies part of criterion (b), Chapter 1.

Fibre failure did not occur in Experiments 3 and 9 and only in the non-trimmed edges in Experiment 5. In each case the absence of fibre failure

was due to experimental difficulties. Table 4.11 and the respective 'Notes and Observations' present relevant information for the specimens which failed.

Fibre failure was always spontaneous and except in Experiments 2 and 8 occurred after approximately 1 minute of constant displacement. On occasions a load crack was heard just before the ultimate failure and, since all gauge measurements were continuous, it is suggested that the noise was due to adhesive failure in the tabs and not fibre failure.

The characteristics of the sustained surface damage indicate that failure must have started in the vicinity of the centre. This is a very important observation since it means that criterion (b) does hold for the plate bending method. The area and depth of failure (fibre and delamination) depended largely on the extent of preferential bending since the path followed the easiest route.

The resultant fibre and delamination failure was often extensive as can be visualised from the diagrams of surface damage in Experiments 1 (Fig. 4.14), 2 (Fig. 4.26), 4 (Fig. 4.32) 6 and 7 ('Notes and Observations'). Only experiments 1 and 2 were identical and their fracture patterns are, as expected, very similar. All the plates attained a final equilibrium position, at a load less than at fracture. But none suffered sufficient damage to render them non load bearing.

Tension-tension was the predominant mode of fibre failure. There are two reasons for the compressive failure found in Experiment 6. First, the experiment was the only one performed without a rubber pad beneath the

loading head. It is therefore likely that the metal indenter induced stress concentrations at its corners which prevented the outer laminae from deforming freely causing the compressive failure. To hopefully eliminate such a failure in future the rubber pad was always inserted.

Second, the plate had already undergone gross bending in Experiment 5 which had caused permanent but not visible damage to the laminate. This is backed by the fact that there is a large difference between corresponding measurements in similar Experiments 6 and 7 (Fig. 4.37 - 4.45).

Because of the factors concerning the compressive failure, Experiment 6 is not representative of the behaviour expected in the plate bending test.

For those specimens which failed initially in the outer lamina, the fibre strain varied from 1.1% to 1.5%, Experiments 1 (Fig. 4.12), 2 (Fig. 4.22), 4 (Fig. 4.30), 7 (Fig. 4.43). These surface strains were recorded by the central gauge and are expected to have been within 3mm of the point of initiation of fibre failure.

The two following factors unfortunately lower their relevance as fibre strains for strength predictions. Although failure started in the outer lamina there is no way of demonstrating if it started in the extreme fibres or not. It may have started at the boundary with the second layer and then progressed to the surface. Although the strain variation across the plate is known not to be ^{bc}linear, there must be a large strain drop across each ply and so the strain causing failure could be below that

measured. However since it is most likely that fibres experiencing the largest strains fail first it has been assumed that the central surface strains represent failure. Also it is known that criterion (c), Chapter 1, is only loosely held by the plate bending method since the actual volume of material experiencing the failure stress is small. Hence, the effect of point defects should not be ignored.

It is encouraging to find that the magnitude for the flexural fibre strain at failure is near the tensile values previously reported (139,140).

No visible damage was found after unloading Experiment 8, even though an extremely load^{up} snap just prior to unloading suggested fibre damage. To explain this, it is proposed that first fibre failure occurred in the second layer. The problem now is how to determine the central stresses when the strains causing failure cannot be determined. It is for this reason that laminates which produce internal fracturing will be very difficult to analyse, and pose a severe limitation on the method.

The experiments have not only demonstrated that providing parameters are sensible failure will start in the test section but that strain runaway is very important to the effectiveness of the method.

For the calculation of central biaxial stresses it is important that in a small area around the centre the transverse strain in the outer lamina exceeded its tensile failure of 0.7%. In fact, this strain was extremely large in Experiments 4 (Fig. 4.30), 7 (Fig. 4.43) and 8 (Fig. 4.48) and meant that there was extensive matrix breakdown along the fibre length and through the thickness. This suggests that at the point of

first fibre failure no material was present to transmit the transverse stress, thus offering a uniaxial state and stress.

The 16 layered cross-ply laminate in Experiment 8 (Fig. 4.46 - 4.49) can be taken to illustrate the effect strain runaway had on the deterioration of the outer layer. In the experiment the deformation made the central strain in the 0° direction, (outer ply orientation) much lower than in the 90° direction. The latter surface strain increased steadily with load to 1.3% at 1300N, and then runaway (Table 4.11 and Fig. 4.47 and 4.49). Just prior to fibre failure in the second layer the 90° strain exceeded the capability of the foil gauge, and the last instantaneous reading was 2.5% at 1650N.

It is of interest to note the relative values of the principal strains at failure since it leads to a new proposal for lamina breakdown under bending. In the experiment it was fortunate that after the 90° gauge had failed its 0° partner still operated. This was because the 0° gauge of the cross-ply had been placed nearest the surface when preparing the specimen, and shows that the breakdown of the 90° gauge was by the foil fracturing and not adhesive weakening.

When the 90° gauge broke its strain was 2.5% and the 0° gauge recorded only 0.6%. From strength tests the composite material has a matrix tensile strain at failure of 0.7% and a fibre flexural tensile strain in the region 1.3-1.5%. It is therefore apparent that the outer lamina (0°) was not going to fail first since the central fibre strain must have been much higher than 0.6% in the second layer. Failure occurred when the load was 2140N and the surface 90° strain was much $> 2.5\%$.

Now immediately before fibre failure the maximum fibre strain in the second lamina must have been below 1.5% or it would have already fractured. From which it is concluded that there must have been a strain drop across the outer-ply in excess of 1.0%. This suggests a new failure mechanism.

Fig. 4.54 illustrates the proposed strain distribution in the outer layers of Experiment 8. With this strain distribution the surface strain could be greater than 2.5% while at the same instance the fibre strain in the second lamina did not exceed 1.5%.

The emergence of the strain runaway also provided two further relevant factors to the work.

If linear strain distribution was applicable the matrix breakdown would have been present several layers deep in the tensile region about the centre, making the localised transverse modulus $E_{22} = \text{zero}$. This should then be taken into account when modelling the experiments by the F.E.M., but since the area of damage is known to be small the result of making $E_{22} = 0$ has not been assessed.

Deformation following the strain runaway indicates that the overall response has not been affected by the local matrix failure, since as a whole the laminate remained intact.

Attention now focuses on the major problem of determining the central biaxial stress ($\tau_{xy} = 0$) ratio in the plate bending method. Before outlining the two procedures which can predict the stresses, a definition

will be made for the directions in which the governing stresses act. The choice is between either the global directions of the plate or, if different, the principal directions of the lamina . The latter was chosen because this characterises first fibre failure.

The first procedure is the application of the C.P.T. and linear elasticity (but with reduced moduli to account for non-linearity) in the geometric non-linear finite element programme ACMBC.

This method would be the most suitable had it not been found unacceptable for the reasons given in Section 3.4. If the analysis had modelled the experiment, only the final load for any arrangement would have been needed to predict the governing biaxial stresses.

The second procedure is to take the measured strains in linear elastic formulae, which also allows for material non-linearity.

However, the observations made from the experiments have provided a number of factors which mean that either procedure will be inaccurate, notably:

The strain does not vary linearly through the thickness and the precise distribution is indeterminate.

If first fibre failure occurred in an internal ply the strains at the centre are unavailable.

The central surface strains are non-linear with load and on occasions difficult to measure.

The material moduli change during the loading and are indeterminate.

Under certain circumstances the central strain transverse to the fibres in the outer layer is likely to cause matrix breakdown, so providing a unidirectional stress state.

Collectively these factors mean that the evaluation of the central biaxial stresses in the plate bending method will be difficult. Hence, the work has demonstrated that criterion (a), Chapter 1 does not apply, and so presents the most significant disadvantage to the method providing relevant strength data.

5.0 Introduction

In Chapter 3 it was demonstrated that the linear programme ACM is capable of accurately representing the plate bending test. Results from the programme will now be compared against experimental measurements, from which several important modelling conditions will be established.

To make comparison simple, the gradients (strain $\mu\epsilon$ / unit load N) were determined from the measurements in the linear region of deformation. The initial gradients were also taken from the test to failure as these gave another good approximation. All values have been presented as the transverse displacements or strains due to a patch load of 100N, with the strain being that which acted in the extreme fibres of the tensile surface. It can also be noted that the measured strains were generally the sum of the bending and a much smaller axial component. Inherent errors in the analyses meant it was sensible to give the strains to the nearest whole number.

The source of experimental error was the variability of the plate thickness, causing the gauge to be out of position compared with the finite element model; the slight misalignment of the strain gauges; the drift in measuring devices whilst taking readings; and an inaccuracy in loading of some $\pm 5N$. These are all thought to have a small influence on the results.

The source of numerical error was the response due to shear

deformation, (subsection 3.3.2.2., assumptions 4,5,7 and 8), which was minimised through the sensible choice of experimental parameters; manufacturing defects,(assumptions 2,3 and 10); material properties; material non-linearities,(assumption 9); and that,due to the difference in the Young moduli in tension and compression, the neutral axis and mid-plane did not coincide,(assumption 11). The latter two factors which could be included in the analysis,(but with increasing computing effort) provided the largest source of concern and will be examined later.

Table 5.1 defines the various mesh constructions used in the comparisons.

5.1 Linear Displacement : Experimental-Numerical Comparison (ACM)

5.1.1 Standard Definitions For The Material Properties

In Section 4.1 it was stated that the precise values for lamina material properties in a laminate were not always available. To reduce the number of numerical models needed to discover if the experiments could be analysed with ACM a set of standard definitions for the material properties was beneficial. To achieve this with speed, it was decided to consider just one mesh, 1SHGE50, (Fig. 5.1.3).

To begin with the fundamental properties E_{11} , E_{22} , G_{12} , ν_{12} and t were taken as the typical measured values for the material system T300/Code 69, Table 4.1.

The numerical results are compared with Experiments 1 and 2 in Table 5.2. The nominal ply thickness $t = 0.127E-03$ m was used in models 1-6. Thereafter it was taken to be equal to the average ply thickness in Specimen 2.

An average for the two specimens would have been preferred, but due to its protective layer the average lamina thickness in specimen 1 was indeterminate.

In models 1-4 the longitudinal Young's modulus, E_{11} , was taken as the mean of the lamina tensile E_{11t} , and compressive E_{22c} . Thereafter, the ply thickness effect was involved through equation 4.1.

The transverse modulus, E_{22} , was taken to be one quarter of its mean tensile, E_{22t} , and compressive, E_{22c} , except in models 1, 11 and 12. For these remaining models it was taken to be some other portion of the mean. The rationale for choosing a quarter of the mean was that it had previously been applied in analytical solutions to fit the experimental data. In the case of the transverse modulus the thickness effect does not apply.

The shear modulus, G_{12} , was expected to remain constant in the linear deformation domain. Since it was not possible to determine the reduction known to occur in laminate manufacturing, the typically measured lamina value was generally taken.

The major Poissons ratio ν_{12} was taken as 0.3, except in model 10, where it was 0.25. This model showed that a reduction produced a slight increase in plate stiffness.

The comparison in Table 5.2 indicates that modelling the patch load with a vertical load only vector (V.L.O.) predicts values which are lower than those with a consistent load vector (C.L.V.) and that the latter are below the measured. In future all numerical models will employ a

consistent vector.

Since it was not a difficult task to produce a series of models with varying parameters that accurately represented the experiments, a set of standard definitions for the material properties was chosen from the 12 models. Model 7 allows for all material factors, except the known reduction in G_{12} , and provides the best fit with the measured values. Therefore the definitions for the material properties used in model 7 have been taken as the standard and will be used exclusively in all future numerical models. The set of standard definitions for the material properties are:

- † The ply thickness is the average plate thickness divided by the number of layers
- E11 The longitudinal Young's modulus is the mean of its tensile and compressive values scaled to take account of the reduction in ply thickness
$$E_{11} = \left[\frac{E_{11t} + E_{11c}}{2} \right] \times \frac{0.127E-03}{t}$$
- E22 The transverse Young's modulus is one quarter of its mean tensile and compressive values
$$E_{22} = \left[\frac{E_{22t} + E_{22c}}{2} \right] \times 0.25 = 0.2889E+10 \text{ N/m}^2$$
- G12 The shear modulus is the typical measured value
$$G_{12} = 0.5771E+10 \text{ N/m}^2$$
- ν_{12} The major Poissons ratio is the typical measured value
$$\nu_{12} = 0.3$$

5.1.2 Plate Modelling of Experiments 1 and 2

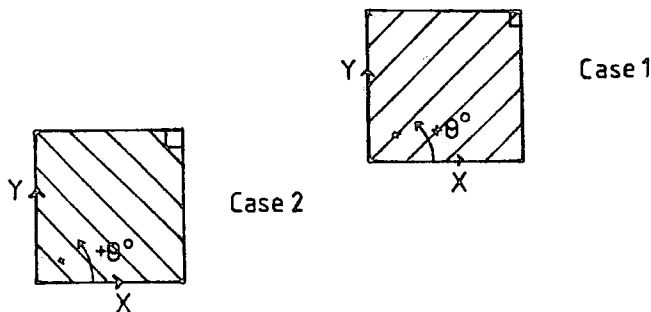
Once a standard set of material properties had been established, it was possible to investigate the accuracy of the different mesh types, as

introduced in subsection 3.3.4. The numerical results from four quarter plate, two half and a full plate mesh as defined in Table 5.1 are compared with Experiments 1 and 2 in Table 5.3.

The range in the calculated values are from model 2 ($.336E-03m$, $145\mu E$, $183\mu E$) to model 7 ($.340E-03m$, $160\mu E$, $201\mu E$) with the exact representation model 11 (full plate mesh with no quarter plate boundary conditions) in the middle.

With the quarter plate models it was possible to simply reverse the orientations of all the $+45^\circ$ and -45° laminae to produce the two distinct modelling cases shown below.

Fig 5.1



Case 1 which has been generally taken gives values which are always higher than those with case 2 and shows the detrimental effect of imposing quarter plate boundary conditions. However it was found that the mean of the two models provides similar results to the exact model. This indicates that the detrimental responses cancelled and that for this particular lamination configuration the contribution of the twisting components to bending were small.

If the $\pm 45^\circ$ orientated laminae were reversed in the half plate models

no difference in the values was found. A similar observation can be made with the full plate models.

As the variation between the models is less than 9% the inclusion of quarter plate boundary conditions are not important with this lamination configuration. Any of the mesh types could be chosen to predict the linear behaviour with good accuracy. But, it would appear sensible to take the average of several different models for the most realistic analysis.

5.1.3 Overall Modelling Of Experiments 1 And 2

To provide further relevant modelling information nearly all the strain and transverse displacement measurements will now be compared with the equivalent numerical. To enable this comparison meshes constructed with a lot of elements were needed.

Numerical results (applying the data presented in Table 5.3) from the four meshes illustrated in Fig. 5.1.1-4 are compared with Experiments 1 and 2 in Table 5.4. The four meshes have been drawn so that with Fig. 4.11 and 4.15 the nodal positions corresponding to the strain and dial gauges can be readily found. Except where noted the measured strains are the surface values which were the result of bending and in-plane (much smaller) components.

For the quarter plate models the average numerical values from the two quarter plate representations (cases 1 and 2) have been presented in the middle. Underneath the mean is the value due to modelling case 2

and above the value due to modelling case 1. If two strain values at a node have been written next to each other, it was because the calculation of that strain by surrounding elements differed, and the mean has been taken.

Collectively, the four models predict the measured response with good accuracy. The calculated transverse displacements and strains are always below that measured, with a maximum difference of 12%.

Mesh 1SQE100 which is the most refined does not give improved accuracy over the coarser meshes and was only included because it has sufficient elements to enable all the measurements to be compared.

The good accuracy does not depend on the position in the plate which implies that the numerical modelling for the patch load and the supports are not critical to the solution, as was noted for point loading examples in subsection 3.3.1. The comparison also shows that the difference between the numerical and experimental results are very similar in both principal directions of the outer lamina. This suggests that the true ratio of E_{11}/E_{22} must be similar to that obtained from the standard material properties.

5.1.4 Central Biaxial Stresses

The experiments illustrated a number of difficulties which prevented the accurate evaluation of the governing central biaxial stresses in the lamina providing first fibre failure, and hence the required strength data. For this reason the stresses reported from the linear and non-linear

analyses are known to be unrealistic. The relative change between linear numerical models (ACM) will however give some idea to the change in central biaxial stresses possible with the plate bending method. To illustrate the range of stress ratios with the lamination used in Experiments 1 and 2 the following examples were examined:

Fig. 5.2 Altering the position of the point supports (but maintaining symmetry) with a constant patch load area, $\frac{A_p}{B_p} = 1$ and plate dimensions $\frac{A}{B} = 1$,

Fig. 5.3 Altering the dimensions of the plate A and B and hence the span distances A_s and B_s with a constant load area $\frac{A_p}{B_p} = 1$.

For both examples the quarter plate mesh 1SQGE100 was used. In Fig. 5.2 the support positions chosen can be seen with reference to Fig. 5.1.4. The values given in Fig. 5.3 were determined by altering the distances illustrated on the plan. A limit was imposed on the maximum side lengths A and B above which it was felt the plate may just slip through the supports, as found in Experiment 5.

The numerical models employed the standard material properties and so E22 was reduced due to thermal cracking caused in manufacturing. Therefore the calculated surface central biaxial stress ratio $\frac{\sigma_y}{\sigma_x}$ was always high.

The plots indicate that by altering these particular geometric parameters the ratio is altered by over 4 times. This factor will be increased once the two effects are combined and other practical changes as defined in Section 2.2 are included.

This simple investigation suggests that the maximum range in the tensile biaxial stress ratio σ_y/σ_x , with $\tau_{xy}=0$, for this particular lamination will be about $10/1$. What effect on the central stresses the nonlinear deformation has could be considerable and requires either numerous experiments or an accurate nonlinear numerical analysis to answer.

Comparing with the biaxial methods studied by Pipes and Coles(4) ($15/1, \tau_{xy}=1$) the plate bending method should provide a similar range in biaxial stress ratios. However unlike the tubular method no compression-tension results are available.

From this investigation it would appear that criteria (d), Chapter 1 will be satisfied by the plate bending method.

5.1.5 Plate Modelling

Subsection 5.1.2 showed that the four mesh types accurately predicted the bending measured in Experiments 1 and 2. By involving the other experiments in an identical analysis those lamination configurations when quarter plate boundary conditions are unacceptable will be established. Then a full plate model (Fig. 3.10.4) will be the single model that represents the linear deformation and a nonlinear solution will not be possible due to computing limitations.

Tables 5.5 - 5.9 have been constructed along the same lines as Table 5.2. The standard set of material properties follow the definitions in subsection 5.1.1. and the meshes are defined in Table 5.1.

As before, central surface strains and transverse displacements were determined from measurements made in the linear (embedding) load range, and an approximation due to the initial gradient of the test to failure. When the values differed considerably both have been reported, otherwise the mean is given.

In Experiments 3,4,5,6,7 and 9 the outer lamina was orientated at $+45^\circ$ to the global axes and the programme (ACM) only predicts the strains in the global directions. To predict the strain parallel and perpendicular to the fibres Mohrs strain circle technique was used to evaluate the $\pm 45^\circ$ strains. This was justifiable because the strain and stress variation with rotation are defined by second order Tensor vectors (3). The strain values are given by:

$$\epsilon_{\pm 45} = \frac{\epsilon_x + \epsilon_y}{2} \pm \gamma_{xy} \quad 5.1$$

where $\gamma_{xy} = 0$ at the centre.

The following observations were made from the comparisons in Tables 5.5 - 5.9.

Quarter plate models are not accurate for Experiments 5,6,7 and 9 nor are half plate models for Experiment 9. Good accuracy is possible for Experiments 5,6,7 by taking the average of the two distinct quarter plate models (cases 1 and 2). These Experiments also show that the number of nodes used in the patch loading has little effect on the accuracy. Only Experiment 9, whose lamination is very anisotropic requires a full plate model for accuracy.

Except for Experiments 3 and 4 all numerical values are lower than

measured and the relevant models from the rest illustrate that the differences are generally less than 10%. Hence, the comparisons show emphatically that the experiments are modelled by the linear analysis ACM to sufficient accuracy.

Furthermore, the values predicted for Experiments 3 and 4 (Table 5.5) can be brought into agreement with the other experiments if the protective layer is included in the average ply thickness. The comparisons also show that Mohrs strain circle technique will determine the strain at any orientation.

In subsection 3.3.4 the idea of taking the relative size of the stiffness ratios D_{11}/D_{16} and D_{22}/D_{26} as a measure of the twisting behaviour was introduced.

Table 5.10 presents the ratios, together with D_{11}/D_{66} for the five laminations tested. With reference to the corresponding tables it can be seen that when D_{11}/D_{16} and D_{22}/D_{26} are above 50 all models are accurate, and that when the ratios are below 20 they are not. However there are not sufficient lamination configurations to be more precise.

5.1.6 Overall Modelling of Experiment 7.

It has already been shown that the bending in Experiments 1 and 2 can be accurately predicted by the programme. The ability of ACM to accurately predict the deformations throughout the specimens can be enhanced by repeating the modelling of the remaining experiments. Models for Experiment 7 will now be presented since the results provide several

new observations. Table 5.11 presents the comparison, Table 5.1 defines the mesh constructions and Diagram 4.41 displays the gauge positions.

The comparison shows that the numerical values are distributed evenly on either side of those measured, as a consequence of the fact that plate modelling is now important. This observation was anticipated since the ratios D_{11}/D_{16} and D_{22}/D_{26} are relatively small implying that the distinct meshes would provide a greater spread in results than for the lamination in Experiments 1 and 2. Fortunately, the twisting components are not too large and the average of the two quarter plate models are within 10% of those measured, except at a few points.

Again Mohrs circle technique provides a good prediction of the $\pm 45^\circ$ strains, but the differences between these and the measured are greater than in the global directions.

The results also show through gauges 9 and 11 that the numerical analysis accurately determines the bending near the free edges. The numerical values had to be determined using linear interpolation since there were no nodes at the gauge positions. This approximation was acceptable in the free edge region since the strain gradients are nearly linear. It is also of interest to note that both analyses established that the lower surface strains near the free edges were compressive.

5.2 Large Displacement : Experimental-Computation Comparison (ACMBC-modified)

It is of interest to this work to examine the modelling ability of

the geometric nonlinear finite element programme ACMBC for one of the experiments, even though it is inaccurate. Experiments 1 and 2 were again analysed using the modified version of ACMBC. Table 5.12 presents the numerical central displacements and strains with the corresponding measurements at several loads. In establishing the five convergent solutions 970s of C.P.U. time were required with the quarter plate mesh 1SQGE36 (Fig. 5.3.2).

Obviously a critical comparison is out of the question since the scale factors introduced into the ACMBC analysis, Section 3.4, have not yet been shown to be universal. However, the results do permit several important observations.

As with the isotropic test examples analysed in Section 3.4 with the unmodified ACMBC analysis the laminate appears stiffer than that recorded experimentally. In fact, at 3600N the central transverse displacement is only half that measured. The modelling suggests that a careful inspection of the deformation throughout the plate would demonstrate that the bending is characteristic of that found in the simple isotropic examples (Fig. 3.13.2) with the unmodified ACMBC analysis.

The comparison also shows that the difference between strains are much lower than for displacements and that if numerical trends are extended there will be no evidence of preferential bending.

If the reasons for the inaccuracy are found to be the same as for the isotropic examples then axial strains presented in Table 5.12 will be lower relative to the bending. This leads to the important conclusion that the

linear bending programme ACM will be accurate when modelling the experiments for a maximum central transverse displacement equal to the plate thickness.

Although the geometric nonlinear finite element analysis constructed cannot be shown to model the experiment, the above does indicate that computing limits are critical to further development. Here a simple construction, with efficient storage and solution techniques, needed most of the 1000s C.P.U. time to determine the bending up to half the failure load. Therefore, further development should concentrate on reducing the computing effort with, at the same time, improved accuracy.

5.3 Numerical Assumptions

The assumptions applied in the formation of ACMBC were introduced in subsection 3.²3.2.2. When designing the experiment care had ensured that assumptions 4,5,7 and 8 held and so the effects of shear deformation and shear stresses could be eliminated from the numerical analysis.

Other assumptions, notably 2,3 and 10 were dependent on the quality of the manufactured laminates. Obviously the specimens were not perfect but it has been assumed that the errors thus introduced were negligible.

Two of the remaining assumptions, namely 9 and 11, could have been involved in the programme and the errors thus omitted from the numerical analysis may reduce the relevance of the numerical comparison .

5.3.1 Material Nonlinearities - Assumption 9.

It has already been stated in Chapter 4 that the moduli E_{22} and G_{12} are nonlinear with strain. The experiments demonstrated that certain laminates contained considerable tensile matrix breakdown around the centre, thus causing E_{22} to become zero. Due to the complex deformation experienced by the laminates in the plate bending test it would be difficult to assess the instantaneous changes in these moduli so their involvement in the numerical analysis is not sought.

It is therefore fortunate that the following factor means that the changes in E_{22} , (except when $E_{22} = 0$) can be neglected.

The nature of the bending means that the strain in the plies about the mid-plane are relatively small compared to the surface. Together with the experimental observation that the surface strain decreases rapidly from the centre to the free edges a change in the modulus will only occur in the outer plies around the centre. Hence except at the centre where complete matrix failure at high loads can occur, the analysis does not have to include the small nonlinearity of E_{22} .

The nonlinearity of the shear modulus, G_{12} , with warping strain, δ_{12} is much more severe. Fig. 4.1 shows that G_{12} decreases substantially with warping stress τ_{12} . The above factor also applies in the determination of the variation throughout the specimen. But the situation is made more difficult since there is no other way of predicting values of δ_{12} , than via the programme, and the analysis is known to be less accurate in determining warping strains than principal strains.

Had ACMEC analysed the experiment accurately the results could have been applied to discover if the shear modulus nonlinearity required involvement. If inclusion was found to be necessary a correction procedure would be needed and the work of Petit and Waddoups (141), Hahn and Tsai (142), Hahn (143), Jones and Morgan (144) and Ditcher, Rhodes and Webber (145) will be of benefit. There would be a drawback if this nonlinearity requires involvement in the numerical work, since it would increase computing time and storage requirements. Further iterations would be necessary for the geometric and material nonlinear solution, so less information would be obtained in the time limit imposed.

5.3.2 Position Of The Neutral Axis - Assumption 11.

Throughout the numerical work presented here, the laminates have been taken as exactly symmetrical, with the layers below the mid-plane possessing geometric and material properties identical to those of corresponding layers above. This assumption means that the terms in matrix $[B]=0$ (3) and that there is no coupling between bending and extension in deformation.

If the moduli are different in tension and compression the laminate properties are not symmetrical about the mid-plane and coupling between bending the extension will exist. Table 4.1 shows that the composite material T300/Code 69 has compressive Young moduli which are 7% and 10% higher than the respective longitudinal and transverse tensile moduli. These differences mean that the neutral axis and the mid-plane do not coincide in the laminates tested, even before the onset of bending deformation. For this reason assumption 11 may not hold. In principle the shift in the neutral axis will be seen as making the terms in $[B] \neq 0$

forcing the linear response to differ from that assumed.

To predict the distance by which the neutral axis was shifted in the specimens from the mid-plane the simple strip analysis constructed by Jones and Morgan (146) was applied. They formulated an iterative procedure which determined the exact location of the neutral axis of a simply supported cross-ply strip with a uniform load. Development of the 1-D analysis enabled generally orthotropic laminates to be solved and a Fortran IV programme was written to solve the equations.

A 2-D analysis was unfortunately not possible due to the complexity of the problem; the basic difficulty being that the differences in the moduli leads to two neutral axes (in the global directions) instead of a single neutral surface of conventional plate theory. Hence, the strip analysis was performed in both the X-Z and Y-Z planes to give an indication of the movement in the global directions.

Table 5.13 gives the shift of the neutral axis in the specimens as a percentage of the average plate thickness. The movement is always into the upper (compressive) portion and is approximately 1% of the average plate thickness. The ensuing terms in [B] provide minute coupling terms which can be ignored. The shift does however slightly alter the values of the surface strains from those calculated by classical theory. A 1% movement into the upper half causes the surface compressive strains to be 2% lower and vice versa for the surface tensile strains. This is very encouraging since it suggests that the error introduced in the numerical comparison can be neglected.

CHAPTER 6.0 CONCLUSIONS

A new biaxial test procedure, the 'plate bending method', has been investigated for thin multi-layered generally symmetrical laminated plate structures. Four criteria for a satisfactory biaxial stress test, identified in Chapter 1, have been investigated with respect to the method. A number of experiments have been performed to determine the applicability of the criteria. A classical 2-D finite element thin plate analysis has been developed to predict the stresses generated. The following conclusions may be drawn from the experimental observations and subsequent numerical comparison.

6.1 The Feasibility Of The 'Plate Bending Method'.

- (i) From this work criterion (a), which states 'The state of stress throughout the test section should be uniform and determinate', cannot be shown to hold for the method. Although the stress state is approximately constant within the volume of the test section the stresses are indeterminate at large deformations. This indeterminacy stems from experimental observations that the lamina providing first fibre failure, and its neighbours, experience complex deformation in the region of the test section. This is a severe obstacle to accurate calculation of stress since it is difficult to evaluate the material properties with sufficient accuracy.
- (ii) Criterion (b), which states 'Failure of the specimen should initiate in the test section so that static strength will be obtained' is applicable. It was noted that with certain

experimental parameters the criterion may be broken as edge effects could become large and cause damage.

- (iii) Criterion (c), which states 'The test section over which the stresses will be uniform should provide a volume of material large enough to eliminate the effects of point defects and hence make the data significant' was assumed to hold for the method since the volume required to eliminate the effects of point defects is unknown.
- (iv) Criterion (d), which states 'The test should be capable of providing a varied combination of stress states in the material' was the hardest to assess. First, too few experiments were performed to be able to provide a guide to the range of biaxial stress ratios obtainable. Second, the nonlinear numerical analysis was inaccurate, so different arrangements could not be evaluated. From reliable linear results the test method will provide a range of biaxial stress ratios of the order ($\max \frac{\sigma_1}{\sigma_2} = 10, \tau_{xy} = 0$).

6.2 Observed Failure Mechanisms

- (i) All the specimens deformed with preferential bending about a centreline. In certain cases there was a continuous growth in the tensile surface strain transverse to the fibres in a small area about the centre. The localised effect measured under constant transverse displacement is known as 'strain runaway'. The severe matrix failure that this implies means there was a uniaxial state of stress in the fibre direction where the governing biaxial stresses are determined.

- (ii) Occurrence of strain runaway in the 16-layered cross-ply plate, in conjunction with first fibre failure in the second layer, has led to the proposal of a new failure mechanism (Fig.4.54.2). At large deformations the strain runaway (which was in the direction of first fibre failure) exceeded the capacity of the foil gauge, with a last instantaneous reading of 2.5%, some time before fibre failure. Since the extreme fibre strain in the second layer could not have been greater than 1.6%, without fibre failure, there must have been a 1% drop in strain across the outer lamina. The figure shows that there was severe matrix cracking through the outer ply, which became wedge shaped to accommodate the high surface strain.

6.3 The Validity Of The Finite Element Analysis To Model The Plate Bending Method

6.3.1 Linear Analysis, ACM

- (i) Numerical comparison demonstrated that the linear analysis accurately predicts deformation, strains and stresses in the experiments to within $\pm 10\%$. Accuracy was restricted to those cases when the standard values for lamina material properties, ($E_{11}, E_{22}, G_{12}, \nu_{12}$ and t) were used, the effect of the twisting stiffnesses D_{16} and D_{26} were allowed for in the modelling and the central transverse displacement, w_c , did not exceed the plate thickness.
- (ii) Effects of shear stresses, nonlinearity of material properties

and exact position of the neutral axis were examined. Their individual effects on the accuracy were small.

- (iii) Greater concern was felt over the error introduced by the omission of shear deformation. A literature research revealed only one promising analytical technique which could be developed to analyse the laminates tested. This high order method broke down for generally orthotropic plates so shear deformation could not be evaluated. Comparison between ACM, several shear flexible elements and exact solution suggested that shear deformation in the experiments will be insignificant providing the span to thickness ratio S is greater than 30.

6.3.2 Nonlinear Analysis, ACMBC

- (i) The basic nonlinear analysis was inaccurate when modelling simple isotropic test examples for the following:

To omit numerical integration techniques in the evaluation of the stiffness coefficients a new definition for the terms in matrix $[H]^e$ (Equ.3.44) was applied. As yet limitation of this definition are not fully realised. Comparing the numerical results with exact analytical solutions has suggested the relative magnitudes of bending and in-plane stiffness terms were incorrect. Numerical models predicted transverse displacements, w , and bending stresses (σ_b), to be too small, and in-plane (σ_{pl}) stresses to be too large near the centre, with the reversed situation near the free edges.

- (ii) Accuracy was improved after introducing scaling factors to

the terms in $[H]^e$ and in evaluating in-plane stiffness coefficients. This modified version of programme ACMBC was inaccurate when analysing the experiments and so scaling factors are thought not to be universally applicable.

- (iii) The importance of persisting with this numerical approach is that the computing effort, although large, was reasonable for the size of the problem undertaken. This appears not to be the case for other nonlinear finite element analyses. This indicated that further development will always be restricted by the computing power available. This limitation may become more pronounced if the approach in ACMBC needs the involvement of shear deformation, material nonlinearities, the exact position of the neutral axis, and the extent of matrix failure prior to first fibre failure for the accurate determination of stresses generated.

CHAPTER 7 FUTURE WORK

The work done in this thesis has laid the foundations for further research on the application of the plate bending method and the analysis of carbon fibre reinforced plastic plates subjected to load. In particular the following areas require more examination.

- (i) The stress in the test section must be established accurately. This is the only way in which the method will be shown to be reliable and accurate in the determination of biaxial strength data. The calculation of the stress field will certainly involve a numerical analysis so the true laminations of ACMBC to analyse laminated structures must be realised.
- (ii) If the ideology of the analysis used in ACMBC is found to be incorrect a critical comparison with other finite element methods should be made. This will be of great benefit to the development of composite structures since it would establish the limits of numerical methods to the solution of structural problems.
- (iii) If the indeterminacy of stresses of the plate bending method can be resolved, then work should be done to discover if the test can provide reliable strength data after the laminates have been subjected to damage. Since, if these results are found to be acceptable, the test will present the aerospace designer with an extremely useful tool.
- (iv) The experiments showed that all the laminates deformed with preferential bending about a centreline, and that in several cases there was a large dynamic growth in strain perpendicular to the fibres near the tensile surface in the test section.

These two observations require further examination so that they can be quantified for the plate bending method.

- (v) A series of experiments should be performed with specimens having different lamination configurations (but the same composite material) to establish the limiting values for the ratios D_{11}/D_{16} and D_{22}/D_{26} which indicate when the finite element models can apply quarter plate boundary conditions without loss in accuracy. With these limiting ratios only the lay-up arrangement of laminates would be required to ascertain if the plate can be modelled with quarter and half plate models, thus saving time.

REFERENCES

- 1 LUBIN, G. Handbook of Fibreglass and Advanced Plastic Composites. Van Nostrand-Reinhold (1969) p.894
- 2 NOYES, J.V. 'Composites in the Construction of the Lear Fan 2100 Aircraft'. Composites Vol.14 No.2 (April 1983) pp.129-139
- 3 ASHTON, J.E., HALPIN, J.C. and PETIT, P.H. 'Primer on Composite Materials : Analysis' Technomic (1969) p124
- 4 PIPES, R.B., COLE, B.W. 'Filamentary Composite Laminates subjected to Biaxial Stress Field' Report AFFDL-TR-73-115 (March 1970 August 1973 June 1974) p412
- 5 GOLDENBAT, I.I., KOPNOV, V.A. 'Strength of glass-reinforced Plastics in Complex Stress State' Mekanika Polimerou Vol.1 (1965) p.70 English Translation - Polymer Mechanics Vol.1 (1966)
- 6 HOFFMAN, O. 'The Brittle Strength of Orthotropic Materials' J. Comp. Mater. Vol.1 (1976) pp.200-206
- 7 BERT, C.W., MAYBERRY, B.E., BAY, J.P. 'Behaviour of Fibre Reinforced Elastic Laminates under Biaxial Loading' Composite Materials : Testing & Design ASTM-STP 460 (1969) pp.362-380
- 8 DOREY, G. 'Fracture Behaviour and Residual Strength of Carbon Fibre Composites subjected to Impact Loads' AGARD CP-163 (October 1975) Strength & Fracture Section Materials Department R.A.E.
- 9 KAEBLE, D.H., DYNES, P.J., CRANE, L.W., MAUS, L. 'Kinetics of Environmental Degradation in Graphite-epoxy Laminates' Composite reliability ASTM STP 580 (1975) pp.247-262
- 10 NAHAS, M.H. 'Failure of Laminated Fibre Reinforced Composite Structures Subjected to Combined Loadings' Ph.D Cranfield Institute of Technology p.406 (1980)
- 11 SODEN, P.D., LEADBETTER, D., GRIGGS, P.P., ECKOLD, G.C. 'The Strength of a Filament Wound Composites under Biaxial Loading' Composites Vol.9 No.9 (October 1978) pp.247-250
- 12 WHITNEY, J.M., PAGANO, N.J., PIPES, R.B. 'Design and Fabrication of Tubular Specimens for Composites Characterization' Composite Materials: Testing & Design (2nd Conf) ASTM STP 479 (1971) pp.52-67

- 13 RICHARDS, G.L. 'Off-Axis Coupon Testing' J. Comp. Mater.
AIRHART, T.P., Vol.3 No.3 (July 1969) pp.586-589
ASHTON, J.E.
- 14 KAMANSKI, B.E., 'Development of Engineering Data for Advanced
LEMON, G.H., McKAGUE, Composite Materials' Tech. Report. AFML-TR-
E.L. 70-108 Vol.1 Static & Thermophysical (October
1972) pp.1-464
- 15 BERT, C.W., MAYBERRY, 'Behaviour of Fiber Reinforced Elastic
B.L., BAY, J.D. Laminates under Biaxial Loading' ASTM STP 460
(1969) pp.362-380
- 16 CHOW, C.C. 'Stress and Strain States in Elliptical
Bulges' Metal Transaction (January 1949)
- 17 RUSHTON, K.R. 'Simply Supported Plates with Corner Free to
Lift' Jour. of Strain Analysis Vol.4 No.4
(1969) pp.306-311
- 18 TIMOSHENKO, S., Theory of Plates and Shells' Engineering
WOINOWSKY-KRIEGER, S. Societies Monographs 2nd Ed. McGraw Hill (1950)
- 19 TURNER, M.J. CLOUGH, 'Stiffness and Deflection Analysis of Complex
R.W., MARTIN, H.C., Structures' J.Aero.Sci. 23 (1956) pp.805-823
TOPP, I.J.
- 20 CLOUGH, R.W. 'The Finite Element in-Plane Stress Analysis'
Proc. 2nd. A.S.C.E. Conf. on Electronic
Computation, Pittsburg, Pa. (September 1960)
- 21 TIMOSHENKO, S. 'Theory of Plates and Shells' 1st Edition
McGraw Hill, New York, (1940),
- 22 REISSNER, E., 'Bending and Stretching of certain types of
STAVSKY, Y. Heterogeneous Anisotropic Elastic Plates'
J. Appl. Mech. Trans. Am. Soc. Mech. Engrs.
(1961) pp.402-
- 23 KIRCHOFF, G. 'Über Das Gleichgewicht und die Bewegung einer
elastischen Scheibe' J. für reine und Angewandte
Mathematik Vol.40 (1850) pp.51-88
- 24 FUNG, Y.C. 'Foundation of Solids Mechanics' Prentice Hall
Inc. Englewood Cliffs, New Jersey (1965)
- 25 ROCKEY, K.C., EVANS, 'The Finite Element Method' A basic Introduction
H.R., GRIFFITHS, D.W., to Engineers. Crosby Lockwood Staples. Granada
NETHERCOT, D.A. Publishing (1970)
- 26 ADINI, A., CLOUGH, 'Analysis of Plate Bending by the Finite Element
R.W. Method and Report' Nat. Sci. Foundation U.S.A.
G.7337 (1961)

- 27 MELOSH, R.J. Basic Derivation of Matrices for the Direct Stiffness Method' J. AIAA (1963) 1 pp.1631-1637
- 28 ZIENKIEWICZ, O.C. The Finite Element Method in Engineering Science' McGraw Hill London (1971)
- 29 BREBBIA, C., CONNOR, J. Geometric Nonlinear Finite Element Analysis' J. of the Eng. Mechanics. Div.Proc. of Am.Soc. Civil Eng. (1969) pp.463-483
- 30 ROBERTS, T.M., ASHWELL, D.G. The Use of Finite Element Mid-Increment Stiffness Matrices in the Post-buckling Analysis of Imperfect Structures' Int.J. Solids Structures (1971) Vol. 7 pp.805-823
- 31 TOCHER, J.L. Analysis of Plate Bending Using Triangular Elements' Ph.D. Thesis. Dept. of Civil Eng., Univ. of California, Berkeley (1962)
- 32 WALZ, J.E., FULTON, R.E., CYRUS, N.J. Accuracy of Convergence of Finite Element Approximations' Proc. of 2nd Conf. on Matrix Methods in Structural Mechanics AFFDL-TR-68-150 Wright Patterson AFB Ohio pp.995-1025
- 33 CLOUGH, R.W., TOCHER, J.L. Finite Element Stiffness Matrices for Analyses of Plate Bending' Conf. on Matrix Meths. on Structural Mechanics, Wright Patterson Air Force Ohio, (Oct.1965) AFFDL-TR-66-80 pp.515-546
- 34 CLOUGH, R.W., FELLIPA, C.A. A Refined Quadrilateral Element for Analyses of Plate Bending' Proc. of 2nd Conf. on Matrix Methods in Structural Mechanics AFFDL-TR-68-150 Wright Patterson AFB Ohio pp.399-440
- 35 BELL, K. A Refined Triangular Plate Bending Element' Inter. Jour. for Numer. Methods in Eng.g. Vol.1.No.1 (Jan.1969) pp.111-122
- 36 BOGNOR, F.R., FOX, R.L., SCHMIT, L.A. The Generation of Interelement Compatible Stiffness and Mass Matrices by the use of the Interpolation Formulas' Conf. on Matrix Meths. in Structural Mechanics, Wright Patterson Air Force Base, Ohio. (Oct.1965) AFFDL-TR-66-80 pp.397-443
- 37 PIAN, T.H.H., TONG, P. Rationalization in Deriving Element Stiffness Matrix by Assumed Stress Approach' Proc. 2nd Conf. on Matrix Methods in Structural Mechanics Wright Patterson Air Force Base, Ohio. AFFDL-TR-68-150 pp.441-471
- 38 MAU, S.T., TONG, P., PIAN, T.H.H. Finite Element Solutions for Laminated Thick Plates' Jour. Comp. Mater. Vol.6 (April 1972) pp.304-311

- 39 ARGYRIS, J.H., BUCK, 'Some New Elements for Matrix Displacement
K.E., FRIED, I., Methods' 2nd. Conf. on Matrix Methods in
MARECZEK, G., SCHARFE, Structural Mechanics. Wright Patterson Air Force
D.W. Base, Ohio AFFDL-TR-68-150 pp.333-399
- 40 HINTON, E., SALONEN, 'A Study of Locking Phenomena in Isoparametric
E.M., BICANIC, N. Elements' 3rd MAPELAP Conf. Brunel University,
Uxbridge (1978)
- 41 SPILKER, R.L. 'A Hybrid Stress Quadratic Serendipity
MUNIR, N.I. Displacement Mindlin Plate Bending Element'
Solids & Structures Vol.12 (1980) pp.11-21
- 42 PAGANO, N.J. 'Exact Solution for Composite Laminates in
Cylindrical Bending' J.Comp. Mater. Vol.3
(1969) pp.398-409
- 43 WHITNEY, J.M. 'Effect on Transverse Shear Deformation on the
Bending of Laminated Plates' J.Comp. Mater.
Vol.3 (1969) pp.534-547
- 44 REDDY, J.N. 'A Penalty Plate Bending Element for the Analysis
of Laminated Anisotropic Composite Plates'
Int.Jour. for Numer. Methods in Eng.g. Vol.15
(1980) pp.1187-1206
- 45 PRYOR, C.W. Jr., 'A Finite Element Analysis Including Transverse
BARKER, R.M. Shear Effects for Applications to Laminated
Plates' J.AIAA Vol.9 (1971) pp.912-917
- 46 MAWENYA, A.S., DAVIES, 'Finite Element Bending Analysis of Multilayered
J.D. Plates' Int. J.Num. Methods in Eng.g Vol.8
(1974) pp.215-225
- 47 PANDA, S.C., 'Finite Element Analysis of Laminated Composite
NATAPAJAN, R. Plates' Int.J.Num. Methods in Eng.g Vol.14 (1979)
pp.69-79
- 48 NOOR, A.K., MATHERS, 'Anisotropy and Shear Deformation in Laminated
M.D. Composite Plates' J.AIAA Vo.14 (1976) pp.282-285
- 49 NOOR, A.K., MATHERS, 'Finite Element Analysis of Anisotropic Plates'
M.D. Int.J.Num. Methods of Eng.g Vol.11 (1977)
pp.289-307
- 50 GALLAGHER, R.H. 'Finite Element Analysis of Geometrically Non-
linear Problems' Theory & Practice in Finite
Element Structural Analysis ed. YAMADA. (1973)
Sem 74/32064/ pp.109-125
- 51 LEVY, S. 'Bending of Rectangular Plates with Large
Deflections' NACA TRN 737 (1942)
- 52 WANG, C.T. 'Nonlinear Large Deflection Boundary Value
Problems of Rectangular Plates' NACA TN 1425
(1948)

- 53 BERGER, H.M. 'A New Approach to the Analysis of Large Deflection of Plates' Jour. of Applied Mechs. (1955) pp.465-472
- 54 RUSHTON, K.R. 'Large Deflection of Plates with Initial Curvature' Int.J.Mech.Sci. (1970) Vol.12 pp.1037-1051
- 55 MAU, S.,
GALLAGHER, R.H. 'A Finite Element Procedure for Nonlinear Pre-buckling and Initial Postbuckling Analysis' NASA CR-1936 (Jan. 1972)
- 56 ODEN, J.T. 'Numerical Formulation of Nonlinear Elasticity Problems' Proc. Am.Soc. Civ. Eng.g 93 ST3 (1967) pp.235-255
- 57 HOFMEISTER, L.D.,
GREENBAUM, G.,
EVENSON, D. 'Large Strain Elastic Plastic Finite Element Analysis' J. AIAA Vol.9 No.7 (July 1971) pp.1248-1254
- 58 RICHTMEYER, R.D.,
MORTON, K.N. 'Difference Methods for Initial-Value Problems' Interscience, New York, (1967)
- 59 TURNER, M.J., DILL,
E.H., MARTIN, H.C.,
MELOSH, R.J. 'Large Deflections of Structures subjected to Heating and External Loads' Jour. of Aerospace Sci. Vol.27 (February 1960) pp 97-106
- 60 ODEN, J.T., SATO, T. 'Finite Strains and Displacements of Elastic Membrane by the Finite Element Method' Inter. Jour. of Solids & Structures Vol.3 (1967) pp.471-488
- 61 MARTIN, H.C. 'On the Derivation of Stiffness Matrices for the Analysis of Large Deflection and Stability Problems' Conf. on Matrix Meths. in Structural Mechs. Wright Patterson Air Force Base, Ohio (1965) AFFDL-TR-66-80 pp.697-716
- 62 PRATO, C. 'A Mixed Finite Element for Thin Shell Analysis' Ph.D Thesis, Dep. of Civil Eng.g Massachusetts Inst. of Tech. (May 1968)
- 63 SCHMIT, L.A., BOGNER,
F.K., FOX R.L. 'Finite Deflection Structural Analysis using Plate and Cylindrical Shell Discrete Elements' Proc. AIAA/ASME 8th Structures/Structural Dynamics & Materials Conference, Palm Spring, California (29-31 March 1967) pp197-211
- 64 GALLAGHER, R.H.,
PADLOG, J. 'Discrete Element Approach to Structural Stability Analysis' J. AIAA Vol.1 No.6 (June 1963) pp.1437-1439
- 65 MARGUERRE, K. 'Zur Theorie Der Gekrümmeten Platte Grosser Formänderung' Proc. 5th Int.Cong.Appl.Mech. (1938) pp 93-101

- 66 KAWAI, T., YOSHIMURA, N. 'Analysis of Large Deflection of Plates by the Finite Element Method' Int. Jour. for Num. Methods in Eng.g Vol.1 (1969) pp.123-133
- 67 GREENE, B.E. 'Stiffness Matrix for Bending of a Rectangular Element with Initial Membrane Stresses' Structural Analysis Research Memo. No.45, The Boeing Co., Seattle (1962)
- 68 YOSHIKI, M., KAWAI, T., YOSHIMURA, N. 'Matrix Method of Analysis of Ship Structures' (3rd Report) J.Soc.Naval.Archit. Japan 123 (1968) pp.188-195
- 69 FUJINO, T., OHSAKA, K. 'Static Structural Analysis of Suspension Bridges' Mitsubishi Nippon Heavy - 2nd Tech. Rev. 3,6 (1966) pp.17-23
- 70 BERGAN, P.G., CLOUGH, R.W. 'Large Deflection Analysis of Plates and Shallow Shells using the Finite Element Method' Int. Jour. for Num.Methods in Eng.g Vol.5 (1973) pp.534-556
- 71 THOMAS, R.G., GALLAGHER, R.H. 'A Triangular Thin Shell Finite Element : Non-linear Analysis' NASA CR-2483 (1975) pp.1-64
- 72 NOOR, A.K., MATHERS, M.D. 'Nonlinear Finite Element Analysis of Laminated Composite Shells' Computational Methods in Nonlinear Mechanics, The Texas Inst. for Comp. Mechs. Texas (1974) pp.1-999
- 73 NOOR, A.K., HARTLEY, S.J. 'Nonlinear Shell Analysis via Mixed Isoparametric Elements' Computers & Structures 7 (1977) pp.615-626
- 74 REDDY, J.N., CHAO, W.C. 'Large Deflection and Large Amplitude Free Vibration of Laminated Composite Material Plates' Computers & Structures Vol.13 (1981) pp.341-347
- 75 REDDY, J.N., BERT, C.W. 'Analysis of Plates Constructed of Reinforced Bimodulus Composite Material' Mechs. of Bimodulus Materials (Ed. C.W. Bert) AMD-Vol.33 ASME NY (1979) pp.67-83
- 76 PICA, A., WOOD, R.D., HINTON, E. 'Finite Element Analysis of Geometrically Nonlinear Plate Behaviour using a Mindlin Formulation' Computers & Structures 11 (1980) pp.203-215
- 77 NOOR, A.K., MATHERS, M.D., ANDERSON, M.S. 'Exploiting Symmetries for Efficient Postbuckling Analysis of Composite Plates' J. AIAA 15 (1976) pp.24-32
- 78 RAZZAQUE, A. 'Program for Triangular Bending Element with Derivative Smoothing' Int. J. Num. Methods in Eng.g 5 (1973) pp.588-589

- 79 NOOR, A.K.,
HARTLEY, S.J. 'Effect of Shear Deformation and Anisotropy on the Nonlinear Response of Composite Plates' Developments in Composite Materials - Ed G. Holister, Applied Science, Barking, Essex (1975) pp.55-65
- 80 MATHERS, M.D. 'Finite Element Analysis of Laminated Composite Plates and Shells' Ph.D Thesis. The George Washington Univ., Dept. of Eng.g Mech. (1976)
- 81 BENNET, J.A. 'Nonlinear Vibration of Simply Supported Angle Ply Laminated Plates' J. AIAA 9 (1971) pp.1997-2003
- 82 BERT, C.W. 'Nonlinear Vibration of a Rectangular Plate Arbitrarily Laminated of Anisotropic Material' J. Appl. Mech. 40 (1973) pp.452-458
- 83 CHAI, C.Y.,
PRABHAKARA, M.K. 'A General Mode Approach to Nonlinear Flexural Vibrations of Laminated Rectangular Plates' J. Appl. Mech. 45 (1978) pp.623-628
- 84 CHAI, C.Y.
PRABHAKARA, M.K. 'Large Deflection of Unsymmetrical Cross-ply and Angle-ply Plates' J.Mech.Eng.g Sci. 18 (4) (1976) pp.178-183
- 85 YANG, P.C., NORRIS,
C.H., STAVSKY, Y. 'Elastic Wave Propagation in Heterogeneous Plates' J.Appl.Mech. 37 (1966) pp.665-684
- 86 CHANG, T.Y.
SAWAMIPHAKDI, K. 'Large Deformation Analysis of Laminated Shells by the Finite Element Method' Computers & Structures, Vol.13 (1981) pp.331-340
- 87 AHMAD, S., IRON, B.M.,
ZIENKIEWICZ, O.C. 'Analysis of Thick and Thin Shell Structures by Curved Finite Elements' Int. J. Num. Methods in Eng.g 2 (1970) pp.419-451
- 88 McMECKING, R.M.,
RICE, J.R. 'Finite Element Formulations for Problems of Large Elastic/Plastic Deformation' Int. J. Solids & Structures 11 (1975) pp.601-616
- 89 HILL, R. 'Some Basic Principles in the Mechanics of Solids without a Natural Time' J. Mech. Phys. Solids 7 (1959) pp.209-225
- 90 CHANG, T.Y.
PRACHUKTAM 'NFAF - A Nonlinear Finite Element Analysis Program' Rep. No. SE16-3, The Univ. of Akron. (October 1976)
- 91 SCHMIT, L.A.,
MONFORTON, G.R. 'Finite Deflection Discrete Element Analysis of Sandwich Plates and Cylindrical Shells with Laminated Faces' J. AIAA 8 (1970) pp.1451-1461
- 92 WASHIZU, K. 'Variational Methods in Elasticity and Plasticity' Pergamon Press (1968)

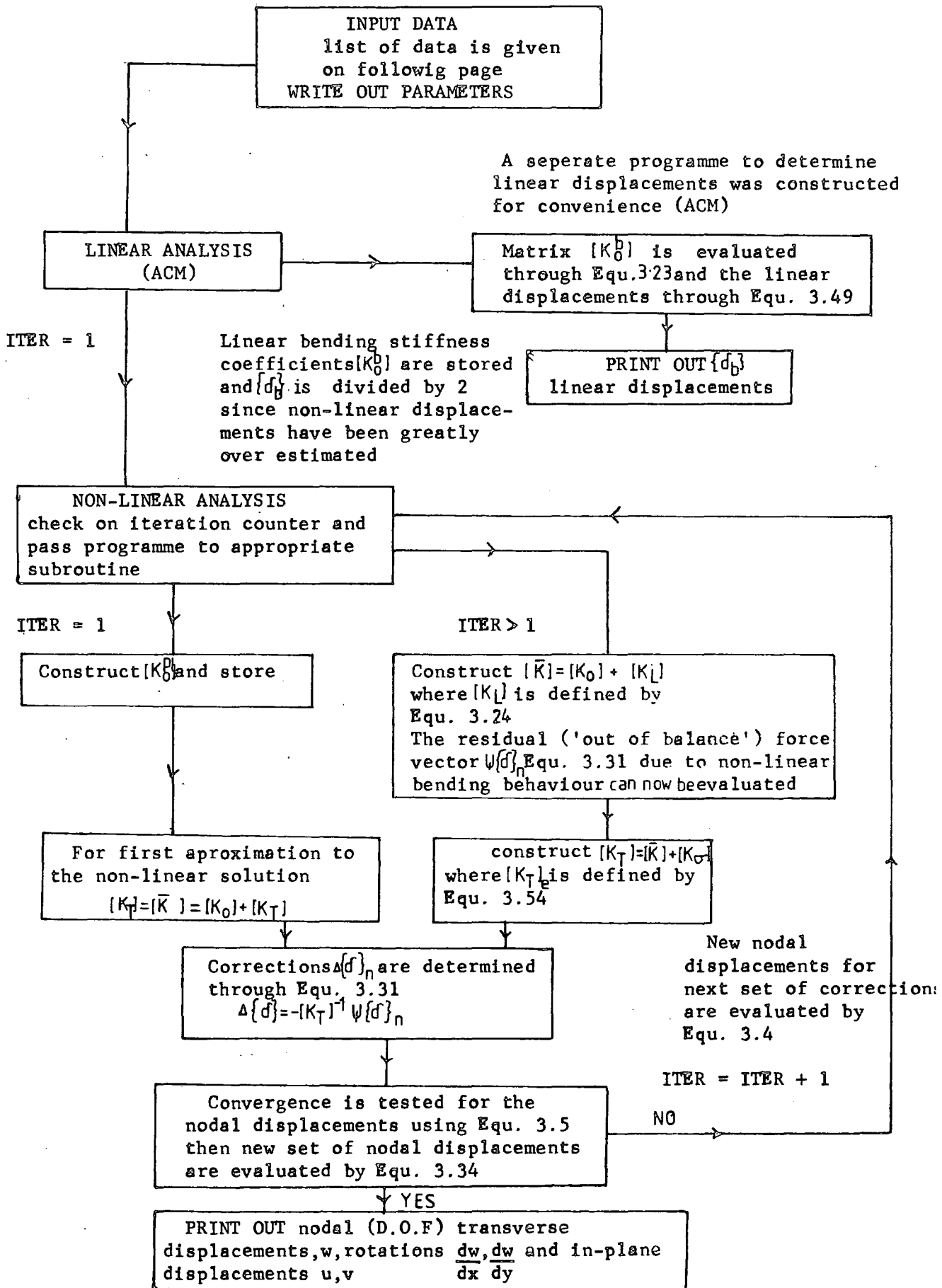
- 93 FRAEIJIS, DE.,
VEUBEKE, B. 'Displacement and Equilibrium Models in the Finite Element Method', Chapt.9 of Stress Analysis ed O.C. Zienkiewicz and G.S. Holister, Wiley, (1965)
- 94 ODEN, J.T. 'Numerical Formulation of Nonlinear Elasticity Problems' Proc. Am. Soc. Civ. Eng., 93 ST3 (1967) pp.235-255
- 95 ARGYRIS, J.H.,
KELSEY, S.,
KAMEL, H. 'Matrix Methods of Structural Analysis' AGARD-ograph 72, Pergamon Press (1963)
- 96 ASPTON, J.E.,
WHITNEY, J.M. 'Theory of Laminated Plates... Progress in Materials Science series... Vol 1V' Technomic (1970)
- 97 MARCUS, H. 'Die Theorie Elastiche Gewebe' 2nd ed. Berlin (1932) p.173
- 98 LEE, S.L.,
BALLESTEROS, P. 'Uniformly loaded Rectangular Plate Supported at Corners' Int. J. Mech. Sci. Vol.2 No.2 (1960) pp.206-211
- 99 LEKHNITSKII, S.G. 'Theory of Elasticity of an Anisotropic Elastic Body', Trans. from Russian by P. Fern, Holden Day, San Francisco (1963)
- 100 WEBBER, J.P.H. 'Experimental and Theoretical Bending Deflection of Laminated Plates' Jour. of Strain Analysis Vol.7 No.2 (1972) pp.87-96
- 101 GALLAGHER, R.H.,
GELLATLY, R.A.,
PADLOG, J.,
MALLET, R.H. 'A Discrete Element Procedure for Thin Shell Instability Analysis' J.AIAA Vol.5 No.1 (1967) pp.138-145
- 102 HANCOX, N.L. 'The Effects of Flaws and Voids on the Shear Properties of C.F.R.P.' J. Mater. Sci. (1977) pp.884-892
- 103 BROWNING, C.E.,
HATNESS, J.T. 'Effects of Moisture on the Properties of High Performance Structural Resins and Composites' Composite Materials:3rd Conf. ASTM STP 546 (1974) pp 284-302
- 104 PAGANO, N.J. 'Exact Solutions for Composite Laminates in Cylindrical Bending' J. Comp. Mater. Vol.3 (1969) pp.398-411
- 105 REISSNER, E. 'The Effect of Transverse Shear Deformation on the Bending of Elastic Plates' Jour. of Appl. Mech. (June 1945) p.A-69,A-77.
- 106 MINDLIN, R.D. 'Influence of Rotatory Inertia and Shear on Flexural Motions of Isotropic Elastic Plates' J. of Appl. Mech. 18 (1951) pp.31-37

- 107 GIRKMAN, K.,
BEER, R. 'Application of Eric Reissner's Refined Plate Theory to Orthotropic Plates' Oster. Ingenieur-Archiv Vol.12 (1958) pp.101-110
- 108 AMBARTSUMYAN, S.A. 'Theory of Anisotropic Plates' ed. Ashton, J.E., Cheron, T. (trans.) Technomic Publishing Co., Stamford Conn, (1970) (Russian publication date unspecified)
- 109 WHITNEY, J.M. 'The Effect of Transverse Shear Deformation on the Bending of Laminated Plates' Jour. of Comp. Mater. Vol.3 (1969) pp.534-547
- 110 YANG, P.C., NORRIS, C.H., STAVSKY, Y. 'Elastic Wave Propagation in Heterogenous Plates' Int. J. Solids. Structures Vol.2 (1966) pp.665-684
- 111 BERT, C.W. 'Analysis of Plates' in Structural Design & Analysis Part I (ed. Chamis, C.C.) Academic Press, New York (1974)
- 112 PAGANO, N.J. 'Exact Solution for Rectangular Bidirectional Composites and Sandwich Plates' J. Comp. Mater. Vol.4 (1970) pp.20-34
- 113 PAGANO, N.J.,
WANG, A.S.D. 'Further Study of Composite Laminates Under Cylindrical Bending' J. Comp. Mater. Vol.5 (1971) pp.521-528
- 114 PAGANO, N.J.,
HATFIELD, S.J. 'Elastic Behaviour of Multilayered Bidirection Composites' J. AIAA Vol.10 No.7 (1972) pp.931-933
- 115 WHITNEY, J.M.,
SUN, C.T. 'A Refined Theory for Laminated Anisotropic, Cylindrical Shells' Jour. of Appl. Mech. Vol.41 No.2 Trans. ASME Vol.96 Series E (1974) pp.471-476
- 116 NELSON, R.B.,
LORCH, D.R. 'A Refined Theory of Laminated Orthotropic Plates' Jour. of Appl Mech. Vol.41 No.1 Trans. ASME Vol.96 Series E (1974) pp.177-183
- 117 HILDEBRAND, F.B.,
REISSNER, E.,
THOMAS, G.B. 'Notes on the Foundations of the Theory of Small Displacements of Orthotropic Shells' NACA T.N. No.1833 (1949)
- 118 REISSNER, E. 'On Transverse Bending of Plates, Including the Effects of Transverse Shear Deformation' Int. Jour. of Solids & Structures, Vol.11 (1975) pp.569-573
- 119 LO, K.H.,
CHRISTENSEN, R.M.,
WU, E.M. 'A High-Order Theory of Plate Deformation - Part 1 : Homogeneous Plates' ASME Paper No.77 WA/APM-23.

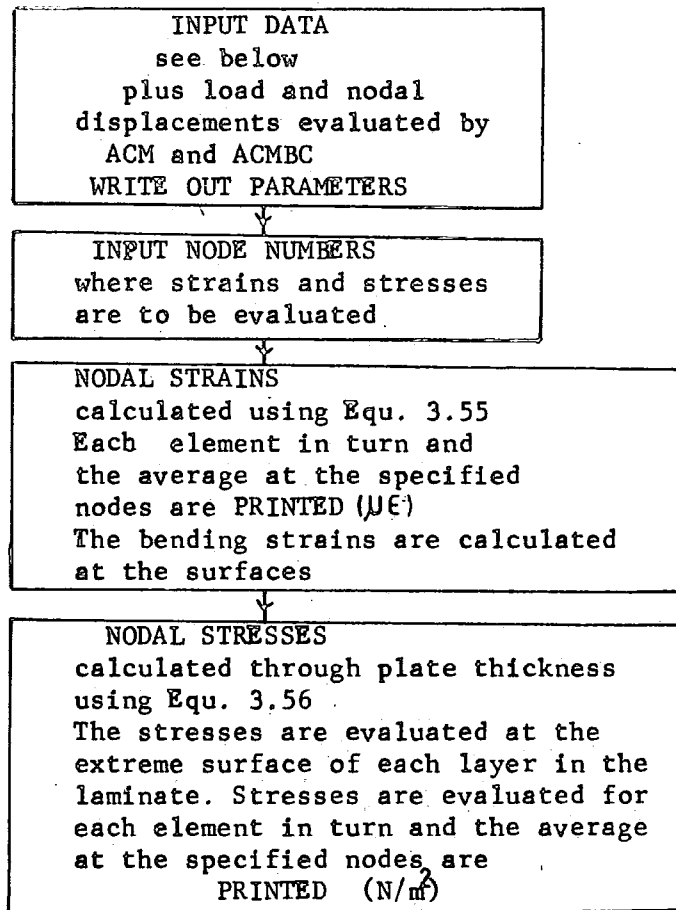
- 120 LO, K.H.,
CHRISTENSEN, R.M.,
WU, E.M. 'A High-Order Theory of Plate Deformation -
Part 2 : Laminated Plates' ASME paper No.77
WA/APM-24
- 121 WHITNEY, J.M. 'The Effect of Transverse Shear Deformation on
the Bending of Laminated Plates' J. Comp.
Mater. Vol.3 (1969) pp.534-547
- 122 LO, K.H.,
CHRISTENSEN, R.M.,
WU, E.M. 'Stress Solution Determination for High Order
Plate Theory' Int. J. Solids. Structures
Vol.14 (1978) pp.655-662
- 123 PIPES, R.B.,
PAGANO, N.J. 'Interlaminar Stresses in Composite Laminates
under Uniform Axial Extension' J. Comp.
Mater. Vol.4 (1970) pp.538-548
- 124 PAGANO, N.J.,
PIPES, R.B. 'The Influence of Stacking Sequence on
Laminate Strength' J. Comp. Mater. Vol.5 (1971)
pp.50-57
- 125 PAGANO, N.J. 'On the Calculation of Interlaminar Normal Stress
in Composite Laminates' J. Comp. Mater. Vol.8(1974)
pp.65-81
- 126 HAYASHI, T. Trans - Japan Soc. Aero Space Sci. 10/17 (1967)
p.43-
- 127 HAYASHI, T.,
SANDOS Proceedings of International Symposium on Space
Technology and Science, Tokyo, Japan
(August 25-30 1969) pp.291-302
- 128 PUPPO, A.H.,
EVENSEN, H.A. 'Interlaminar Shear in Laminated Composites
Under Generalised Plane Stress' J. Comp. Mater.
4 (1970) pp.204-220
- 129 PAGANO, N.J.,
PIPES, R.B. 'Some Observations on the Interlaminar Strength
of Composite Laminates' Int. J. Mech. Sci. (1973)
Vol.15 pp.679-688
- 130 OPLINGER, D.N. 'Edge Effects in Angle-Ply Composites' AMHRC
TR-71-62, Army Materials & Mechanics Research
Center, Watertown, Mass. (1971)
- 131 RYBICKI, E.F. 'Approximate 3-D Solutions for Symmetric
Laminates under Inplane Loading' J. Comp. Mater.
5 (1971) pp.354-361
- 132 WANG, S.S. Ph.D Thesis, MIT Hayden Memorial Library,
Massachusetts Institute of Technology (1974)
- 133 WANG, A.S.D,
CROSSMAN, F.W. 'Some New Results on Edge Effect in Symmetric
Composite Laminates' J. Comp. Mater. Vol.11
(1977) pp.92-106

- 134 PAGANO, N.J. 'Stress Fields in Composite Laminates' Int. J. Solids Structures Vol.4 (1978) pp.385-400
- 135 REISSNER, E. 'On a Variational Theorem in Elasticity' J. Math. Phys. 29 (1950) p.29-
- 136 TANG, S. 'Interlaminar Stresses of Uniformly Loaded Rectangular Composite Plates' J. Comp. Mat. Vol.10 (1976) pp.69-78
- 137 SALAMON, N.J. 'Interlaminar Stresses in a Layered Composite Laminate in Bending' Fibre Science Technology 11 (1978) pp.305-317
- 138 REIFSNIDER, K.L., FENNEK, E.G. II, STINCHCOMB, W.W. 'Delamination in Quasi-Isotropic Graphite-Epoxy Laminates' Composite Materials : Testing & Design (4th Conf) ASTM STP 617 (1977) pp.93-105
- 139 WHITNEY, J.M. KNIGHT, M. 'The Relationship Between Tensile Strength and Flexure Strength in Fiber-reinforced Composites' Exp. Mech. (1980) pp.211-216
- 140 MAYBURY, A. 'An Investigation of the Failure Mechanisms of a Carbon-fibre Reinforced Composite Material in Bending' Ph.D Thesis. Univ. of Aston, (April 1973)
- 141 PETIT, P.H., WADDOUPS, M.E. 'A method of Predicting the Non-linear Behaviour of Laminated Composites' Jour. Comp. Mater. 3 (1969) pp2-19
- 142 HAHN, H.T., TSAI, S.W. 'Non-linear Elastic Behaviour of Uni-directional Composite Laminae' Jour. Comp. Mater 7 (1973) pp. 102-118
- 143 HAHN, H.T. 'Non-linear Behaviour of Laminated Composites' Jour. Comp. Mater. 7 (1973) pp257-271
- 144 JONES, R.M., 'Analysis of Non-linear Stress-Strain Behaviour of Fibre Reinforced Composite Materials' J. AIAA 15 (1977) pp1669-1676
- 145 DITCHER, A.K., RHODES, F.E., WEBBER, J.P.H. 'Non-linear Stress-Strain Behaviour of Carbon Fibre Reinforced Plastic Laminates' Jour. Strain Analysis v16 No1 (1981) pp43-51
- 146 JONES, R.M., MORGAN, H.S. 'Bending and Extension of Cross-ply Laminates with Different Moduli in Tension and Compression' Computers & Structures 11 (1980) pp181-191

APPENDIX I ACMBC Displacements : Programme Flow Chart



APPENDIX I ACM and ACMBC Strains and Stresses : Programme Flow Chart



INPUT DATA FOR FINITE ELEMENT ANALYSIS

Title
 No. of Nodes , No. of Elements
 Boundary Conditions { Bending
 In-plane
 No of layers in half the plate
 Orientations of each layer
 Topology of each finite element {repeated for the number
 Material Properties and Dimensions {of Elements in the mesh
 Load vector (Transverse)
 Node No. where $\epsilon_{xy} = 0$ along the Quarter Plate Boundaries
 No. of Load Increments
 β Factor applied in reducing the number of iterations to a
 convergent solution through Equ 3.4
 No. of Elements along each side of the Finite Element Mesh

High Order Differential Equations Governing Flexural Displacement Components of a Symmetrical Laminated Plate

$$-A55 \frac{d^2 w_o}{dx^2} - 2A45 \frac{d^2 w_o}{dx dy} - A44 \frac{d^2 w_o}{dy^2} - A55 \frac{d \psi_x}{dx} - A45 \frac{d \psi_x}{dy} - A45 \frac{d \psi_y}{dx} - A44 \frac{d \psi_y}{dy} - D55 \frac{d^2 \xi_z}{dx^2} - 2D45 \frac{d^2 \xi_z}{dx dy} - D44 \frac{d^2 \xi_z}{dy^2} - 3D55 \frac{d \phi_x}{dx} - 3D45 \frac{d \phi_x}{dy}$$

$$- 3D45 \frac{d \phi_y}{dx} - 3D44 \frac{d \phi_y}{dy} = \sigma_z \left(\frac{h}{2} \right)$$

$$-A55 \frac{d w_o}{dx} - A45 \frac{d w_o}{dy} + D11 \frac{d^2 \psi_x}{dx^2} + 2D16 \frac{d^2 \psi_x}{dx dy} + D66 \frac{d^2 \psi_x}{dy^2} - A55 \psi_x + D16 \frac{d \psi_y}{dx} + (D12 + D66) \frac{d \psi_y}{dx dy} + D26 \frac{d \psi_y}{dy} - A45 \psi_y + (2D13 - D55) \frac{d \xi_z}{dx}$$

$$+ (2D36 - D45) \frac{d \xi_z}{dy} + H11 \frac{d^2 \phi_x}{dx^2} + 2H16 \frac{d^2 \phi_x}{dx dy} + H66 \frac{d^2 \phi_x}{dy^2} - 3D55 \phi_x + H16 \frac{d \phi_y}{dx} + H26 \frac{d \phi_y}{dy} + (H12 + H66) \frac{d \phi_y}{dx dy} - 3D45 \phi_y = 0$$

$$-A45 \frac{d w_o}{dx} - A44 \frac{d w_o}{dy} + D16 \frac{d^2 \psi_x}{dx^2} + (D12 + D66) \frac{d^2 \psi_x}{dx dy} + D26 \frac{d^2 \psi_x}{dy^2} - A45 \psi_x + D66 \frac{d \psi_y}{dx} + 2D26 \frac{d \psi_y}{dx dy} + D22 \frac{d \psi_y}{dy} - A44 \psi_y + (2D36 - D45) \frac{d \xi_z}{dx}$$

$$+ (2D23 - D44) \frac{d \xi_z}{dy} + H16 \frac{d^2 \phi_x}{dx^2} + (H12 + H66) \frac{d^2 \phi_x}{dx dy} + H66 \frac{d^2 \phi_x}{dy^2} + 2H26 \frac{d^2 \phi_x}{dx dy} + H22 \frac{d \phi_y}{dy} - 3D44 \phi_y + H26 \frac{d^2 \phi_y}{dy^2} = 0$$

$$-D55 \frac{d^2 w_o}{dx^2} - 2D45 \frac{d^2 w_o}{dx dy} - D44 \frac{d^2 w_o}{dy^2} + (2D13 - D55) \frac{d \psi_x}{dx} + (2D36 - D45) \frac{d \psi_x}{dy} + (2D36 - D45) \frac{d \psi_y}{dx} + (2D23 - D44) \frac{d \psi_y}{dy} - H55 \frac{d^2 \xi_z}{dx^2}$$

$$- 2H45 \frac{d^2 \xi_z}{dx dy} - H44 \frac{d^2 \xi_z}{dx^2} + 4D33 \xi_z + (2H13 - 3H55) \frac{d \phi_x}{dx} + (2H36 - 3H45) \frac{d \phi_x}{dy} + (2H36 - 3H45) \frac{d \phi_y}{dx} + (2H23 - 3H44) \frac{d \phi_y}{dy} = \sigma_z \left(\frac{h}{2} \right) \times \frac{h^2}{4}$$

$$- 3D55 \frac{d w_o}{dx} - 3D45 \frac{d w_o}{dy} + H11 \frac{d^2 \psi_x}{dx^2} + 2H16 \frac{d^2 \psi_x}{dx dy} + H66 \frac{d^2 \psi_x}{dy^2} - 3D55 \psi_x + H16 \frac{d \psi_y}{dx} + (H12 + H66) \frac{d \psi_y}{dx dy} + H26 \frac{d \psi_y}{dy} - 3D45 \psi_y + (2H13 - 3H55) \frac{d \xi_z}{dx}$$

$$+ (2H36 - 3H45) \frac{d \xi_z}{dy} + L11 \frac{d^2 \phi_x}{dx^2} + 2L16 \frac{d^2 \phi_x}{dx dy} + L66 \frac{d^2 \phi_x}{dy^2} - 9H55 \phi_x + L16 \frac{d \phi_y}{dx} + (L12 + L66) \frac{d \phi_y}{dx dy} + L26 \frac{d \phi_y}{dy} - 9H45 \phi_y = 0$$

$$- 3D45 \frac{d w_o}{dx} - 3D44 \frac{d w_o}{dy} + H16 \frac{d^2 \psi_x}{dx^2} + (H12 + H66) \frac{d^2 \psi_x}{dx dy} + H26 \frac{d^2 \psi_x}{dy^2} - 3D45 \psi_x + H66 \frac{d \psi_y}{dx} + 2H26 \frac{d \psi_y}{dx dy} + H22 \frac{d \psi_y}{dy} - 3D44 \psi_y + (2H36 - 3H45) \frac{d \xi_z}{dx}$$

$$+ (2H23 - 3H44) \frac{d \xi_z}{dy} + L16 \frac{d^2 \phi_x}{dx^2} + (L12 + L66) \frac{d^2 \phi_x}{dx dy} + L26 \frac{d^2 \phi_x}{dy^2} - 9H45 \phi_x + L66 \frac{d \phi_y}{dx} + 2L26 \frac{d \phi_y}{dx dy} + L22 \frac{d \phi_y}{dy} - 9H44 \phi_y = 0$$

174

High Second Order Differential Equations Governing In-plane Displacement Components of a Symmetrical Laminated Plate

$$A11 \frac{du_o^2}{dx^2} + 2A16 \frac{du_o^2}{dx dy} + A66 \frac{du_o^2}{dy^2} + A16 \frac{dv_o^2}{dx^2} + (A12 + A16) \frac{dv_o^2}{dx dy} + A26 \frac{dv_o^2}{dy^2} + A13 \frac{d\psi_z}{dx} + A36 \frac{d\psi_z}{dy} + D11 \frac{d\zeta_x^2}{dx^2} + 2D16 \frac{d\zeta_x^2}{dx dy} + D66 \frac{d\zeta_x^2}{dy^2} + D16 \frac{d\zeta_y^2}{dx^2} + (D12 + D66) \frac{d\zeta_y^2}{dx dy} + D26 \frac{d\zeta_y^2}{dy^2} = 0$$

$$A16 \frac{du_o^2}{dx^2} + (A12 + A66) \frac{du_o^2}{dx dy} + A26 \frac{du_o^2}{dy^2} + A66 \frac{dv_o^2}{dx^2} + 2A26 \frac{dv_o^2}{dx dy} + A22 \frac{dv_o^2}{dy^2} + A36 \frac{d\psi_z}{dx} + A23 \frac{d\psi_z}{dy} + D16 \frac{d\zeta_x^2}{dx^2} + (D12 + D66) \frac{d\zeta_x^2}{dx dy} + D26 \frac{d\zeta_x^2}{dy^2} + D66 \frac{d\zeta_y^2}{dx^2} + 2D26 \frac{d\zeta_y^2}{dx dy} + D22 \frac{d\zeta_y^2}{dy^2} = 0$$

$$A13 \frac{du_o}{dx} + A36 \frac{du_o}{dy} + A36 \frac{dv_o}{dx} + A23 \frac{dv_o}{dy} - D55 \frac{d\psi_z}{dx^2} - 2D45 \frac{d\psi_z}{dx dy} - D44 \frac{d\psi_z}{dy^2} + A33 \psi_z + (D13 - 2D55) \frac{d\zeta_x}{dx} + (D36 - 2D45) \frac{d\zeta_x}{dy} + (D36 - 2D45) \frac{d\zeta_y}{dx} + (D23 - D44) \frac{d\zeta_y}{dy} = \sigma_z \left(\frac{h}{2}\right) \times \frac{h}{2}$$

$$D11 \frac{d\zeta_x^2}{dx^2} + 2D16 \frac{d\zeta_x^2}{dx dy} + D66 \frac{d\zeta_x^2}{dy^2} + D16 \frac{d\zeta_y^2}{dx^2} + (D12 + D66) \frac{d\zeta_y^2}{dx dy} + D26 \frac{d\zeta_y^2}{dy^2} + (D13 - 2D55) \frac{d\psi_z}{dx} + (D36 - 2D45) \frac{d\psi_z}{dy} + H11 \frac{d\zeta_x^2}{dx^2} + 2H16 \frac{d\zeta_x^2}{dx dy} + H66 \frac{d\zeta_x^2}{dy^2} - 4D55 \zeta_x + H16 \frac{d\zeta_y^2}{dx^2} + (H12 + H66) \frac{d\zeta_y^2}{dx dy} + H26 \frac{d\zeta_y^2}{dy^2} - 4D45 \zeta_y = 0$$

$$D16 \frac{d\zeta_x^2}{dx^2} + (D12 + D66) \frac{d\zeta_x^2}{dx dy} + D26 \frac{d\zeta_x^2}{dy^2} + D66 \frac{d\zeta_y^2}{dx^2} + 2D26 \frac{d\zeta_y^2}{dx dy} + D22 \frac{d\zeta_y^2}{dy^2} + (D36 - 2D45) \frac{d\psi_z}{dx} + (D23 - 2D44) \frac{d\psi_z}{dy} + H16 \frac{d\zeta_x^2}{dx^2} + (H12 + H66) \frac{d\zeta_x^2}{dx dy} + H26 \frac{d\zeta_x^2}{dy^2} - 4D45 \zeta_x + H66 \frac{d\zeta_y^2}{dx^2} + 2H26 \frac{d\zeta_y^2}{dx dy} + H22 \frac{d\zeta_y^2}{dy^2} - 4D44 \zeta_y = 0$$

Coefficients which are non zero

11	12	13	-	-	16
21	22	23	-	-	26
31	32	33	-	-	36
-	-	-	44	-	-
-	-	-	-	55	-
61	62	63	-	-	66

and 16, 26, 36 exist only for θ orientated layers to the global axes of the plate

$$A_{ij}, D_{ij}, H_{ij}, L_{ij} = \int (1, z^2, z^4, z^6) \bar{Q}_{ij} dz$$

Matrix Governing Flexural Displacements for a General Symmetrical Laminated Rectangular Plate, Simply Supported along its edges and Subjected to the Transverse Loading $q = q_0 \sin \frac{\pi x}{A} \sin \frac{\pi y}{B}$

$\pi^2 cs \left[\frac{D11+D66+A55}{A^2} + \frac{2D16}{B^2} + \frac{2D16}{\pi^2 AB} \right]$	$\pi^2 cs \left[\frac{H11+H66+3D55}{A^2} + \frac{2H16}{B^2} + \frac{2H16}{\pi^2 AB} \right]$	$\pi^2 cs \left[\frac{D12+D66}{A B} + \frac{D16+D26}{A^2} + \frac{D16+D26}{B^2} \right]$	$\pi^2 cs \left[\frac{H12+H66}{A B} + \frac{H16+H26}{A^2} + \frac{H16+H26}{B^2} \right]$	$\pi cs \frac{A55}{A}$	$\pi cs \left[\frac{D55-2D13}{A} - \frac{2D36}{B} \right]$	K_1	0
	$\pi^2 cs \left[\frac{L11+L66}{A^2} + \frac{9H55}{B^2} + \frac{2L16}{\pi^2 AB} \right]$	$\pi^2 cs \left[\frac{H12+H66}{A B} + \frac{H16+H26}{A^2} + \frac{H16+H26}{B^2} \right]$	$\pi^2 cs \left[\frac{L12+L66}{A B} + \frac{L16+L26}{A^2} + \frac{L16+L26}{B^2} \right]$	$\pi cs \frac{3D55}{A}$	$\pi cs \left[\frac{3H55-2H13}{A} - \frac{2H36}{B} \right]$	K_2	0
THESE TERMS ARE SYMMETRICAL		$\pi^2 cs \left[\frac{D66+D22+A44}{A^2} + \frac{2D26}{B^2} + \frac{2D26}{\pi^2 AB} \right]$	$\pi^2 cs \left[\frac{H66+H22+3D44}{A^2} + \frac{2H26}{B^2} + \frac{2H26}{\pi^2 AB} \right]$	$\pi cs \frac{A44}{B}$	$\pi cs \left[\frac{D44-2D23}{B} - \frac{2D36}{A} \right]$	K_3	0
			$\pi^2 cs \left[\frac{L66+L22+9H44}{A^2} + \frac{2L26}{B^2} + \frac{2L26}{\pi^2 AB} \right]$	$\pi cs \frac{3D44}{B}$	$\pi cs \left[\frac{3H44-2H13}{B} - \frac{2H36}{A} \right]$	K_4	0
$\pi ss \frac{A55}{A}$	$\pi ss \frac{3D55}{A}$	$\pi ss \frac{A44}{B}$	$\pi ss \frac{3D44}{B}$	$\pi ss \left[\frac{A55+A44}{A} + \frac{A44}{B} \right]$	$\pi ss \left[\frac{D55+D44}{A} + \frac{D44}{B} \right]$	K_5	$ss q_0$
$\pi ss \left[\frac{D15-2D13}{A} - \frac{cs2D36}{B} \right]$	$\pi ss \left[\frac{3H55-2H13}{A} - \frac{cs2H36}{B} \right]$	$\pi ss \left[\frac{D44-2D23}{B} - \frac{sc2D36}{A} \right]$	$\pi ss \left[\frac{3H44-2H12}{B} - \frac{sc2H36}{A} \right]$	$\pi ss \left[\frac{D55+D44}{A} + \frac{D44}{B} \right]$	$\pi^2 ss \left[\frac{H55+H44}{A^2} + \frac{4D33}{B^2} + \frac{4D33}{\pi^2} \right]$	K_6	$ss q_0$

where $s = \sin \frac{\pi x}{A}$ and $c = \cos \frac{\pi y}{B}$

The above can be solved when the terms 16, 26, and 36 are zero, but when there are lamina at θ° to the global axes the matrix coefficients are dependent on the x-y co-ordinates.

Figure 1.1 PLATE GEOMETRY

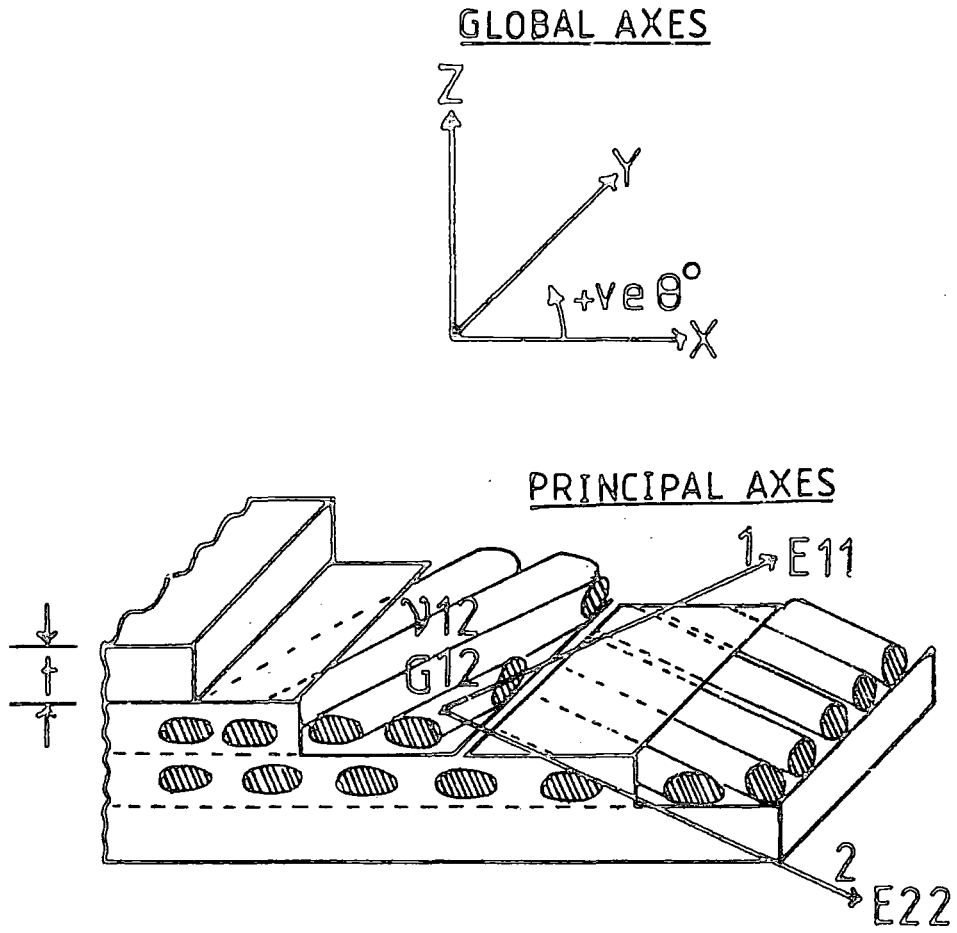


Figure 2.1 BIAXIAL TEST METHODS FOR COMPOSITES

Figure 2.1.1
TUBULAR SPECIMEN
(filament wound)

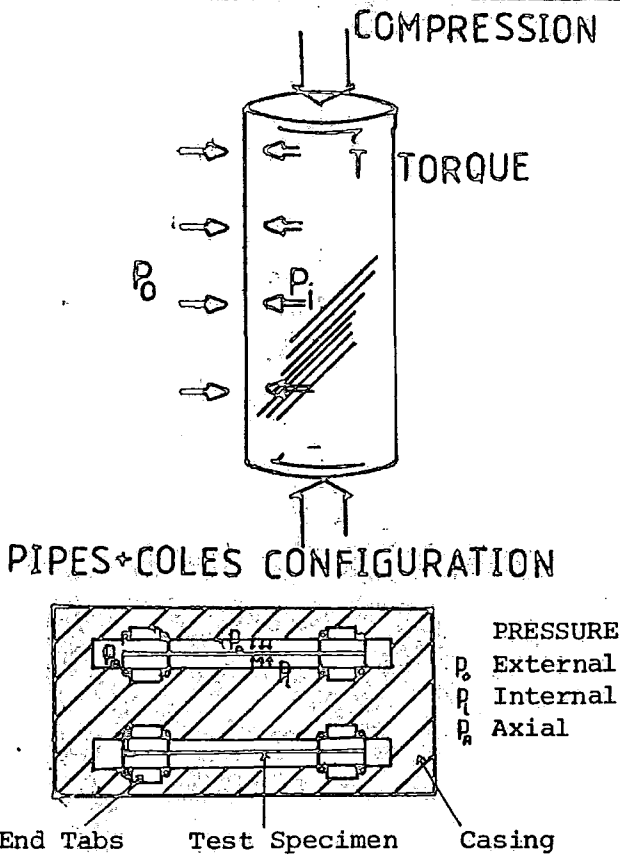


Figure 2.1.2
OFF-AXIS COUPON

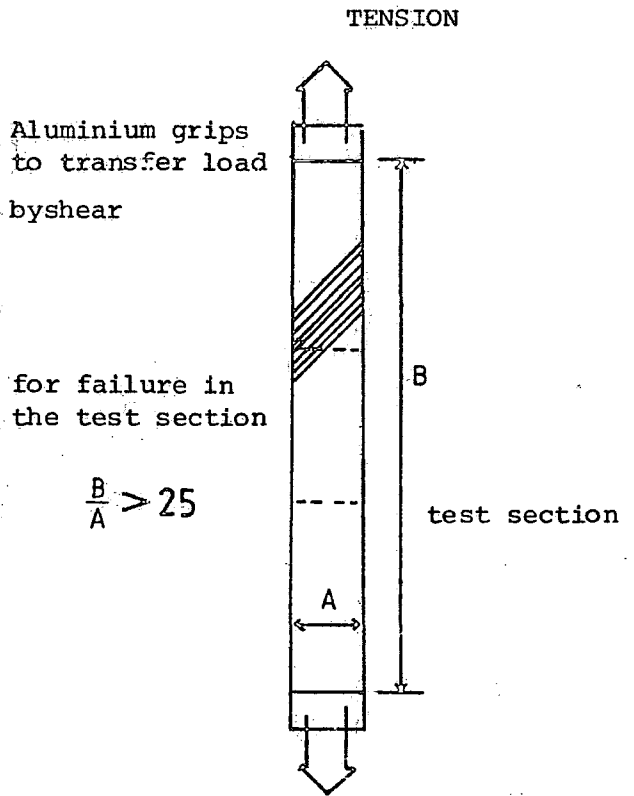


Figure 2.1.3
CROSS BEAM SPECIMEN

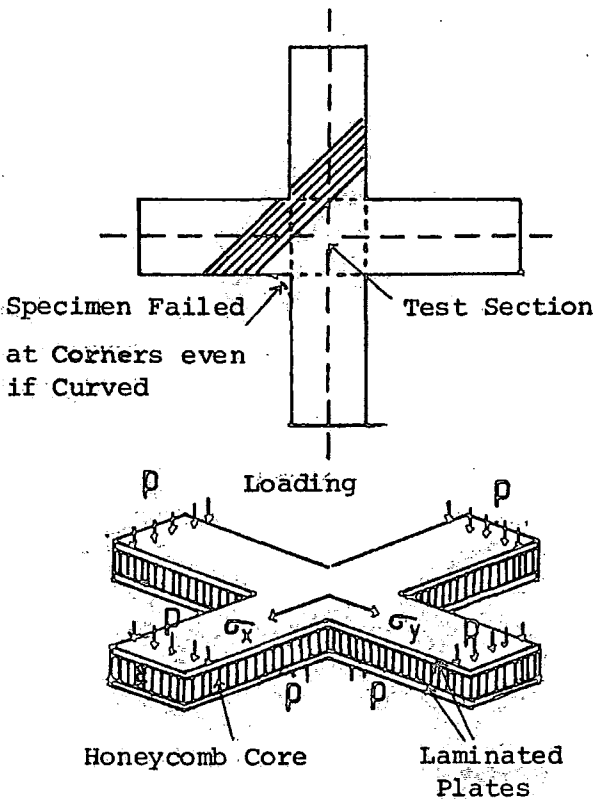


Figure 2.1.4
BULGE TEST
(elliptical plate)

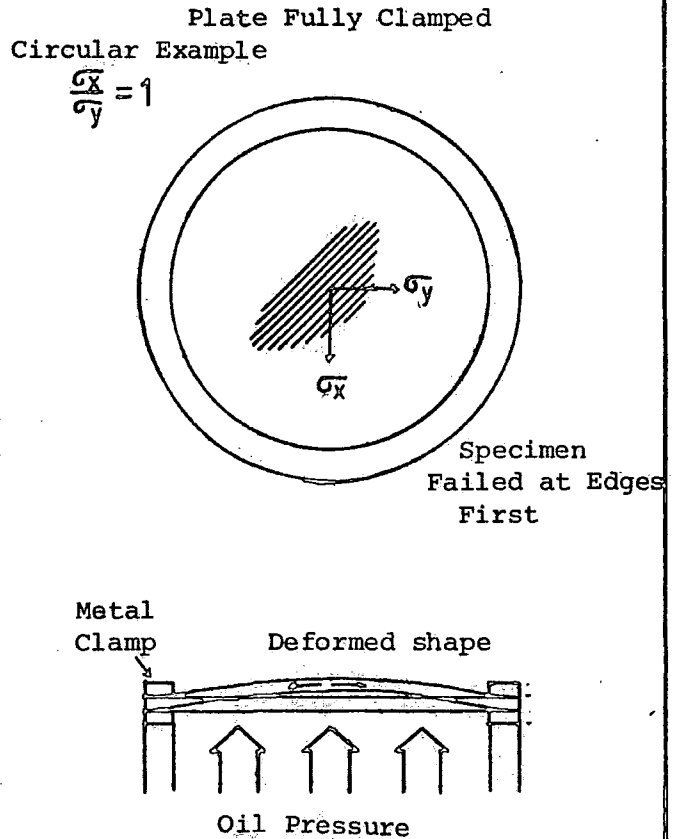


Figure 2.2 PLAN OF PLATE BENDING METHOD

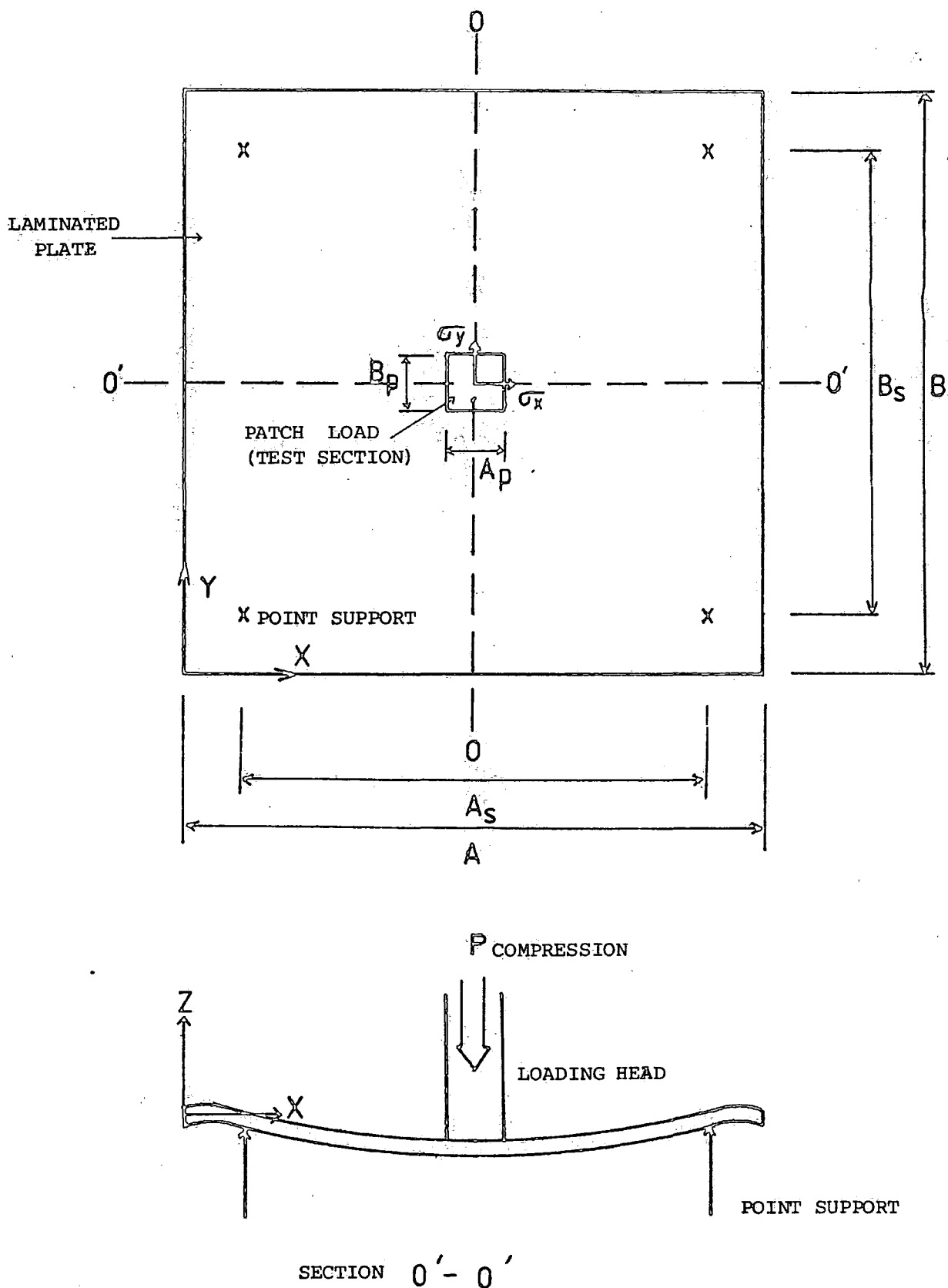


Figure 2.3 BIAxIAL STRESS RATIO $\frac{\sigma_x}{\sigma_y}$ FOR A SIMPLY SUPPORTED RECTANGULAR PLATE SIDE RATIO $\frac{A}{B}$ WITH UNIFORM PRESSURE OVER AN AREA $\frac{A_p}{B_p}=1$ ABOUT THE CENTRE

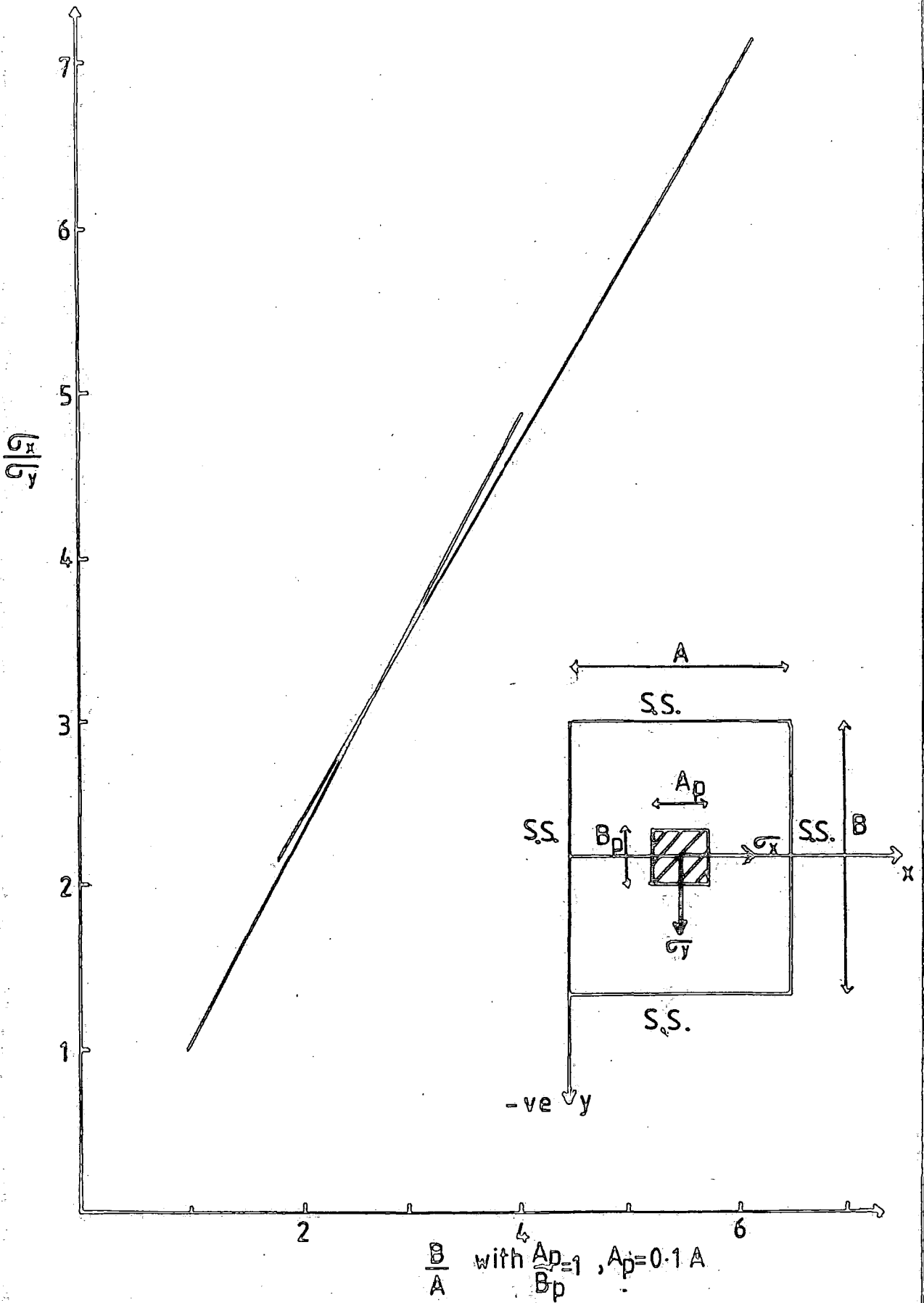


Figure 2.4 BIAxIAL STRESS RATIO $\frac{\sigma_x}{\sigma_y}$ FOR A SIMPLY SUPPORTED SQUARE PLATE WITH A CHANGING CENTRAL PATCH LOAD $\frac{A_p}{B_p}$

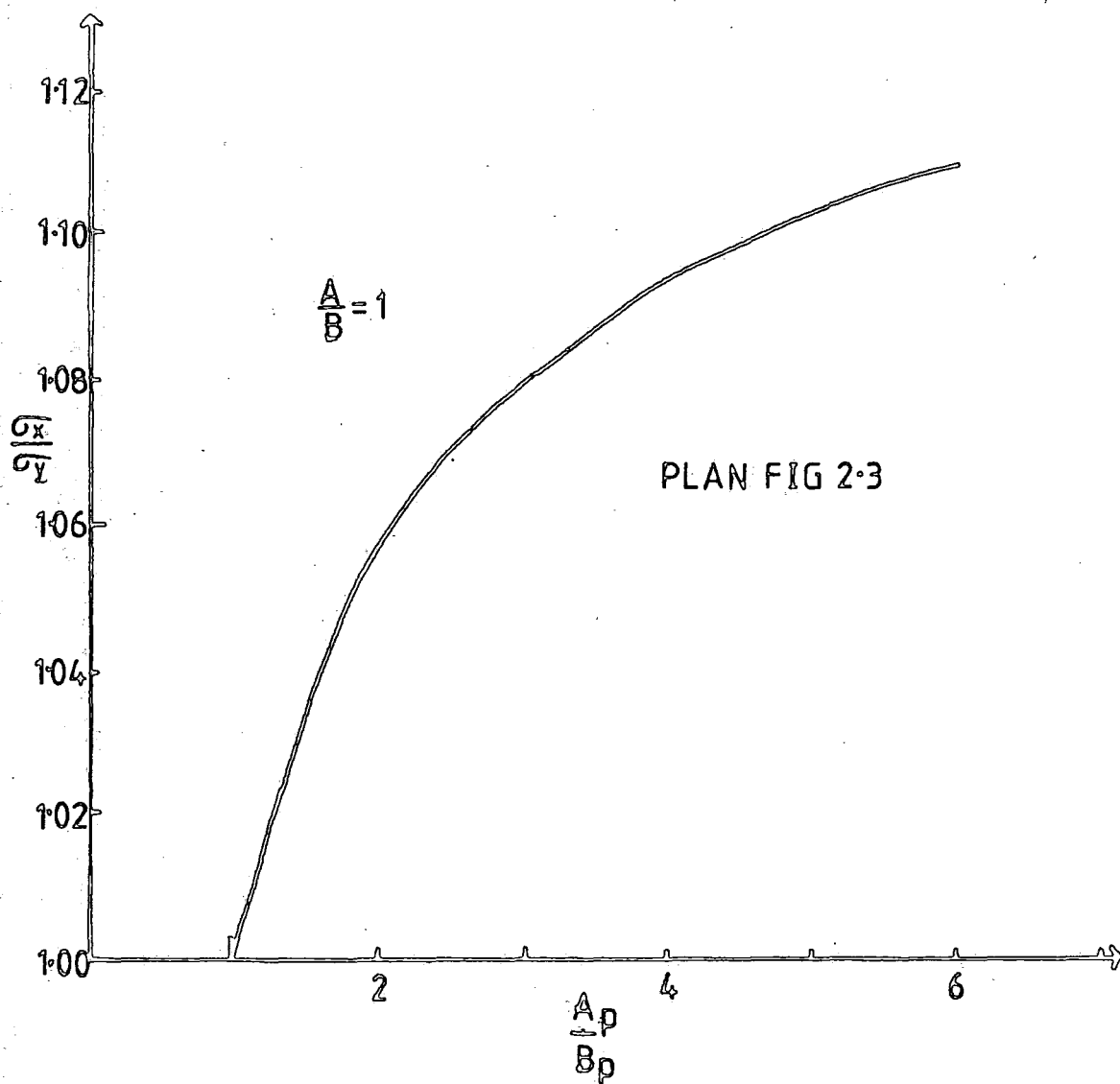


Figure 3.1 ACMBC ELEMENTS

RECTANGULAR FOUR NODED PLATE BENDING ELEMENT

Figure 3.1.1

BASIC ELEMENT

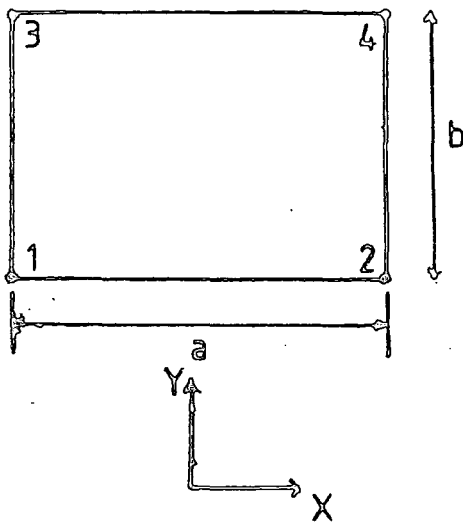
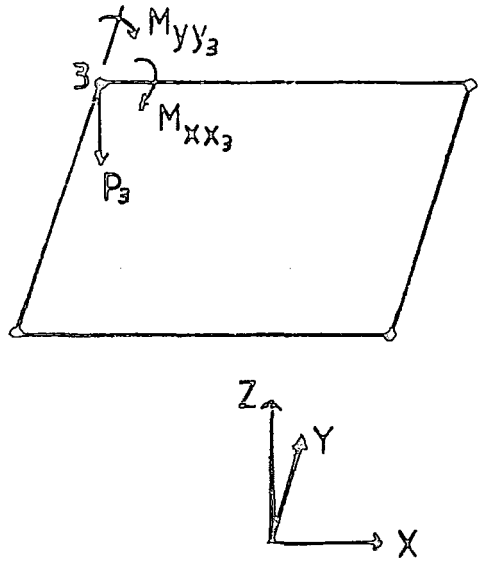


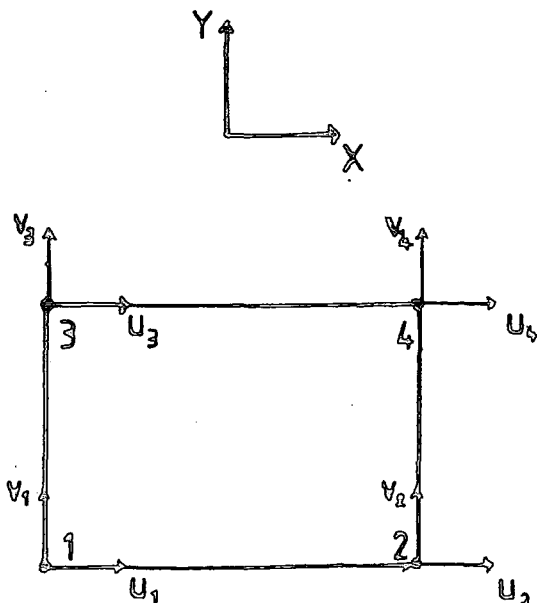
Figure 3.1.2

NODAL LOADS



ELEMENT DEGREES OF FREEDOM

IN-PLANE Figure 3.1.3



BENDING (ACM) Figure 3.1.4

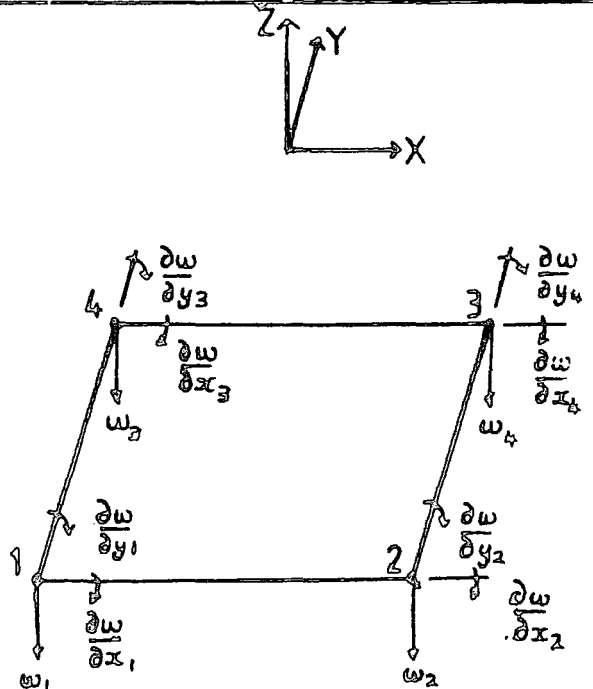


Figure 3.2 PLATE GEOMETRY

Figure 3.2.1 CO-ORDINATE SYSTEM FOR FINITE ELEMENT ANALYSIS

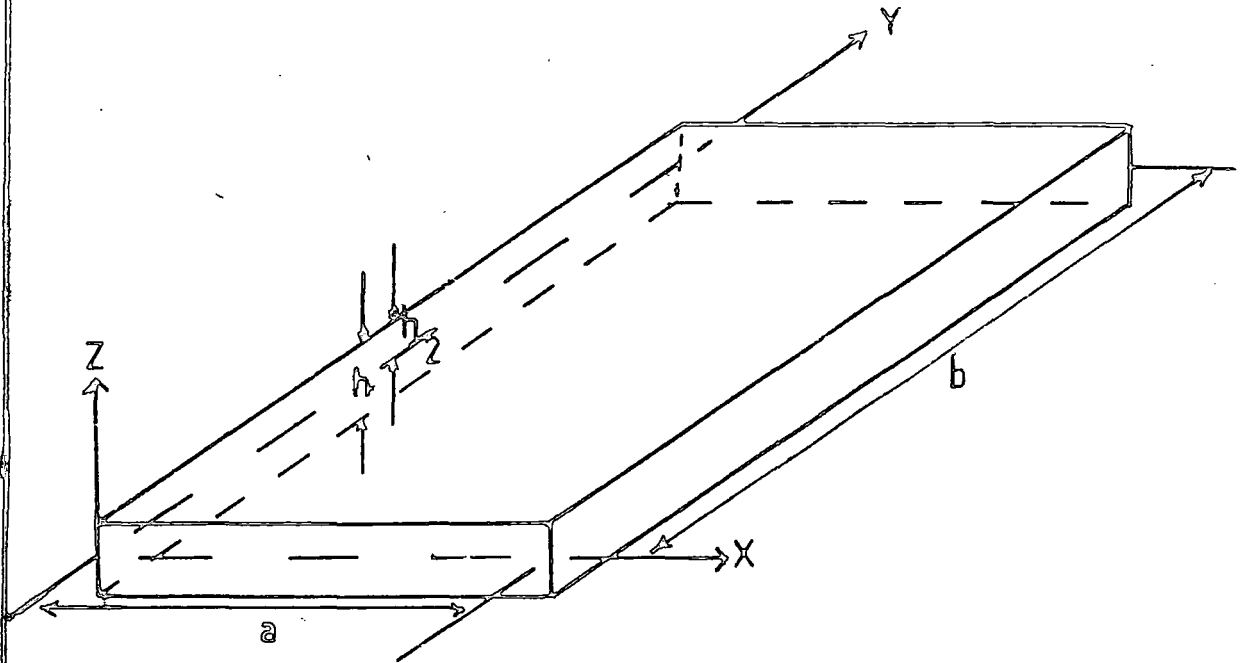


Figure 3.2.2 INCREASE IN MIDDLE SURFACE LENGTH DUE TO LATERAL DISPLACEMENT

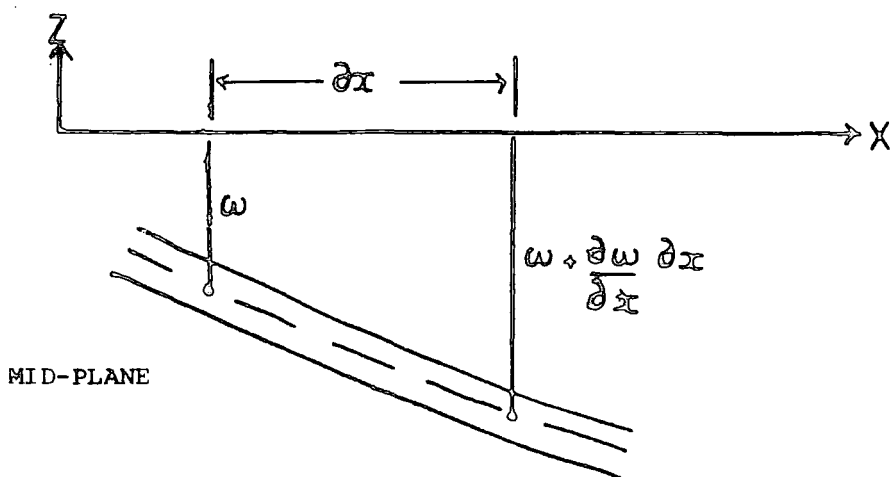


Table 3.1 Mesh Constructions

Subscripts

Q = Quarter plate model H = Half plate F = Full plate

U = Uniform sized elements in mesh G = Graded mesh

S = Square mesh R = Rectangular mesh

E = Experiment (mesh constructed to model plate bending experiment)

Graded meshes have the smaller elements around the centre of the plate that they are representing. Unless otherwise stated the meshes have non-dimensional lengths.

Mesh Label	Plate Dimension		No. of elements (along each side)		Size of elements along sides
	A	B			
1SQU	.2	.2	1	(1)	.1 * 1
2SQU	.2	.2	4	(2)	.05 * 2
3SQU	.2	.2	9	(3)	.0333 * 3
4SQU	.2	.2	16	(4)	.025 * 4
5SQU	.2	.2	25	(5)	.02 * 5
6SQU	.2	.2	36	(6)	.01667 * 6
7SQU	.2	.2	64	(8)	.0125 * 8
8SQU	.2	.2	100	(10)	.01 * 10
9SQU	.2	.2	144	(12)	.00833 * 12
1SQG	.2	.2	9	(3)	.05 * 1, .04 * 1, .01 * 1
2SQG	.2	.2	36	(6)	.03 * 1, .015 * 4, .01 * 1
3SQG(A)	.2	.2	49	(7)	.02 * 3, .015 * 2, .005 * 2
3SQG(B)	.2	.2	49	(7)	.016 * 5, .01 * 2
4SQG	.2	.2	64	(8)	.02 * 3, .01 * 3, .005 * 2
5SQG	.2	.2	100	(10)	.02 * 2, .01 * 4, .005 * 4
6SQG	.2	.2	144	(12)	.02 * 1, .015 * 2, .01 * 1, .005 * 8
1RFU	3.81 cm 2.25		16	(4)	.9525 * 4 and 0.5625 * 4
1SFGE144	.26m.26		144	(12)	.03 * 1, .02 * 1, .03 * 2, .01 * 4 .03 * 2, .02 * 1, .03 * 1
1SHGE50	.26m.26		50	(5)	.03 * 4, .01 * 1
				(10)	.03 * 4, .01 * 2, .03 * 4
1SHGE72	.26m.26		72	(6)	.03 * 3, .02 * 1, .01 * 2
				(12)	.03 * 3, .02 * 1, .01 * 4, .02 * 1 .03 * 3
1SQGE100	.26m.26		100	(10)	.015 * 6, .01 * 4

Table 3.2 Finite elements for linear evaluation

ACM (26,27)	
4 noded non-conformal 12 D.O.F.	simple polynomial (Equ. 3.3)
S (36)	
8 noded 48 D.O.F.	conformal Hermitian. Displacement method
<p>Based on complex Hermitian interpolation functions. A high order plate bending element using a hyperoscillatory polynomial.</p> $w(x,y) = \sum_{i=1}^2 \sum_{j=1}^2 \left[H_{0i}^{(2)}(x) H_{0j}^{(2)}(y) w_{ij} + H_{1i}^{(2)}(x) H_{0j}^{(2)}(y) w_{xij} + H_{0i}^{(2)}(x) H_{1j}^{(2)}(y) w_{yij} + H_{2i}^{(2)}(x) H_{0j}^{(2)}(y) w_{xxij} + H_{0i}^{(2)}(x) H_{2j}^{(2)}(y) w_{yyij} + H_{1i}^{(2)}(x) H_{1j}^{(2)}(y) w_{xyij} \right]$ <p>where $w_{ij}, w_{xij}, w_{yij}, w_{xxij}, w_{yyij},$ and w_{xyij} are the D.O.F. and</p> $H_{01}^{(2)}(x) = \frac{1}{5} (a^5 - 10a^2x^3 + 15ax^4 - 6x^5), H_{02}^{(2)}(x) = \frac{1}{5} (10a^2x^3 - 15ax^4 + 6x^5), H_{12}^{(2)}(x) = \frac{1}{a^4} (4a^2x^3 + 7ax^4 - 3x^5)$ $H_{11}^{(2)}(x) = \frac{1}{a^4} (4x^4 - 6a^2x^3 + 8ax^4 - 3x^5), H_{21}^{(2)}(x) = \frac{1}{2a^3} (a^3x^2 - 3a^2x^3 + 3ax^4 - x^5), H_{22}^{(2)}(x) = \frac{1}{2a^3} (a^2x^3 - 2ax^4 + x^5)$ <p>where for y the x's become y's and the a's become b's</p> <p>For compatibility</p> <ul style="list-style-type: none"> (i) all four elements at a node must have identical w_{ij}, w_{xij}, w_{yij} and w_{xyij} at common corners (ii) the elements joining along edge $x = \text{const.}$ must have identical w_{yyij}. (iii) similarly $y = \text{const.}$ identical w_{xxij} <p>Tables are required for stiffness coefficients. The element has also been incorporated into a non-linear analysis, (65).</p>	
SM (41)	
8 noded 24 D.O.F.	conformal Hybrid-stress. Shear deformation model
<p>Hybrid-stress representation of a serendipity element. Stiffness coefficients were evaluated using 3×3 Gaussian numerical integration. The hybrid-stress approach was applied to prevent locking found with Serendipity elements and prevent the spurious zero energy modes found with Lagrangian elements.</p> <p>Stress distributions are given by the following:-</p> $\sigma_x = \beta_1 + x\beta_2 + y\beta_3 + xy\beta_4 + x^2\beta_5 + y^2\beta_6 + xy^2\beta_7 + x^2y\beta_8$ $\sigma_y = \beta_9 + x\beta_{10} + y\beta_{11} + xy\beta_{12} + x^2\beta_{13} + y^2\beta_{14} + xy^2\beta_{15} + x^2y\beta_{16}$ $\sigma_{xy} = \beta_{17} + x\beta_{18} + y\beta_{19} + xy\beta_{20} + x^2\beta_{21} + y^2\beta_{22}, \sigma_z = 2(\beta_5 + \beta_{14} + \beta_{20}) + 2x\beta_{15} + 2y\beta_8$ $\sigma_{xz} = \beta_2 + \beta_{19} + x(2\beta_5 + \beta_{20}) + y(\beta_4 + 2\beta_{22}) + 2xy\beta_8 + y^2\beta_7$ $\sigma_{yz} = \beta_{11} + \beta_{18} + x(\beta_{12} + 2\beta_{22}) + y(2\beta_{14} + \beta_{20}) + 2\beta_{15}xy + x^2\beta_{16}$ <p>The paper gives an explanation for the formulation of the above eqs.</p> <p>The displacement functions for the Serendipity element are:-</p> $\frac{dw}{dx} = \alpha_1 + \xi\alpha_2 + \eta\alpha_3 + \xi\eta\alpha_4 + \xi^2\alpha_5 + \eta\alpha_6 + \xi\eta^2\alpha_7 + \xi^2\eta\alpha_8$ $\frac{dw}{dy} = \alpha_9 + \xi\alpha_{10} + \eta\alpha_{11} + \xi\eta\alpha_{12} + \xi\alpha_{13} + \eta\alpha_{14} + \xi\eta^2\alpha_{15} + \xi^2\eta\alpha_{16}$ $w = \alpha_{17} + \xi\alpha_{18} + \eta\alpha_{19} + \xi\eta\alpha_{20} + \xi\alpha_{21} + \eta\alpha_{22} + \xi\eta^2\alpha_{23} + \xi^2\eta\alpha_{24}$ <p>where $\xi = \frac{x}{a}, \eta = \frac{y}{b}$</p>	

Table 3.2 Finite elements for linear evaluation (contd.)

T (31)

3 noded non-conformal simple polynomial. Displacement method
9 D.O.F.

Tocher tried to improve the simple function applied by Adini .
The proposed displacement function is :-

$$w = \alpha_1 + x\alpha_2 + y\alpha_3 + x^2\alpha_4 + xy\alpha_5 + y^2\alpha_6 + x^3\alpha_7 + (x^2y + xy^2)\alpha_8 + y^3\alpha_9$$

HCT (33)

7 noded based on simple polynomials
9 D.O.F Displacement method

Although the element T describes triangular displacement compatability between adjacent elements, it does not provide normal slope compatability in a triangular plate bending system, (c.f. ACM).

A correct element can be achieved by dividing the element into three subsections. The stiffness analysis is then based on assuming an independent polynomial displacement function for each sub-element. The displacement function is:-

$$w = \alpha_1 + x\alpha_2 + y\alpha_3 + x^2\alpha_4 + xy\alpha_5 + y^2\alpha_6 + x^3\alpha_7 + xy^2\alpha_8 + y^3\alpha_9$$

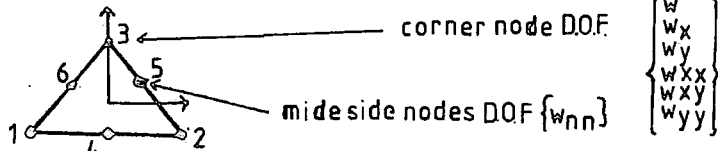
where x,y are the co-ordinate system for each sub-element.
The complete element involves a total of 27 D.O.F., 18 are employed in satisfying internal compatability between adjacent sub-elements while the remaining 9 D.O.F. are bending D.O.F of the element. A reduction technique then reduces the unknowns to leave just the governing D.O.F..

B (35)

3 noded conformal Refined polynomial. Displacement method
18 D.O.F

This refined element is based on an assumed displacement function which forms a complete 5th order polynomial expression in x and y.

The expression contains 21 terms and requires an element with mid-side nodes.



These mid-side nodes were undesirable in the analysis and were eliminated using a condensation process to leave the 18 bending D.O.F.. The stiffness coefficients were evaluated by numerical integration.

Figure 3.3 SIMPLY SUPPORTED SQUARE ISOTROPIC PLATE UNDER UNIFORMLY DISTRIBUTED LOAD (V.L.O.)

Figure 3.3.1 CENTRAL DISPLACEMENT α

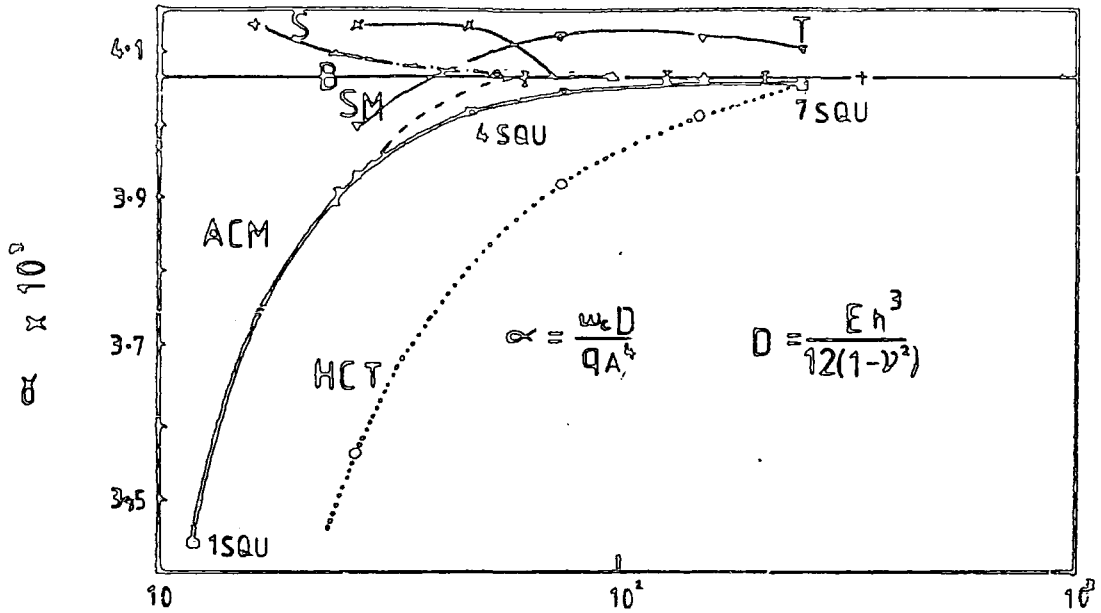
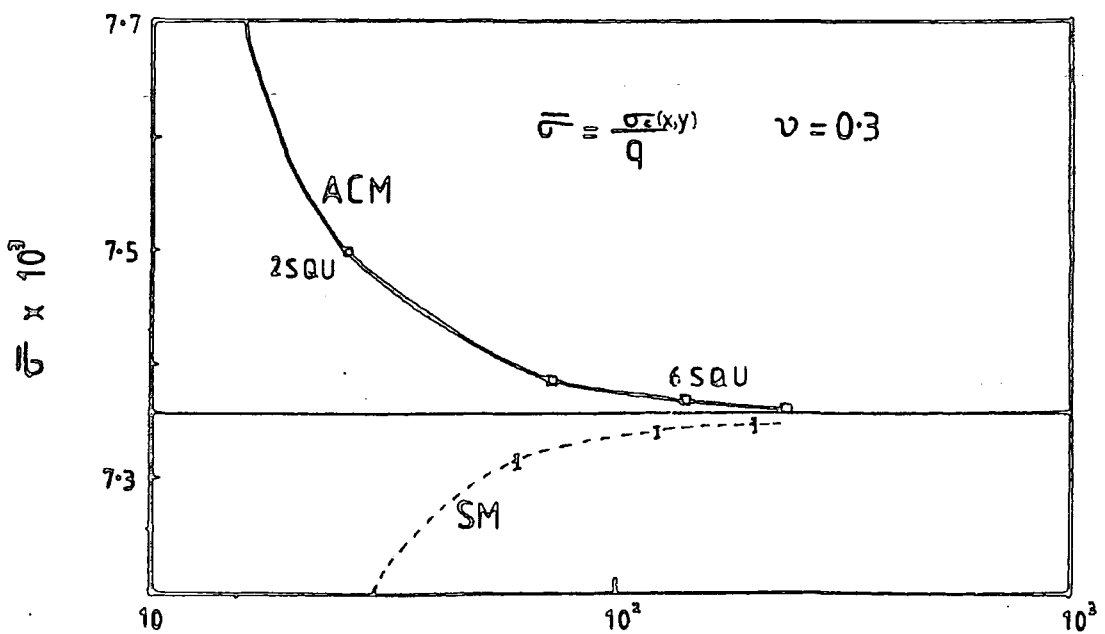


Figure 3.3.2 central surface STRESS $\bar{\sigma}$ (TENSILE)



TOTAL NUMBER OF DEGREES OF FREEDOM FOR A QUARTER OF THE PLATE

Figure 3.4 SQUARE ISOTROPIC PLATE WITH A CONCENTRATED LOAD AT THE CENTRE

Figure 3.4.1 SIMPLY SUPPORTED . CENTRAL DISPLACEMENT β

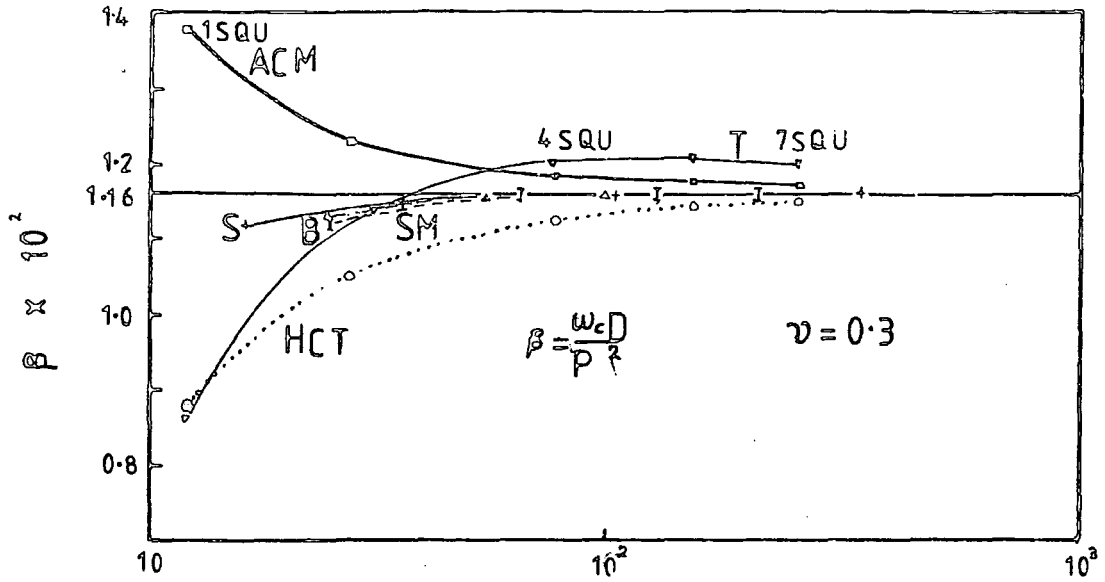
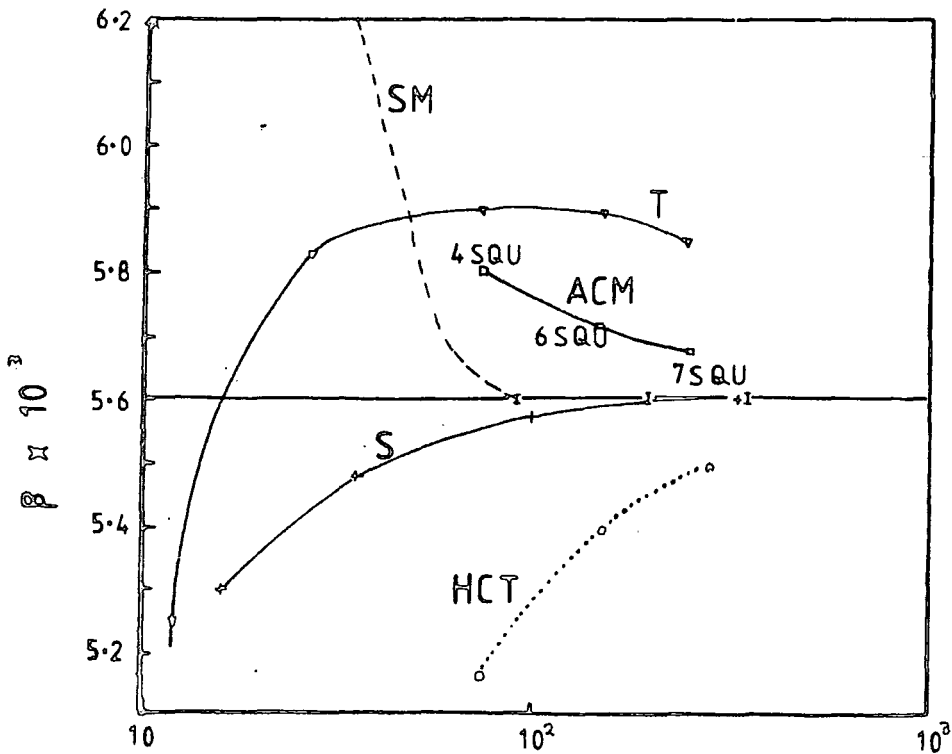


Figure 3.4.2 CLAMPED. CENTRAL DISPLACEMENT β



TOTAL NUMBER OF DEGREES OF FREEDOM FOR A QUARTER OF THE PLATE

Figure 3.5 SQUARE ISOTROPIC PLATE WITH CORNER POINT SUPPORTS UNDER UNIFORMLY DISTRIBUTED LOAD (V.L.O.)

Figure 3.5.1 central DISPLACEMENT α

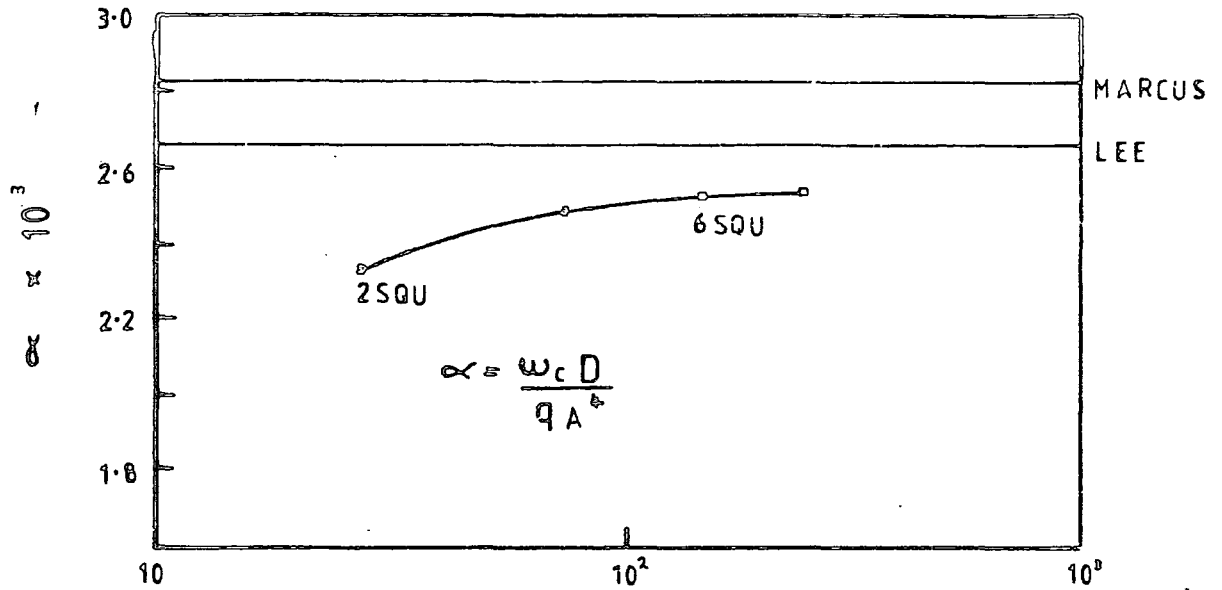


Figure 3.5.2 CENTRAL SURFACE STRESS

$\bar{\sigma}$ (TENSILE)

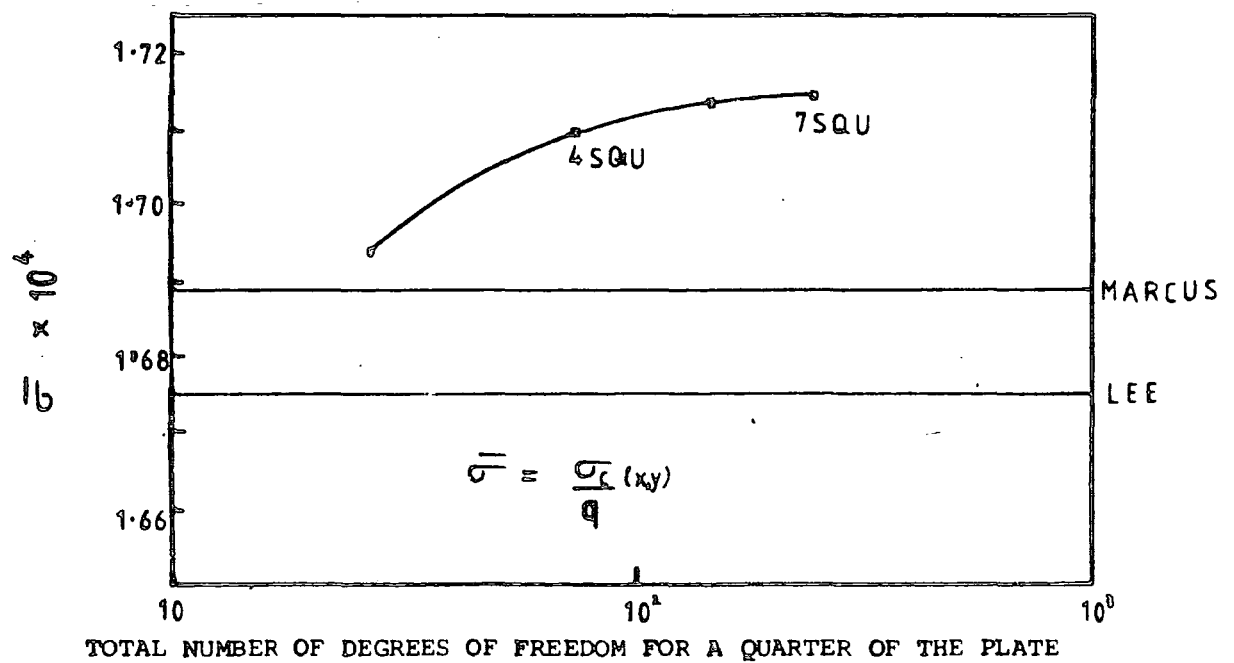


Figure 3.6 SQUARE ISOTROPIC PLATE WITH CORNER POINT SUPPORTS UNDER CENTRAL PATCH LOAD. (V.L.O.)

$$\left\{ \frac{A}{A'} P = \frac{B}{B'} P = 0.1 \right\}$$

Figure 3.6.1 CENTRAL DISPLACEMENT α

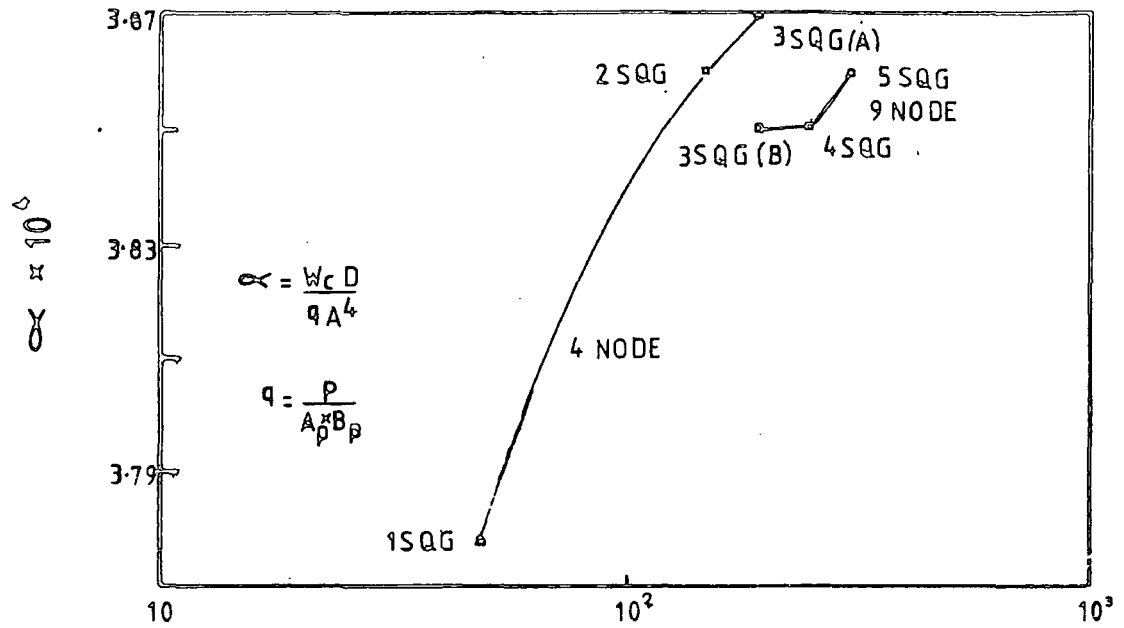


Figure 3.6.2 CENTRAL SURFACE STRESS (σ) (TENSILE)

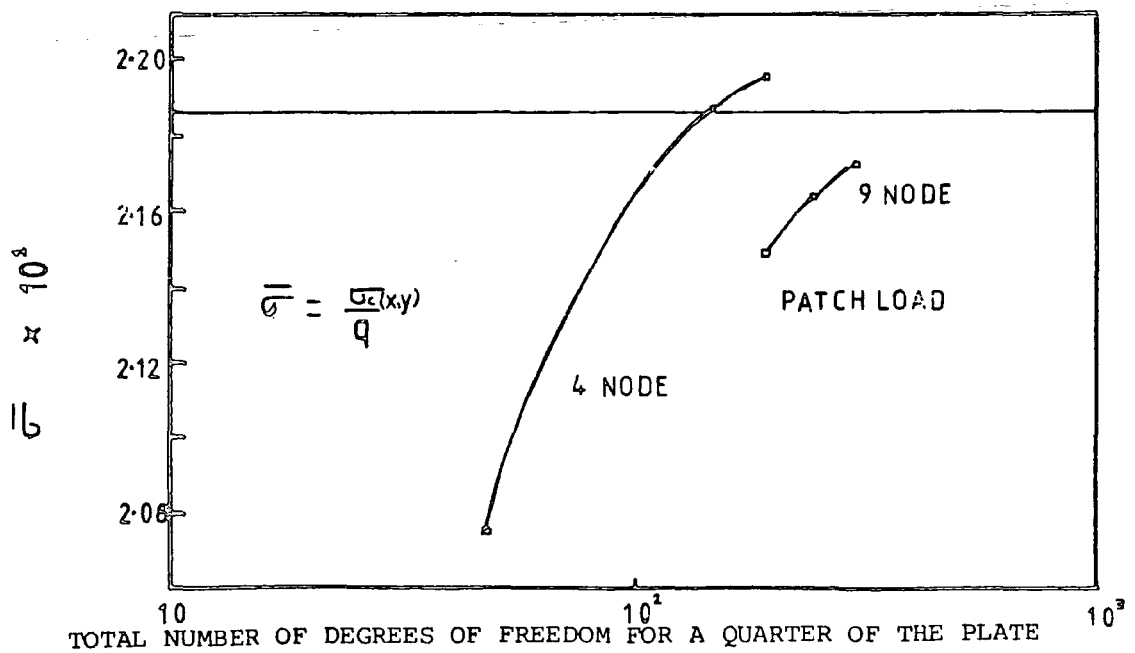


Figure 3.7 ORTHOTROPIC CROSS-PLY TEST EXAMPLE

Figure 3.7.1 TEST PARAMETERS

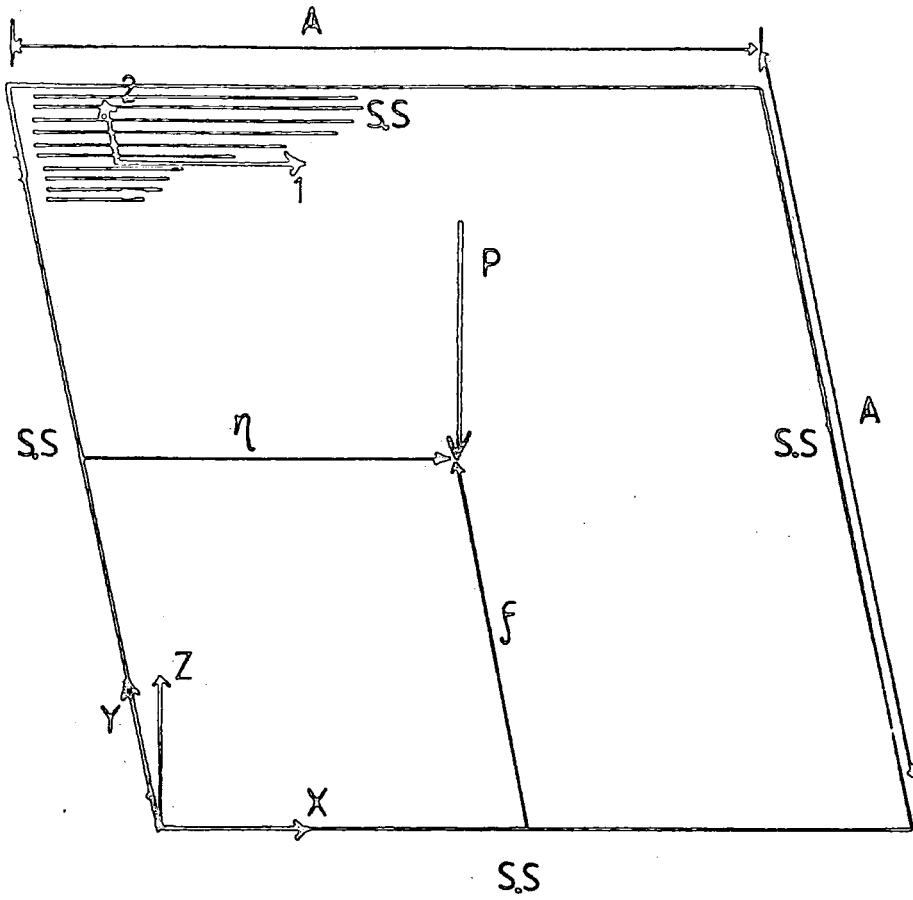


Figure 3.7.2 LAMINATION CONFIGURATION

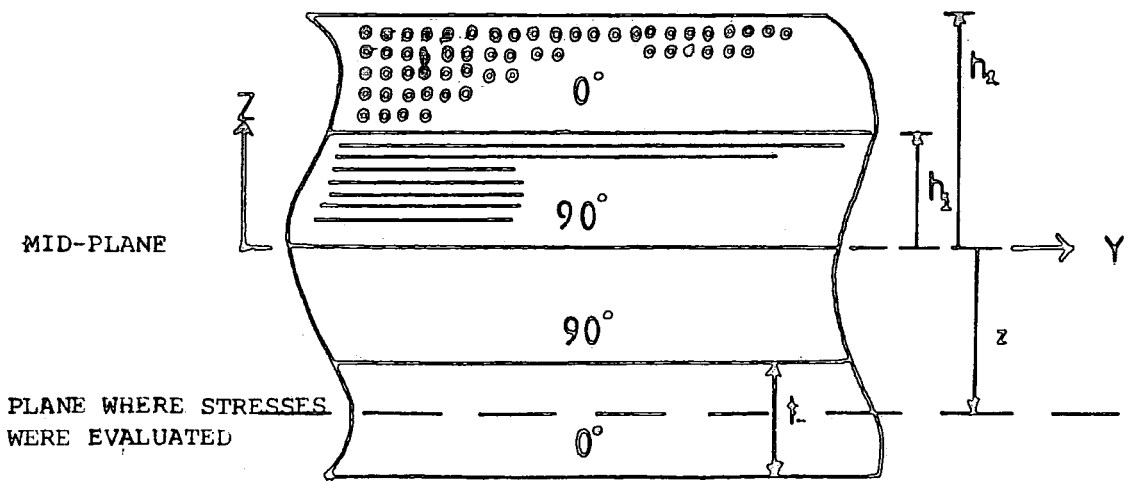


Figure 3.8 FINITE ELEMENT MODELS

Figure 3.8.1 MESH 3SQG(A)

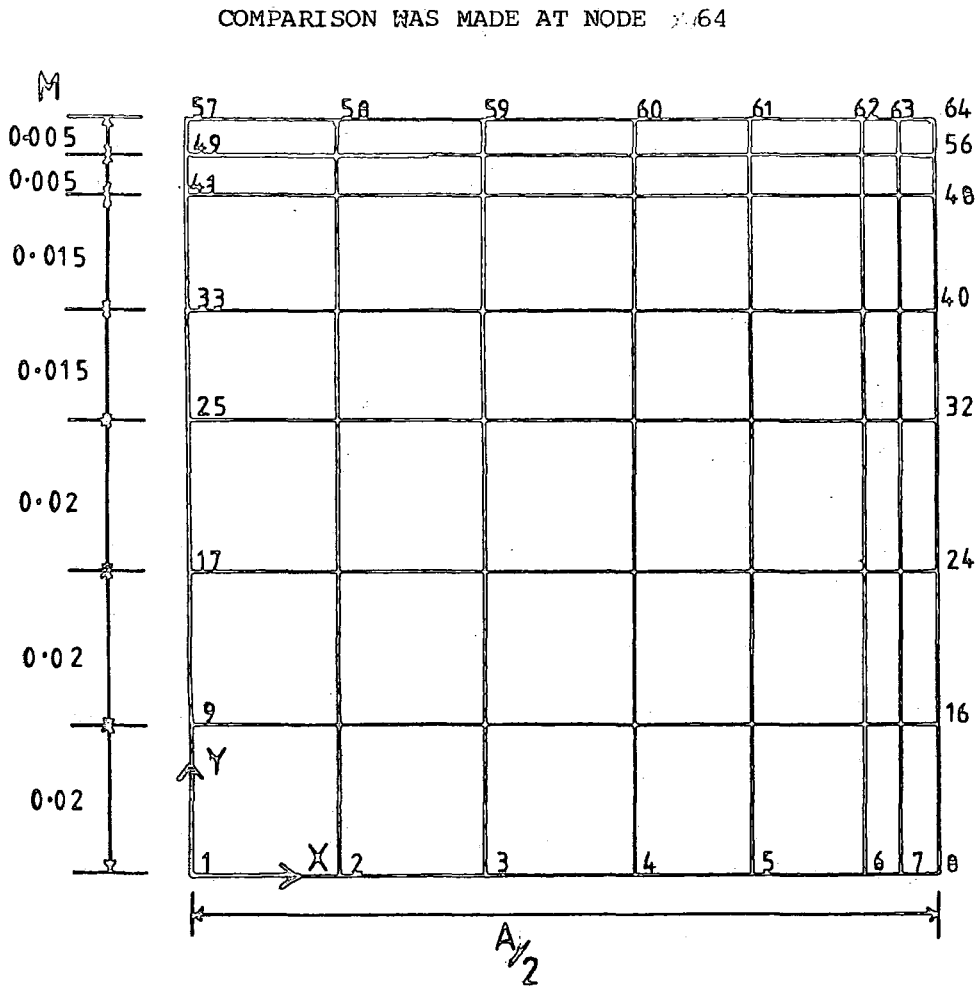


Figure 3.8.2 BOUNDARY CONDITIONS (A) AEM (B) PAFEC 75

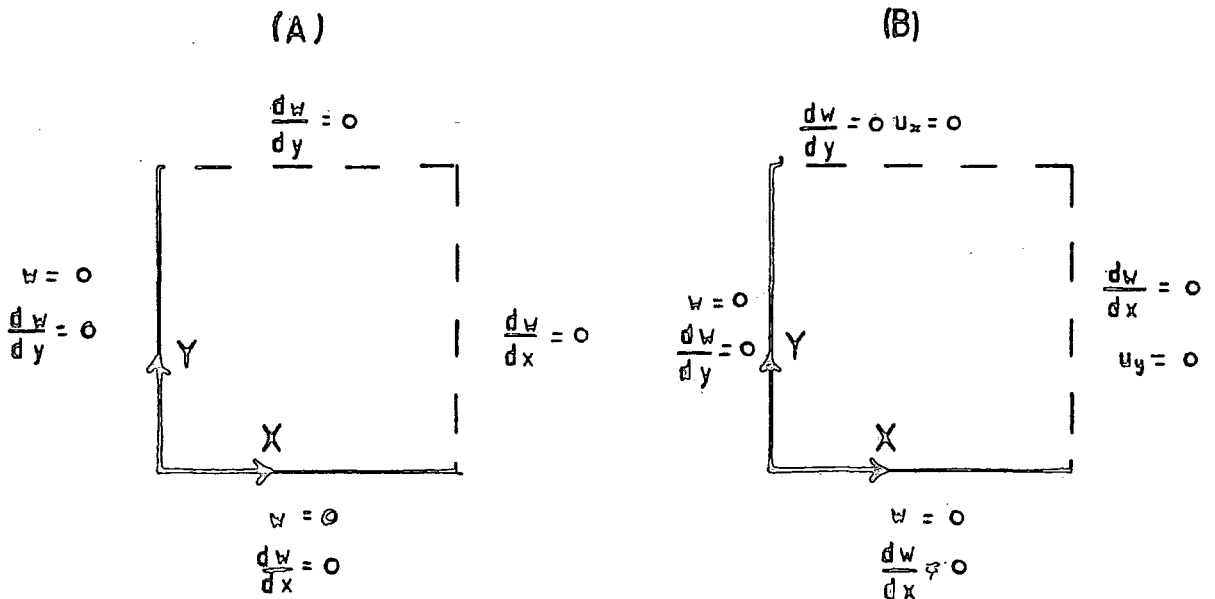


Table 3.3 Deflections

All transverse displacements are * E-03m

Except when otherwise stated results were calculated using mesh 3SQ(A)

Position in plate Node number	PAFEC 75		ACM element	Analytical m=n=1,23(odd)
	4-noded	8-noded		
64 w_c	9.239	8.050	7.605 7.584*	7.562
63	9.081	7.975	7.553	7.508
56	9.046	7.942	7.520	7.481
55	8.995	7.896	7.481	7.440
28	4.940	4.397	4.203	4.169
10	0.0637	0.0570	0.0543	0.0539

Table 3.4 Stresses

Stresses at the mid-plane of the outer lamina (0°) * E+08 N/m²

Position in plate Node number	PAFEC 75		ACM element	Analytical m=n=1,2ol(odd)
	4-noded	8-noded		
64 σ_x σ_y	3.83 0.701	5.75 0.942	5.46(5.50*) 0.864(0.869*)	7.38 $\{m=n=1,801\text{odd}\}$ 0.887
63 σ_x σ_y	3.17 ± 20% 0.57 ± 3%	3.16 ± 24% 0.63 ± 3%	2.88 0.62	3.11 0.40
56 σ_x σ_y	3.15 ± 2% 0.51 ± 34%	3.91 ± 1% 0.38 ± 21%	3.36 0.35	3.48 0.38
55 σ_x σ_y	2.92 ± 7% 0.49 ± 15%	3.35 ± 14% 0.47 ± 14%	3.28 0.43	3.18 0.36
28 σ_x σ_y	0.99 ± 15% 0.095 ± 33%	1.10 ± 7% 0.082 ± 16%	1.09 0.076	1.07 0.101
10 σ_x σ_y	0.13 ± 49% .0089 ± 59%	0.15 ± 22% .0046 ± 58%	0.150 .0027	0.144 .0012

* Results using mesh 5SQ

Table 3.5 C.P.U Time

Model	Mesh	D.O.F	C.P.U sec. (IBM 370/167)
ACM	3SQG(A)	192	<10 *
ACM	5SQG	363	<15
PAFEC 75			
4-node	3SQG(A)	320	70 *
8-node	3SQG(A)	880	320
12-node	3SQG(A)	1440	>900

* Identical models

Figure 3.9 WEBBER'S ANGLE PLY CANTILEVER EXAMPLE

Figure 3.9.1 MESH IRFU . TEST PARAMETERS

SCALE 5:1

lay-up (45°, -45°, -45°, 45°)

Length 0.228 E-01 m
 Width 0.381 E-01 m
 Thickness 0.1 E-01 m

$E_{11} = 0.230 \text{ E}+12 \text{ N/M}^2$

$E_{22} = 0.135 \text{ E}+11 \text{ N/M}^2$

$G_{12} = 0.525 \text{ E}+10 \text{ N/M}^2$

$\nu_{12} = 0.43$

$P = 26.75 \text{ N}$

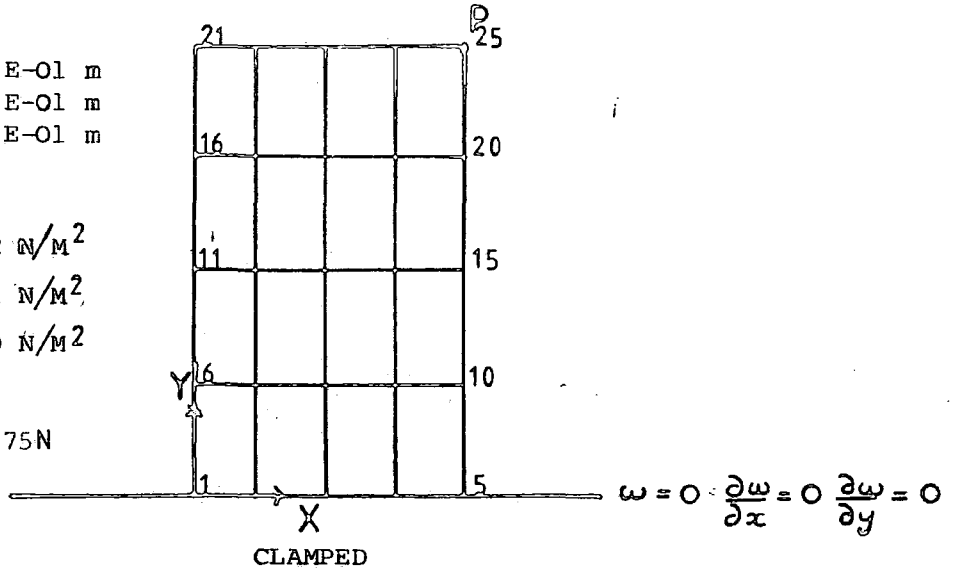


Figure 3.9.2 DISPLACEMENT OF CANTILEVER PLATE WITH POINT LOAD AT NODE 25

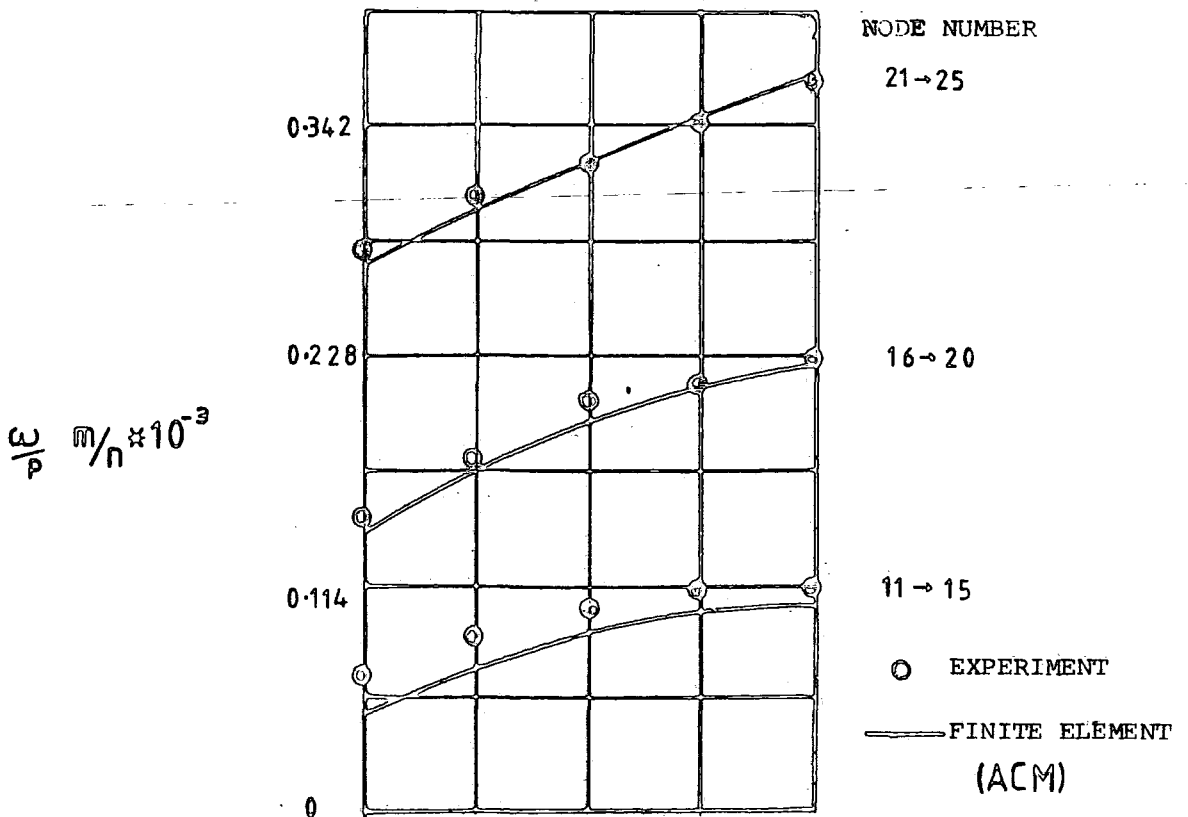
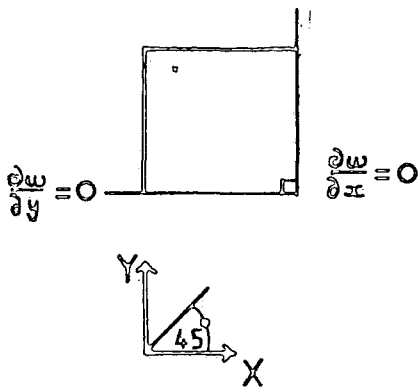


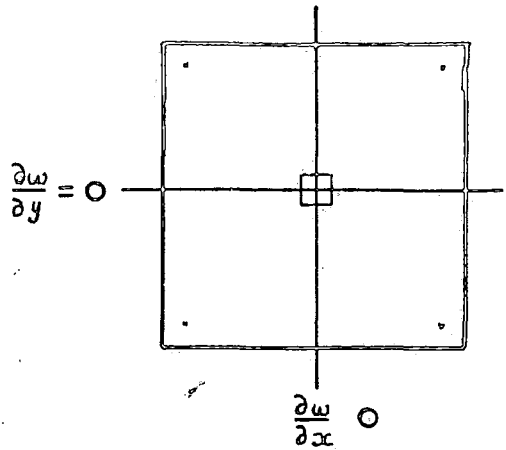
Figure 3.10 QUARTER PLATE BOUNDARY LIMITATIONS
45° LAMINATE TEST EXAMPLE

FINITE ELEMENT BOUNDARY CONDITIONS (ACM,ACMBC)

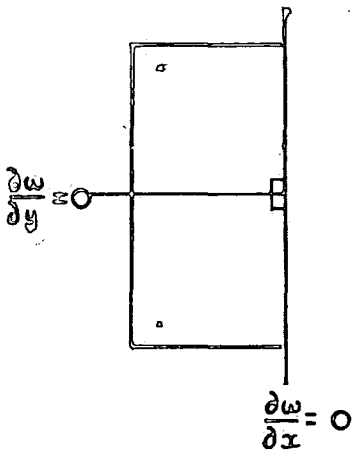
QUARTER PLATE Fig. 3.10.1



FULL PLATE (QUARTER PLATE B.C.)
Fig. 3.10.3



HALF PLATE Fig. 3.10.2



FULL PLATE Fig. 3.10.4

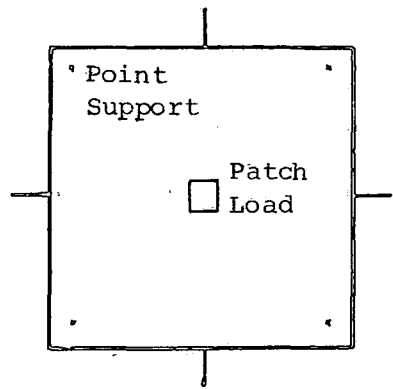


Figure 3.10.5: LOCATION OF THE ZERO CURVATURES FOR THE 45° LAMINATE EXAMPLE

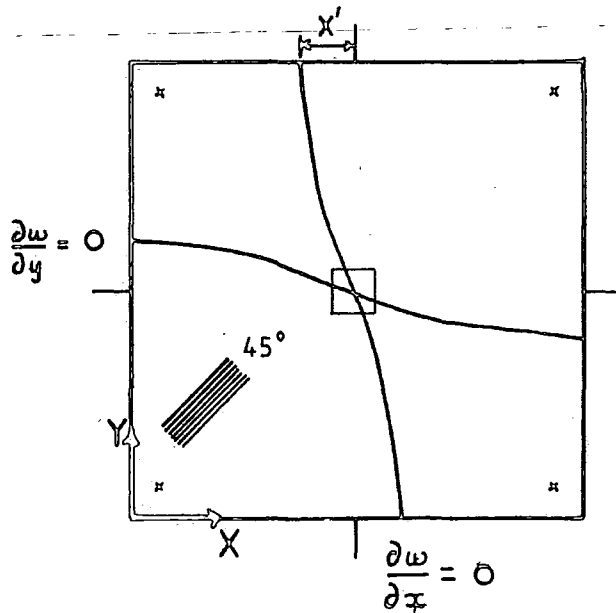


Table 3.6 Modelling a 45° laminate plate in the plate bending test.

Plate dimensions

A = 0.26m B = 0.26m
 h = 0.2E-02m
 A_S = 0.2m B_S = 0.2m
 A_p = 0.02m B_p = 0.0m

Central patch load P = 100N (C.L.V)

Material properties

E₁₁ = 0.25E+12 N/m
 E₂₂ = 0.10E+11 N/m
 G₁₂ = 0.58E+10 N/M
 ν₁₂ = 0.3

Model	Orientation	Central transverse displacement	Tensile surface strains at the centre	
		* E-02m	X(0°) μE	Y(90°)
1SFGE144 (Fig. 3.10.4)	±45°	0.270	1017	1017
1SFGE144 (Fig. 3.10.3)	±45°	0.240	449	449
1SHGE50 (Fig. 3.10.2)	±45°	0.324	637 637	1961 189
1SHGE72 (Fig. 3.10.2)	±45°	0.324	620 620	2098 182
1SQGE100 (Fig. 3.10.1)	+45° (Case 1)	0.433	3291	3291
1SQGE100 (Fig. 3.10.1)	-45° (Case 2)	0.379	-28	-28

Table 3.7 Geometric non-linear examples- Load increments

SIMPLY SUPPORTED		CLAMPED	
\bar{q}	No. of iterations	\bar{q}	No. of iterations
32.8	6	31.3	12
98.3	4	93.8	10
163.8	6	156.2	11
229.4	6	218.8	12
294.4	6	281.3	12
Approximate C.P.U. time 50 + sec.		Approximate C.P.U. Time 140+ sec.	

Table 3.8 ACMBC -Analytical comparison(Levy)

Parameters non-dimensional	Simply Supported	Clamped
\bar{w}_D	yes	yes
$\bar{\sigma}_{Dx}$	yes	yes
$\bar{\sigma}_{B Dx}$	yes	yes
$\bar{\sigma}_{R Dx}$	yes	yes
$\bar{\sigma}_{R Bx}$	yes	no
$\bar{\sigma}_{PL Cx}$	yes	no
$\bar{\sigma}_{Cx}$	no	yes
$\bar{\sigma}_{B Axy}$	yes	no

See Figures 3.11 to 3.17

Figure 3.11 SIMPLY SUPPORTED SQUARE PLATE UNIFORM PRESSURE LOAD (C.L.V.), LEVY INPLANE RESTRAINTS

Figure 3.11.1 CENTRAL TRANSVERSE DISPLACEMENT

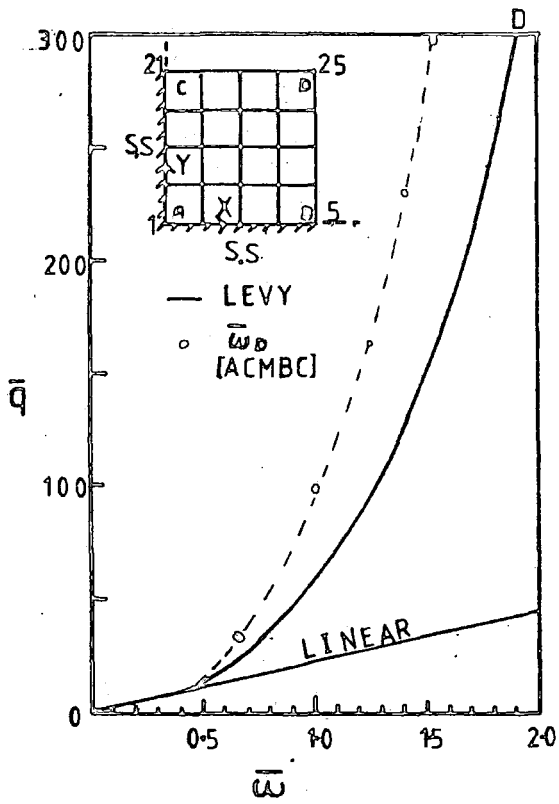


Figure 3.11.2 CENTRAL SURFACE TENSILE STRESS

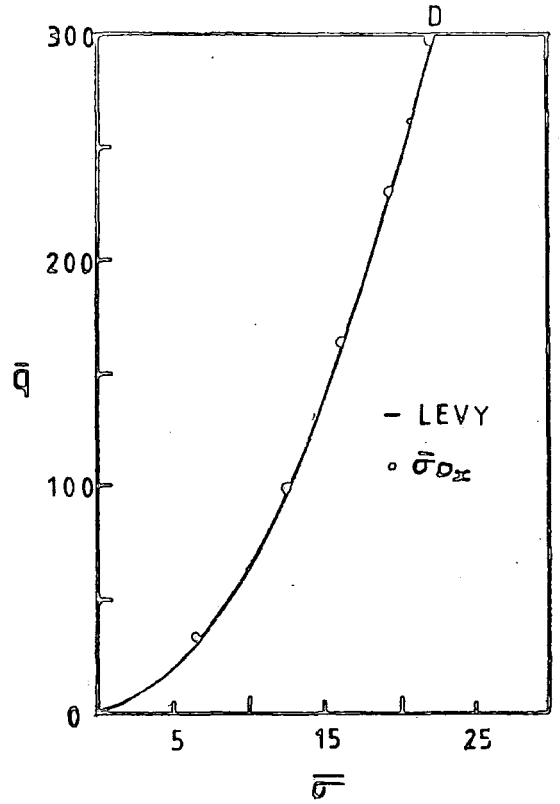


Figure 3.11.3 IN-PLANE SURFACE TENSILE STRESSES

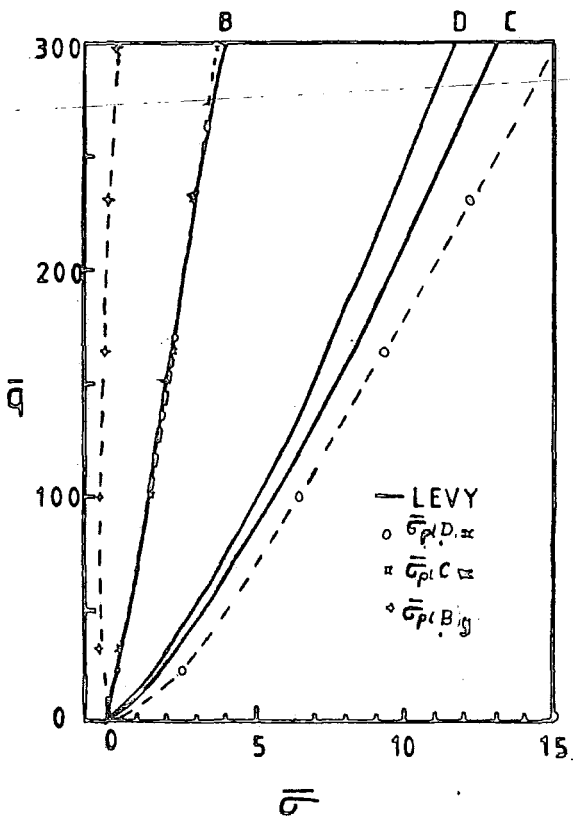


Figure 3.11.4 BENDING SURFACE TENSILE STRESSES

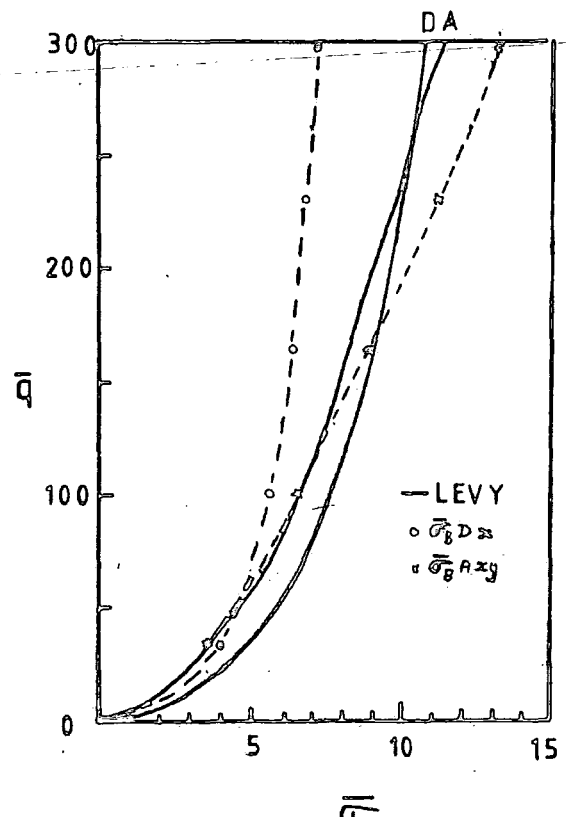


Figure 3.12 CLAMPED SQUARE ISOTROPIC PLATE UNIFORM PRESSURE LOAD (C.L.V.), LEVY IN-PLANE RESTRAINTS

Figure 3.12.1 CENTRAL TRANSVERSE DISPLACEMENT

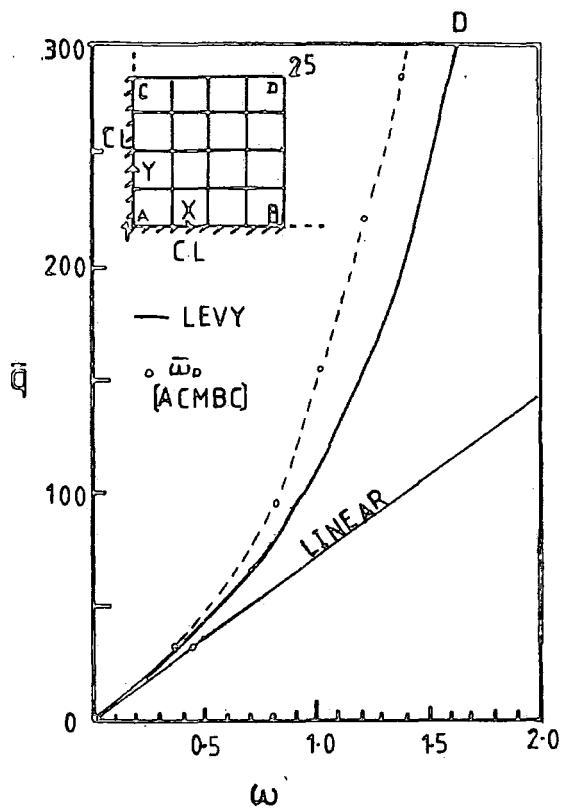


Figure 3.12.2 CENTRAL SURFACE TENSILE STRESS

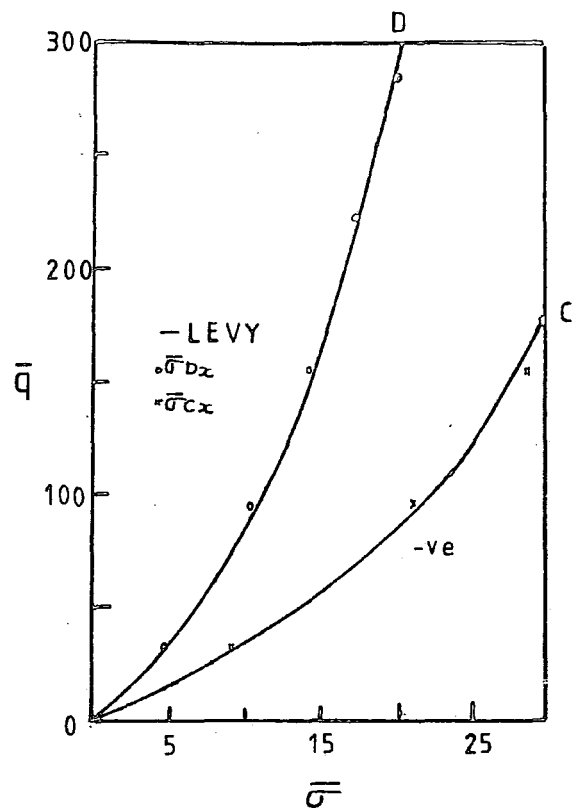


Figure 3.12.3 IN-PLANE SURFACE TENSILE STRESS

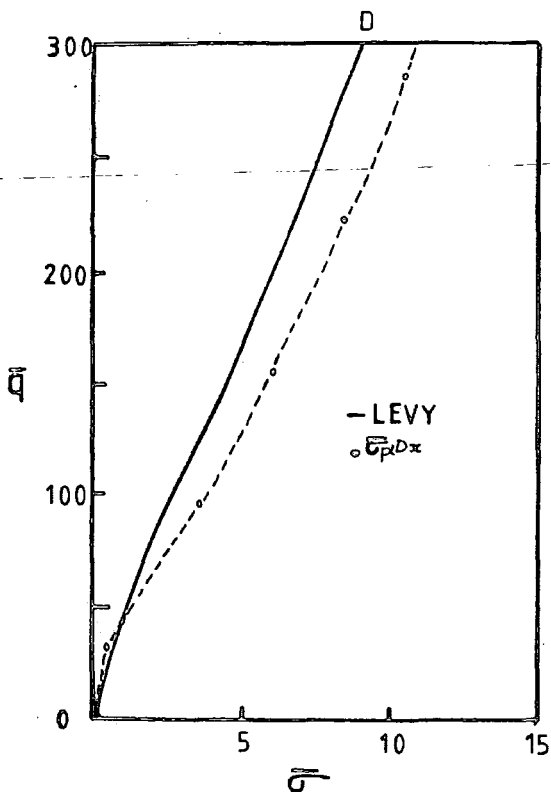


Figure 3.12.4 BENDING SURFACE TENSILE STRESS

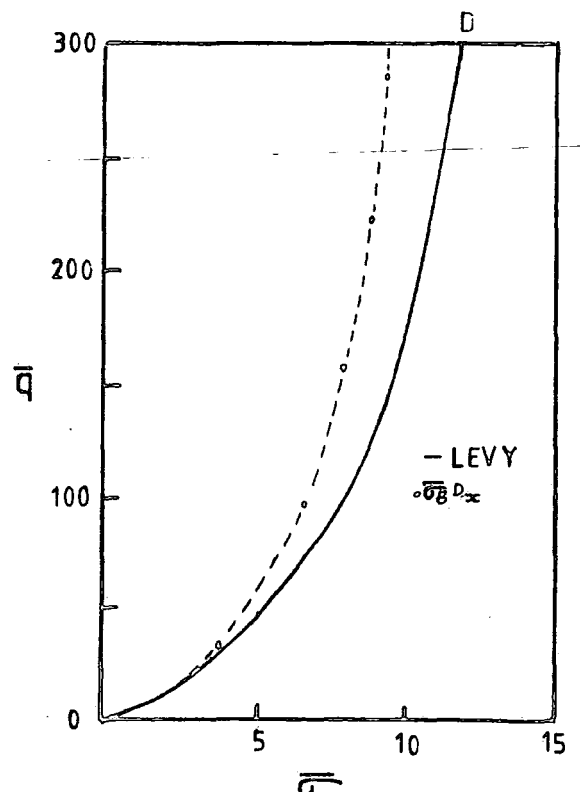


Table 3.9 Percentage errors for the non-linear isotropic simply supported plate, with a load factor $\bar{q} = 200$
(Fig. 3.11)

(ref) Author	Element	Analysis	Mesh	\bar{w}_D %	$\bar{\sigma}_{Dx}$ %	$\bar{\sigma}_B D_x$ %	$\bar{\sigma}_{PL} D_x$ %
	simply polynomials ACMBC (4 noded)	laminated	4 x 4 (125)	≈ 20.0L	≈ 1.0L	32.5L	27.0L
Bergan + Clough (70)	Q-19 (bending) lagrangian(in-plane) (4-noded)	isotropic	4 x 4 (125)	≈ 1.1L	≈ 15.3L	10.3L	5.0L
Pica +	Heterosis QH (9-noded)	isotropic	4 x 4 (425)	0.3L	0.7H		
Wood +	Serendipity QS (8-noded)	isotropic	4 x 4 (325)	0.3L	1.0H		
Hinton (76)	Lagrangian QL (9-noded)	isotropic	4 x 4 (405)	0.3L	0.9H		
Reddy +	Serendipity linear (4-noded)	laminated	4 x 4 (125)	8.4H		≈ 7.3L	
Chao (74)	Serendipity quartic (8-noded)	laminated	4 x 4 (325)	1.5L		≈ 7.3L	
Chang + Sawamiphakdi (86)	Serendipity (8-noded)	laminated	4 x 4 (325)	≈ 1.0L			
	Lagrangian (9-noded)	laminated	4 x 4 (405)	≈ 1.0L			

L = lower than analytical H = higher than analytical

Table 3.10 Percentage errors for the non-linear isotropic clamped plate, with a load factor $\bar{q} = 200$ (Fig. 3.12)

Author (ref.)	Element	Analysis	Mesh	\bar{w}_D %	$\bar{\sigma}_{Dx}$ %	$\bar{\sigma}_{Cx}$ %
	simply polynomials ACMBC (4-noded)	laminated	4 x 4 (125)	16.0L	≈1.0L	5.0H
Brebbia + Connor(29)	simply polynomials ACMBC (4-noded)	isotropic	4 x 4 (125)	7.5H		
Thomas + Gallagher (71)	inconsistent quad. '4 triangles' (4-noded)	isotropic	4 x 4 ?	4.4H		
Pica +	Heterosis QH (9-noded)	isotropic	4 x 4 (425)	≈1.8L	≈2.0H	≈1.4L
Wood +	Serendipity QS (8-noded)	isotropic	4 x 4 (325)	≈1.8L	≈3.0H	≈4.0L
Hinton(76)	Lagrangian QL (9-noded)	isotropic	4 x 4 (405)	≈1.7L	≈3.5H	≈1.3L
Bogner + Fox + Schmit (63)	Hermitian (4-noded) 24 D.O.F.	isotropic	? ?	≈2.0L	≈3.0H	≈4.0L
Reddy +	Serendipity linear (4-noded)	laminated	4 x 4 (125)	18.5H		
Chao (74)	Serendipity quartic(8-noded)	laminated	4 x 4 (325)	4.0H		

L = lower than analytical H = higher than analytical

Figure 3.13

ACMBC FINITE ELEMENT ANALYSIS

Figure 3.13.1 3SQU QUARTER PLATE MESH . NONLINEAR BOUNDARY CONDITIONS

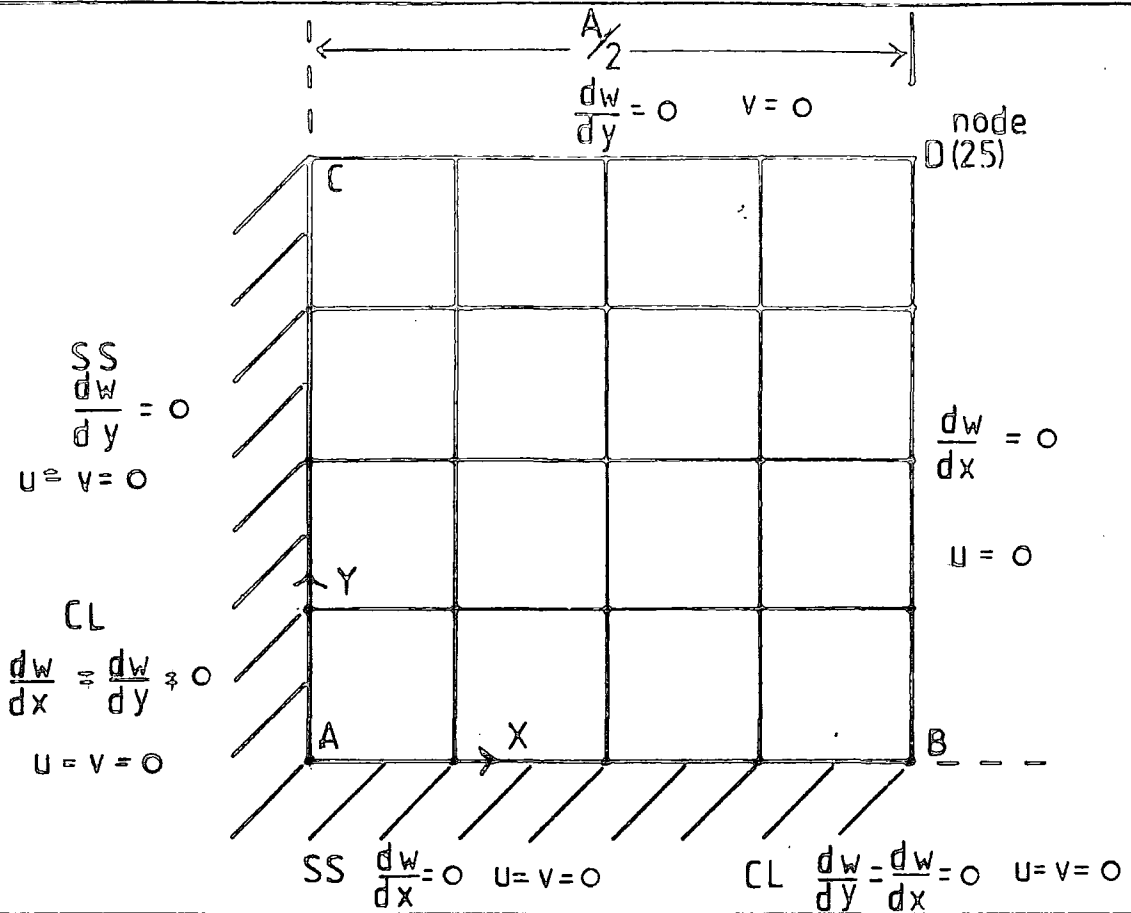


Figure 3.13.2 SECTION (B-D) OF PLATE SHOWING TRANSVERSE DISPLACEMENT

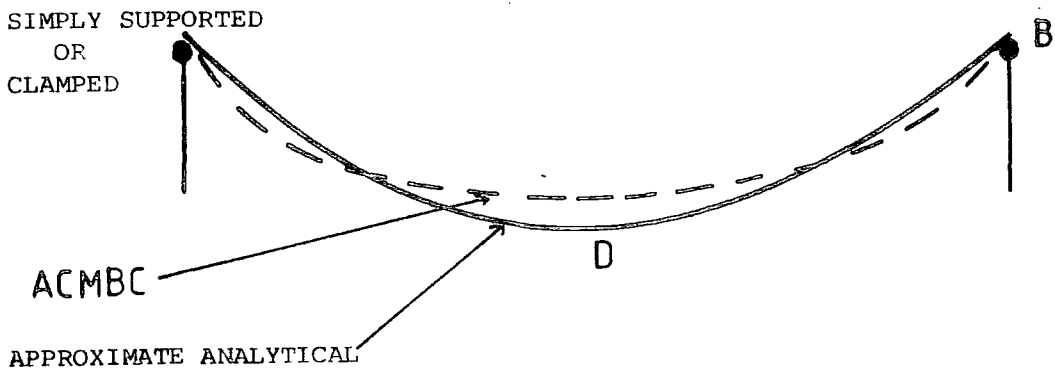


Figure 3.14. SIMPLY SUPPORTED SQUARE ISOTROPIC PLATE UNIFORM PRESSURE LOAD (C.L.V.), LEVY IN-PLANE RESTRAINTS
 ROTAV $\left[\frac{dw}{dx_e}, \frac{dw}{dy_e} \frac{3}{4} \rightarrow \frac{5}{6} \right]$

Figure 3.14.1 CENTRAL TRANSVERSE DISPLACEMENT

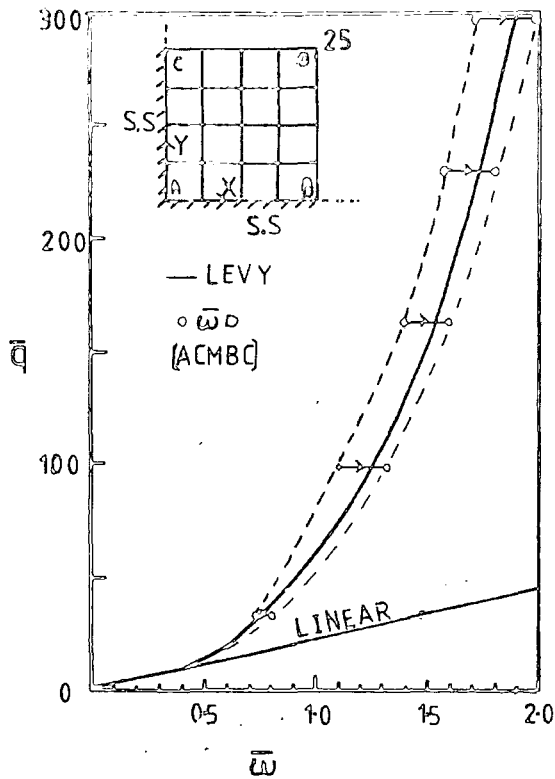


Figure 3.14.2 CENTRAL SURFACE TENSILE STRESS

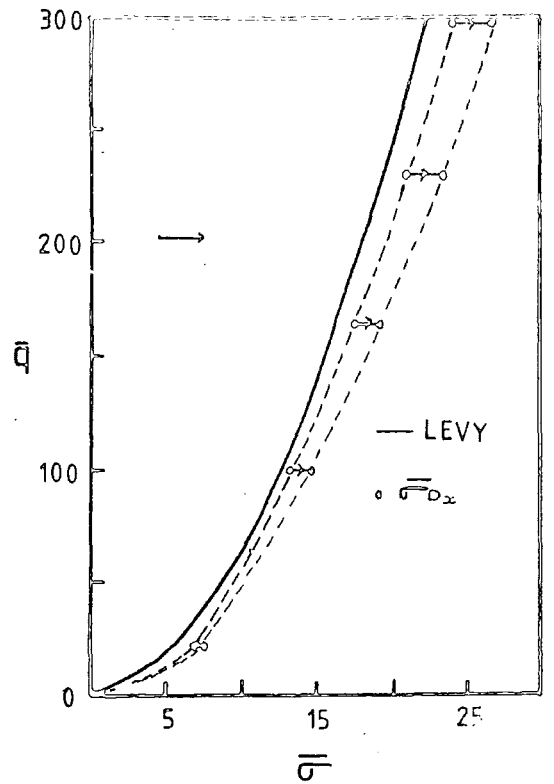


Figure 3.14.3 IN-PLANE SURFACE TENSILE STRESSES

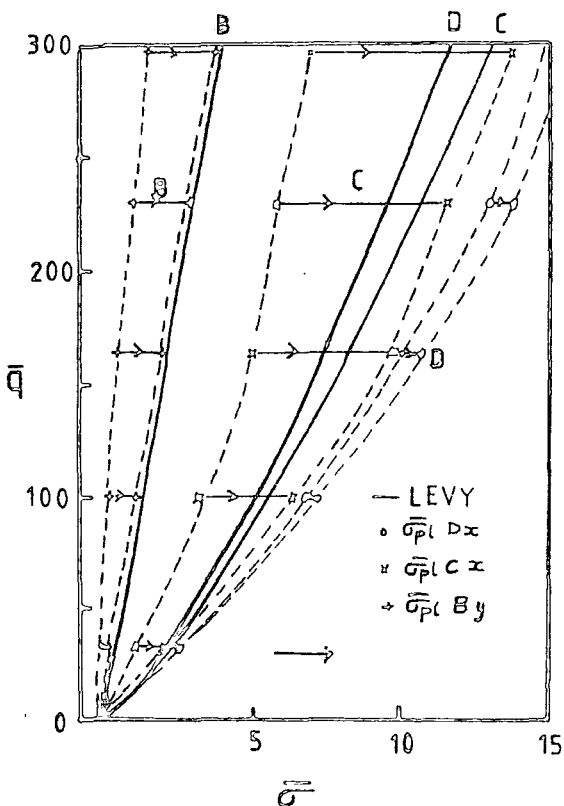


Figure 3.14.4 BENDING SURFACE TENSILE STRESSES

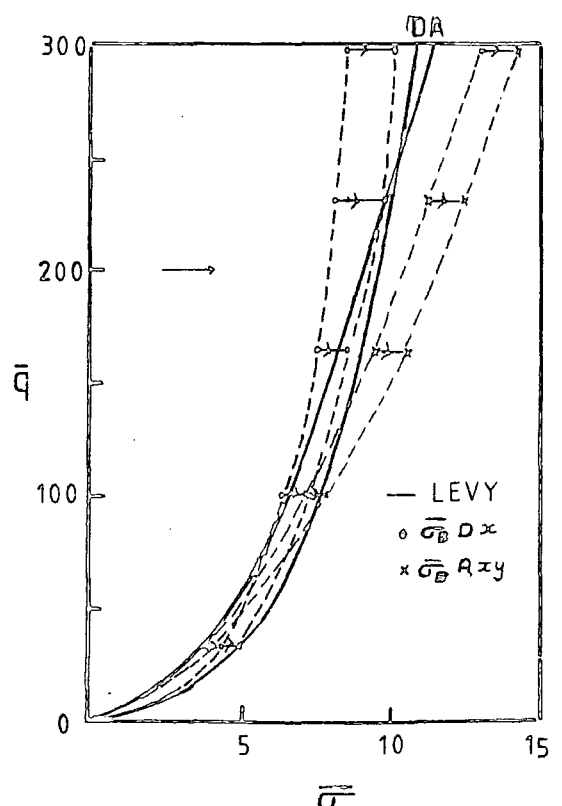


Figure 3.15 SIMPLY SUPPORTED SQUARE ISOTROPIC PLATE UNIFORM PRESSURE LOAD (C.L.V), LEVY IN-PLANE RESTRAINTS IN-PLANE STIFFNESS COEFFICIENTS 1.3 - 1.5

Figure 3.15.1 CENTRAL TRANSVERSE DISPLACEMENT

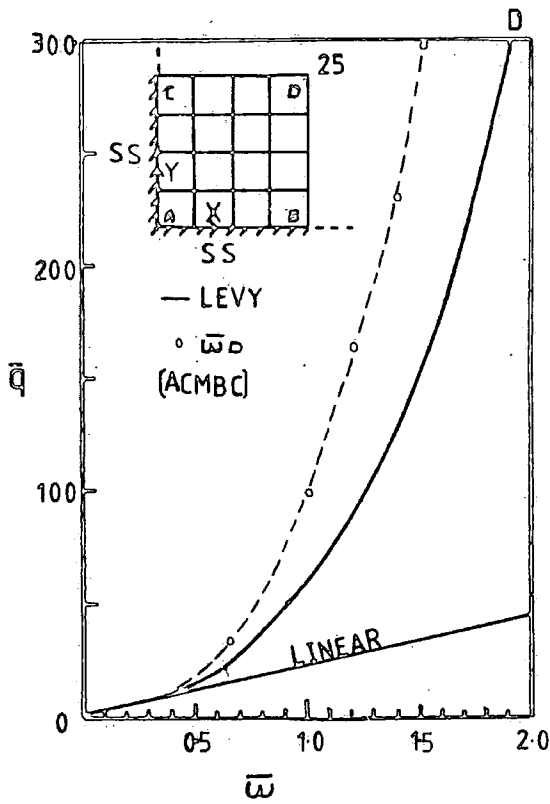


Figure 3.15.2 CENTRAL SURFACE TENSILE STRESSES

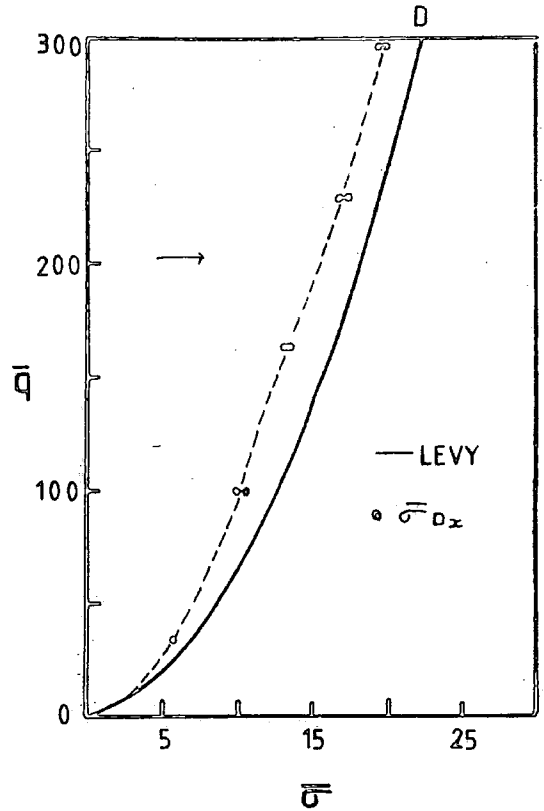


Figure 3.15.3 IN-PLANE SURFACE TENSILE STRESSES

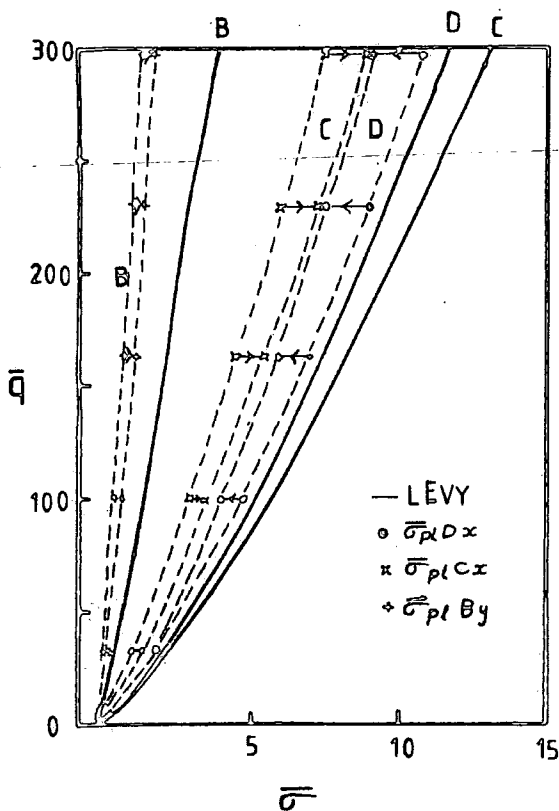


Figure 3.15.4 BENDING SURFACE TENSILE STRESSES

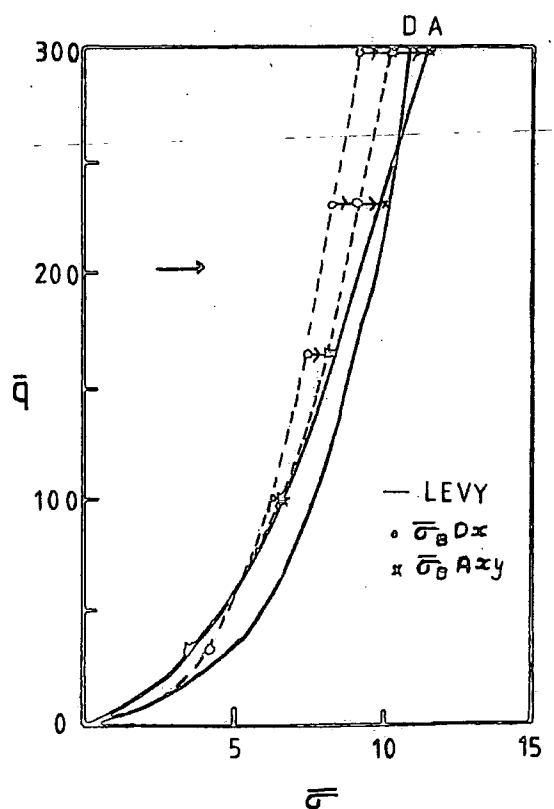


Figure 3.16. SIMPLY SUPPORTED SQUARE ISOTROPIC PLATE UNIFORM PRESSURE LOAD (C.L.V.), LEVY IN-PLANE RESTRAINTS
 ROTAV $\left\{ \begin{array}{l} \frac{dw}{dx} = 3 \\ \frac{dw}{dy} = 4 \end{array} \right\}$ IN-PLANE STIFFNESS COEFFICIENTS 1.3

Figure 3.16.1 CENTRAL TRANSVERSE DISPLACEMENT

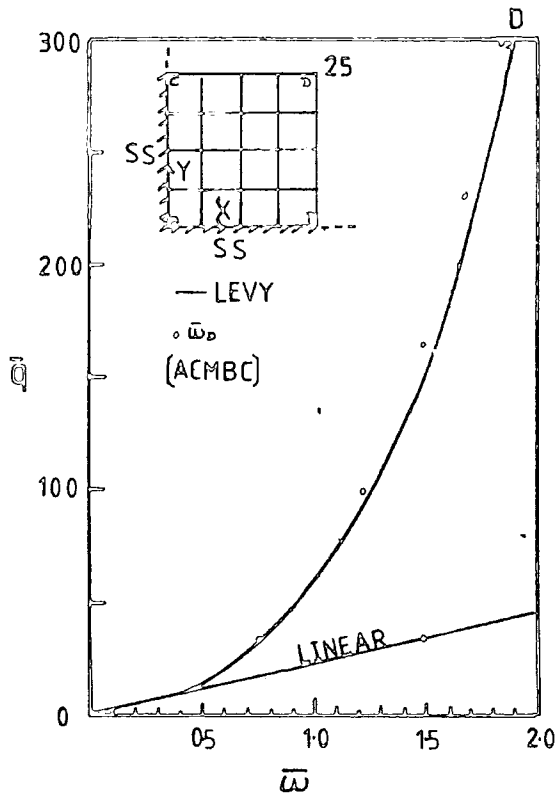


Figure 3.16.2 CENTRAL SURFACE TENSILE STRESS

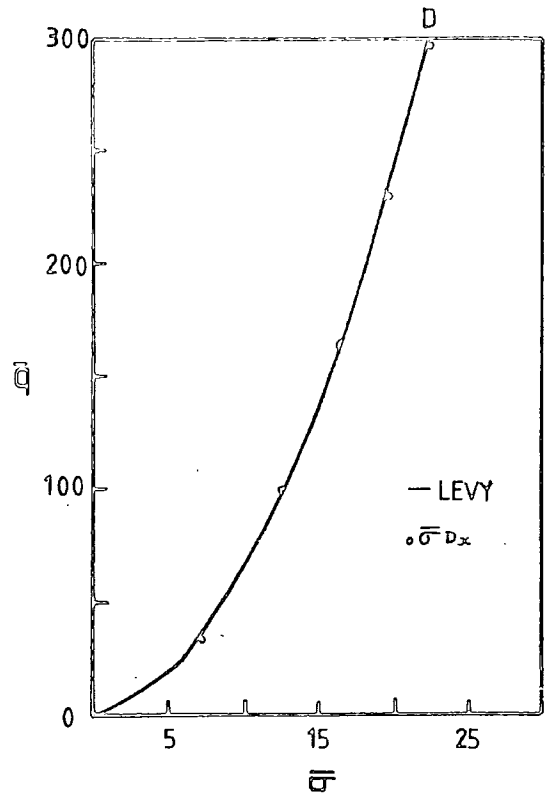


Figure 3.16.3 IN-PLANE SURFACE TENSILE STRESSES

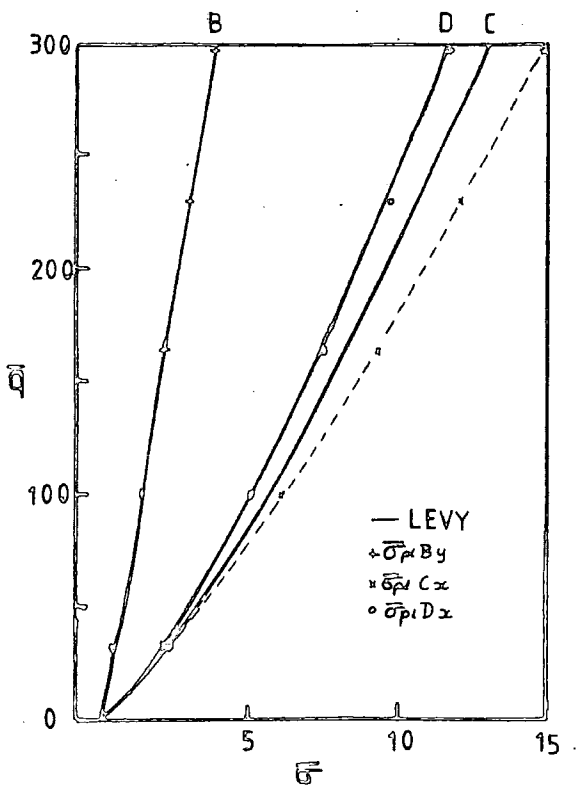


Figure 3.16.4 BENDING SURFACE TENSILE STRESSES

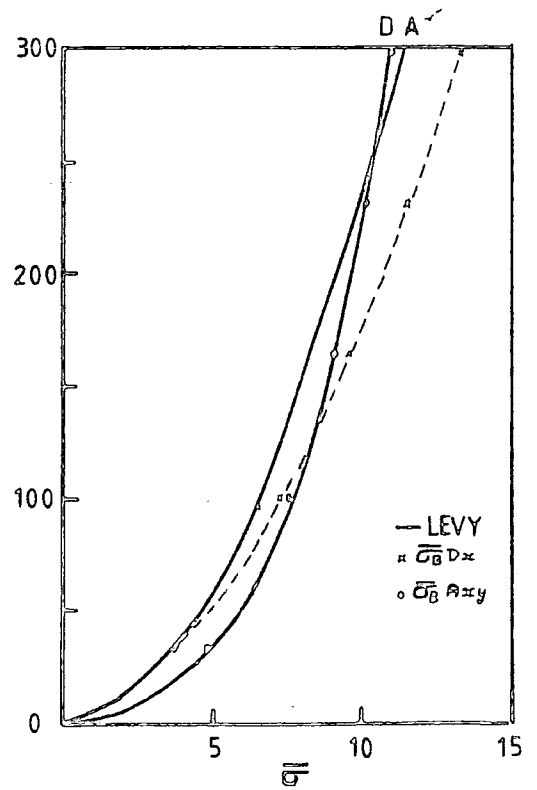


Figure 3.17 CLAMPED SQUARE ISOTROPIC PLATE UNIFORM PRESSURE
 LOAD (C.L.V.), LEVY IN-PLANE RESTRAINTS
 $\left. \begin{matrix} \text{ROTAV} \\ \left\{ \frac{dw}{dx} \frac{dw}{dy} \right\} \end{matrix} \right\} \text{IN-PLANE STIFFNESS COEFFICIENTS 1.3}$

Figure 3.17.1 CENTRAL TRANSVERSE DISPLACEMENT

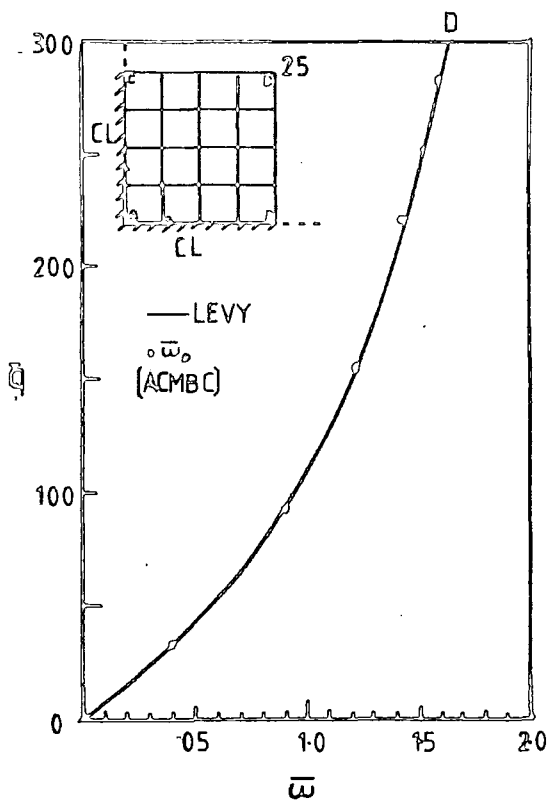


Figure 3.17.2 CENTRAL SURFACE TENSILE STRESS

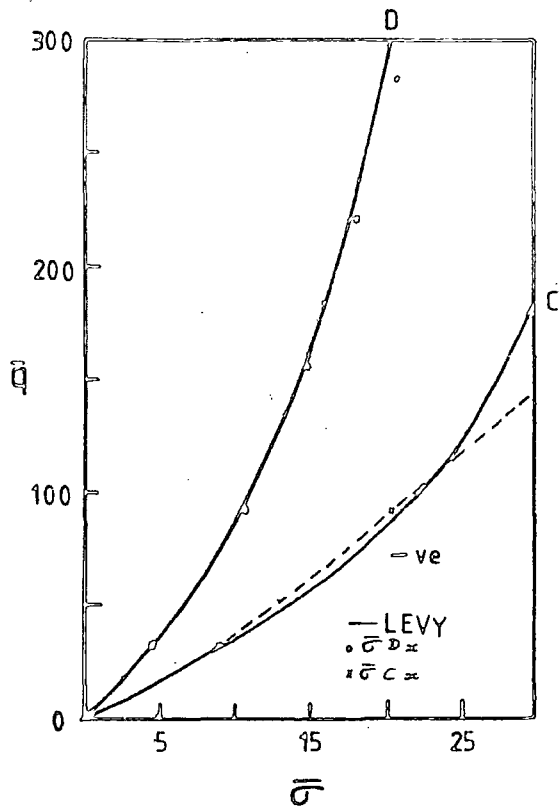


Figure 3.17.3 IN-PLANE SURFACE TENSILE STRESS

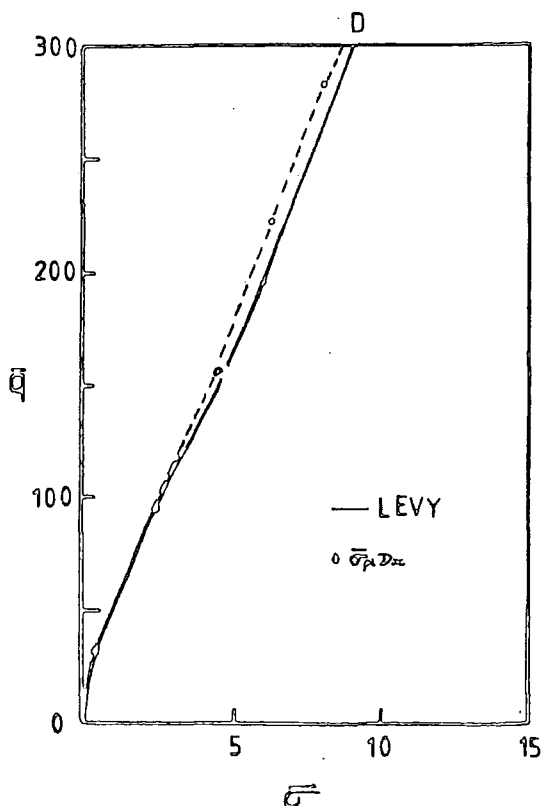


Figure 3.17.4 BENDING SURFACE TENSILE STRESS

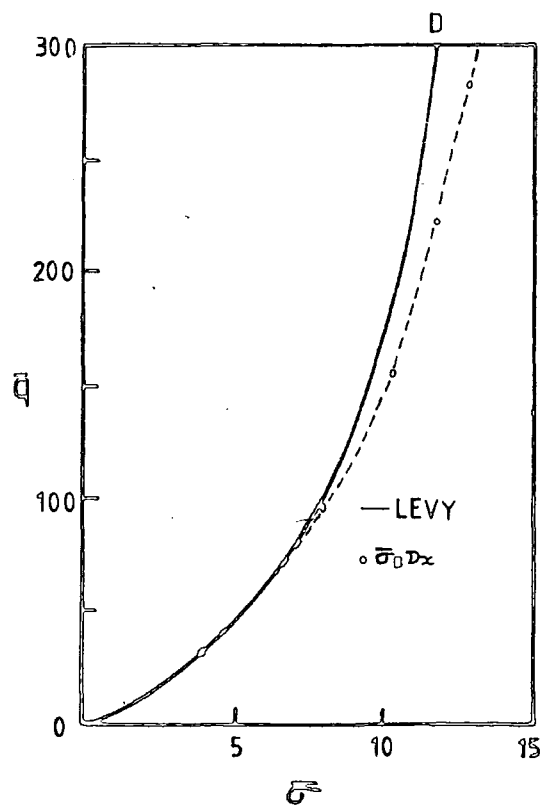


Table 4.1 T300/Code69 lamina material properties

The properties are for a unidirectional laminate with nominal ply thickness (0.127E-03m) and 60% fibre volume.

Material property (Symbol)	Design permissible	Typical value measured
Longitudinal tensile strength	0.117E+10 N/m ²	0.177E+10 N/m ²
Longitudinal tensile Youngs modulus (E11 _t)	0.123E+12 N/m ²	0.135E+12 N/m ²
Longitudinal tensile strain to failure	1.1 %	~
Transverse tensile strength	0.494E+08 N/m ²	0.550E+08 N/m ²
Transverse tensile Youngs modulus (E22 _t)	0.748E+10 N/m ²	0.1096E+11 N/m ²
Transverse tensile strain to failure	0.7%	~
Longitudinal compressive strength	0.707E+09 N/m ²	0.139E+10 N/m ²
Longitudinal compressive Youngs modulus (E11 _c)	0.123E+12 N/m ²	0.144E+12 N/m ²
Transverse compressive strength	0.100E+09 N/m ²	0.253E+09 N/m ²
Transverse compressive Youngs modulus (E22 _c)	0.549E+10 N/m ²	0.121E+11 N/m ²
Interlaminar shear strength	0.706E+08 N/m ²	0.122E+09 N/m ²
Shear modulus (G12)	0.440E+10 N/m ²	0.577E+10 N/m ²
Poissons ratio (ν12)	0.3	0.3
Longitudinal coefficient of thermal expansion	-0.32E-06 /°C	-0.32E-06 /°C
Transverse coefficient of thermal expansion	0.23E-04 /°C	0.23E-04 /°C

Figure 4.1 SHEAR MODULUS G_{12} WITH SHEAR STRESS τ_{12}

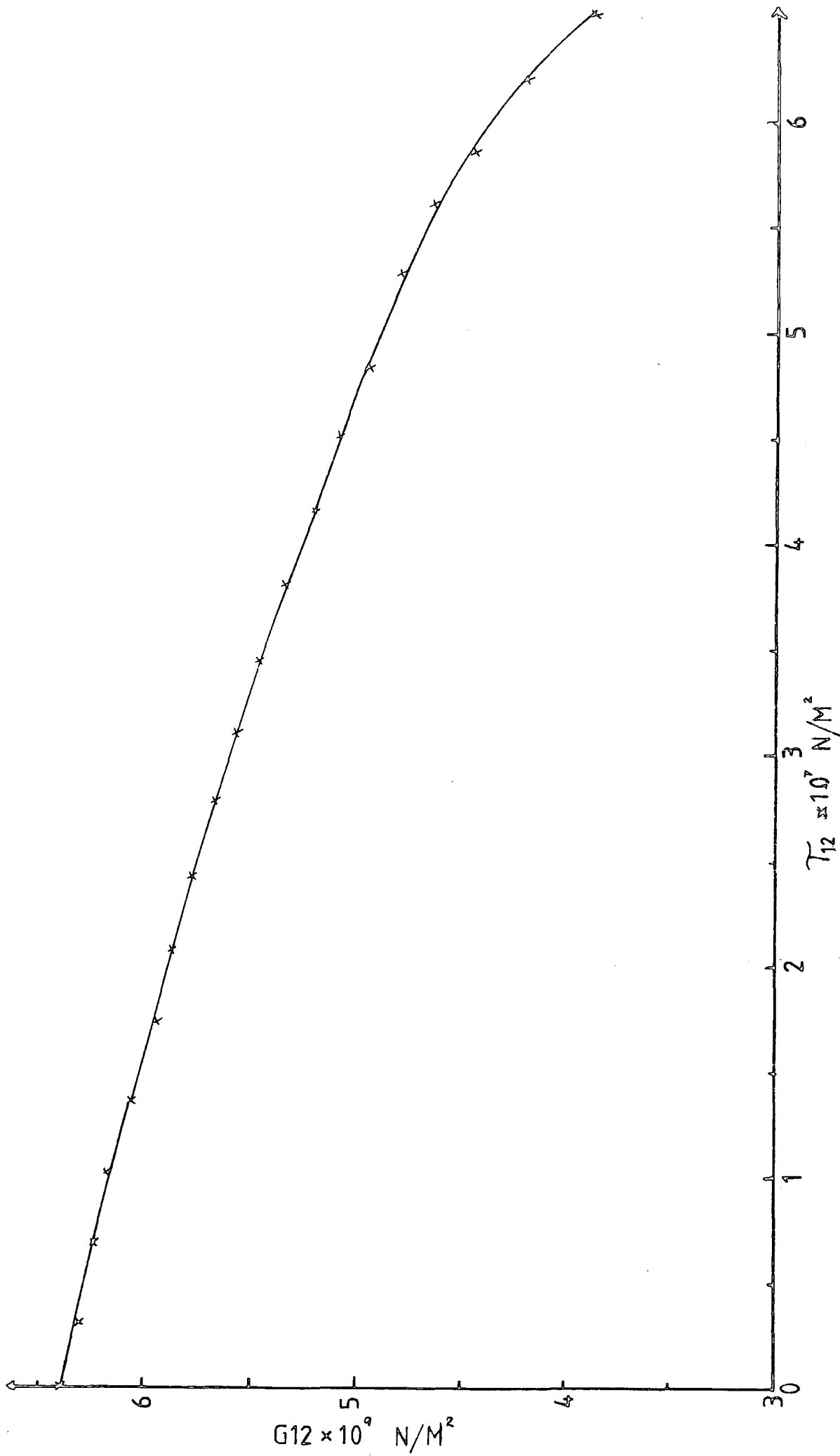
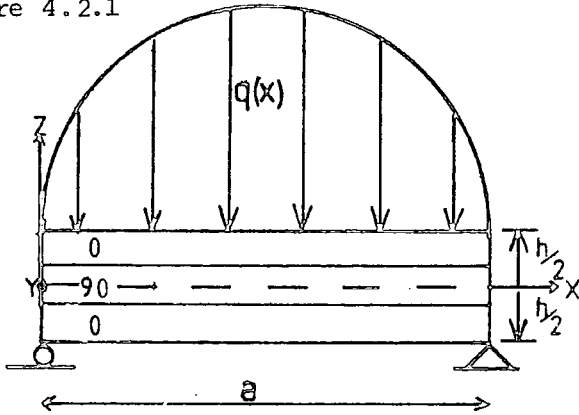


Table 4.2 Specimens

Exp.	Lay-up (T300/Code69)	A m	B m	h E-03 m	h(norm)E-03 m	Remarks
1	(90°;0°;90°;+45°;0°;-45°;0°;0°; -45°;0°;+45°;0°;0°;+45°;0°; -45°;0°) _s	.258	.258	4.40	4.318	The lower surface had a protective layer which was approx. two ply thick (0.254E-03m) (Reference B-A H6/2) Cured 1978-9
2	"	.253	.251	4.66	4.318	Void content ≤ 0.6% (Reference B-A CF-1074) Cured 1982
3	(+45°;90°;-45°;0°;0°;-45°;90°; +45°) _s	.258	.258	5.49	5.08	The upper surface had a protective layer which was approx. two ply thick (0.254E-03m) The plate was tested twice because adhesive caused the gauges to peel off during Exp. 3 (Reference B-A H5/2) Cured 1978-9
4	"					
5	(+45°;0°;-45°;90°;90°;-45°;0° +45°) _s	.205	.273	1.91±1%	2.032	The specimen was not failed in Exp. 5 because poor choice of supporting distances allowed it to just slip through the supports Support distances were changed for Exp 6. (Reference B-A CF-1050) Cured 22/12/81
6	"					
7	"	.204	.272	1.91±1%	2.032	(Reference B-A CF-1051) Cured 5/1/82
8	(0°;90°;0°;90°;0°;90°;0°;90°) _s	.204	.202	1.88±1%	2.032	Void content < 1.2% (Reference B-A CF-1075) Cured 4/82
9	(0°;+45°;0°;+45°;0°;-45°;0°; -45°) _s	.202	.200	1.91±2%	2.032	Void content < 1.2% (Reference B-A CF-1076) Cured 4/82

Figure 4.2 PAGANO'S 3-CROSS-PLY STRIP BENDING EXAMPLE

Figure 4.2.1



TEST PARAMETERS

$$q(x) = q_0 \sin^2 \frac{\pi x}{a}$$

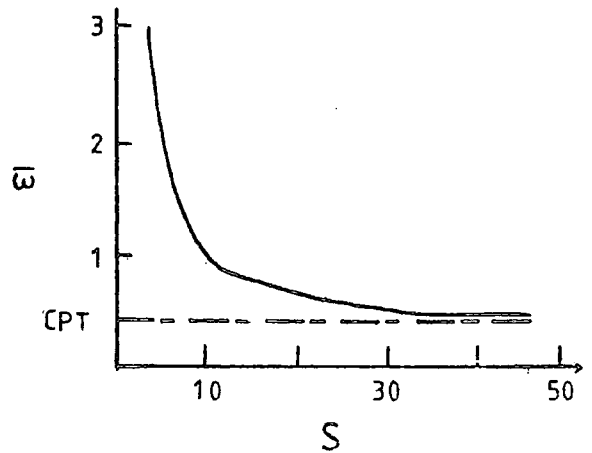
$$\frac{E_{11}}{E_{22}} = 25$$

$$\frac{G_{12}}{E_{22}} = 0.5$$

$$\frac{G_{23}}{E_{22}} = 0.2$$

$$\nu_{12} = \nu_{23} = 0.25$$

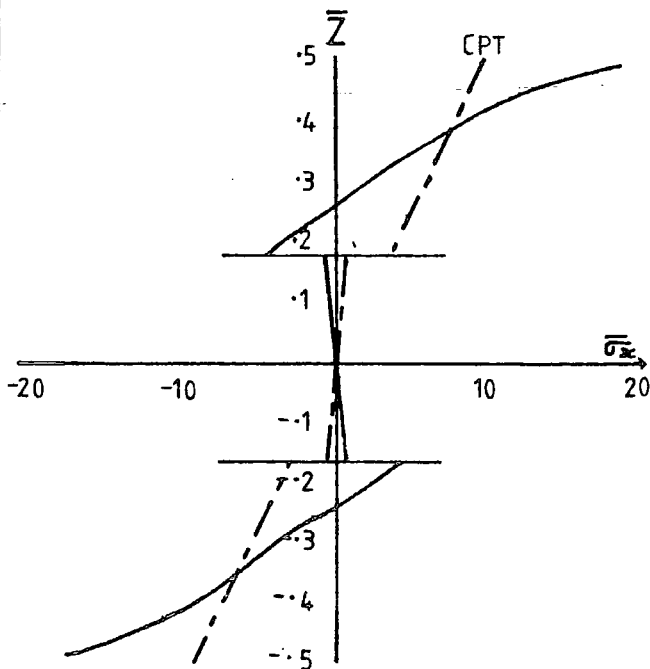
Figure 4.2.2 MAXIMUM DISPLACEMENT \bar{w} WITH SPAN TO THICKNESS RATIO S



$$\bar{w} = \frac{w_c}{h} \quad S = \frac{a}{h}$$

Figure 4.2.3 CENTRAL INTERFACE STRESS $\bar{\sigma}_x$ Figure 4.2.4 CENTRAL INTERFACE STRESS $\bar{\sigma}_x$

$S=4$



$$\bar{z} = \frac{z}{h} \quad \bar{\sigma}_x = \frac{\sigma_x(\frac{a}{2}, z)}{q_0}$$

$S=10$

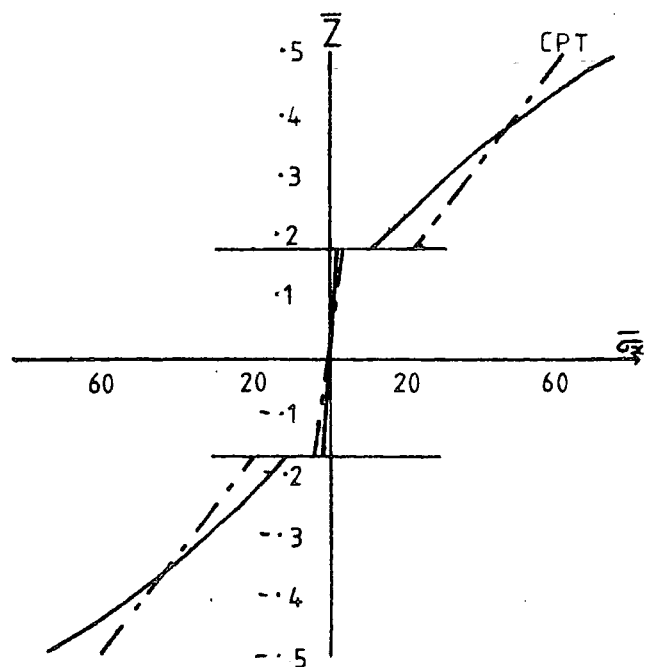


Figure 4.2 contd. PAGANO'S 3-CROSS-PLY STRIP BENDING EXAMPLE

Figure 4.2.5 SHEAR STRESS $\bar{\tau}_{xz}$

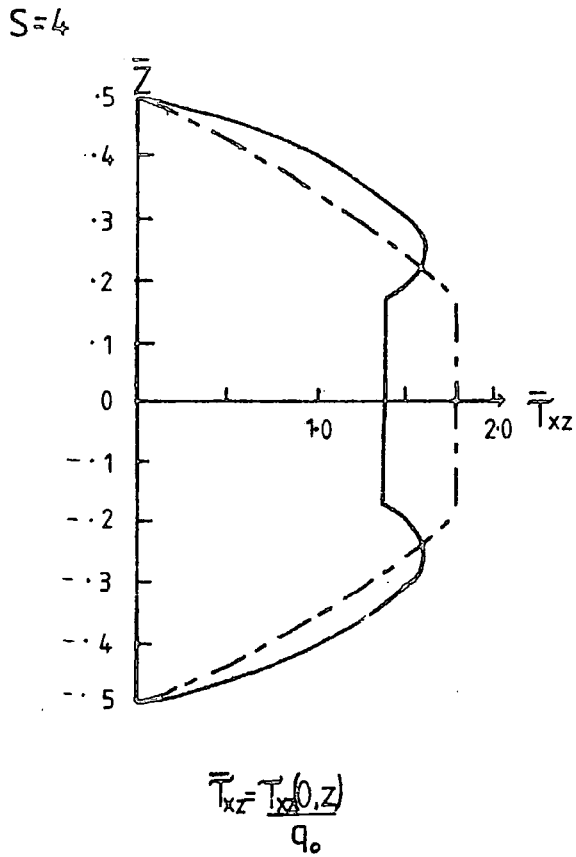


Figure 4.2.6 SHEAR STRESS $\bar{\tau}_{xz}$

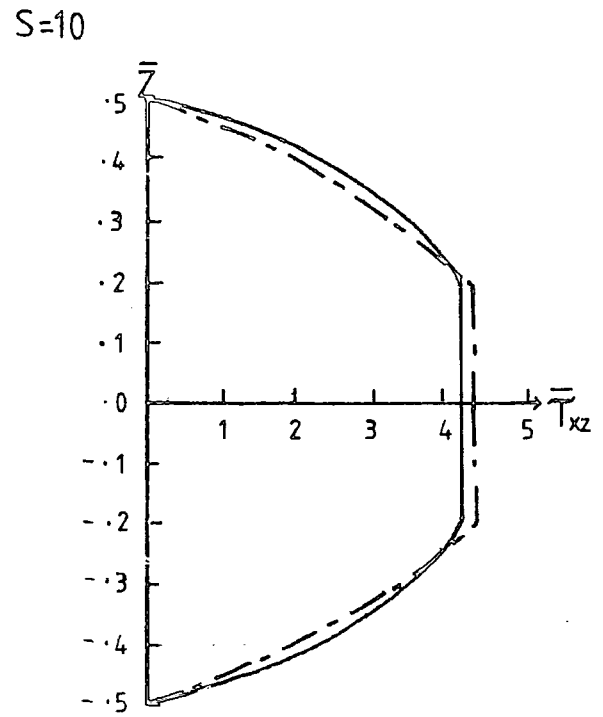


Figure 4.2.7 X-DISPLACEMENT \bar{u}_x

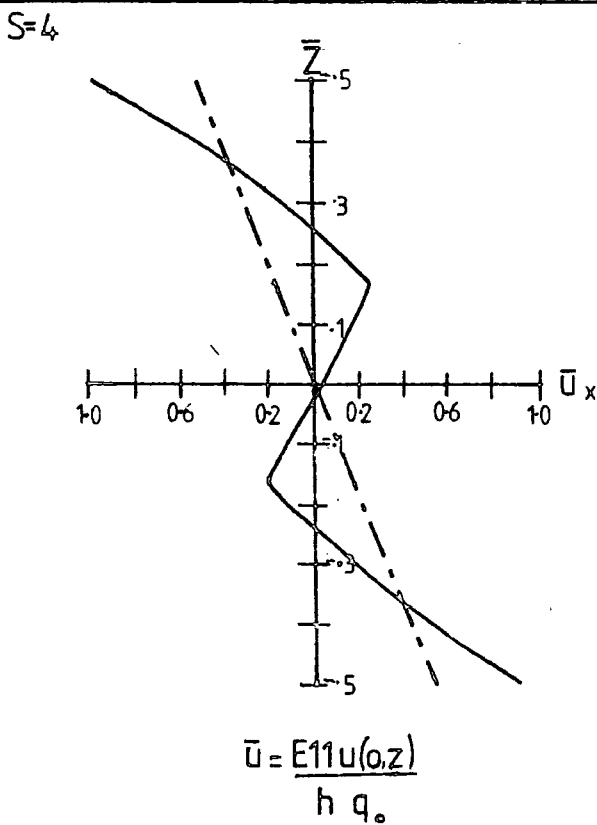


Figure 4.2.8 X-DISPLACEMENT \bar{u}_x

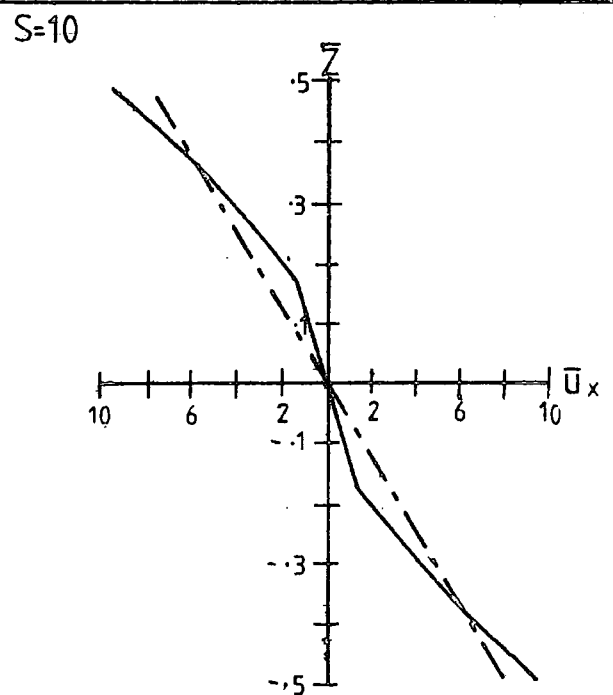


Table 4.3 Shear flexible finite elements

Author (ref)	Element type	F.E.M	No. of nodes D.O.F.	Displacement Function	Remarks
Mau + Tong + Pian (38)		Hybrid-stress	4 $((n+1) \times 2 + 1) \times 4$	Quartic	The rotations of normals for different layers were considered to be different.
Mawenya + Davies (46)	Iso- parametric	Displacement	8 $((n+1) \times 4 + 1) \times 8$	Quartic Numerical integ. (2x2) Gaussian	The normal rotations, though assumed uniform for any layer, vary from layer to layer and are independent of the transverse displacement.
Panda + Natarajan (47)	Super- parametric	Displacement	8 40	Quartic Numerical integ. (2x2) Gaussian	Assumed normal rotations to be the same for all layers, and the elasticity at different layers was taken into account by applying a "thickness" concept in the numerical integration. This analysis showed that Mawenya's analysis did not necessarily give improved accuracy
Reddy (44)	Serendipity	Displacement	8 40	Quartic Numerical integ. (2x2) Gaussian	Used a Lagrange penalty function to take into account that normals did not remain normal. The analysis also included shear correction factors in the 3-D stress-strain relationships.

n = No. of layers

Figure 4.3 PAGANO'S CROSS-PLY RECTANGULAR PLATE BENDING EXAMPLE

MATERIAL PROPERTIES

$$\frac{E_{11}}{E_{22}} = 25$$

$$\frac{G_{12}}{E_{22}} = 0.5$$

$$\frac{G_{23}}{E_{22}} = 0.2$$

$$\nu_{12} = \nu_{23} = 0.25$$

TRANSVERSE LOAD

$$q(x, y) = q_0 \sin \frac{\pi x}{A} \sin \frac{\pi y}{B}$$

$$q_0 = 1$$

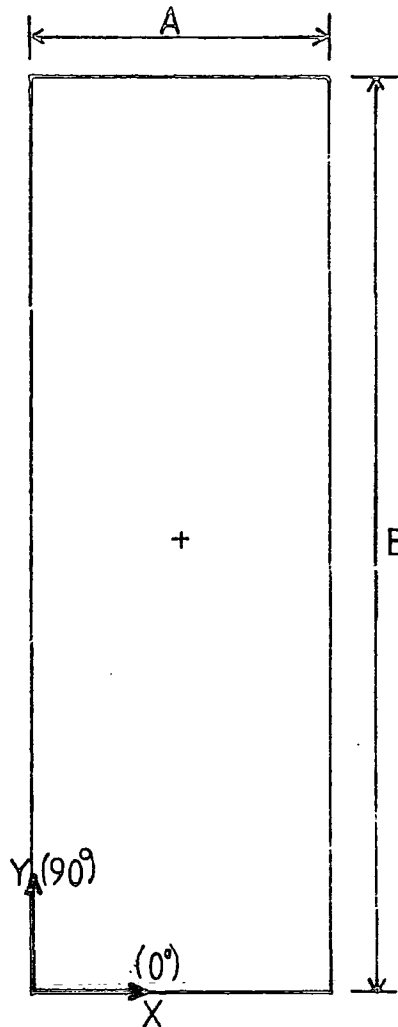
BOUNDARY CONDITIONS

SIMPLY SUPPORTED EDGES

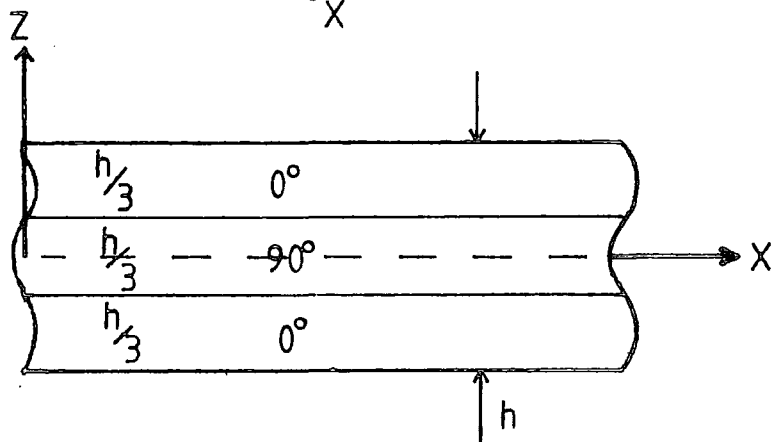
$$X = 0, a \quad v = w = 0$$

$$Y = 0, b \quad v = w = 0$$

$$B = 3A$$



MID-PLANE



$$\bar{w} = \frac{100 E_{11} w}{q_0 h S^4}$$

$$\bar{\sigma}_x = \frac{\sigma_x(x, y)}{q_0 S^2}$$

$$S = \frac{A}{h}$$

Figure 4.4 CENTRAL DISPLACEMENT $\bar{w}\left(\frac{A}{2}, \frac{B}{2}\right)$ WITH SPAN TO THICKNESS S FOR SHEAR FLEXIBLE FINITE ELEMENTS, ACM, C.P.T., AND PAGANO'S EXACT SOLUTION

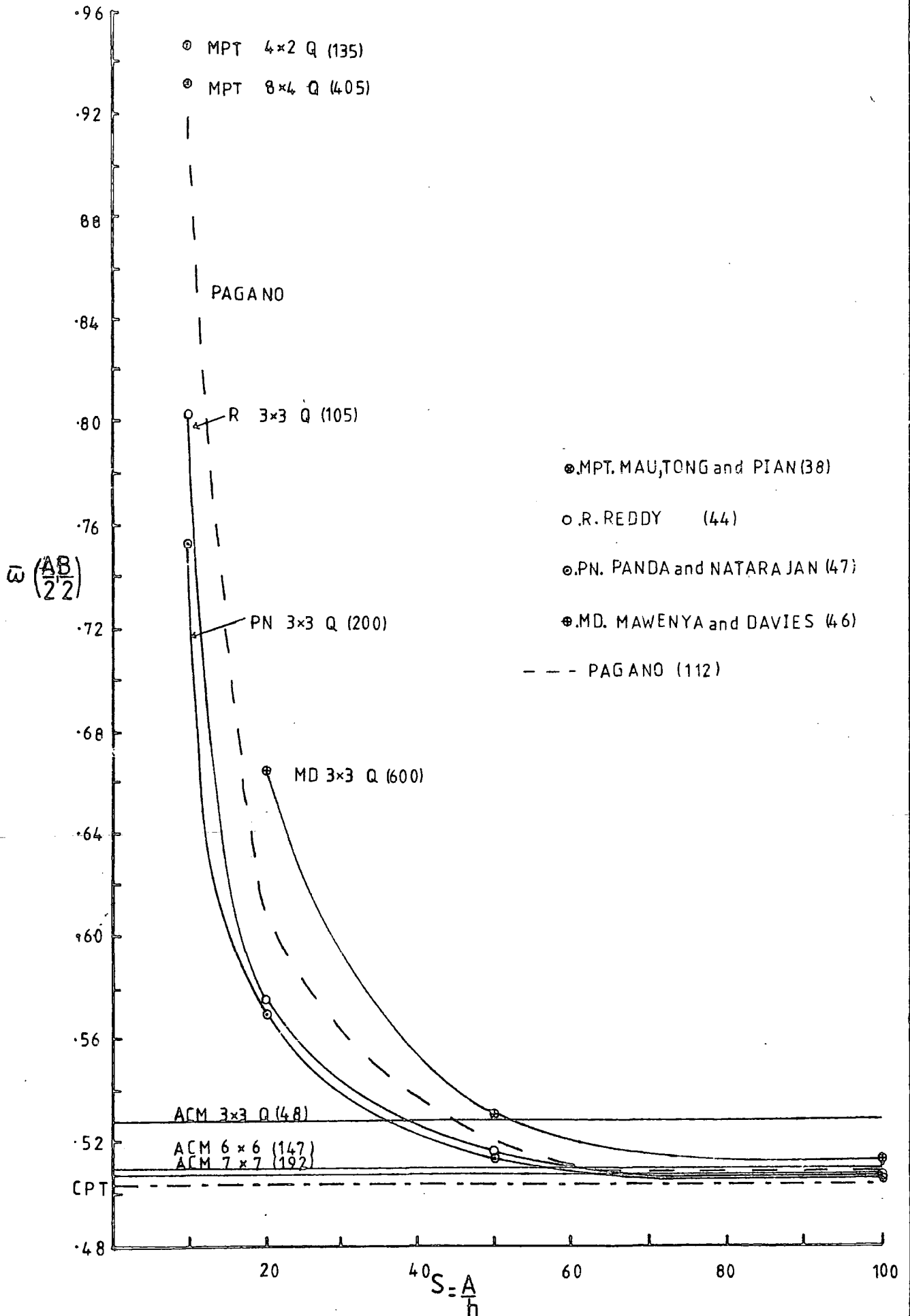


Figure 4.5 CENTRAL STRESS $\bar{\sigma}_x \left(\frac{A}{2}, \frac{B}{2}, \frac{h}{2} \right)$ WITH SPAN TO THICKNESS RATIO S FOR SHEAR FLEXIBLE FINITE ELEMENTS, ACM, C.P.T., AND PAGANO'S EXACT SOLUTION

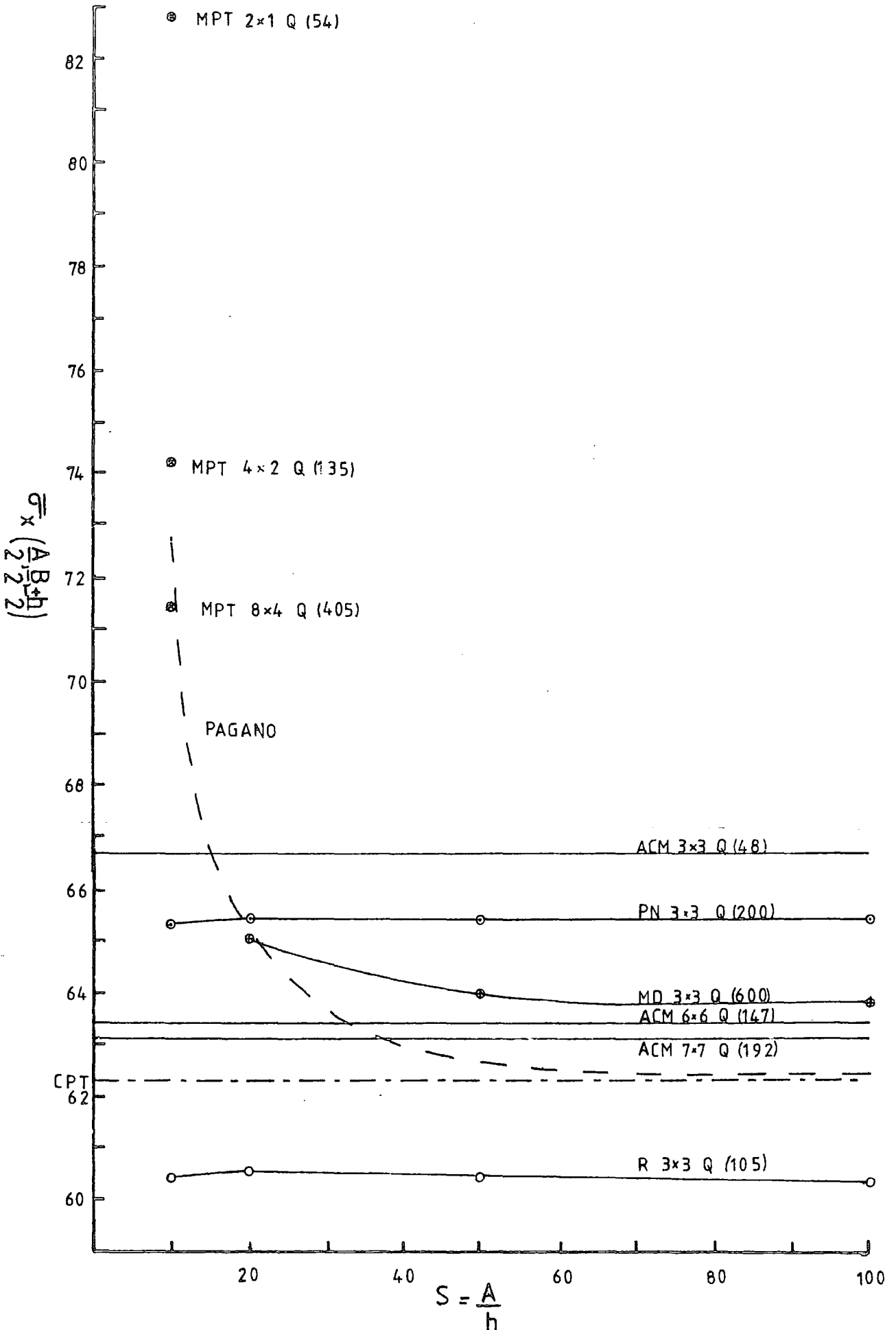


Table 4.5 Comparison of High order plate deformation theory with the exact elasticity solution of a rectangular simply supported bi-directional plate with a sinusoidal load (Fig. 4.3)

S	Pagano $\bar{\sigma}_x(\frac{A}{2}, \frac{B}{2}, \frac{h}{2})$	Lo $\bar{\sigma}_x(\frac{A}{2}, \frac{B}{2}, \frac{h}{2})$	Pagano $\bar{\sigma}_y(\frac{A}{2}, \frac{B}{2}, \frac{h}{2})$	Lo $\bar{\sigma}_y(\frac{A}{2}, \frac{B}{2}, \frac{h}{2})$	Pagano $\bar{w}(\frac{A}{2}, \frac{B}{2})$	Lo $\bar{w}(\frac{A}{2}, \frac{B}{2})$
4	1.14 -1.1	1.07	0.109 -0.119	±0.123	2.82	3.98
10	±0.725	0.725 -0.727	0.0418 -0.0435	±0.0492	0.919	1.083
20	±0.650	0.655 -0.652	0.0294 -0.0435	±0.0327	0.610	0.649
100	±0.624	±0.627	±0.0253	±0.0277	0.508	0.509
ACM	±0.631		±0.0260		0.507	
CPT	±0.623		±0.0252		0.503	

Table 4.6 Bending and in-plane components using the High Order plate deformation theory to solve the rectangular simply supported bi-directional plate with a sinusoidal load, (Fig 4.3).

S	Component	$w(\frac{A}{2}, \frac{B}{2})_m$	$\sigma_x(\frac{A}{2}, \frac{B}{2}, \frac{h}{2})_{N/mm^2}$	$\sigma_y(\frac{A}{2}, \frac{B}{2}, \frac{h}{2})$	$\sigma_z(\frac{A}{2}, \frac{B}{2}, \frac{h}{2})$
10	Bending	0.1300E-03	-.7266E+02	-.4923E+01	-.1498E+01
10	In-plane	0.2816E-06	0.2966E+00	0.1434E+00	0.5044E+00
20	Bending	0.6237E-03	-.2619E+03	-.1309E+02	-.6940E+01
20	In-plane	0.1408E-06	0.3529E+00	0.1462E+00	0.5052E+00
100	Bending	0.6111E-01	-.6300E+04	-.2712E+03	-.1809E+03
100	In-plane	0.2816E-07	0.3729E+00	0.1470E+00	0.5050E+00

All parameters for the test example are given with Fig. 4.3.

References. Pagano (112); Lo, Christensen, Wu (119,120,122)

Figure 4.7 INTERLAMINAR STRESSES IN LAMINATES UNDER AXIAL EXTENSION (123)

Figure 4.7.1 STRESSES AT INTERFACE $(+45^\circ/45^\circ)_s$

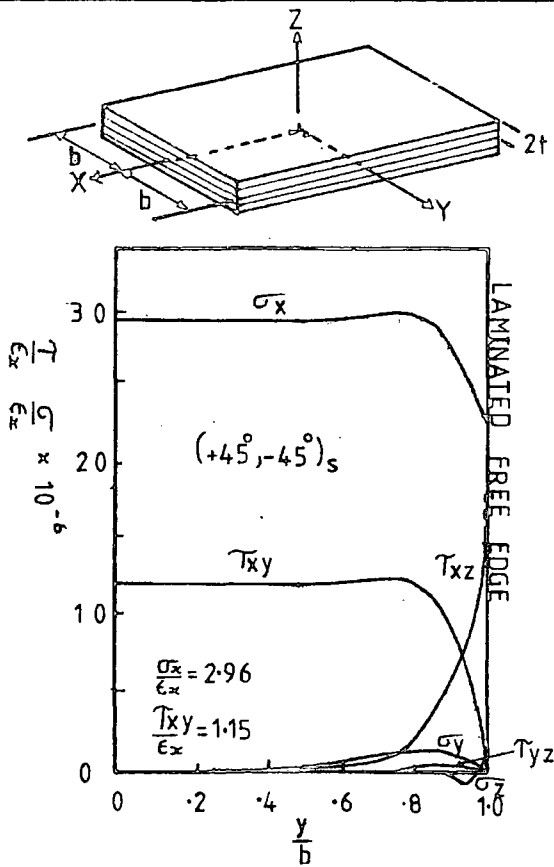


Figure 4.7.2 $\frac{\sigma_z}{E_x}$ DISTRIBUTION ALONG CENTRELINE $z=0$

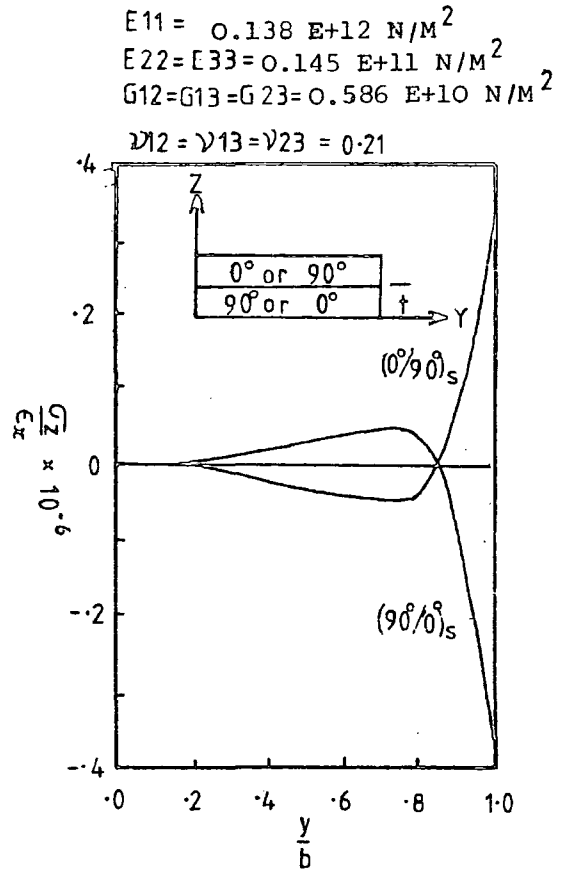


Figure 4.7.3 $\frac{\sigma_z}{E_x}$ DISTRIBUTION ALONG $90^\circ-0^\circ$ INTERFACE $z=t$

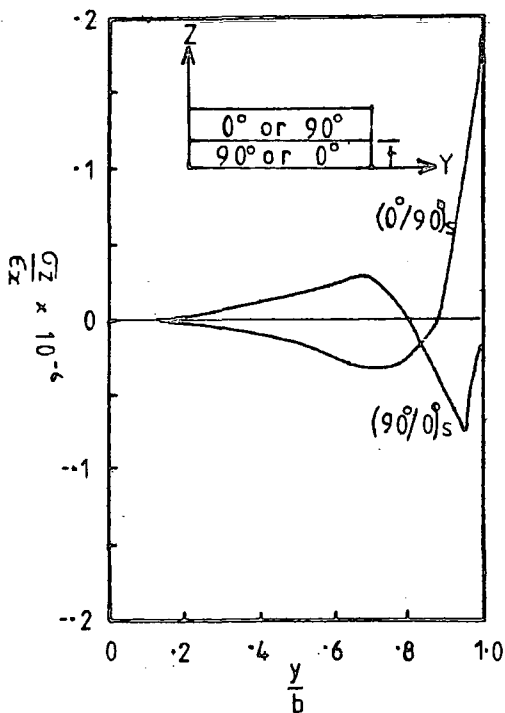


Figure 4.7.4 $\frac{\tau_{yz}}{E_x}$ DISTRIBUTION ALONG $90^\circ-0^\circ$ INTERFACE $z=t$

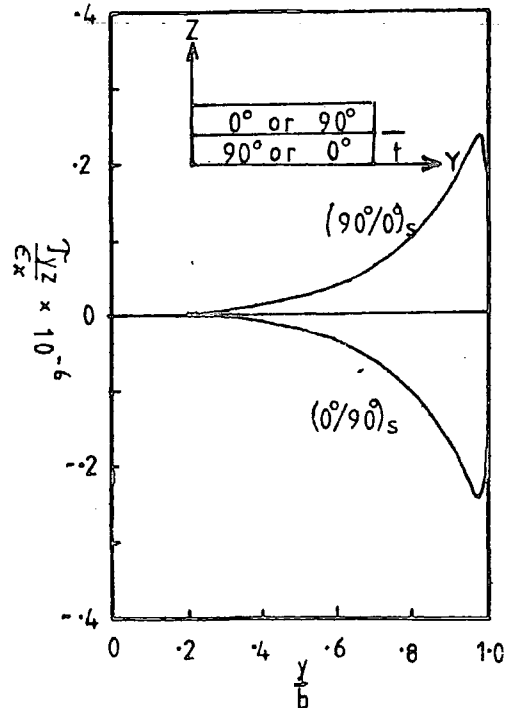


Figure 4.8 APPARATUS FOR PLATE BENDING EXPERIMENT

Figure 4.8.1 BASE PLATE (MILD STEEL)

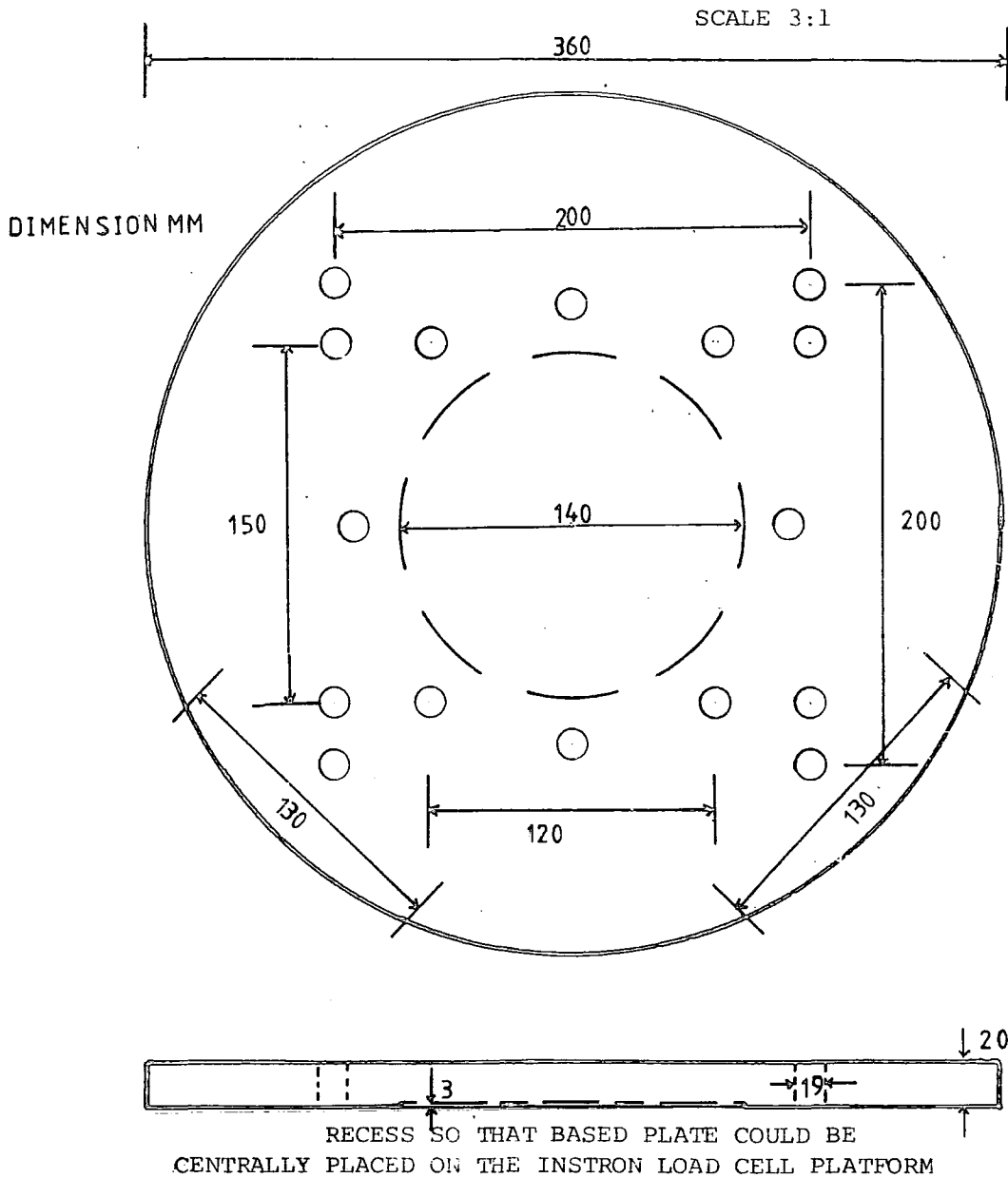


Figure 4.8.2 SUPPORT COLUMNS

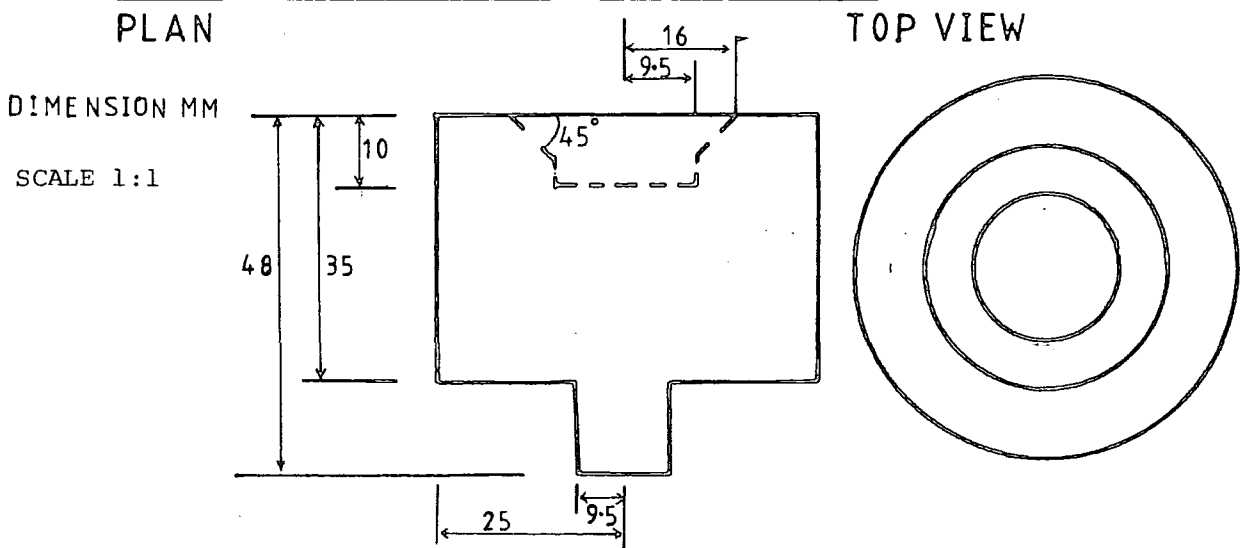


Figure 4.8 APPARATUS FOR PLATE BENDING EXPERIMENT

PLATES EXPERIMENT 5

PLATE
4.1

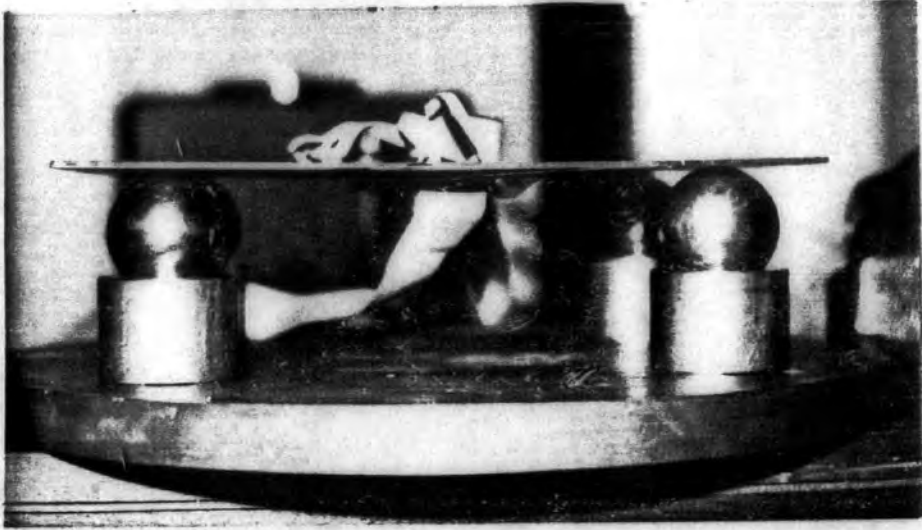


PLATE
4.2

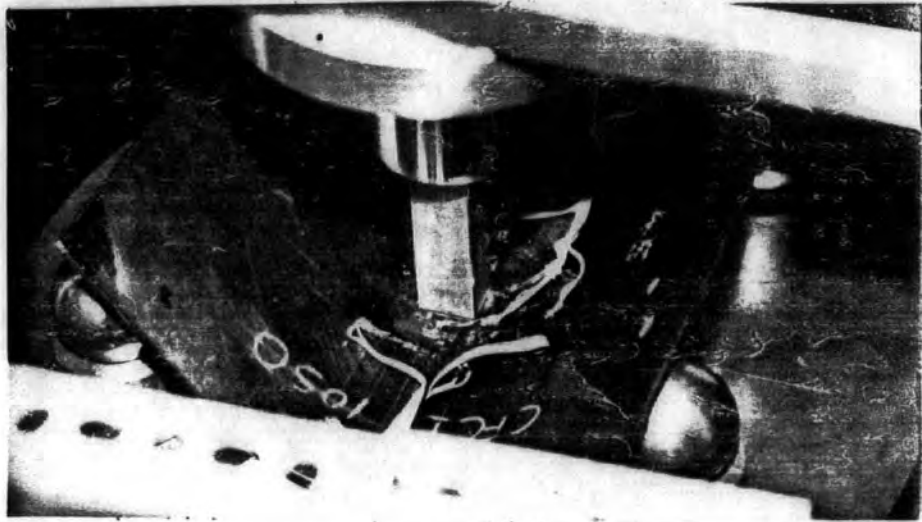
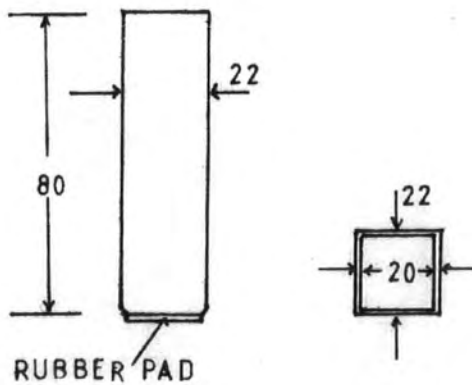


Figure 4.8.3 METAL LOADING HEADS

20 x 20 MM



10 x 10 MM

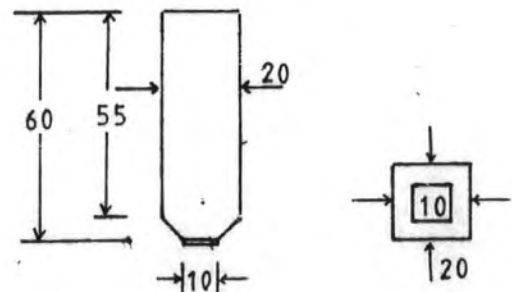


Figure 4.9 STRAIN MEASUREMENTS

Figure 4.9.1 NONLINEAR BENDING STRAIN DISTRIBUTION

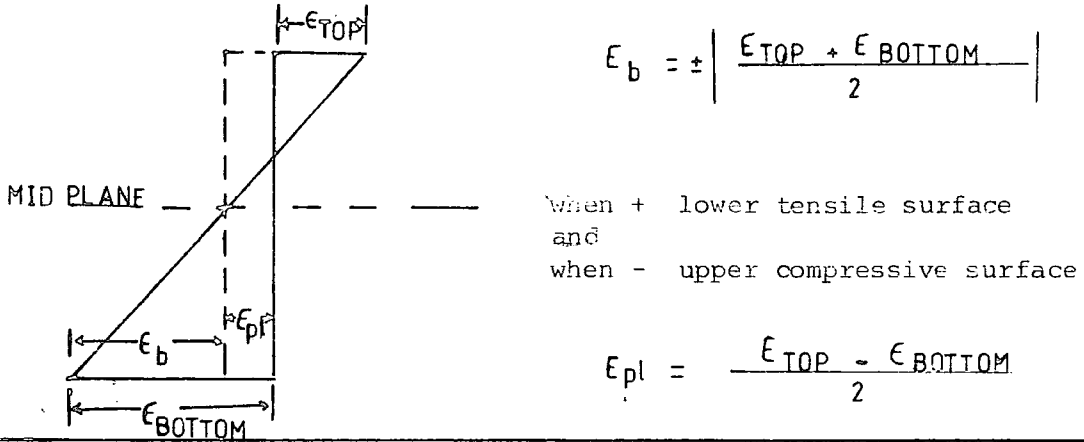
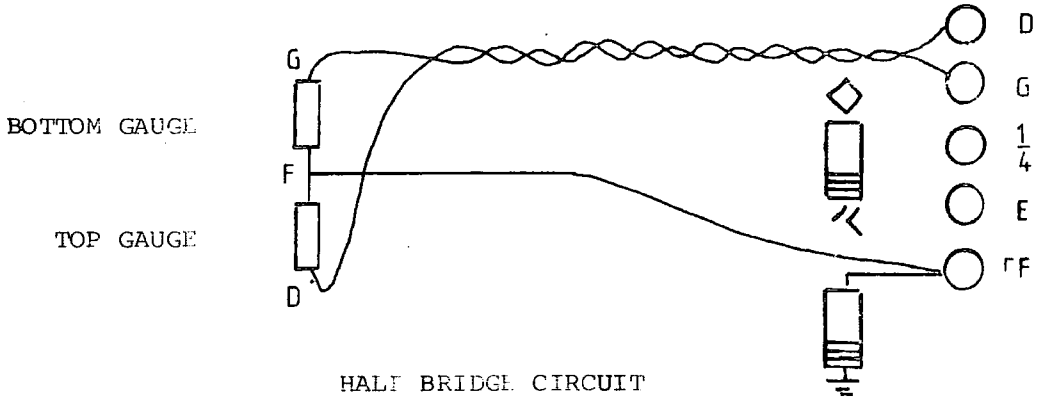
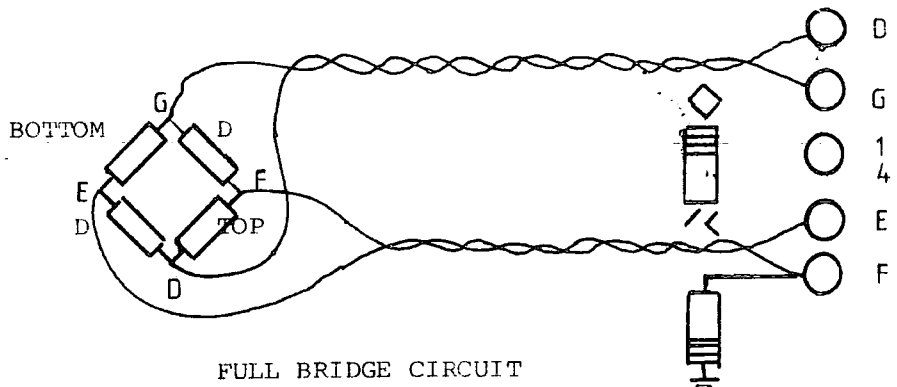


Figure 4.9.2 CONNECTIONS FOR STRAIN GAUGE MEASUREMENTS

BENDING STRAIN MEASUREMENT (TWICE ACTUAL VALUE)



AXIAL STRAIN MEASUREMENT (TWICE ACTUAL VALUE)



SURFACE (BENDING + IN-PLANE) MEASUREMENT

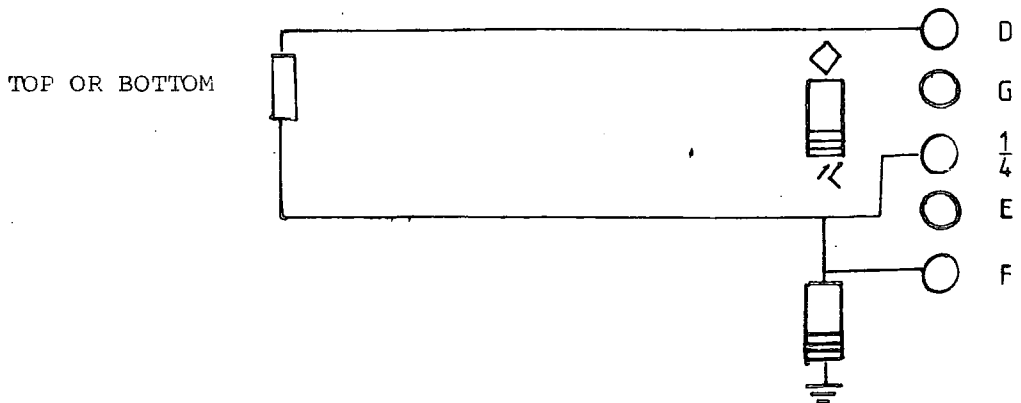


Figure 4.10 EXPERIMENTAL ARRANGEMENT

PLATE 4.3 EXPERIMENT

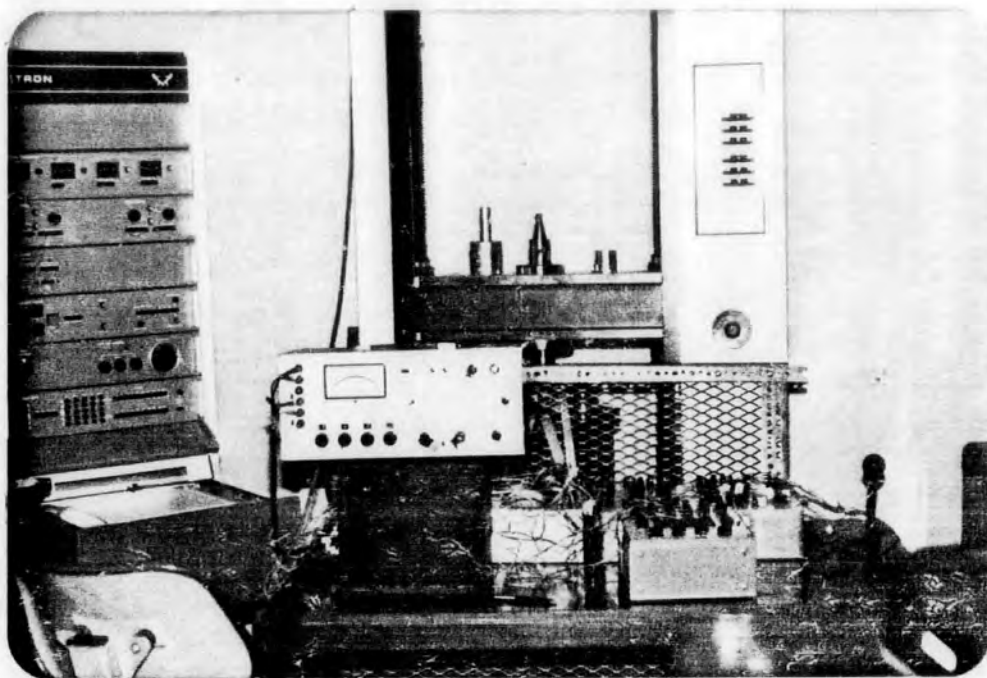


Figure 4.10.1 STRAIN INSTRUMENTATION

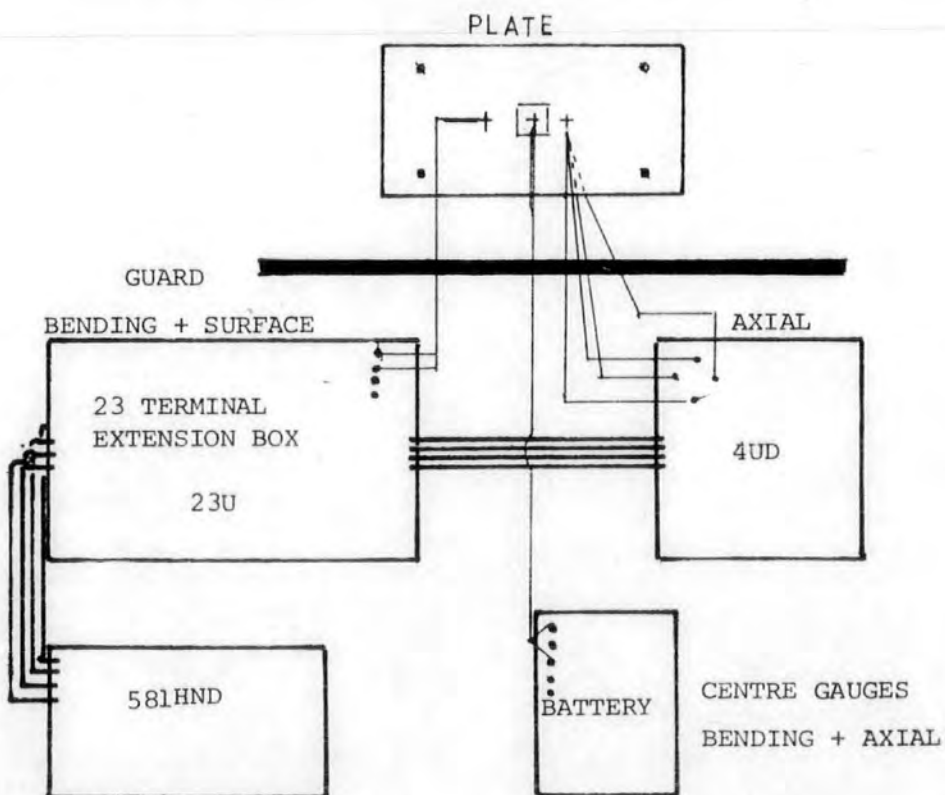


Table 4.7 Plate bending test parameters

Exp.	Lay-up	A _m	B _m	h E-03 _m	A _s _m	B _s _m	S(min)	A _p _m	B _p _m
1	(90°,0°,90°,+45°,0°,-45°,0°,0°,-45°,0°,+45°,0°,0°,+45°,0°,-45°,0°) _s	0.258	0.258	4.40	0.2	0.2	46	0.02	0.02
2		0.253	0.251	4.06	0.2	0.2	49	0.02	0.02
3	(+45°,90°,-45°,0°,0°,-45°,90°,+45°) _s	0.258	0.258	5.49	0.2	0.2	36	0.02	0.02
4									
5	(+45°,0°,-45°,90°,90°,-45°,0°,+45°) _s	0.205	0.273	1.91±1%	0.15	0.2	$\frac{A_s}{h}$ 79	0.02	0.02
6					0.15	0.12	$\frac{B_s}{h}$ 63	0.01	0.01
7		0.204	0.272	1.91±1%	0.15	0.12	$\frac{B_s}{h}$ 63	0.01	0.01
8	(0°,90°,0°,90°,0°,90°,0°,90°) _s	0.204	0.202	1.88±1%	0.13	0.13	69	0.01	0.01
9	(0°,+45°,0°,+45°,0°,-45°,0°,-45°) _s	0.202	0.200	1.91±2%	0.13	0.13	68	0.01	0.01

Table 4.8 Linear (embedding) load cycles

Exp.	Max. load N	Increment N	Period of time load was maintained (min)
1	300	100	5
2	300	100	5
3	400	100	4
4	400	100	4
5	100	20	3
6	100	20	3
7	100	20	3
8	100	20	3
9	100	20	3

Table 4.9 Load increments for test to failure

Exp.	Linear deform. N max. increment		Test to failure N increment
1	300	50	200 to fibre failure at 8200
2	400	100	400 to 7200 then 300 to fibre failure at 7960
3	—	—	400 to 11200 (adhesive failure)
4	400	50	400 to 2000 then 800 to fibre failure at 13750
5	80	20	50 to 1200 then plate just slipped through the supports
6	50	10	100 to fibre failure at 2500
7	50	10	100 to fibre failure at 2600
8	100	20	100 to fibre failure at 2100
9	100	20	100 to 400 then 50 to 500 and then had to be stopped due to plate rotation

EXPERIMENT 1 .NOTES AND OBSERVATIONS

Date of test : July 81

Plate dimensions

A = 0.258 m

B = 0.258m

h = 0.44E-02m(Includes protective layer)

A_s = 0.2m

B_s = 0.2m

A_p = 0.02m

B_p = 0.02m (Rubber pad 0.178E-02m)

Lay-up (90°,0°,90°,+45°,0°,45°,0°,45°,0°,+45°,0°,+45°,0°,45°,0°)_s

Ball bearings 0.4445E-01m

The plate was arranged with the protective layer as the lower surface.

Central transverse displacement was increased at 0.5E-03m/min in increments of 200 N.

No transverse displacement measurements were made.

Strain gauge measurements not plotted

3 90° B was always less than 4 90° B ,the trend was the same and at 8200N strain=10825 με

7 0° A maximum value 700 με at 5200N, and at 8200N strain=668 με

12 90° A maximum value 500 με at 4400N, decreasing to 0 με at 8200N.

5 90° B and 9 90° A were connected to a ultraviolet recorder.

The information was loss due to electrical noise when the deformation was still small.

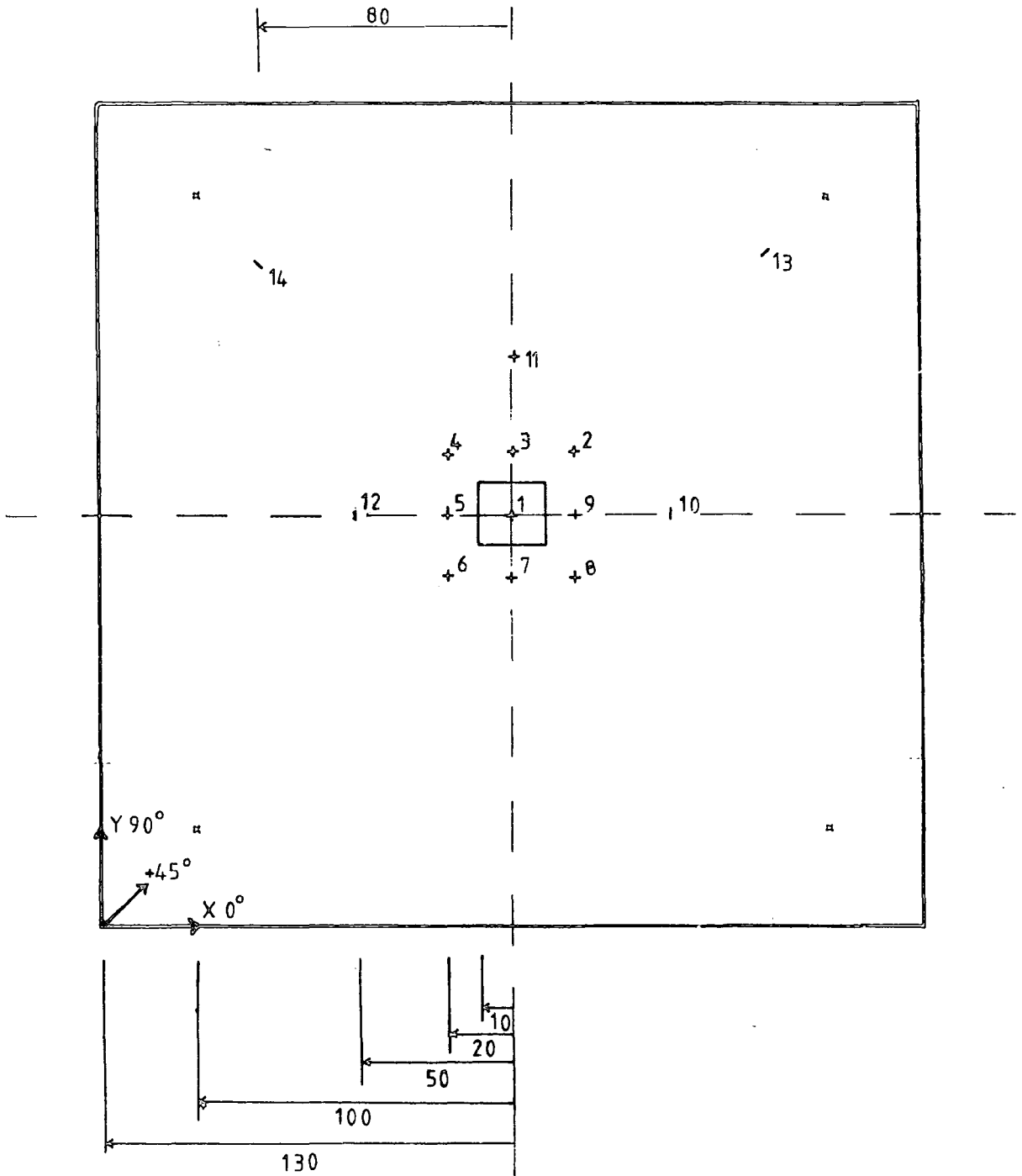
Sudden catastophic first fibre failure occurred after approx. 1min with the load equal to 8400N. Failure started near the centre in the outer tensile layer. There had been no previous sign of visible failure ,and the occasional loud crack heard suggested adhesive breakdown. The final load after failure was not recorded.

Figure 4.11 EXPERIMENT 1. STRAIN GAUGE ARRANGEMENT

34 LAYERS (90,0,90,+45,0,-45,0,0,-45,0,+45,0,0,+45,0,-45,0)s

SCALE 1:4

STRAIN GAUGES	+	CROSS-PLY	TYPE FCA3-11	3MM	TOKYO SUKKI
	-	SINGLE	TYPE FLA3-11	3MM	KENKYUJO Co Ltd.



• POINT SUPPORT

□ PATCH LOAD

Figure 4.12 EXPERIMENT 1. STRAIN MEASUREMENTS TO FIRST FIBRE FAILURE

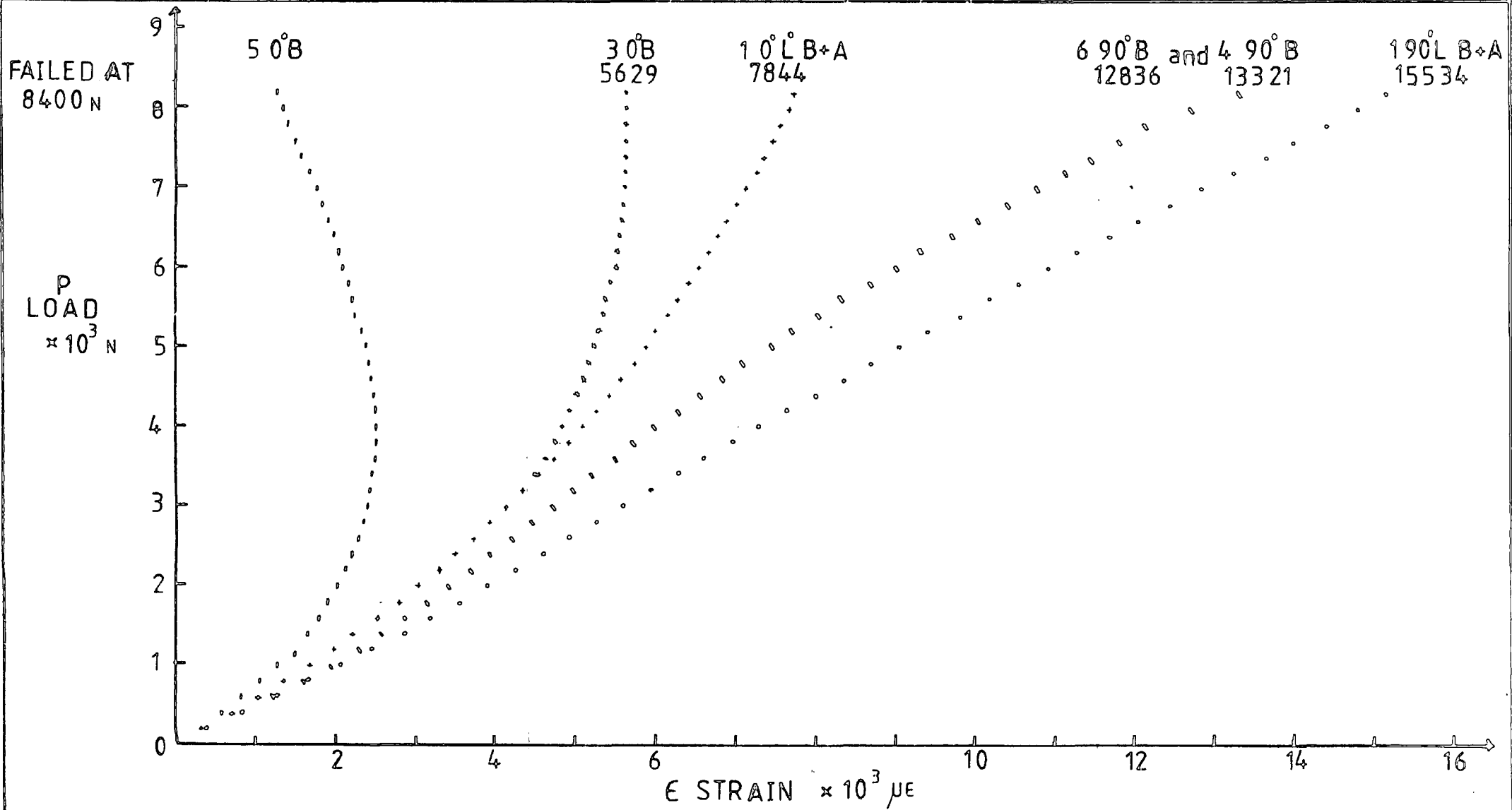


Figure 4.13 EXPERIMENT 1. STRAIN MEASUREMENTS TO FIRST FIBRE FAILURE

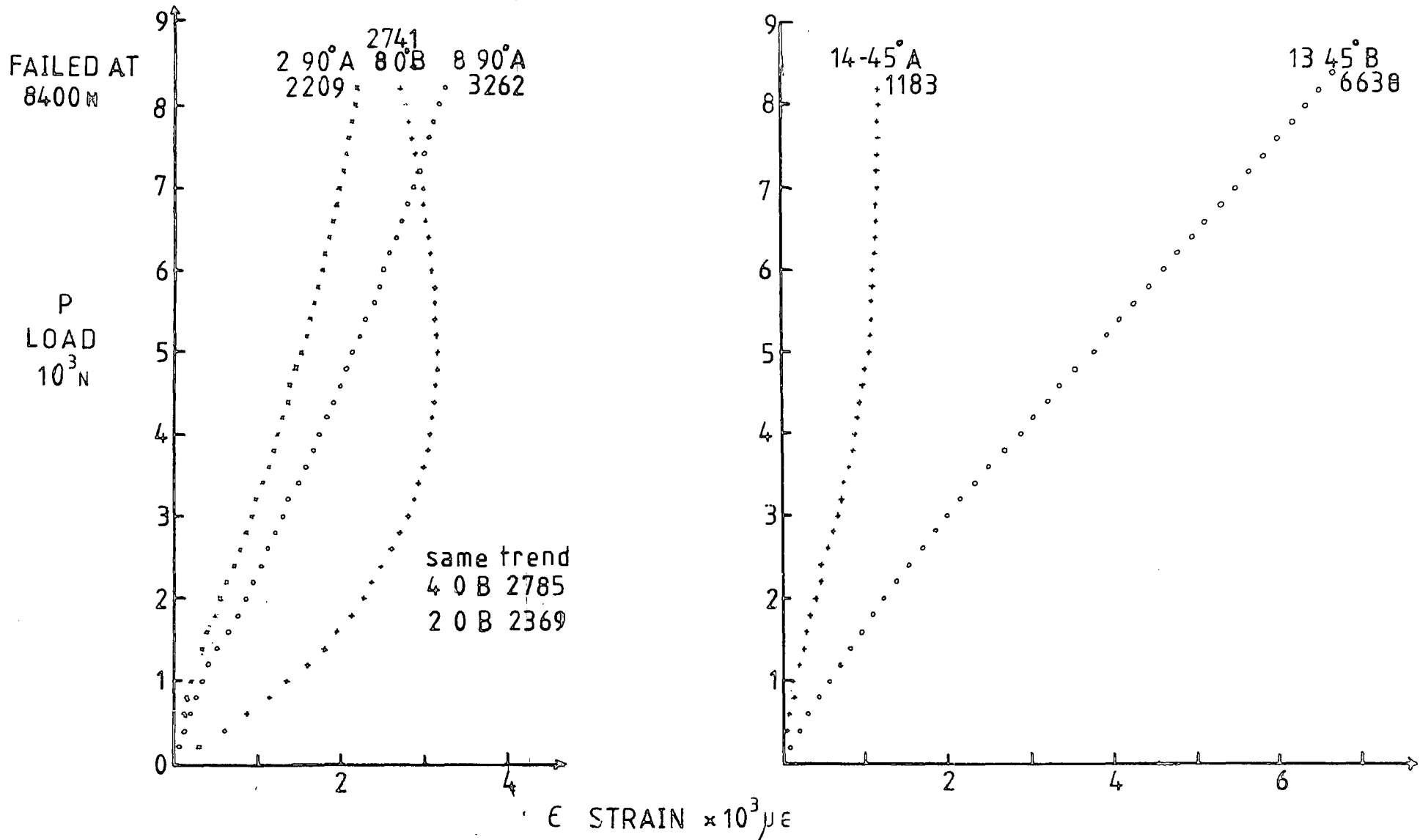
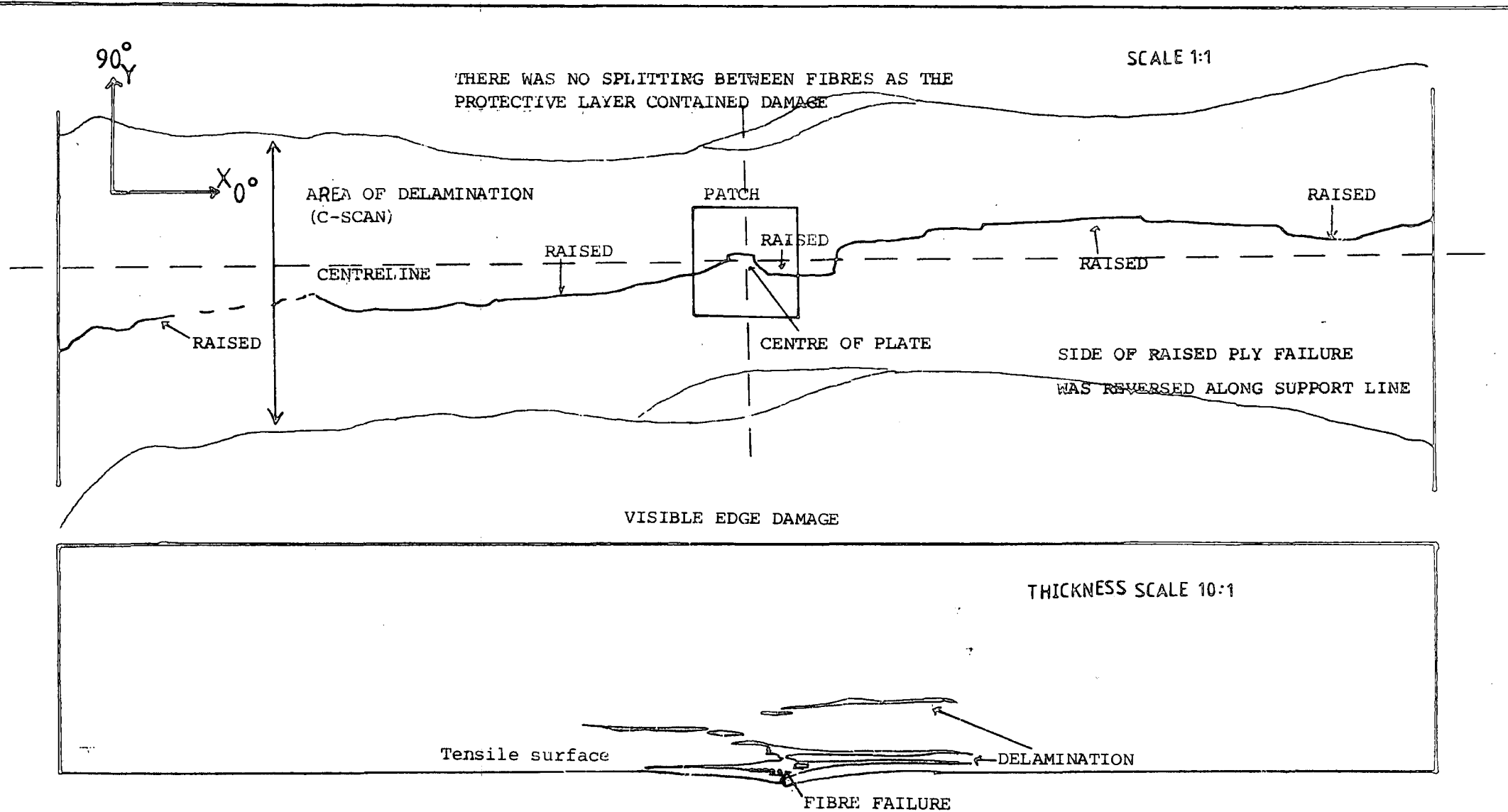


Figure 4.14 VISIBLE FAILURE ON TENSILE SURFACE



EXPERIMENT 2. NOTES AND OBSERVATIONS

Date of test : June 82

Plate dimensions

A = 0.253m B = 0.251m

h = 0.406E-02m

A_S = 0.2m B_S = 0.2m

A_P = 0.02m B_P = 0.02m

Lay-up (90°, 0°, 90°, 45°, 0°, 45°, 0°, 45°, 0°, 45°, 0°, 45°, 0°, 45°, 0°)_S

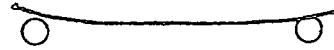
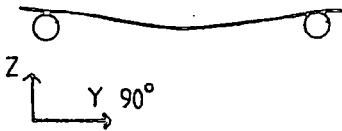
Ball bearings 0.4445E-01m

Central transverse displacement was increased at 0.5E-03m/min in increments of 400N.

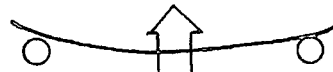
All strains and displacements recorded have been presented in the plots.

Approximate deformation observed

At 4000N



At 6000N



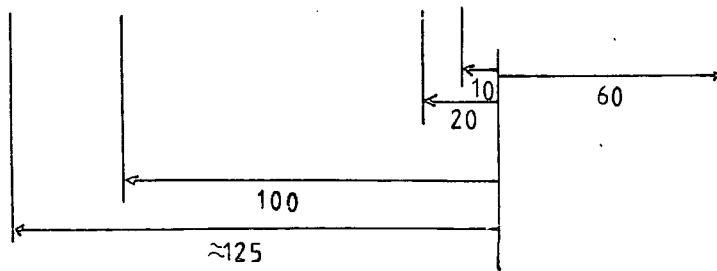
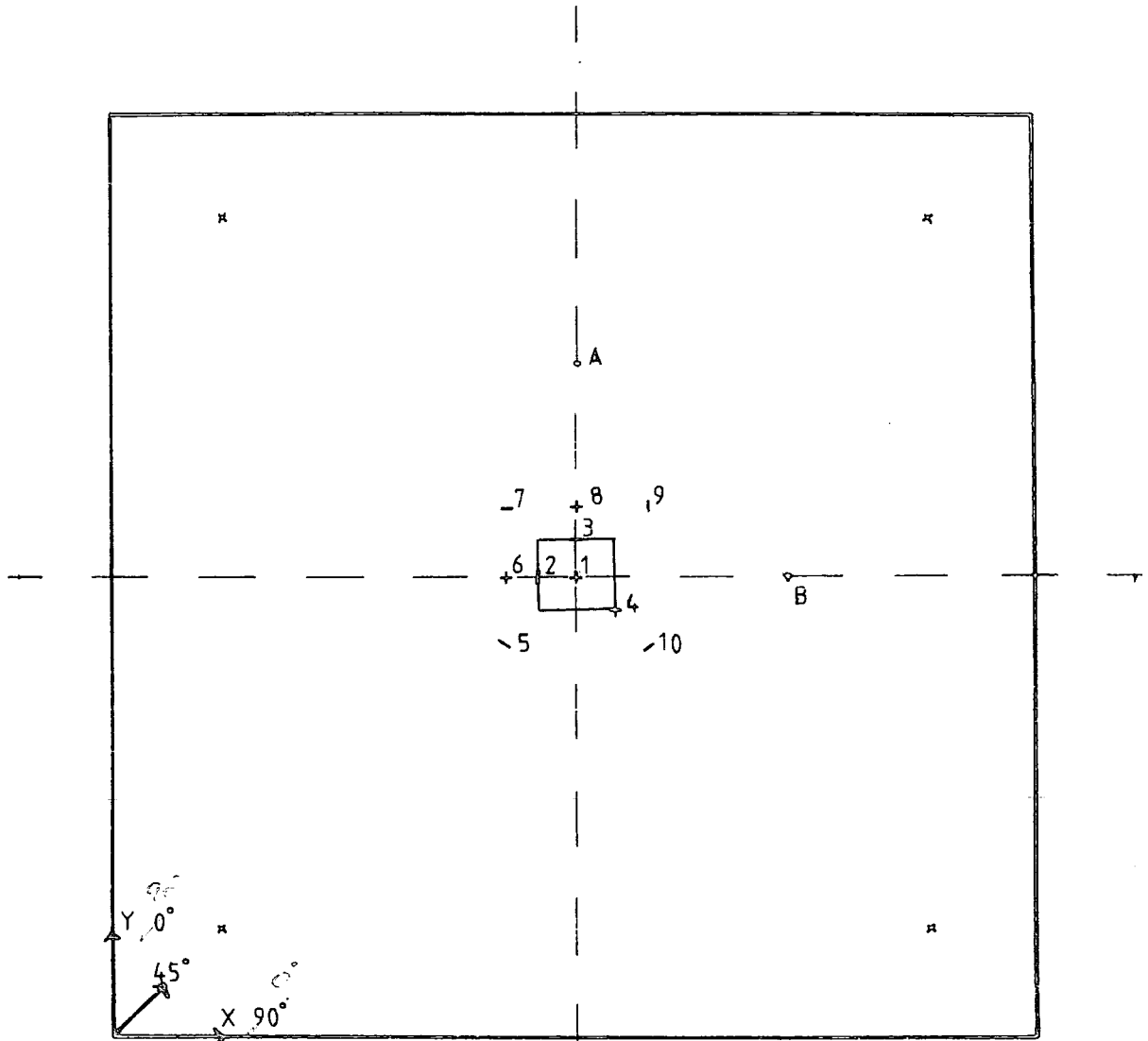
When load exceeded 6400N the occasional snap was heard, (adhesive breakdown). First fibre failure occurred as the transverse displacement was increasing at 7960N. Failure started near the centre in the outer tensile lamina. The resultant failure caused sufficient weakening that final equilibrium was attained at 1250N.

On inspecting the area where the patch load was subjected the chalk impression left indicated that load had been applied fairly evenly, with a heavy line along one side.

Figure 4.15 EXPERIMENT 2. STRAIN GAUGE ARRANGEMENT
 34 layers (90,0,90,+45,0,-45,0,0,-45,0,+45,0,0,+45,0,-45,0)s
 SCALE 1:4

STRAIN GAUGES + CROSS-ply TYPE FCA3-11 3MM
 - SINGLE-PLY TYPE FLA3-1E 3MM

VIEW : FROM BELOW



▪ POINT SUPPORT

□ PATCH LOAD

Figure 4.16 EXPERIMENT 2. DISPLACEMENT MEASUREMENTS DURING LINEAR DEFORMATION

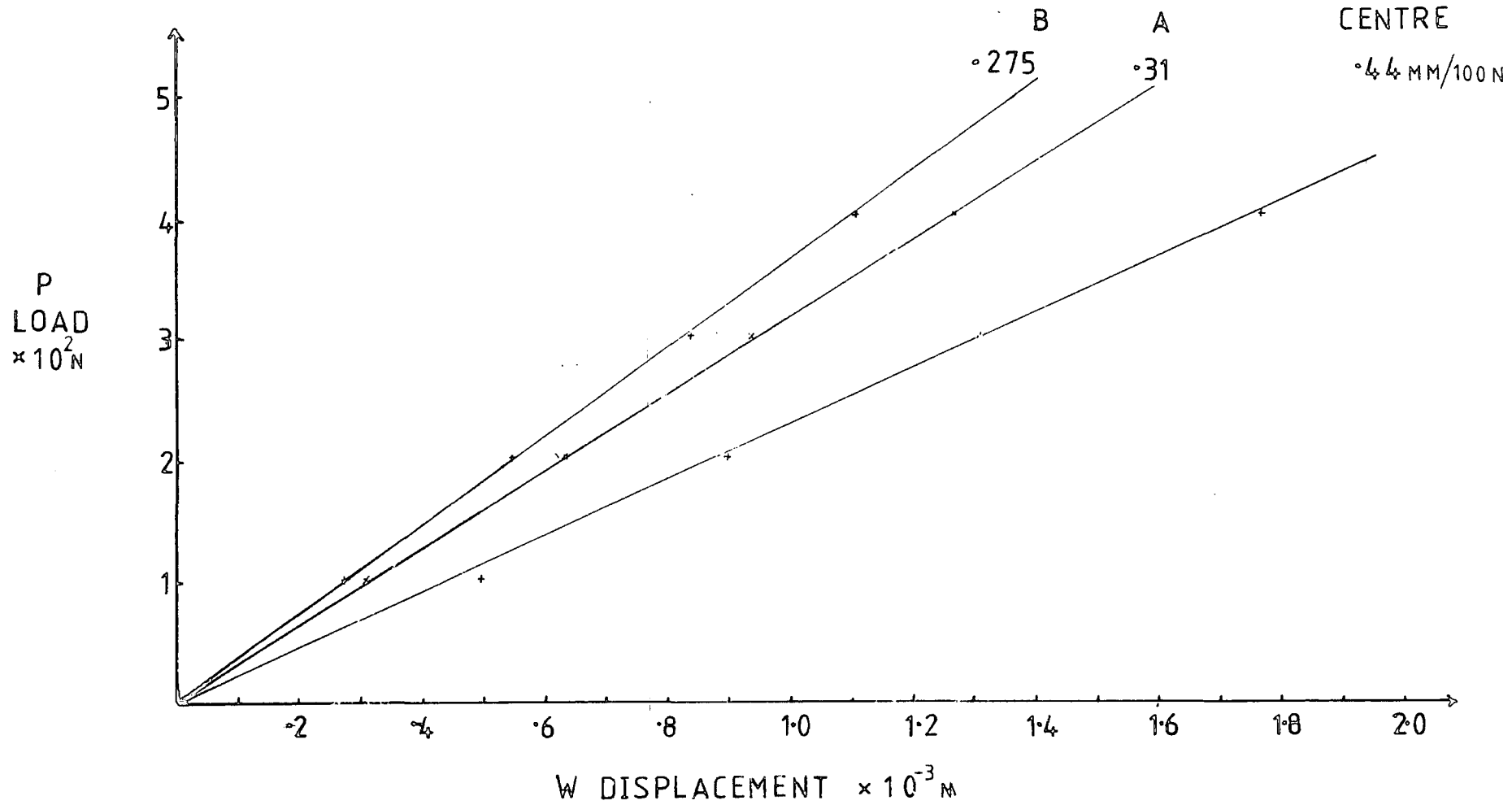


Figure 4.17 EXPERIMENT 2. STRAIN MEASUREMENTS DURING LINEAR DEFORMATION

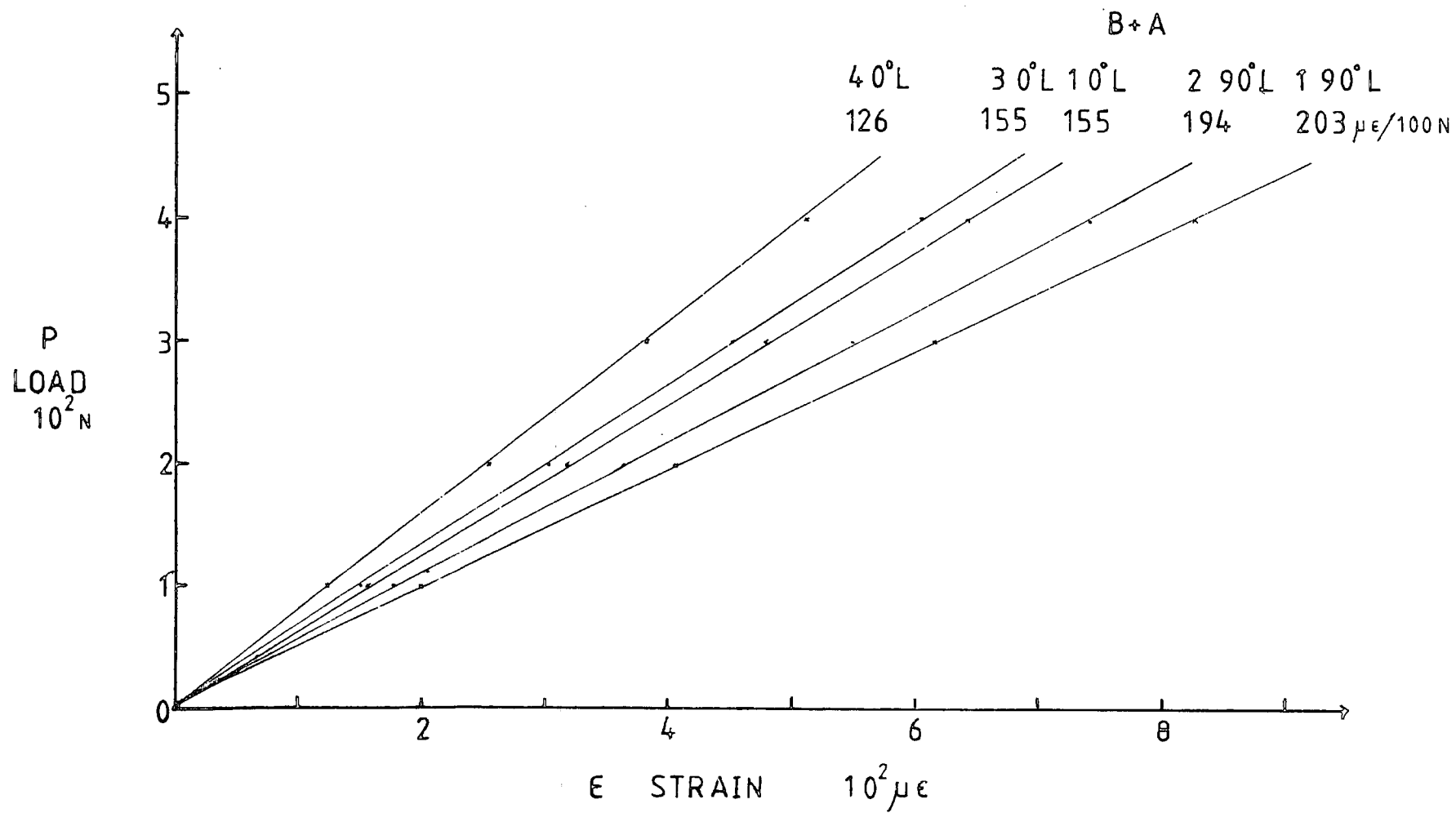


Figure 4.18 EXPERIMENT 2. STRAIN MEASUREMENTS DURING LINEAR DEFORMATION

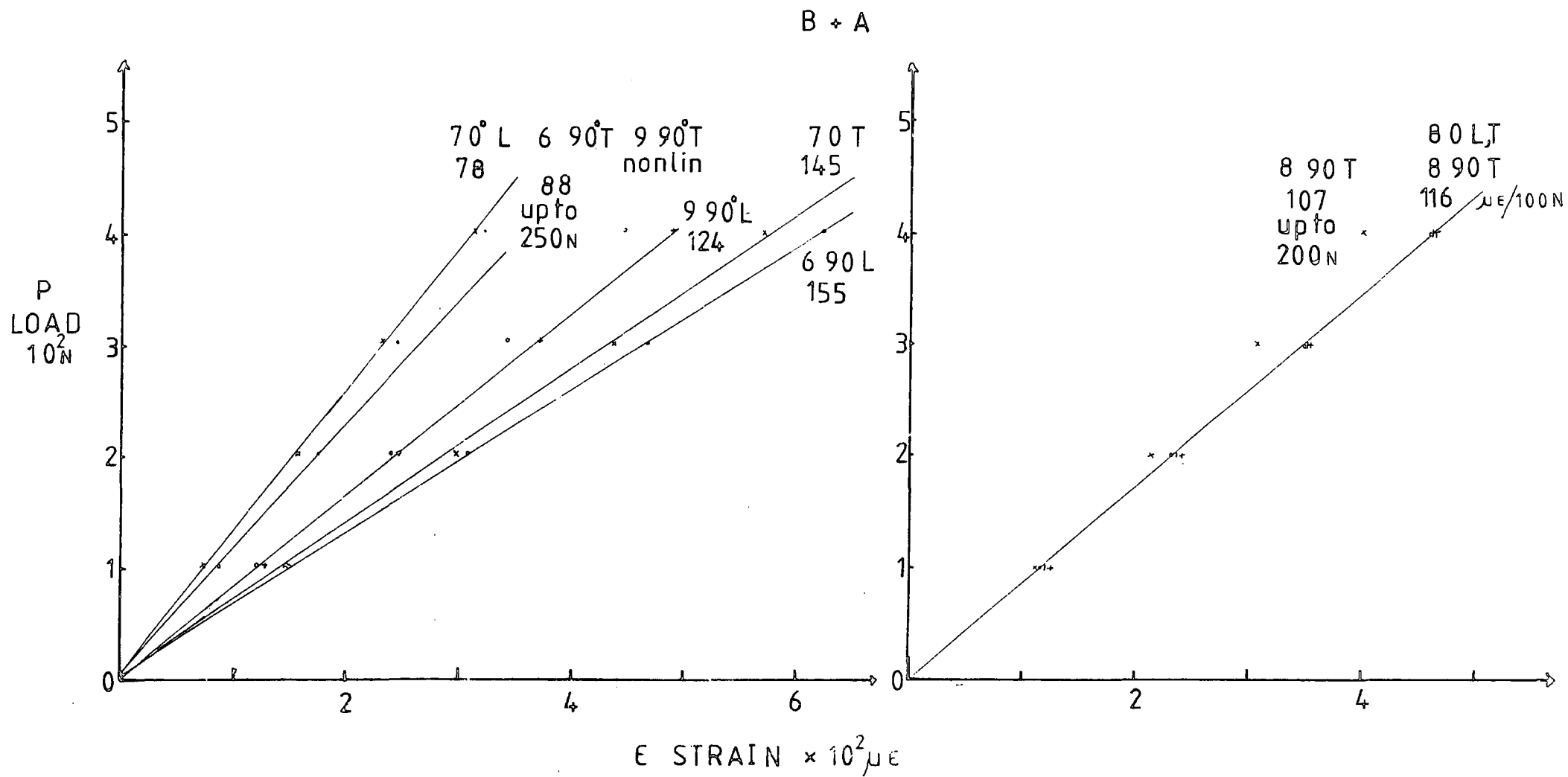


Figure 4.19 EXPERIMENT 2. STRAIN MEASUREMENTS DURING LINEAR DEFORMATION

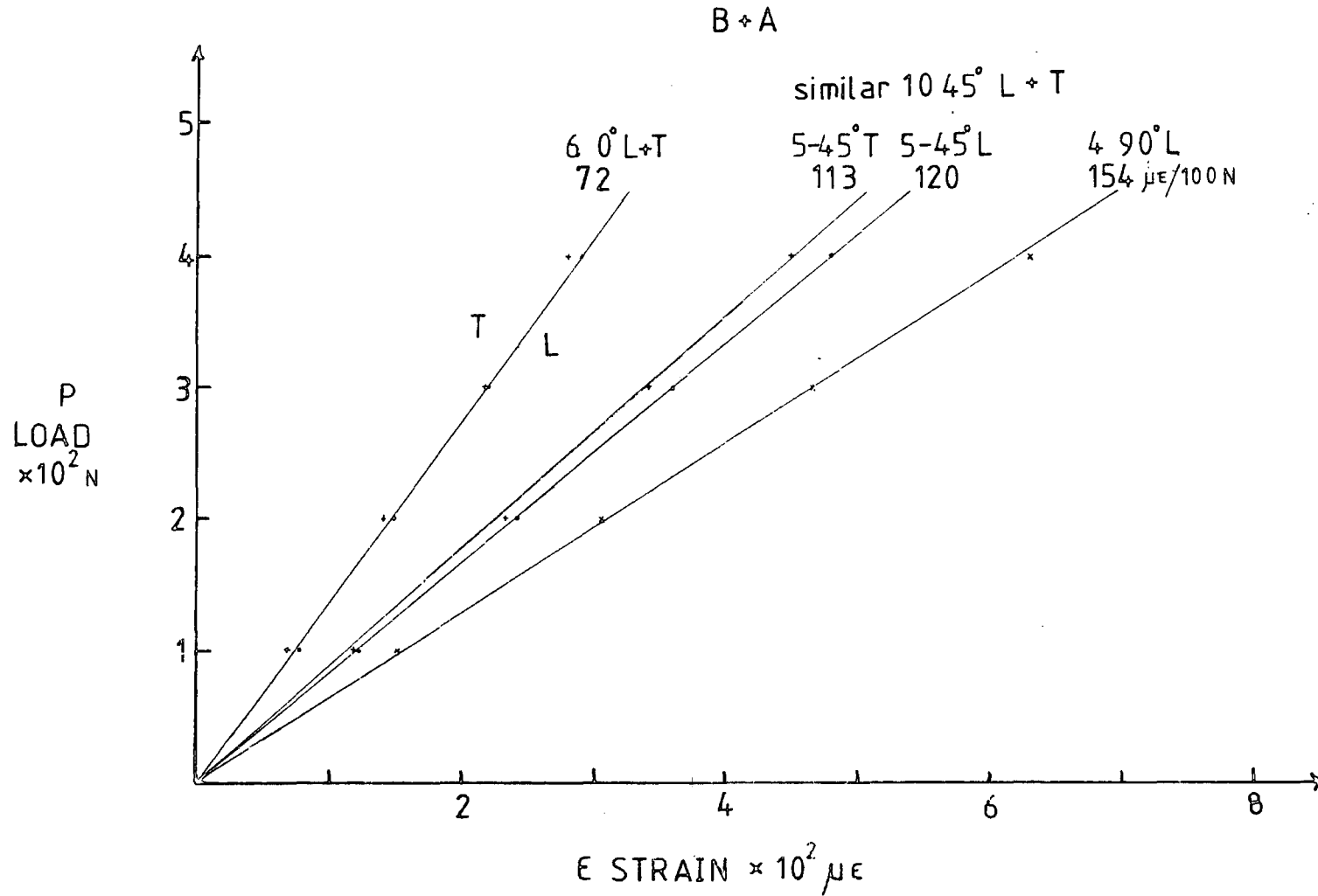
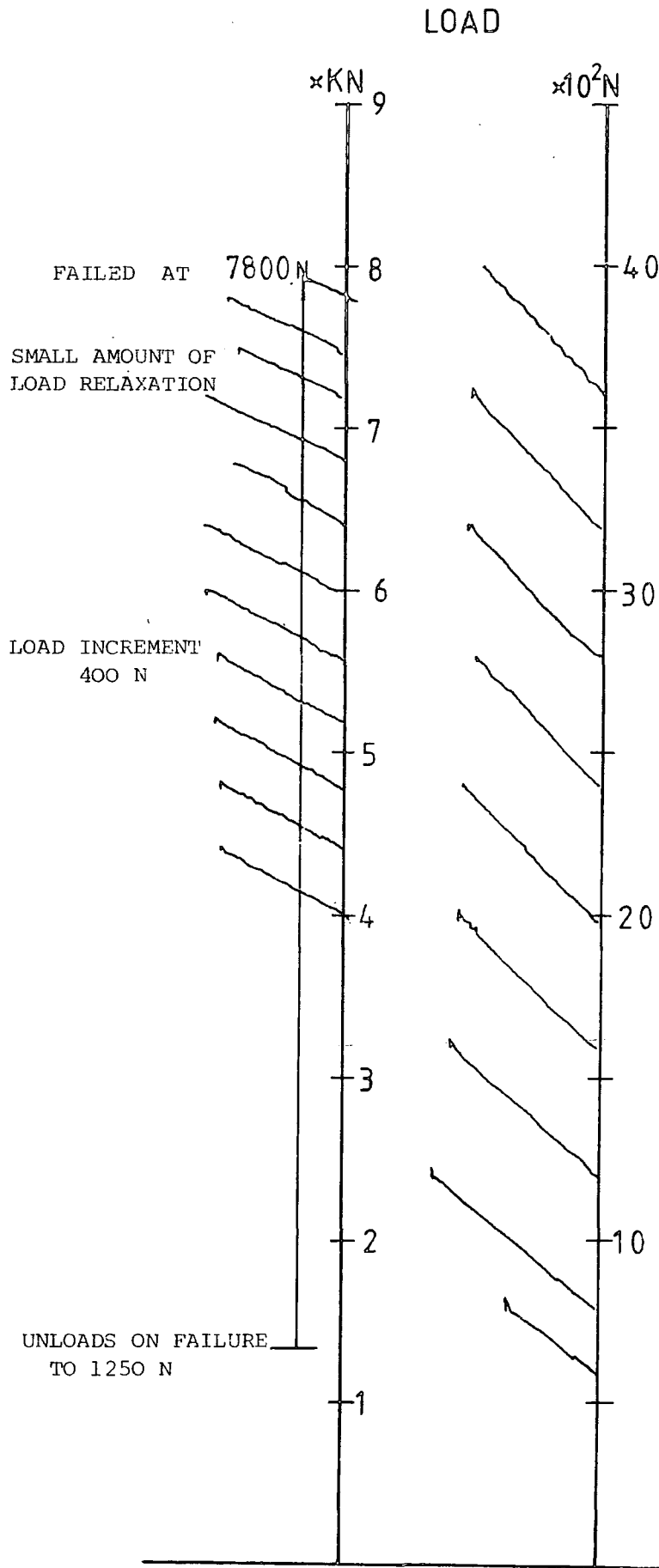


Figure 4.20 EXPERIMENT 2. LOAD / TRANSVERSE DISPLACEMENT RECORDED ON THE CHART RECORDER OF THE INSTRON



20 MM CHART MOVEMENT IS EQUIVALENT TO 1 MM MOVEMENT OF CROSSHEAD

Figure 4.21 EXPERIMENT 2. TRANSVERSE DISPLACEMENTS TO FIRST FIBRE FAILURE

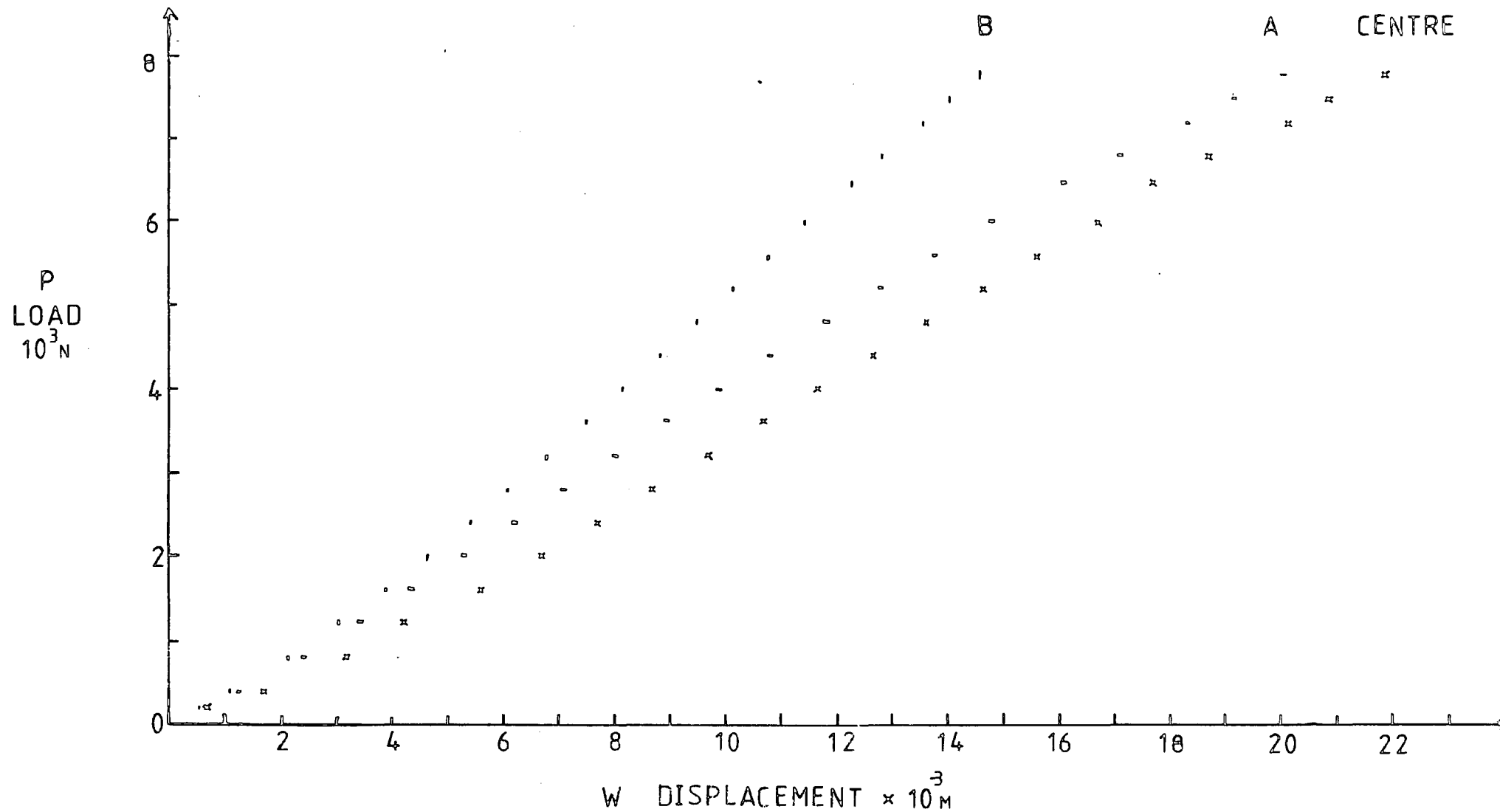


Figure 4.22 EXPERIMENT 2. STRAIN MEASUREMENTS TO FIRST FIBRE FAILURE

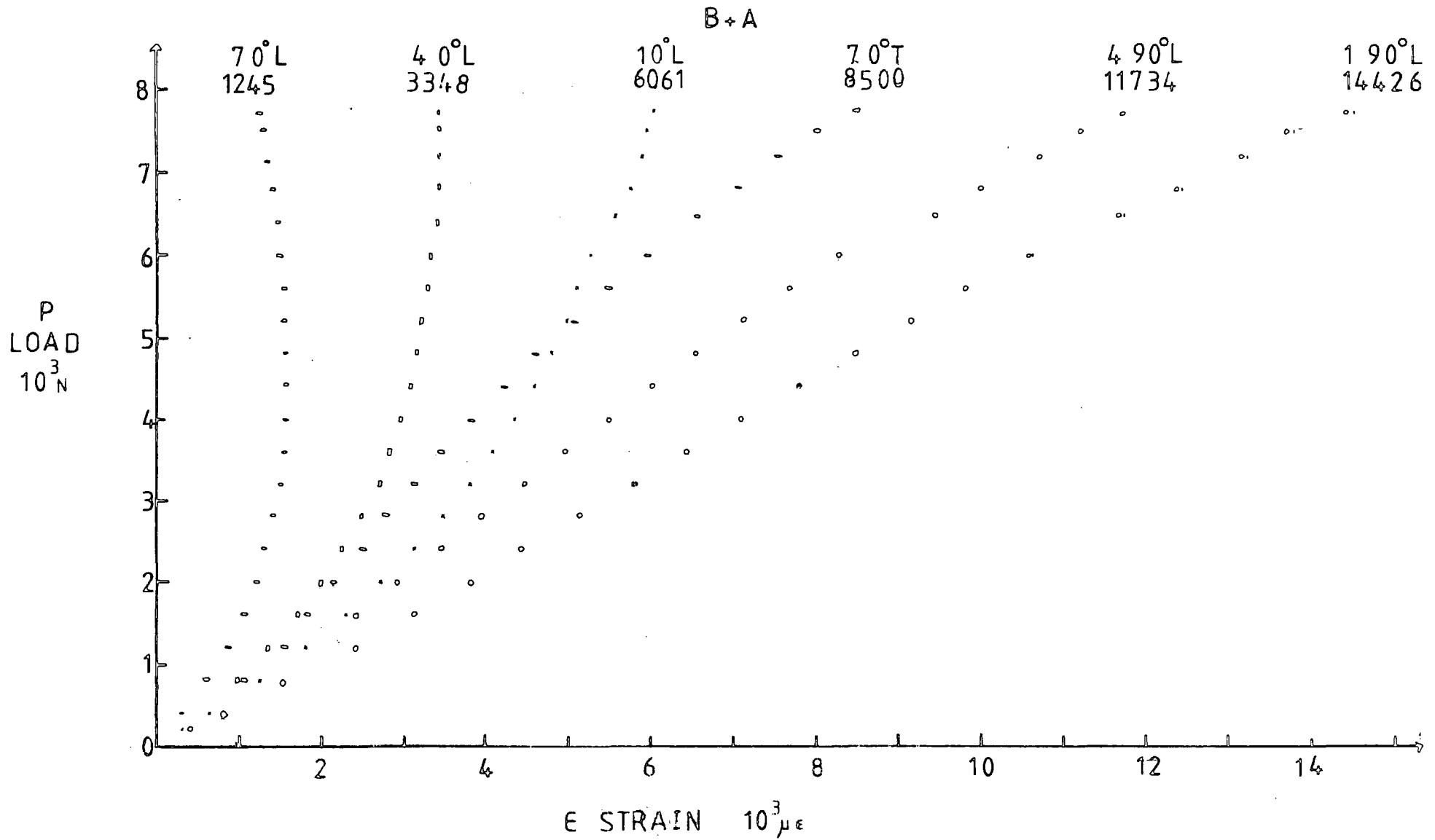


Figure 4.23 EXPERIMENT 2. STRAIN MEASUREMENTS TO FIRST FIBRE FAILURE

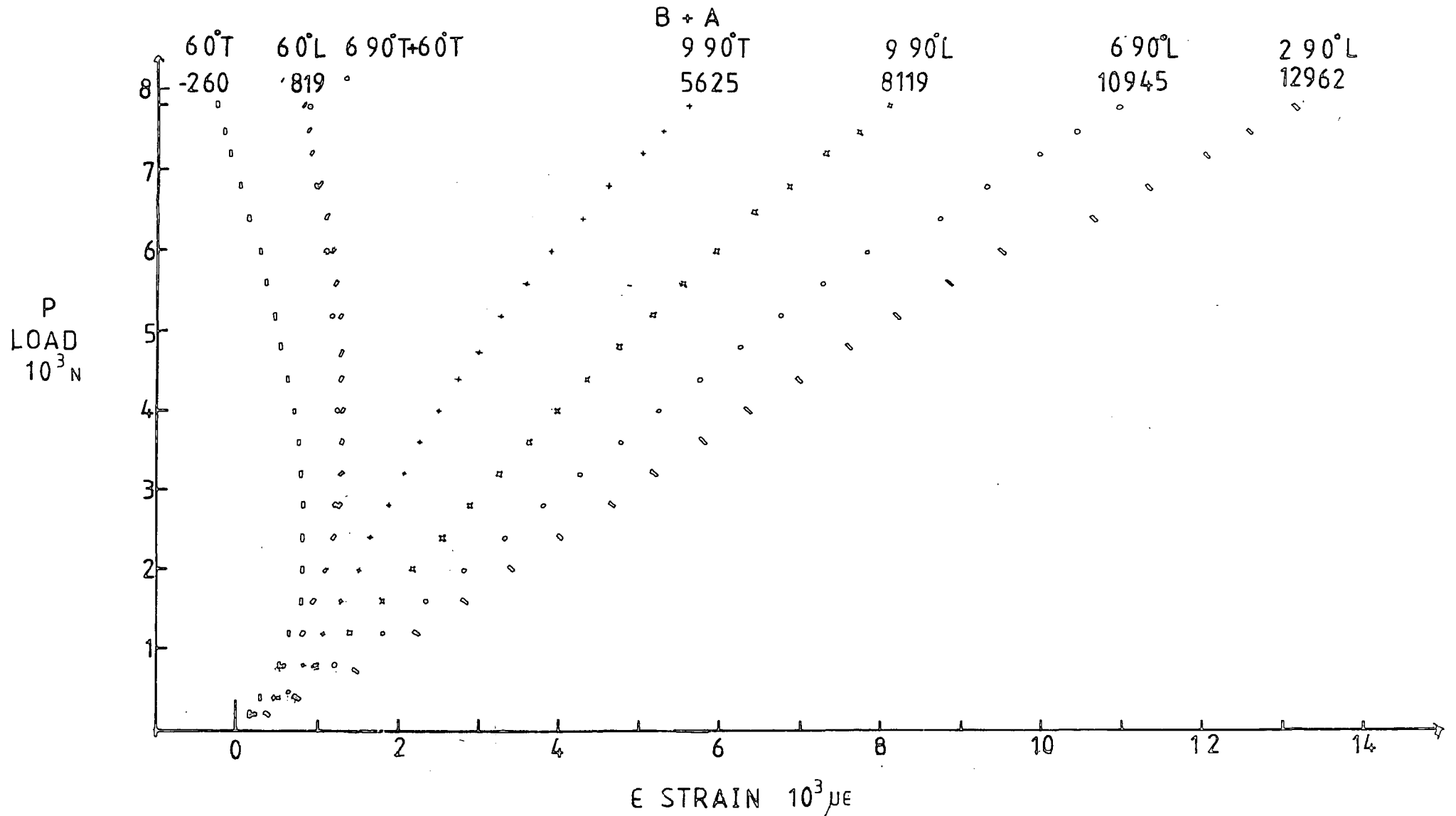


Figure 4.24 EXPERIMENT 2. STRAIN MEASUREMENTS TO FIRST FIBRE FAILURE

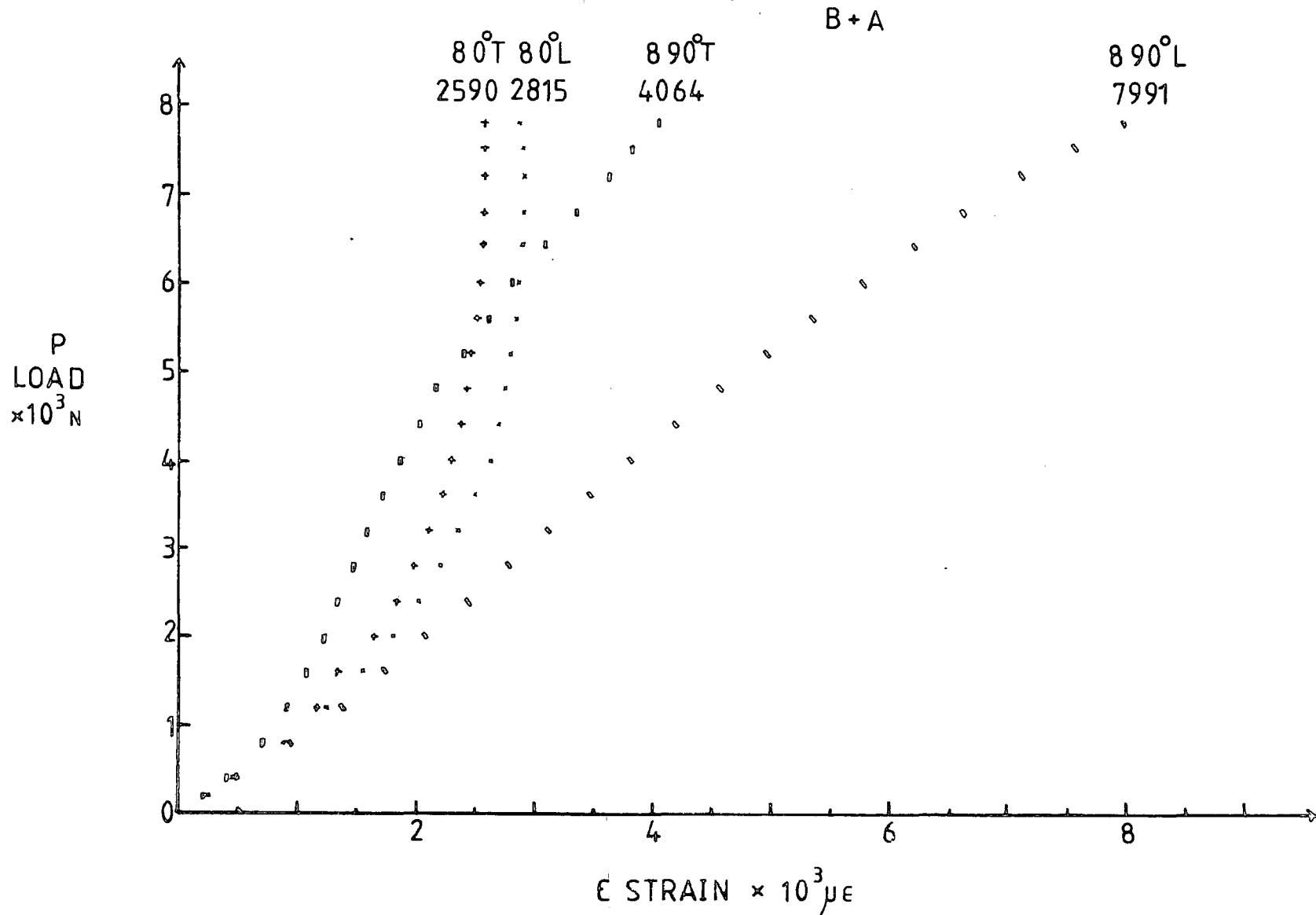


Figure 4.25 EXPERIMENT 2. STRAIN MEASUREMENTS TO FIRST FIBRE FAILURE

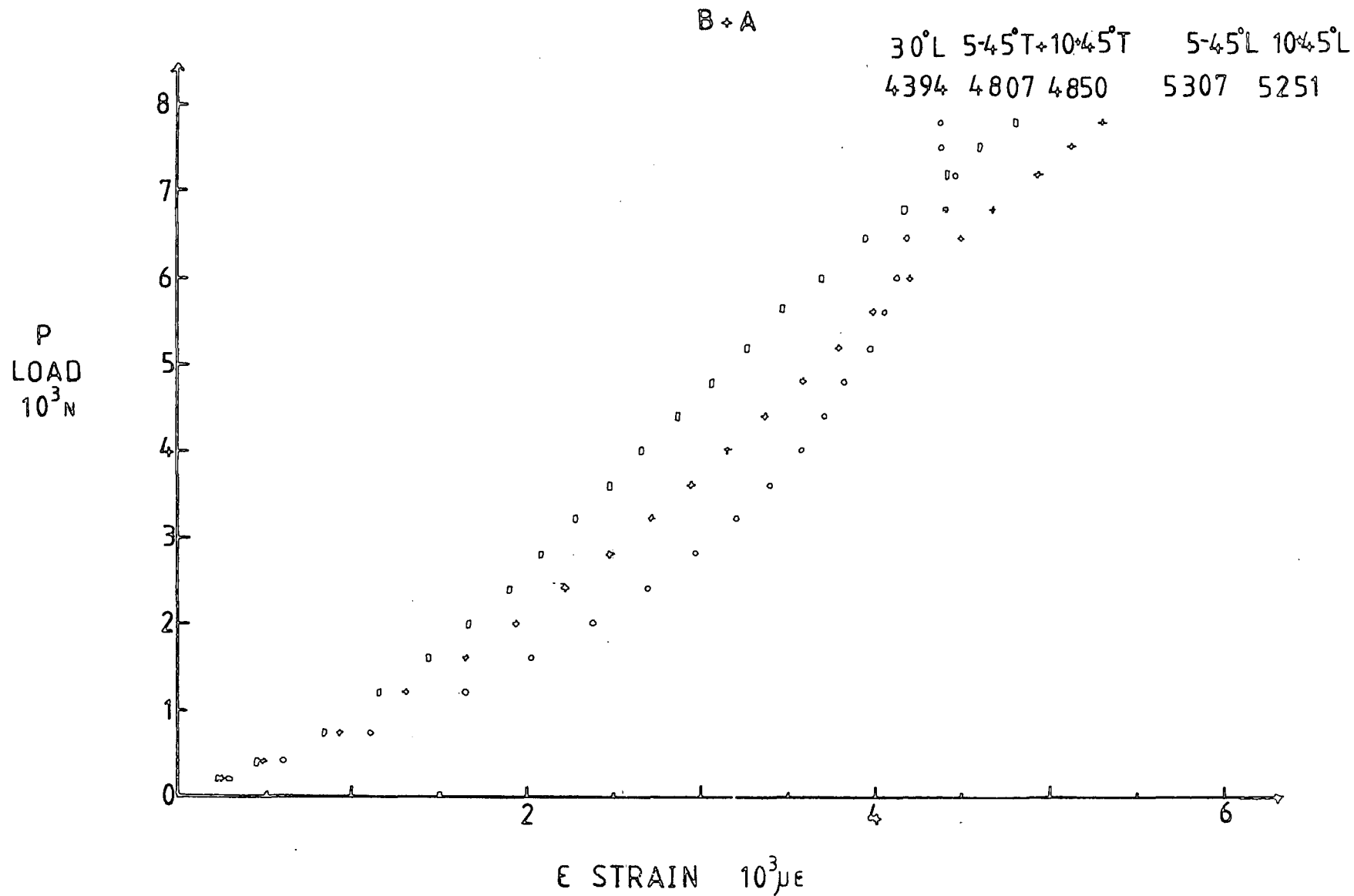
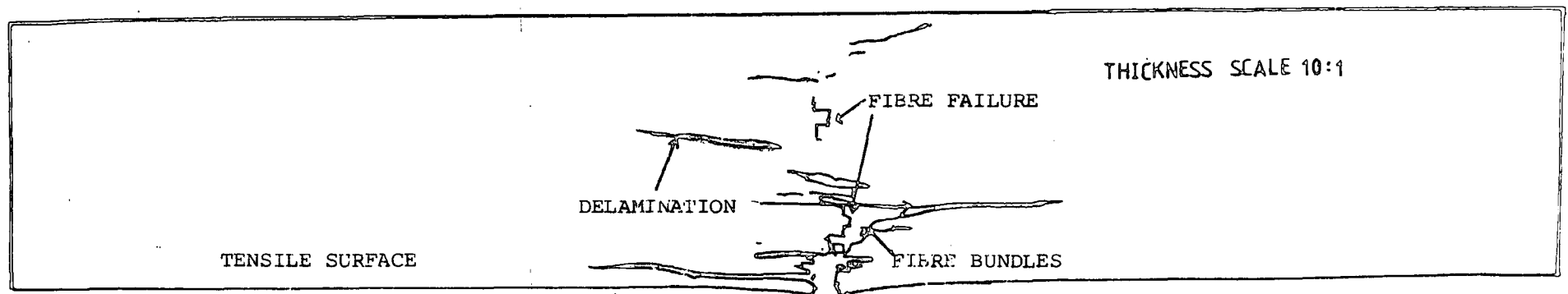
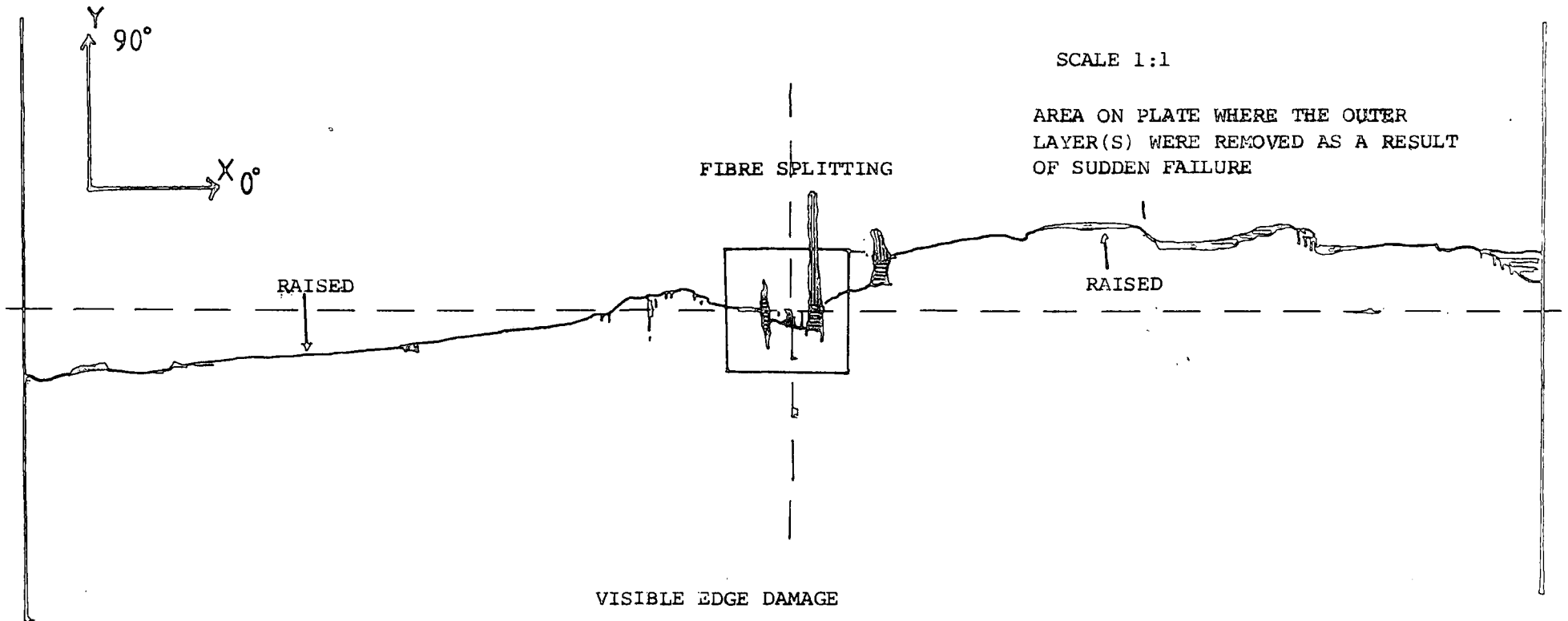


Figure 4.26 EXPERIMENT 2. VISIBLE FAILURE ON TENSILE SURFACE



EXPERIMENT 3 and 4. NOTES AND OBSREVATIONS

Date of test : Exp. 3 Oct 81 . Exp. 4 May 82

Plate dimensions

A = 0.258m

B = 0.258m

h = 0.549E-02m (includes protective layer)

A_s = 0.2m

B_s = 0.2m

A_p = 0.02m

B_p = 0.02m(rubber pad 0.178E-02m)

Lay-up (45°,90°,-45°,0°,0°,-45°,90°,+45°)₅

Ball bearings 0.4445-01m (Exp 3) , 0.3175E-01m (Exp 4)

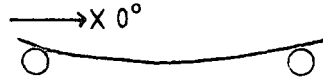
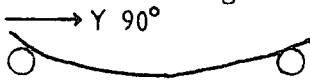
Experiment 3

The plate was arranged with the protective layer as the top surface. Central transverse displacement was applied at 0.1E-02m/min in increments of 400N.

At 400N a small amount of load relaxation(25N) was recorded, but the size of load relaxation did not increase with load.

At 6000N a small amount of strain increase was measured at the centre during the time required to take the readings.

At 8000N the bending deformation was:



At 9600N there was no visible damage along the edges, a loud snap was heard and gauge 1 90° L suddenly recorded an increase.

At 10800N the central strains decreased rapidly as adhesive failure due to poor quality M-bond 200 caused the gauges to peel off.

Strain gauge measurements not plotted

The values below were recorded at 8000N when the adhesive failure had not appeared.

	μE		μE		μE
2 90° B	3139	4 0° A	249	7 90° L B+A	5812
2 0° B	3147	6 90° L B+A	5903	7 -45° L "	6475
3 90° A	577	6 0° L "	4905	8 0° L "	2671
3 0° A	319	6 45° L "	6142	8 90° L "	4769
4 90° A -23(1400 N) 80		7 0° L "	7150	8 +45 L "	4577

All B and B+A gradually increased and showed stiffening.

All A were small and practically linear above 4000N.

EXPERIMENT 3 and 4. NOTES AND OBSERVATIONS (contd.)

Experiment 4

The plate had been C-scanned by British Aerospace(Woodford) after Experiment 3 ,which showed that there was no internal damage.

A similar procedure as that for Exp. 3 was followed ,but with 800N increments of load. Observations up to 13750N were also similar to Exp. 3. No damage was observed until ultimate first fibre failure ,which occurred at 13750N after 1 minute of constant central transverse displacement. Like Exp. 2 a chalk impression indicated that the load had been uniformly distributed. The resultant fibre failure which initiated at the centre was not as extensive as in Exp. 1 and 2 .The final load after failure was 9600N.

Strain gauge measurements not plotted

The value below were recorded at 13000N since failure prevented the full set of readings to be made at 13750 N.

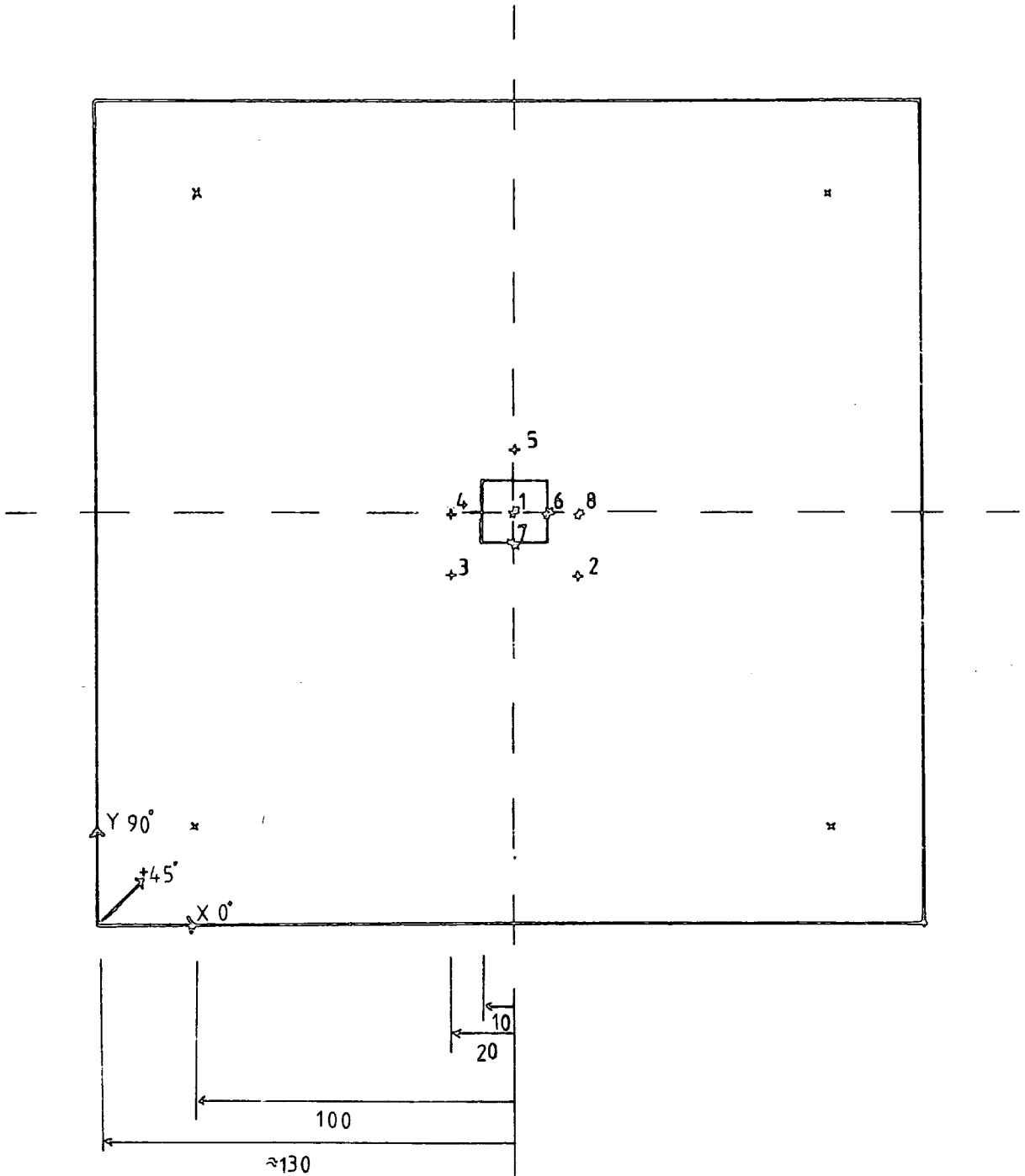
	$\mu\epsilon$		$\mu\epsilon$
6 0° L B+A	5276	9 90°L B+A	6103
6 0° T "	2029	9 90 T B+A	5629
7 90° L "	4564	10 0°L "	6866
7 90°T "	2240	10 0°T "	6360

Figure 4.27 EXPERIMENT 3. STRAIN GAUGE ARRANGEMENT
 40 LAYERS (45,90,-45,0,0,-45,90,+45)₅

SCALE 1:4

STRAIN GAUGES	+	CROSS-PLY	TYPE FCA3-11	3MM
	-	SINGLE-PLY	TYPE FLA3-11	3MM

VIEW: FROM ABOVE



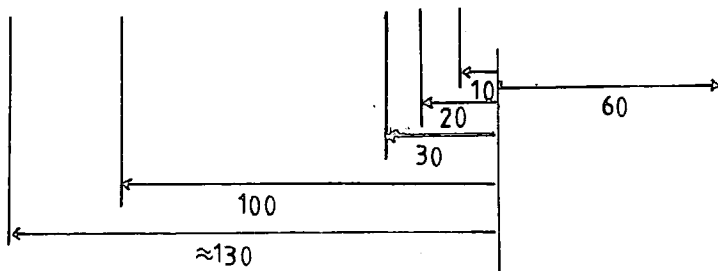
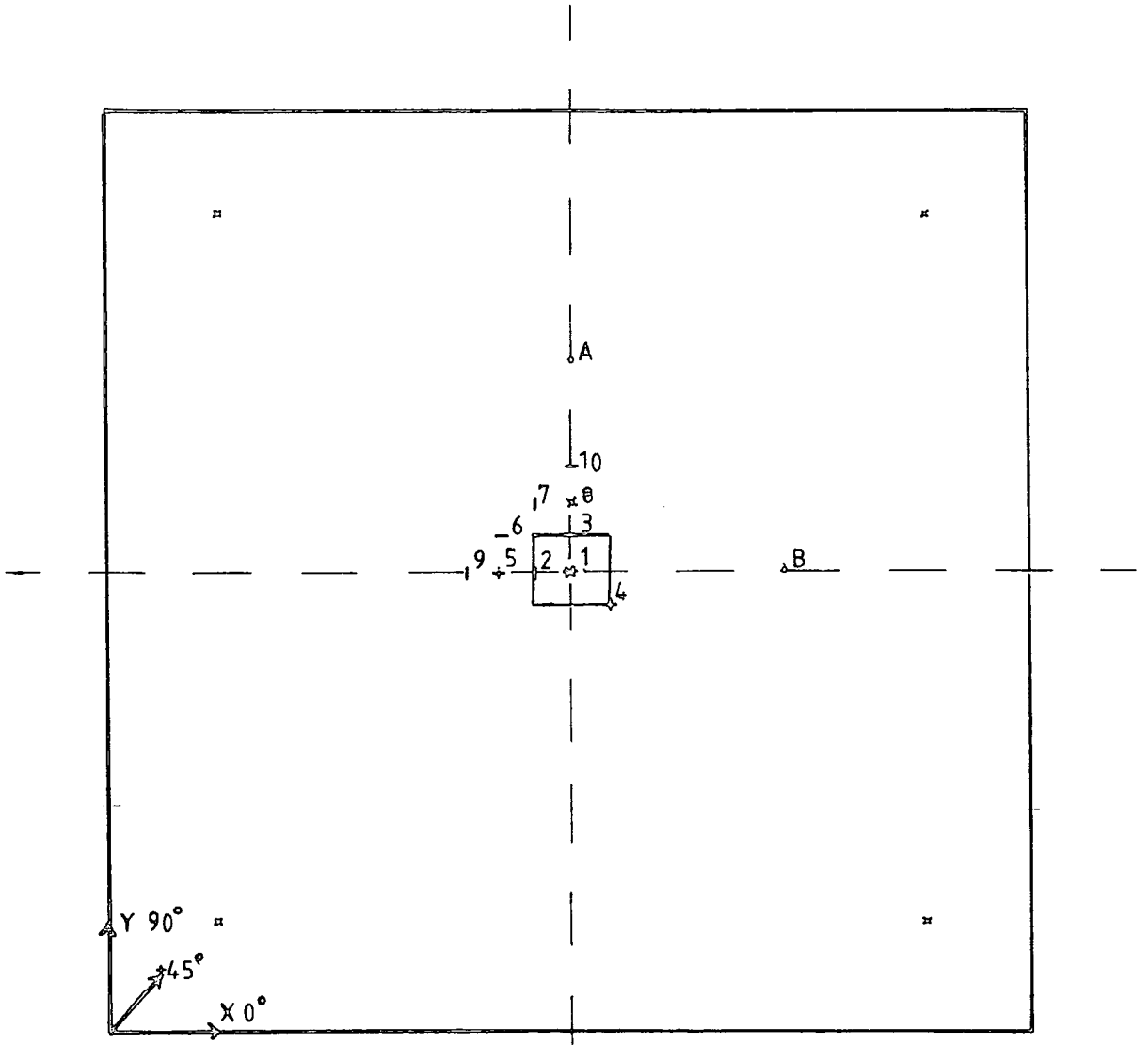
x POINT SUPPORT
 □ PATCH LOAD

Figure 4.28 EXPERIMENT 4. STRAIN AND DAIL GAUGE ARRANGEMENT
 40 LAYERS (+45,90,-45,0,0,-45,90,+45)₅

SCALE 1:4

STRAIN GAUGES	◇	CROSS-PLY	TYPE FCA3-11	3MM
	-	SINGLE-PLY	TYPE FLA3-11	3MM

VIEW : FROM ABOVE



□ POINT SUPPORT
 □ PATCH LOAD

Figure 4.29 EXPERIMENTS 3 AND 4 . TRANSVERSE DISPLACEMENT MEASUREMENTS

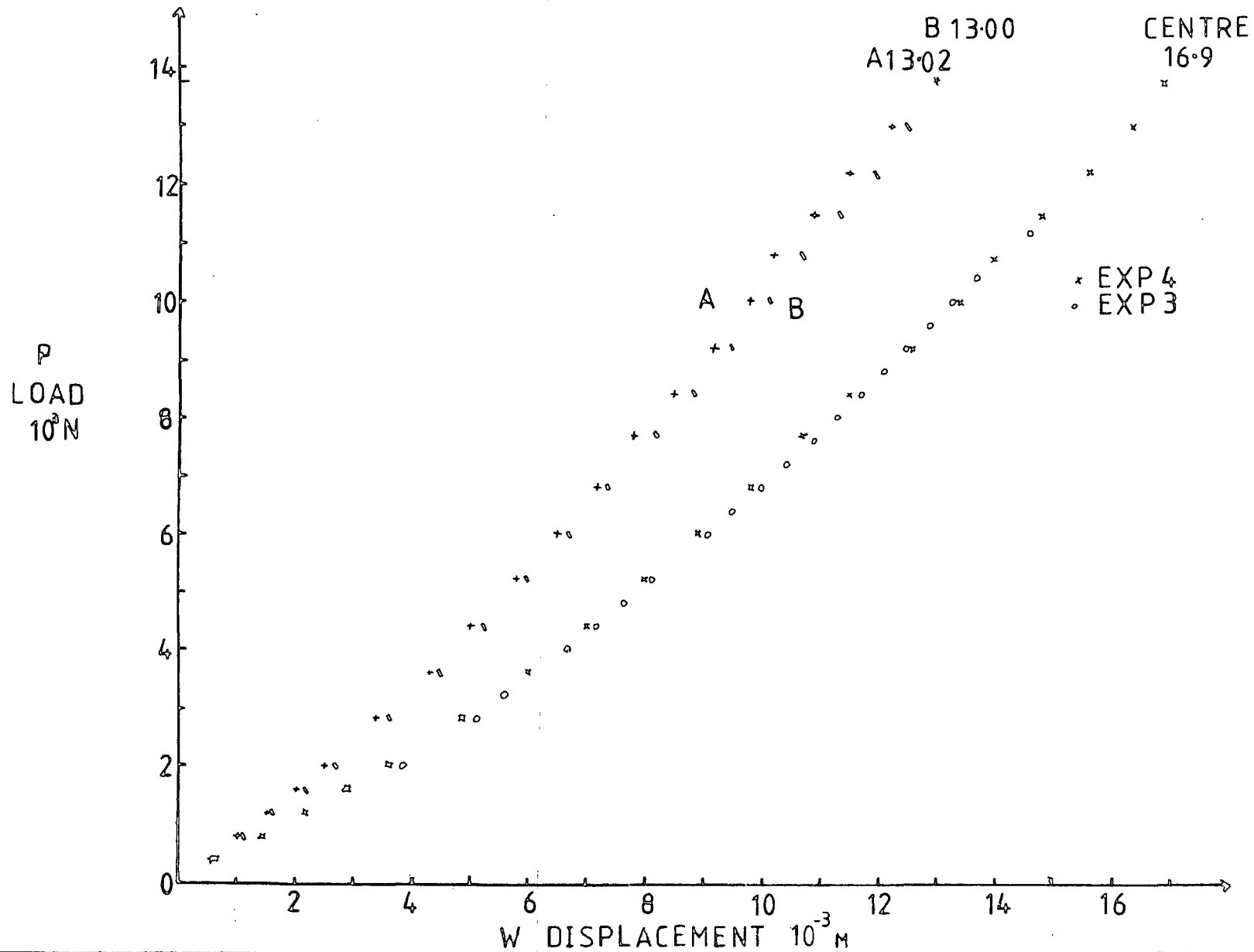


Figure 4.30 EXPERIMENTS 3 AND 4. STRAIN MEASUREMENTS

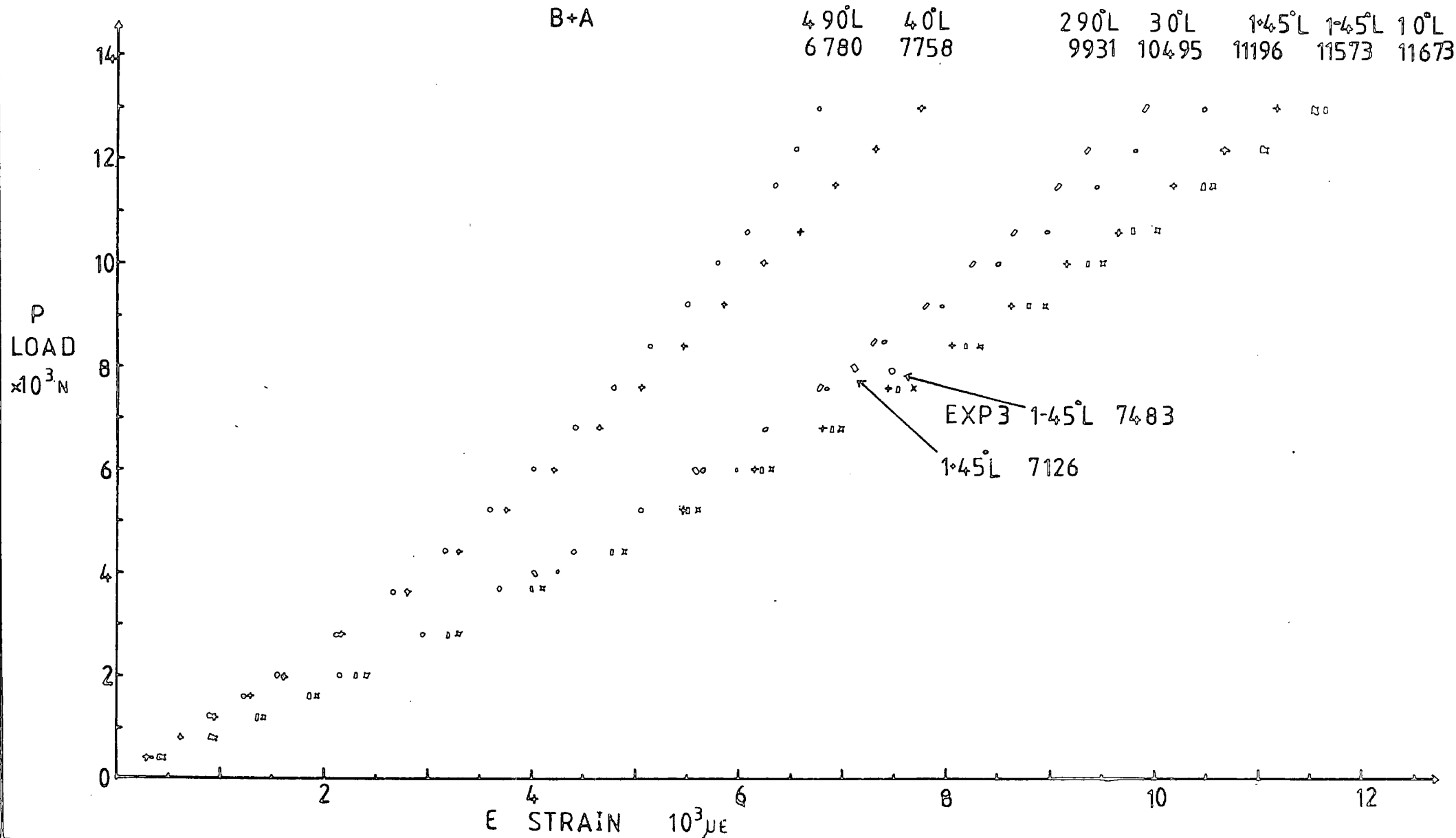


Figure 4.31 EXPERIMENTS 3 AND 4. STRAIN MEASUREMENTS

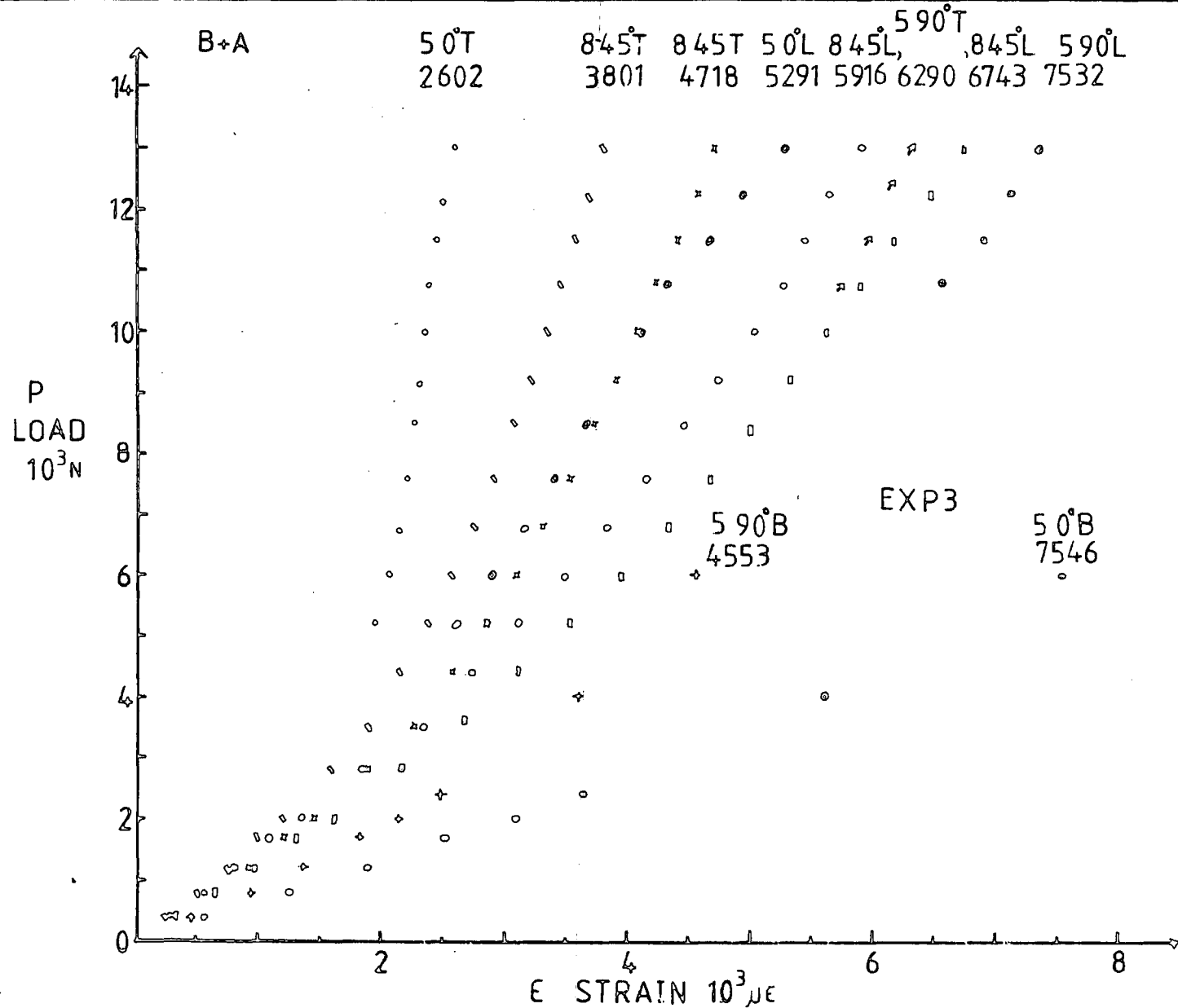
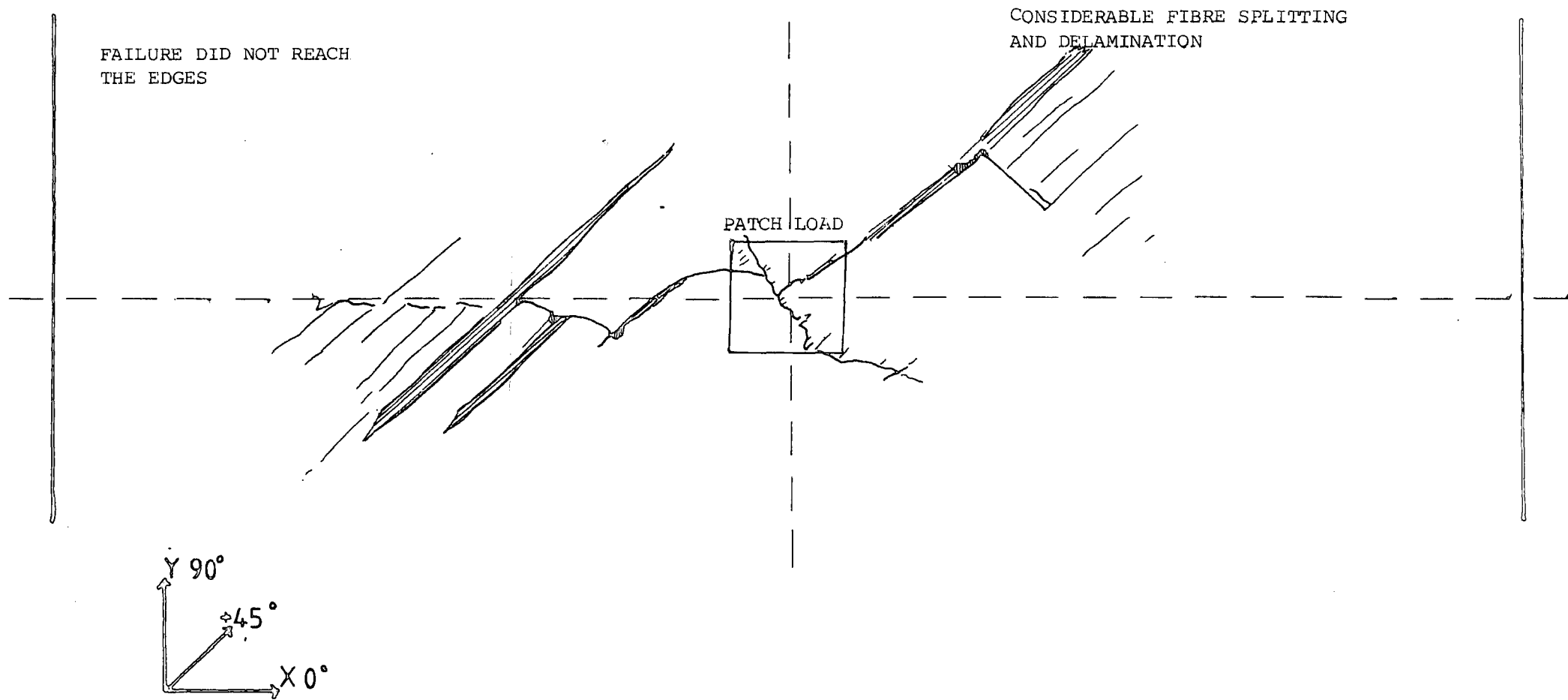


Figure 4.32 EXPERIMENT .4. VISIBLE FAILURE ON TENSILE SURFACE



EXPERIMENT 5. NOTES AND OBSERVATIONS

Date of test: Feb 82

Plate dimensions

A = 0.205m B = 0.273m

h = 0.191E-02m

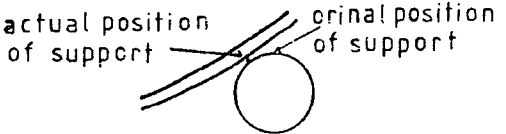
A_S = 0.15m B_S = 0.2m

A_P = 0.02m A_P = 0.02m

Lay-up (+45°, 0°, -45°, 90°, 90°, -45°, 0°, +45°)_S

Ball bearings 0.4445E-01m

Central transverse displacement was increased at 0.5E-03m/min in increments of 100N.

LOAD N	REMARKS
400	The plate started to behave like a pure beam, with a very small amount of bending about the Y-centrelne
550	No load relaxation
650	No visible edge delamination
750	Load relaxation(10N)
950	The laminate was bending as a beam. Load relaxation(10N)
1000	It was noted that the point of support had moved down the surface of the ball bearings. 
	This change was only observed in the Y-direction.
1050	No sign of edge delamination.
1100	There was noticeable flutter in the load recorded.
1150	Load crack - which resulted in minor fibre failure in the non trimmed edges.
1200	Further fibre failure. Load relaxation(10N)

EXPERIMENT 5. NOTES AND OBSERVATIONS (contd.)

LOAD N

REMARKS

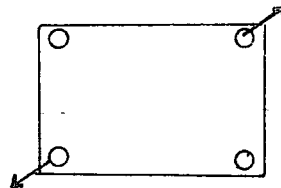
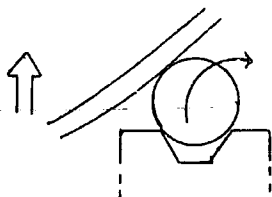
1250 and above

Continuing to increase central transverse displacement did not increase load and there was immediate load relaxation. This was due to poor choice of experimental parameters which allowed the plate to just slip through the supports, Plate 4.2.

The experiment was stopped (without central fibre failure) when the central transverse displacement was 0.66E-01m. It was then noted that a little amount of delamination had occurred along the highly strain edges. But, as with the fibre failure appeared to have happened in the waste material of the edges.

The laminate was subjected to the maximum displacement for 1 hr, and the final load was still above 1200N.

It was then decided to take readings on unloading to measure recovery. Unfortunately the displacement was released too quickly and the unbending caused two diagonally opposite ball bearings to come out of their sockets.



No further gauge measurements than those plotted will be given since the experiment was not successful.

Inspection of the chalk impression left on the plate where the patch loading was imposed indicated that load was uniformly distributed, except at one corner where it was slightly higher.

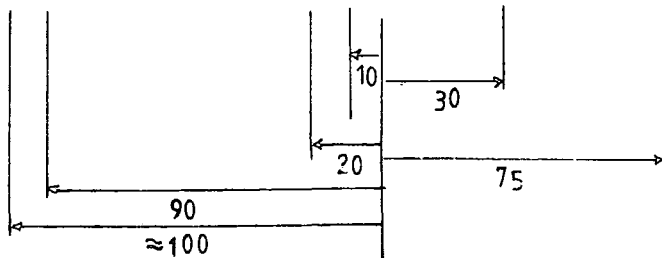
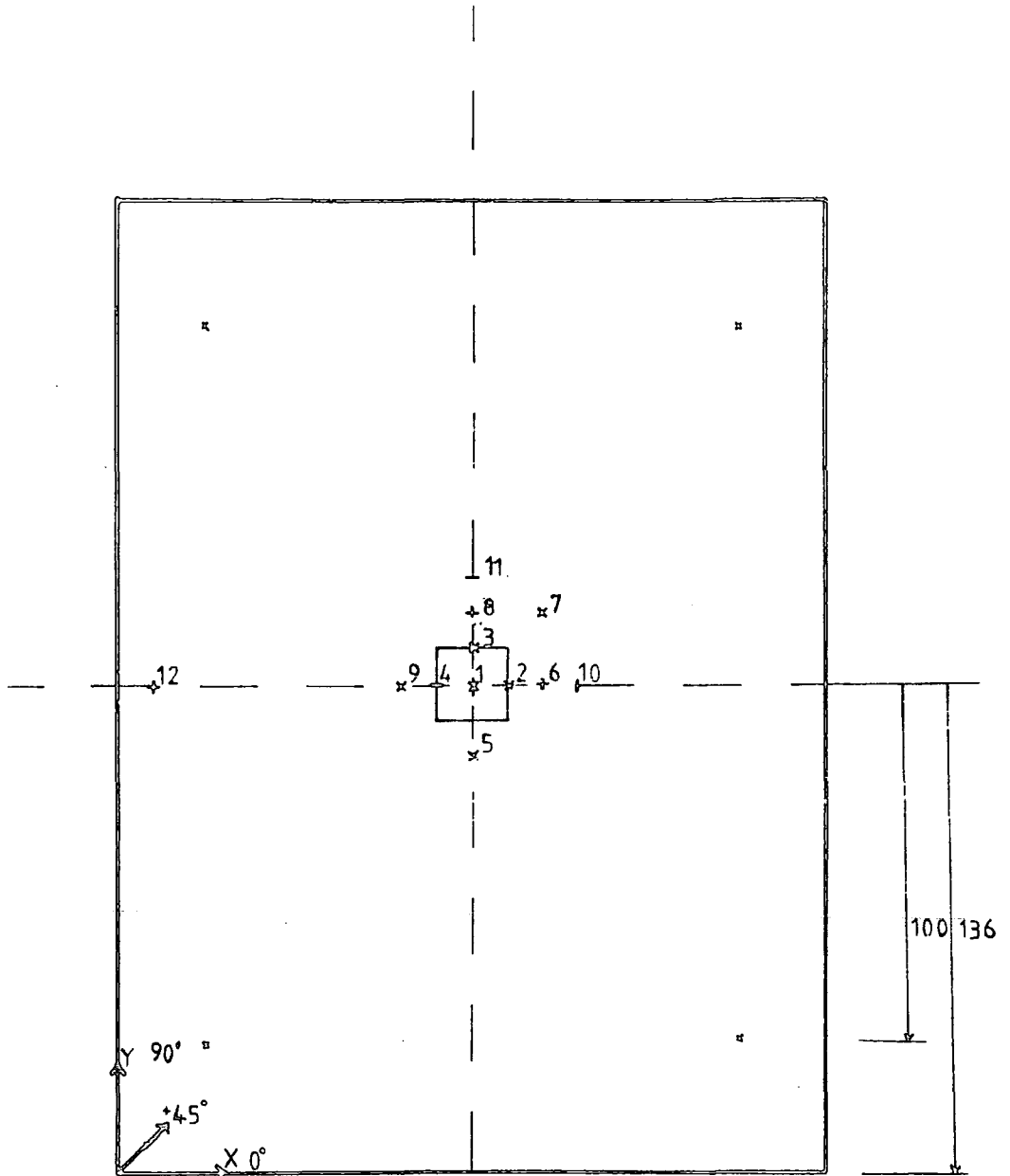
Figure 4.33 EXPERIMENT 5. STRAIN GAUGE ARRANGEMENT

16 LAYERS (+45,0,-45,90,90,-45,0,+45)s

SCALE 1:4

STRAIN GAUGES +	CROSS-PLY	type fca3-11	3MM
-	SINGLE-PLY	TYPE FLA3-11	3MM

VIEW : FROM ABOVE



△ POINT SUPPORT

□ PATCH LOAD

Figure 4.24 EXPERIMENT 5. CENTRAL TRANSVERSE DISPLACEMENT

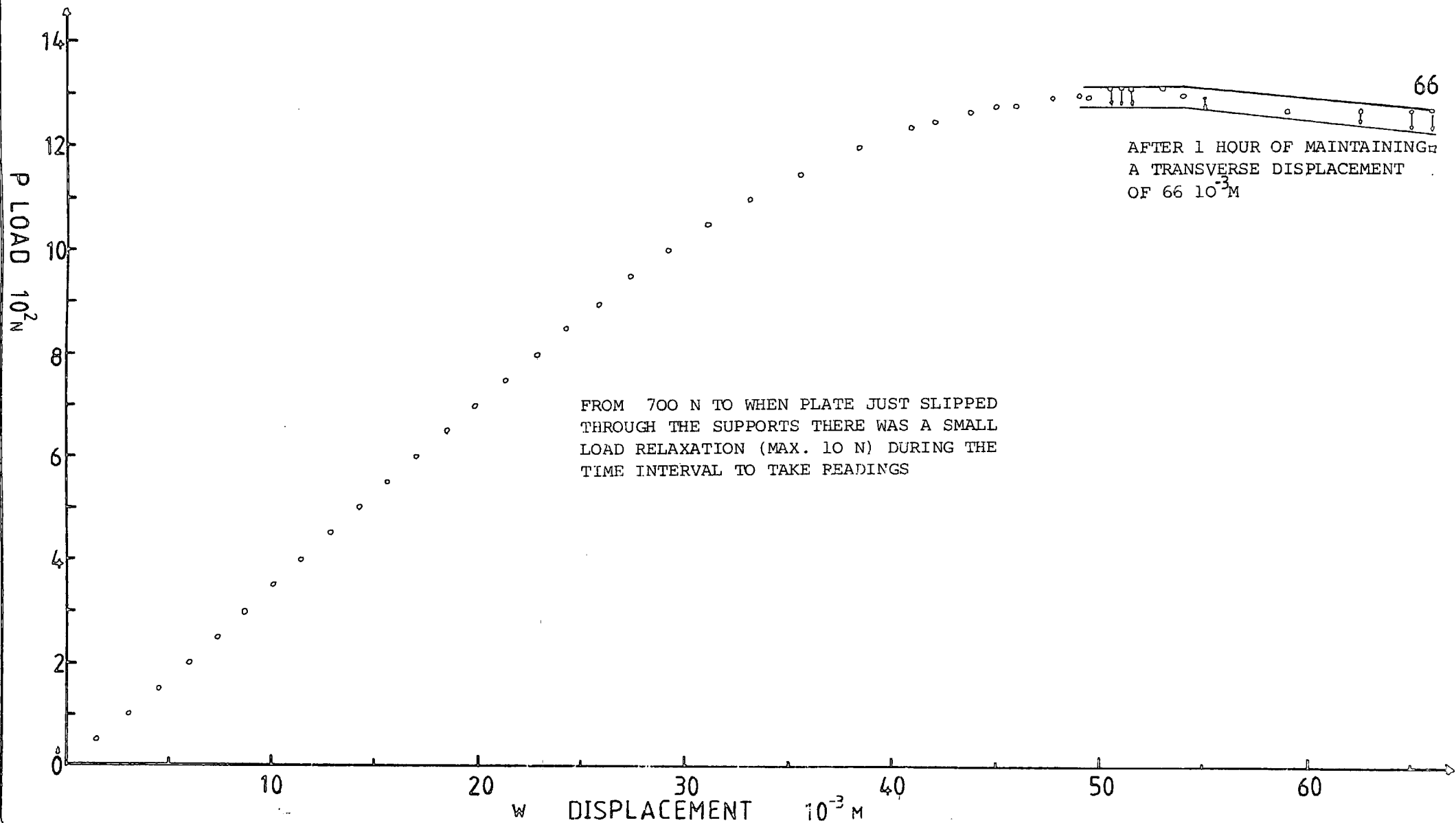


Figure 4.35 EXPERIMENT 5. STRAIN MEASUREMENTS

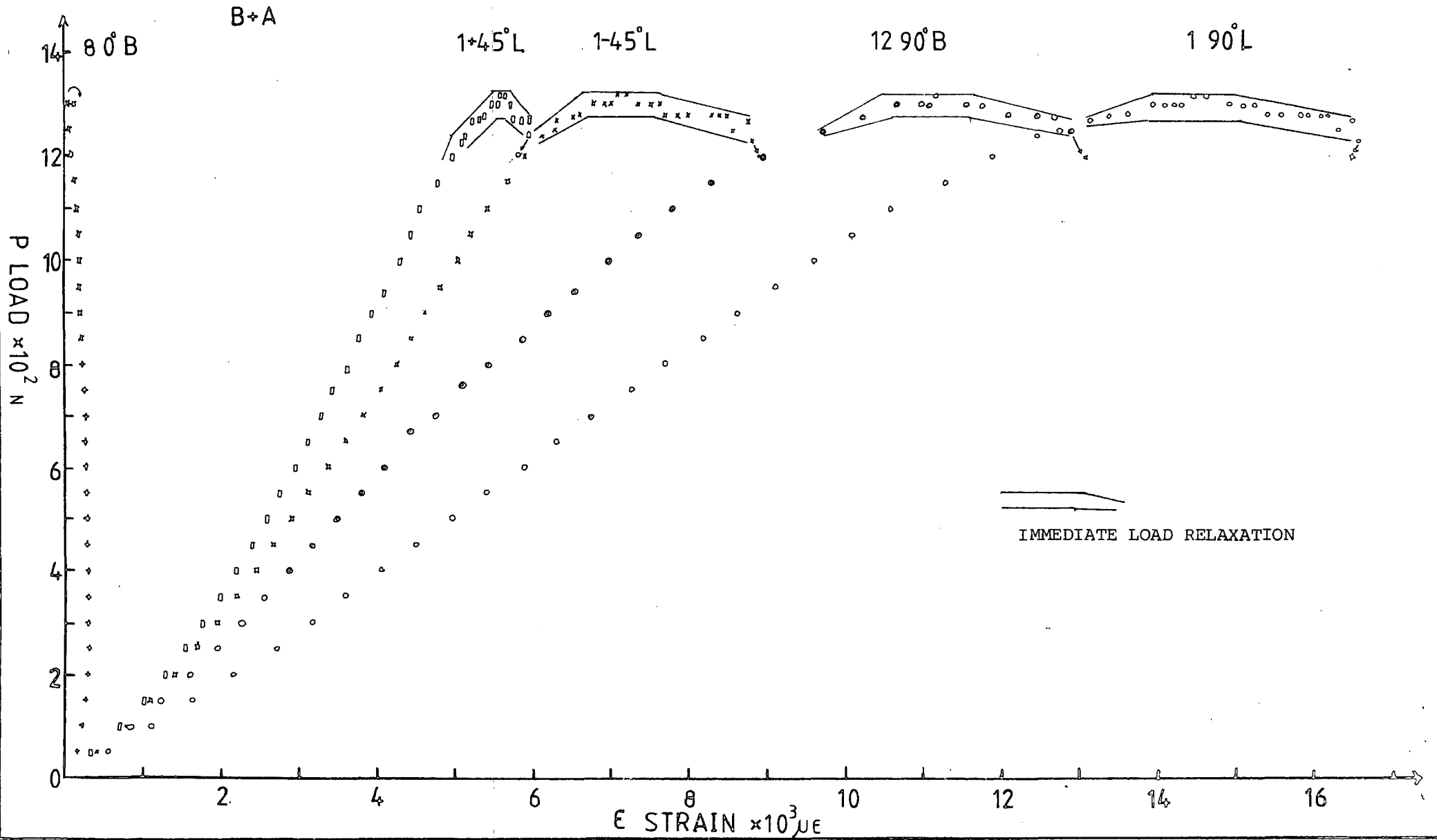
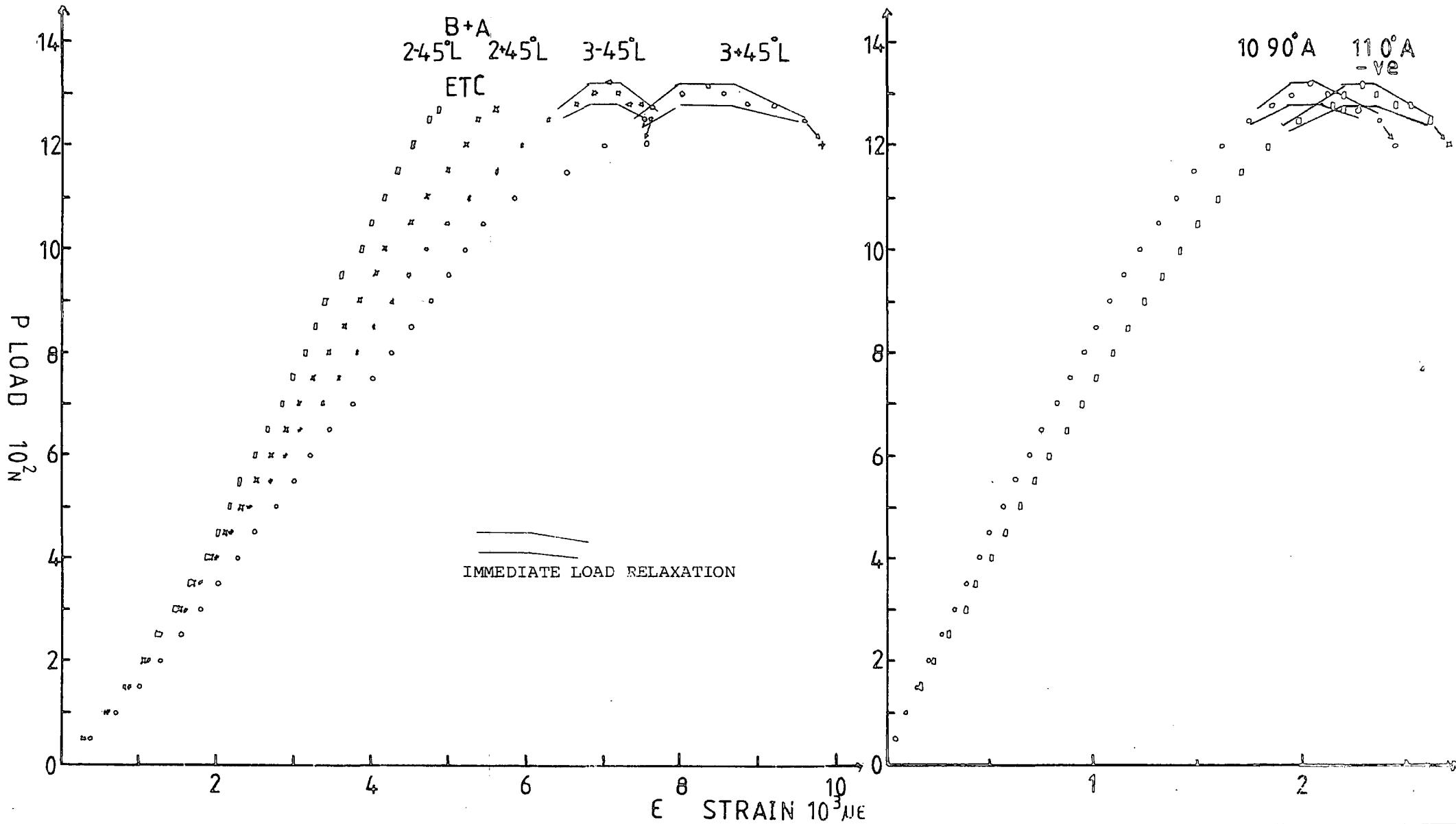


Figure 4.36 EXPERIMENT 5. STRAIN MEASUREMENTS



EXPERIMENT 6. NOTES AND OBSERVATIONS

Date of test : March 82

Plate dimensions

Same as Experiment 5

$A_s = 0.15m$

$B_s = 0.12m$

$A_p = 0.01m$

$B_p = 0.01m$ (rubber pad not inserted)

Lay-up $(+45^{\circ}, 0^{\circ}, -45^{\circ}, 90^{\circ}, 90^{\circ}, -45^{\circ}, 0^{\circ}, +45^{\circ})_s$

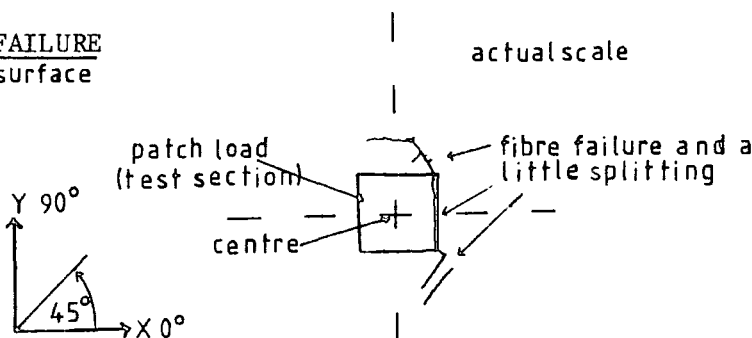
Ball bearings 0.3175E-01m

The plate was that used in the unsuccessful Exp. 5. Changes were made to the supporting distances A_s and B_s and the patch load dimensions A_p and B_p , so that the dominant preferential bending found in Exp.5 did not occur. The other important difference was that the load was imposed without the rubber pad.

There was no check to find out if Exp.5 had caused permanent damage. Central transverse displacement was increased at 0.5E-03m/min in increments of 100N.

LOAD N	REMARKS
800	Small jump in load
1900	Loud crack probably as the result of adhesive failure in the tabs
2500	The bending behaviour was now preferential about the Y-centreline. Much louder crack, fibre failure occurred around patch load in the compressive outer layers. The central strain gauge readings reduced dramatically as load fell to 2375N. This happened about 0.5 minute after the load had reached 2500N. There was no sign of any further damage at the edges than that introduced by Exp.5.

FIBRE FAILURE
Compressive surface



EXPERIMENT 6. NOTES AND OBSERVATIONS (contd.)

The strains and displacements plotted correspond to those presented from Exp. 5.

Strain gauge measurements not plotted

The values below were recorded at 2400N.

trend	$\mu\epsilon$	trend	$\mu\epsilon$
4 0°L B+A (also 0 0°B)	10905	6 90°B (maximum 1400 at 900N)	101
5+45°B { similar to }	9560	9+45°B similar to gauge 5	6346
5-45°B { gauges 2+3 }	8000	9-45°B	5086
6 0° B (also 0 0°B)	11540		

The gauge 12 90° which was used in Exp. 5 to measure edge strains could not be used since this experiment had caused adhesive failure.

Figure 4.37 EXPERIMENT 6. STRAIN GAUGE ARRANGEMENT

16 LAYERS (+45,0,90,90,-45,0,+45)s

SCALE 1:4

STRAIN GAUGES + CROSS-PLY TYPE FCA3-11 3MM
- SINGLE-PLY TYPE FLA3-11 3MM

VIEW : FROM ABOVE

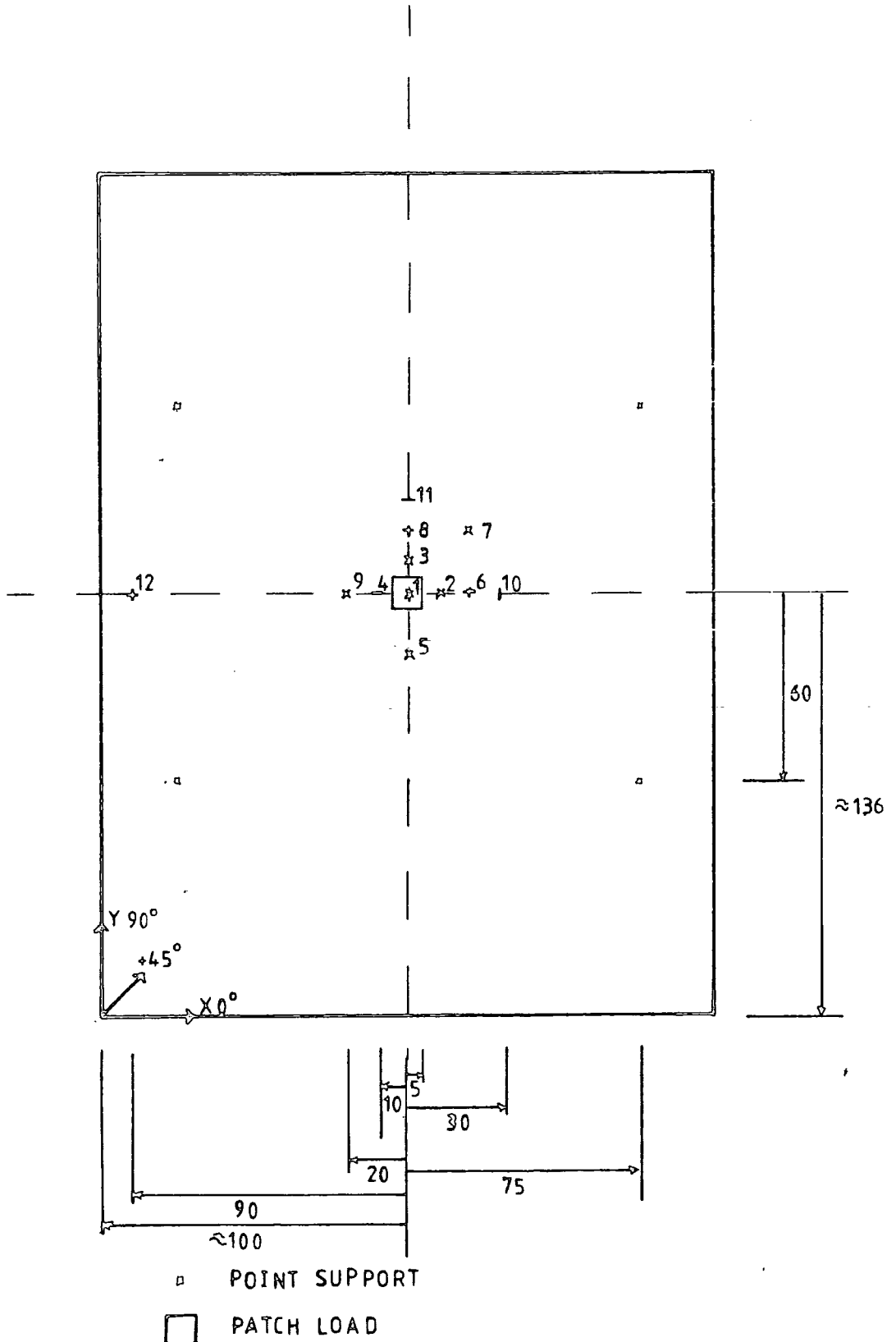


Figure 4.38 EXPERIMENT 6. CENTRAL TRANSVERSE DISPLACEMENT TO FIRST FIBRE FAILURE

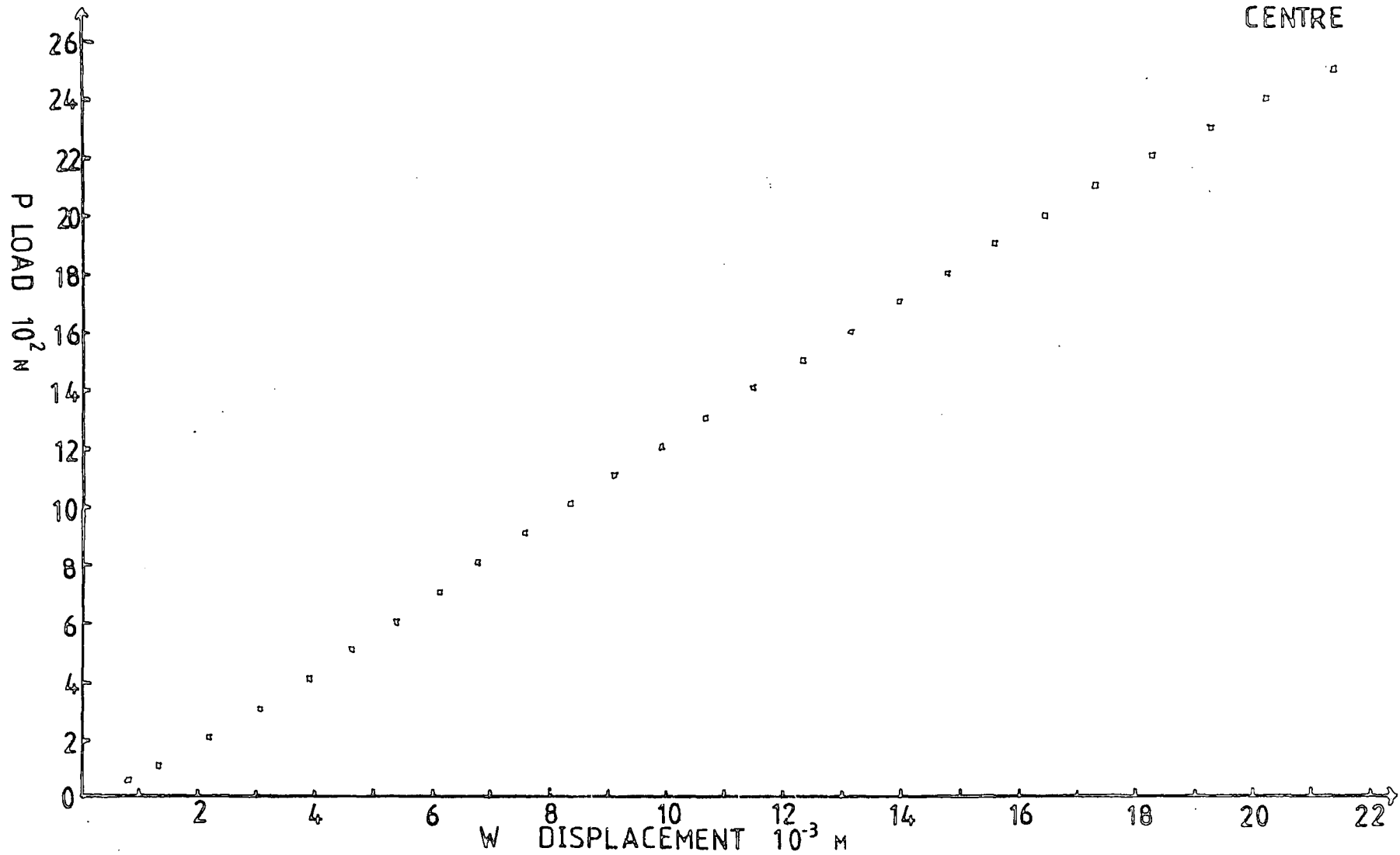


Figure 4.39 EXPERIMENT 6. STRAIN MEASUREMENTS TO FIRST FIBRE FAILURE

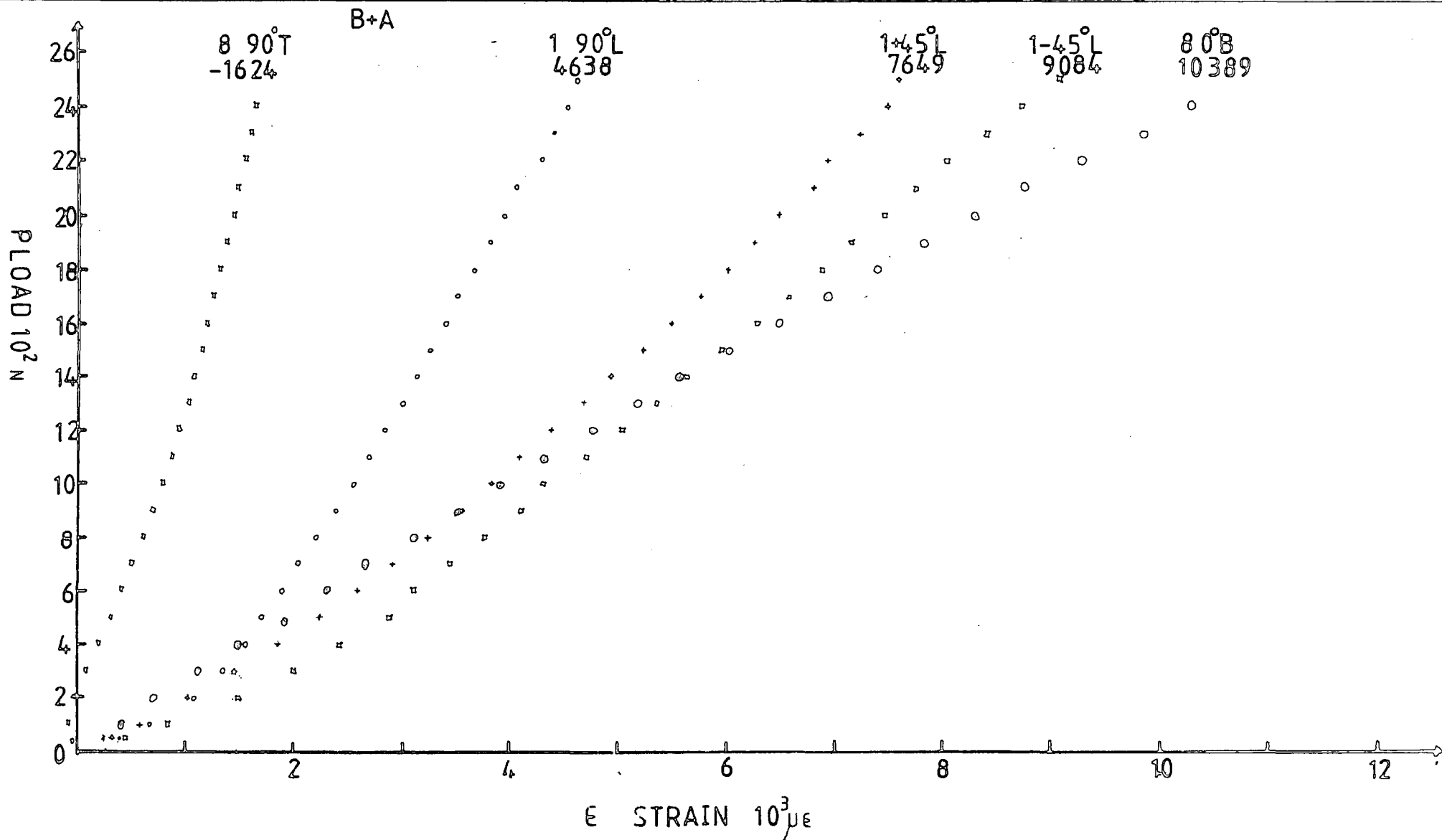
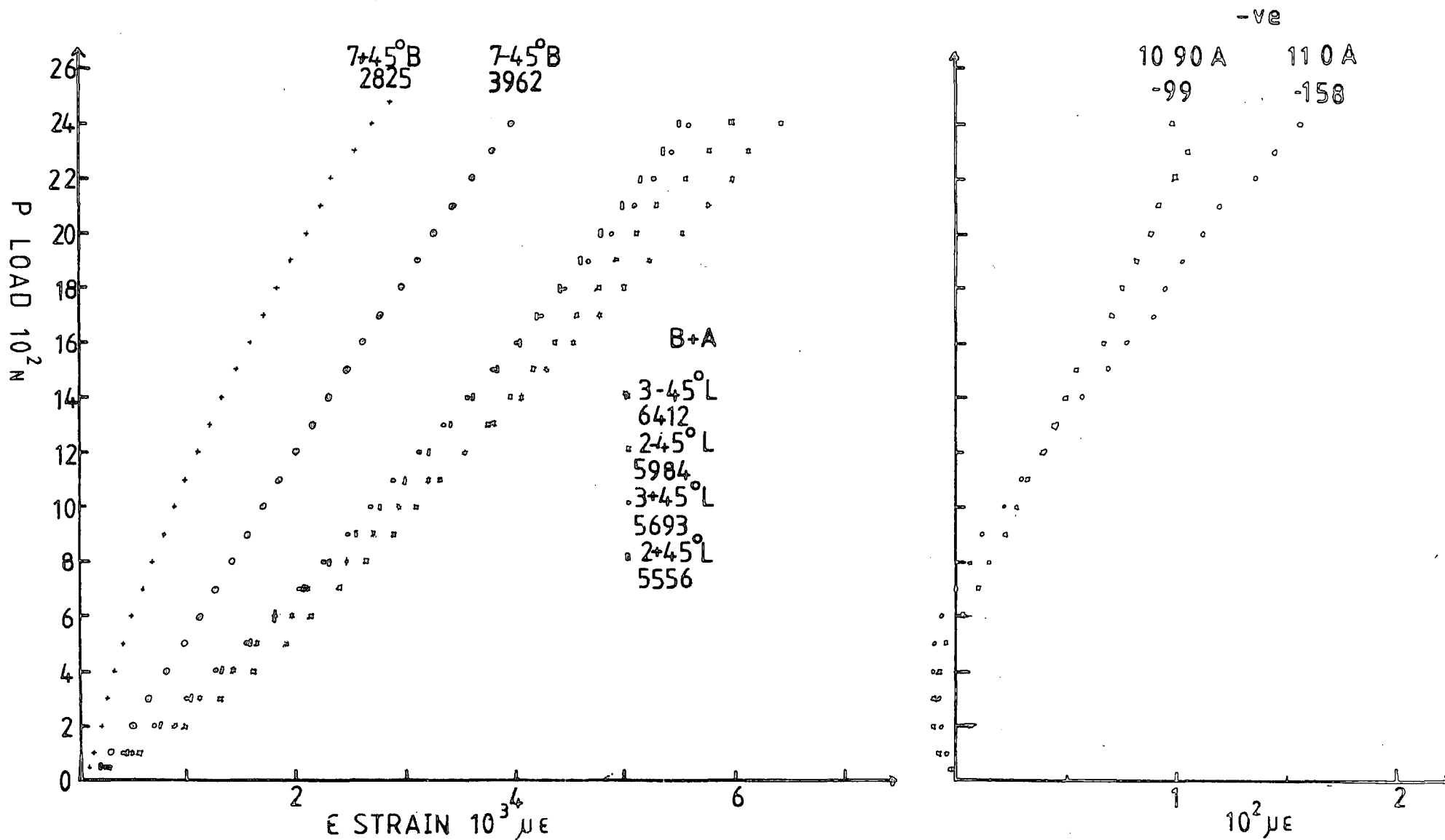


Figure 4.40 EXPERIMENT 6. STRAIN MEASUREMENTS TO FIRST FIBRE FAILURE



EXPERIMENT 7. NOTES AND OBSERVATIONS

Date of test : March 82

Plate dimensions

A = 0.204m

B = 0.272m

h = 0.191E-02m

A_S = 0.15m

B_S = 0.12m

A_P = 0.01m

B_P = 0.01m (rubber pad 0.178E-02m)

Lay-up (+45°₁, 0°₁, -45°₂, 90°₂, 90°₃, -45°₃, 0°₄, +45°₄)_S

Ball bearings 0.3175E-01m

Central transverse displacement was increased at 0.5m/min in increments of 200N.

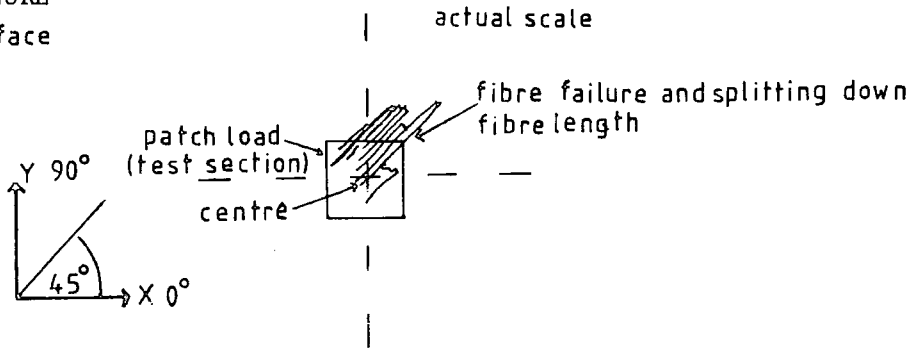
LOAD N	REMARKS
300	Small load relaxation (10N)
600	Jerky load increase was recorded on Instron chart recorder.
700	Preferential bending about X centreline Load relaxation (10N)
1400	No visible sign of edge delamination
1600	Load relaxation (20N). There was a crack which indicated adhesive failure in the strain gauge tabs. A definite increase in strain was measured by gauge 1-45° ₁ B+A during the time to take the set of readings.
1700	Load relaxation (10N)
1800	Further indication of adhesive failure
2100	Load increase was more jerky than usual.
2200	There was a dramatic increase in the central displacement needed for next increment of load. Load relaxation (30N)
2300	There were signs of the some shift in the positions of support.
2600	Tensile first fibre failure occurred at the centre after a period of 1 to 1.5 minutes of constant central displacement. There was an immediate reduction in load to 2420N.

EXPERIMENT 7. NOTES AND OBSERVATIONS (contd.)

Just before the onset of failure the deformed shape was :



FIBRE FAILURE
Tensile surface



The laminate did not possess any edge damage as a result of the test.

Strain gauge measurements not plotted

The values below were recorded at 2500N.

trends	$\mu\epsilon$		$\mu\epsilon$
3+45° B { very similar to }	6243	5+45° B { trends the }	6387
3-45° B { gauges 2±45° B }	5718	7+45° B { same as gauges }	6072
5 90°L B+A (max 1044 $\mu\epsilon$ at 600N)	463	7-45° B { 2±45° B }	6443

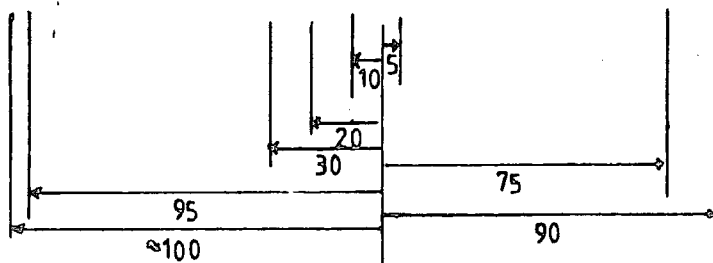
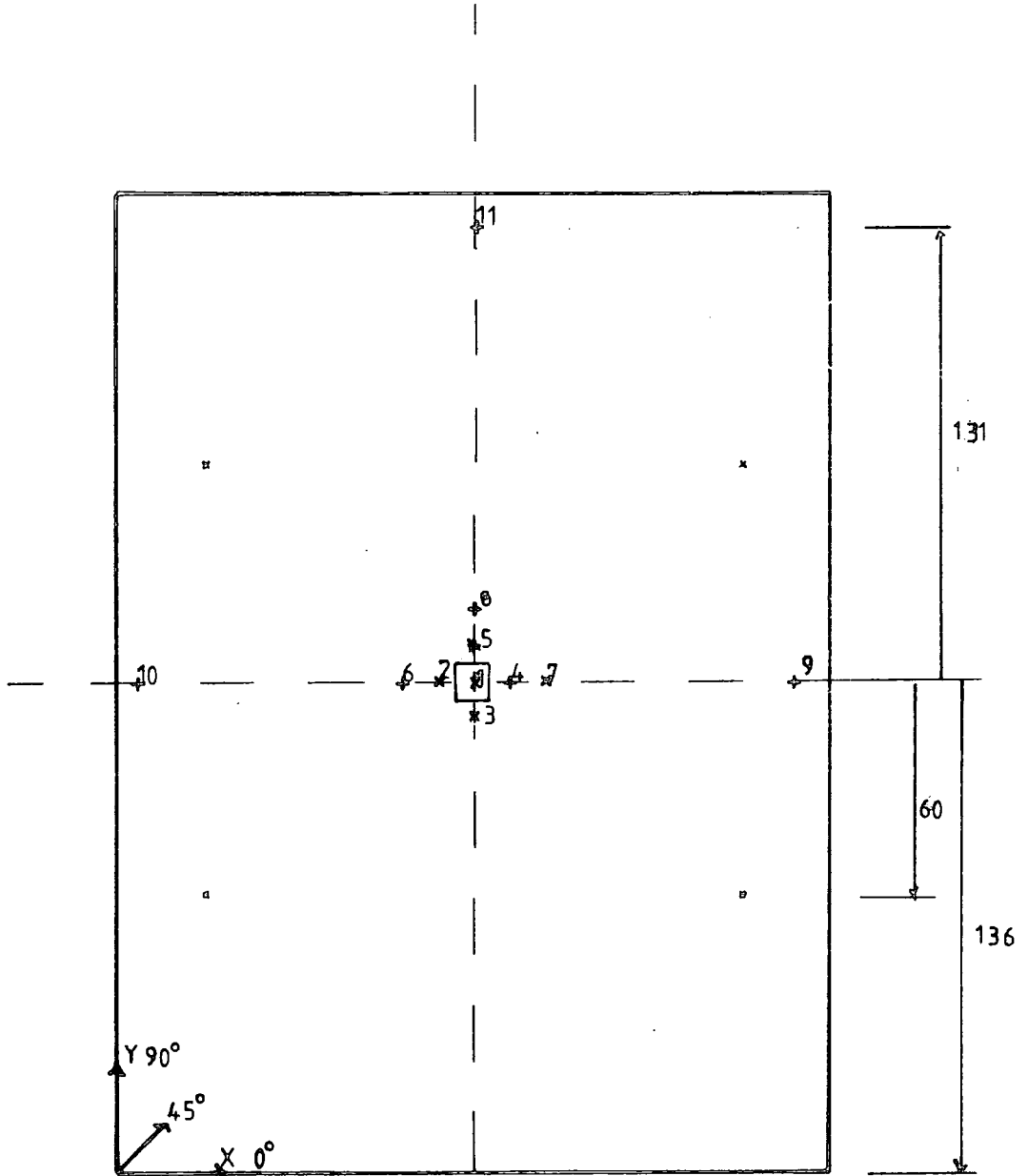
Figure 4.41 EXPERIMENT 7. STRAIN GAUGE ARRANGEMENT

16 LAYERS (+45,0,-45,90,90,-45,0,+45)_s

SCALE 1:4

STRAIN GAUGES + CROSS-PLY TYPE FCA3-11 3MM
- SINGLE-PLY TYPE FLA3-11 3MM

VIEW : FROM BELOW



○ POINT SUPPORT
□ PATCH LOAD

Figure 4.42 EXPERIMENT 7. CENTRAL TRANSVERSE DISPLACEMENT TO FIRST FIBRE FAILURE

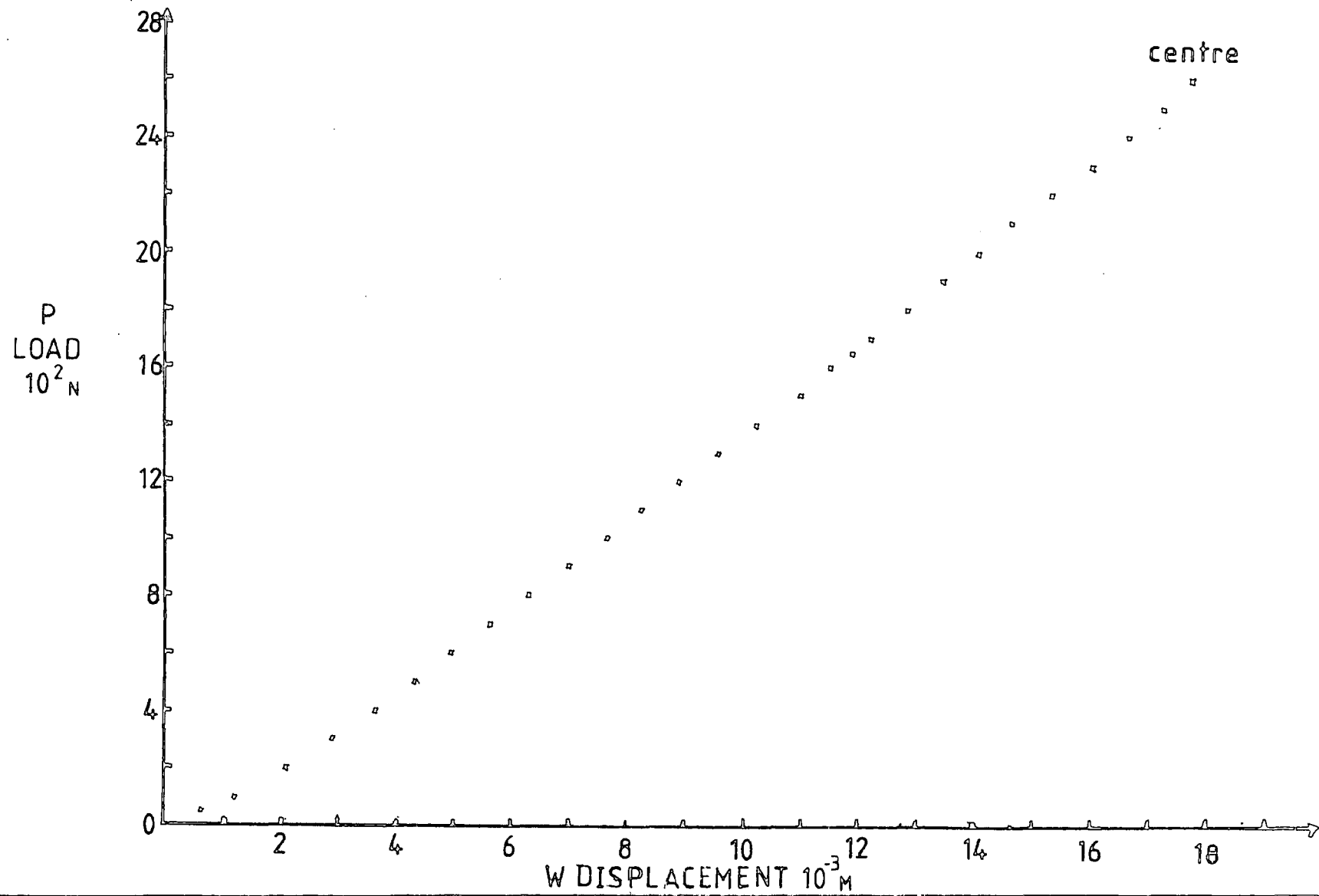


Figure 4.43 EXPERIMENT 7. STRAIN MEASUREMENTS TO FIRST FIBRE FAILURE

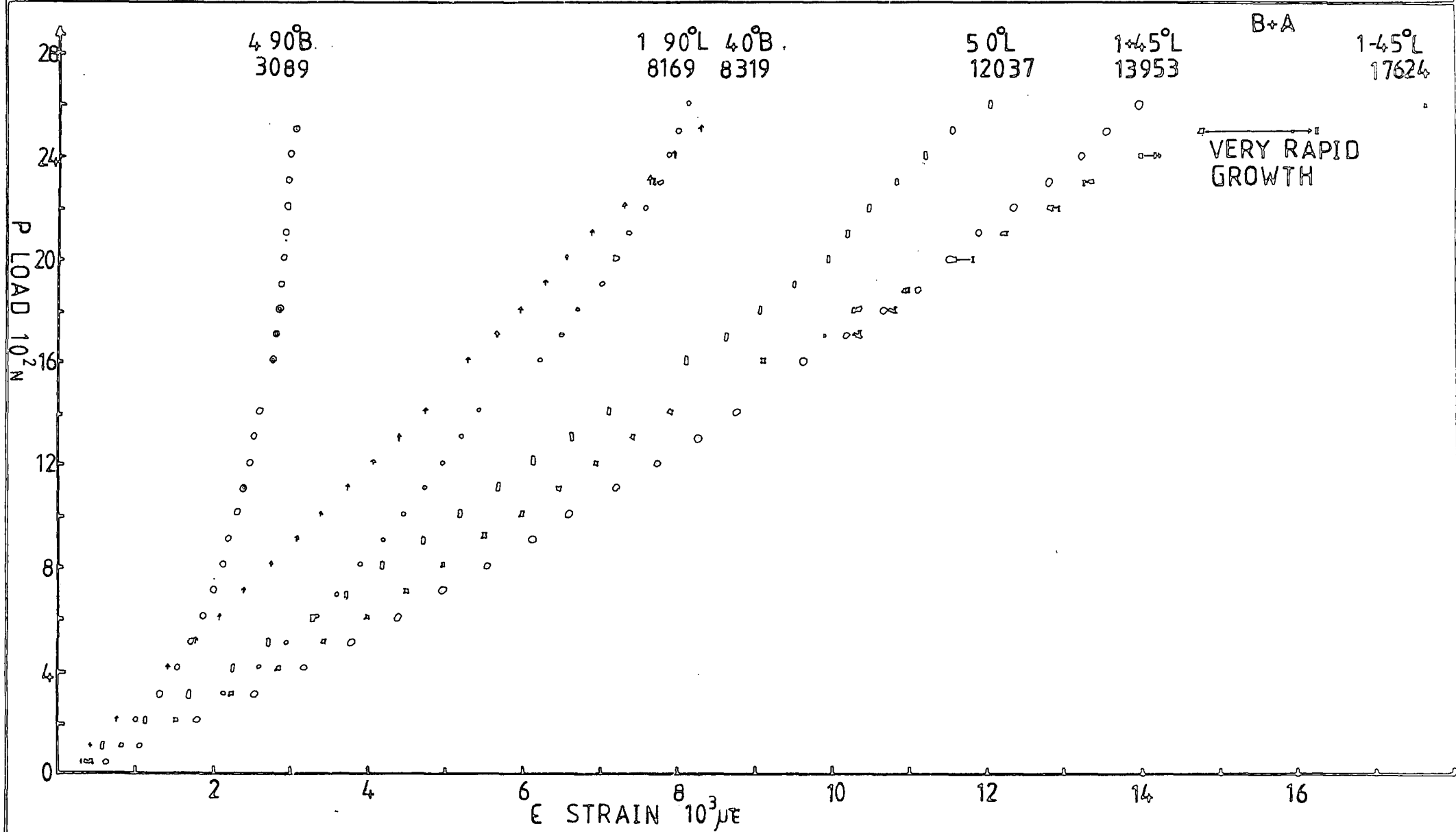


Figure 4.44 EXPERIMENT 7. STRAIN MEASUREMENTS TO FIRST FIBRE FAILURE

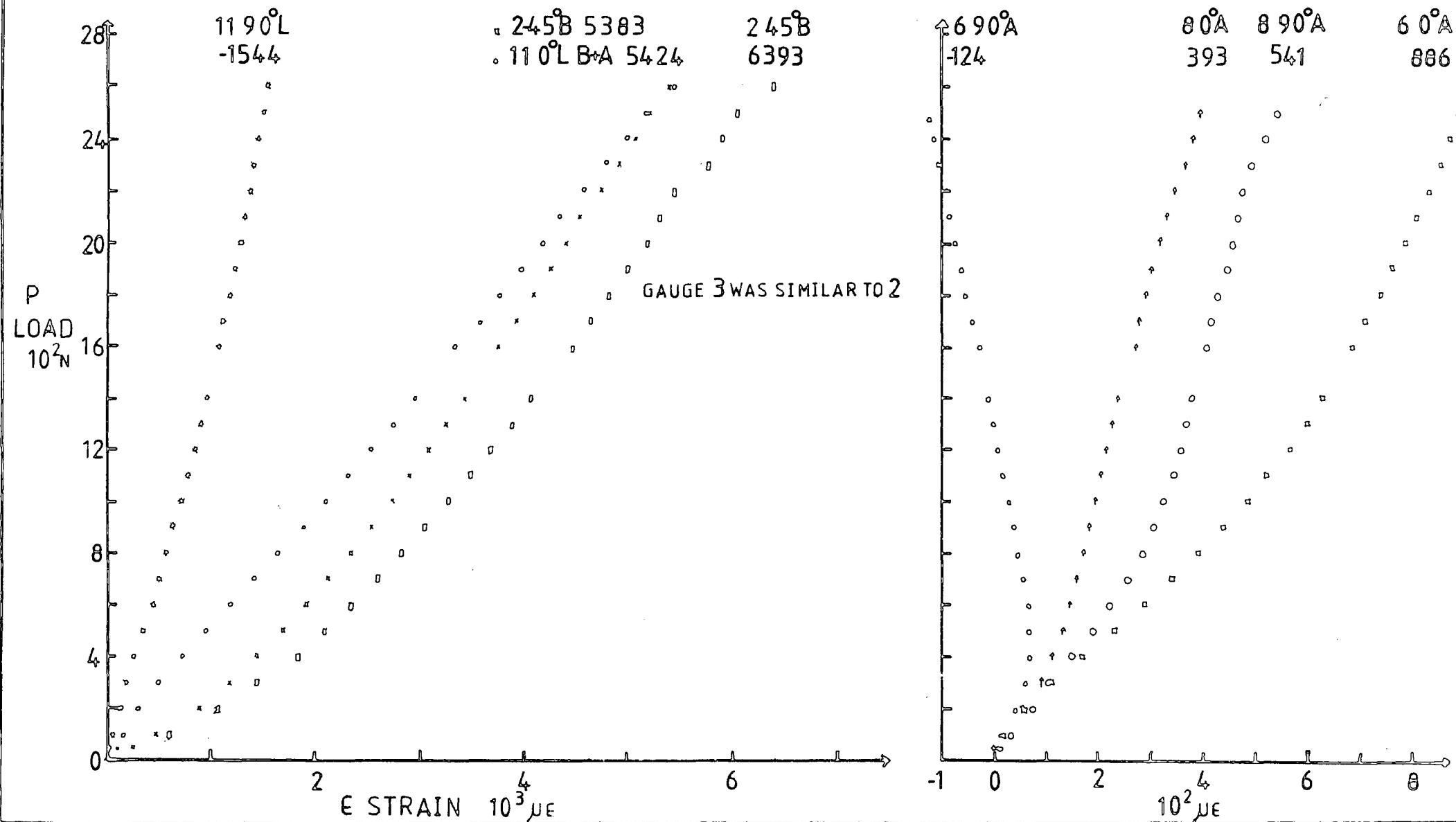
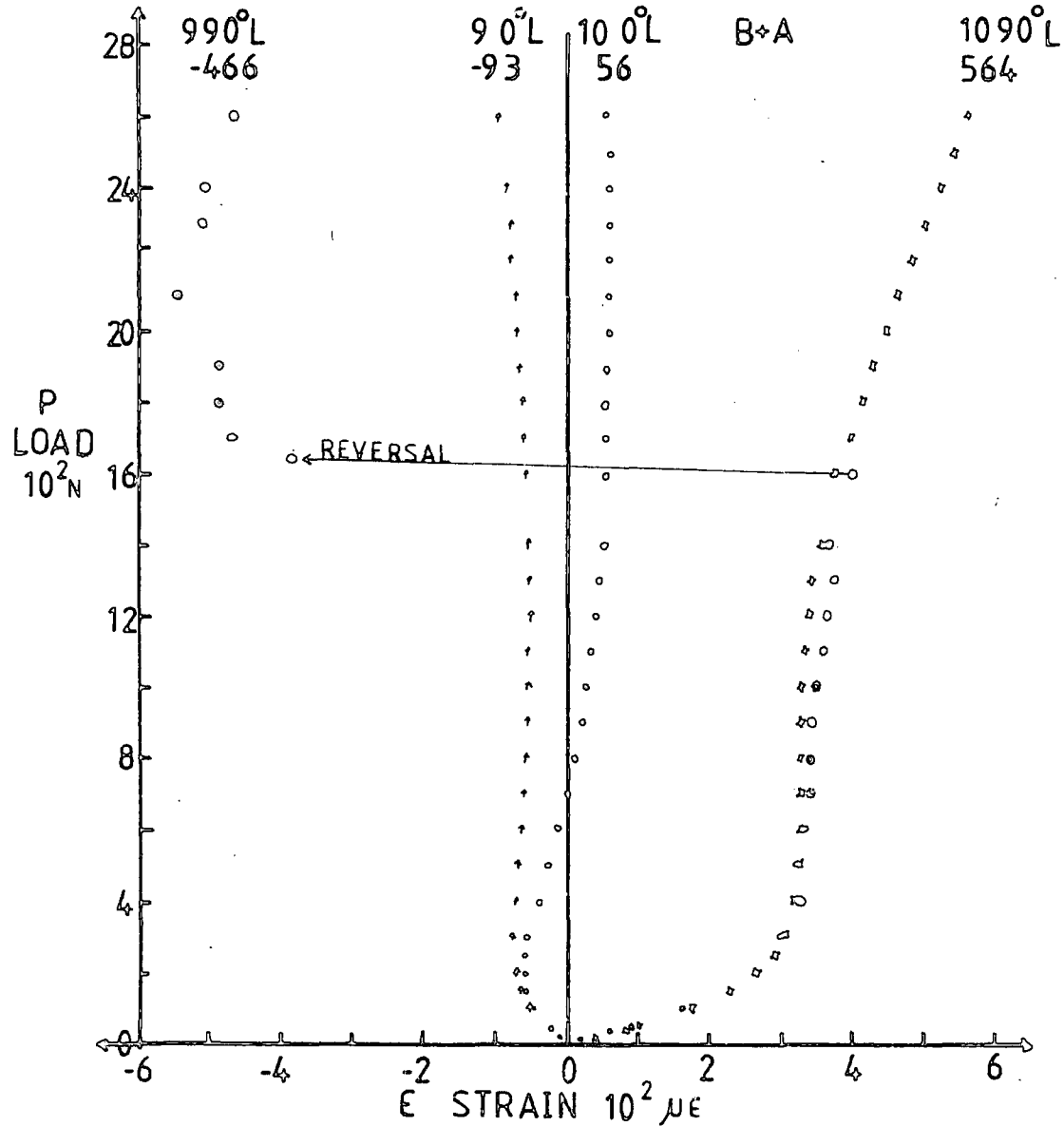


Figure 4.45 EXPERIMENT 7. STRAIN MEASUREMENTS TO FIRST FIBRE FAILURE



EXPERIMENT 8. NOTES AND OBSERVATIONS

Date of test : May 82

Plate dimensions

A = 0.204m

B = 0.202m

h = 0.2032E-02m

A_S = 0.13m

B_S = 0.13m

A_P = 0.01m

B_P = 0.01m (rubber pad 0.178E-02m)

Lay-up (0°90°0°90°0°90°0°90°)_S

Ball bearings 0.3175E-01m

Central transverse displacement was increased at 0.5m/min in increments of 100N.

LOAD N	REMARKS
400	Load relaxation (5N) , it was noted that there was preferential bending about the X-centreline.
800	Load relaxation (10N)
1500	Adhesive failure
1600	Load relaxation (10N). The preferential bending about the X-centreline was becoming more dominant.
2140	As the central transverse displacement was being increased a very loud snap associated with first fibre failure was heard, and the plate was unloaded. There was a small reduction in load to 2060N.

Inspecting the surfaces around the highly strained centre region no visible damage was found. It has been suggested that first fibre failure occurred in the second tensile layer .

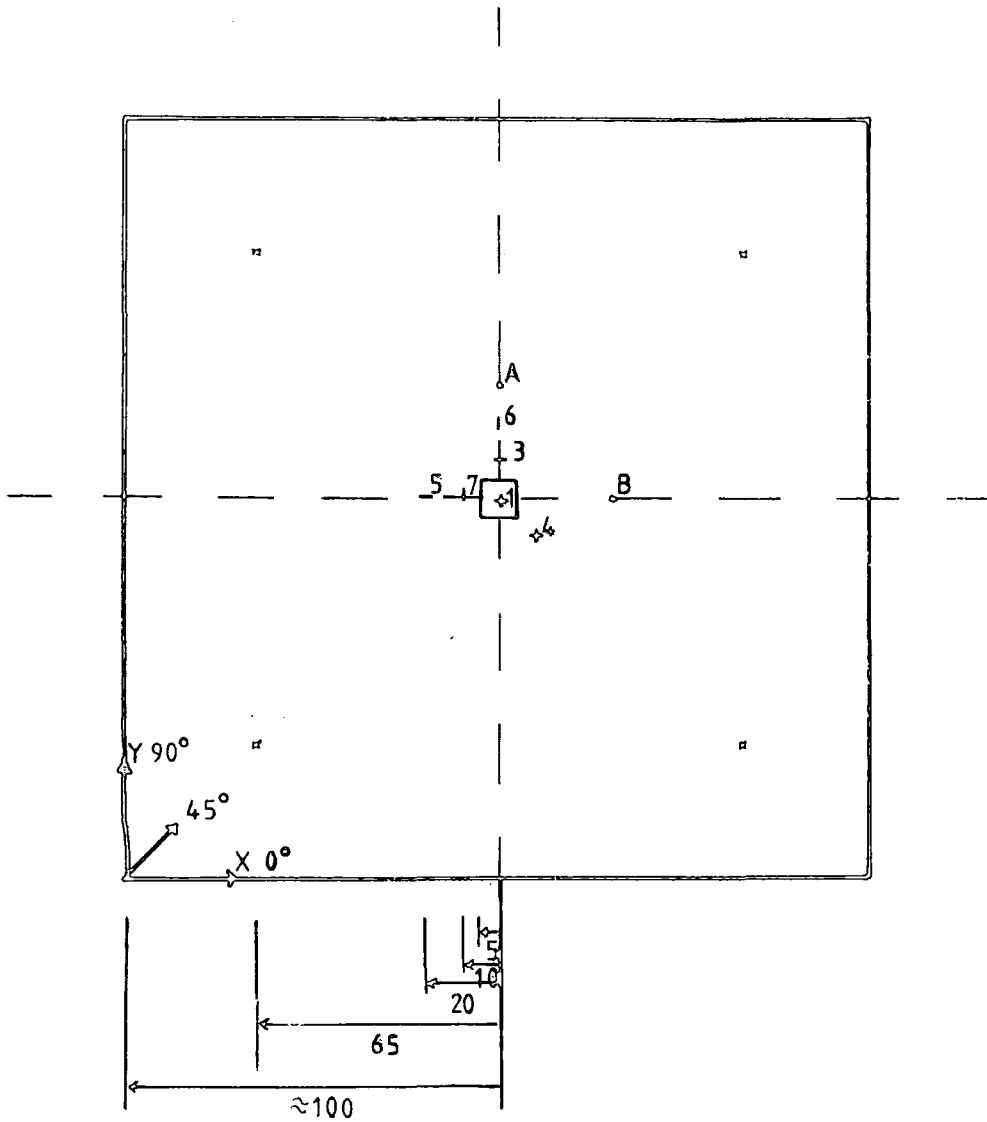
Figure 4.46 EXPERIMENT 8. STRAIN GAUGE ARRANGEMENT

16 LAYERS ($0^{\circ}, 90^{\circ}, 0^{\circ}, 90^{\circ}, 0^{\circ}, 90^{\circ}, 0^{\circ}, 90^{\circ}, 0^{\circ}, 90^{\circ}$) S

SCALE 1:4

STRAIN GAUGES	◇	CROSS-PLY	TYPE	FCA3-11	3MM
	-	SINGLE-PLY	TYPE	FLA3-11	3MM

VIEW : FROM BELOW



■ POINT SUPPORT

□ PATCH LOAD

Figure 4.47 EXPERIMENT 8. TRANSVERSE DISPLACEMENTS TO FIRST FIBRE FAILURE

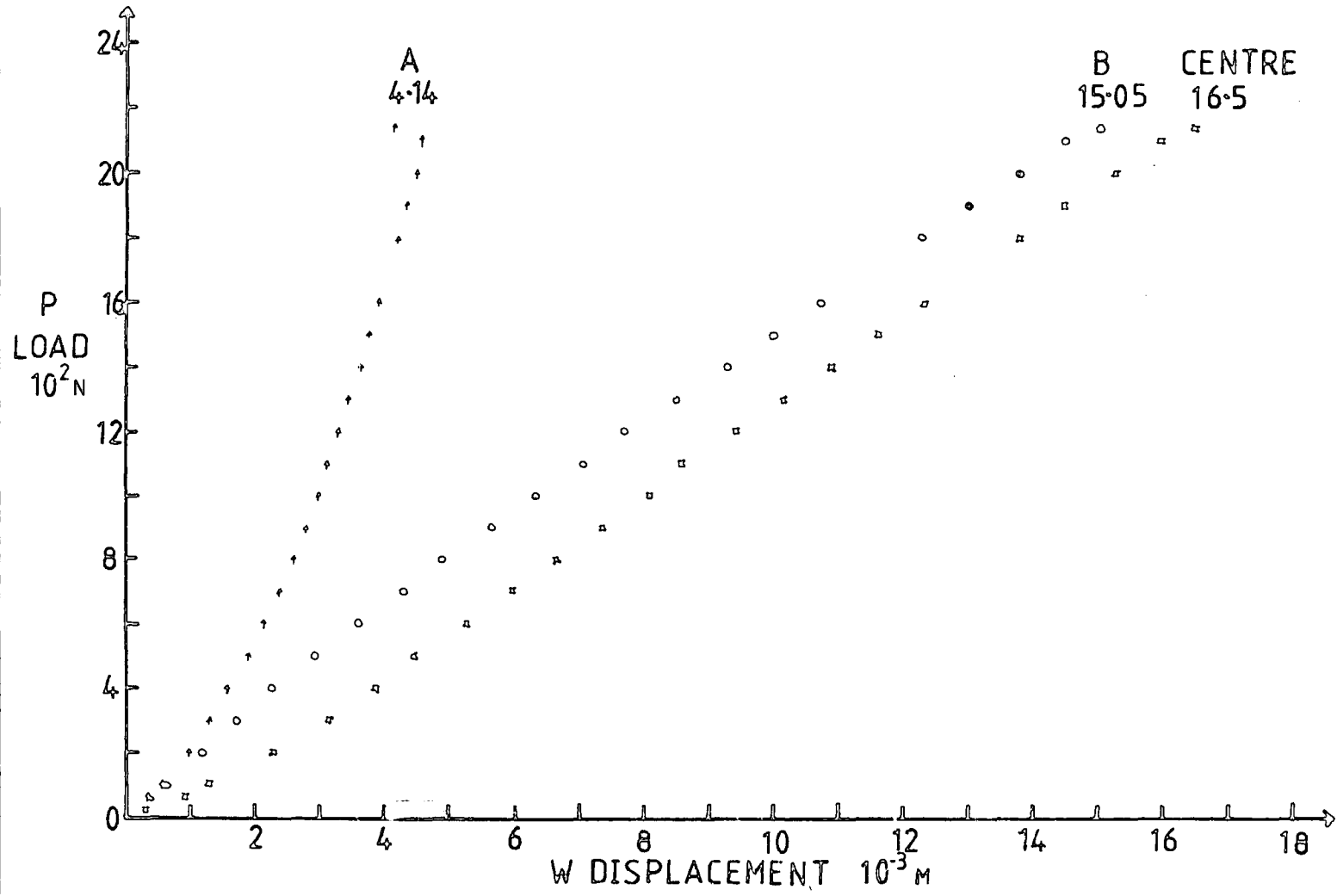


Figure 4.48 EXPERIMENT 8. STRAIN MEASUREMENTS TO FIRST FIBRE FAILURE

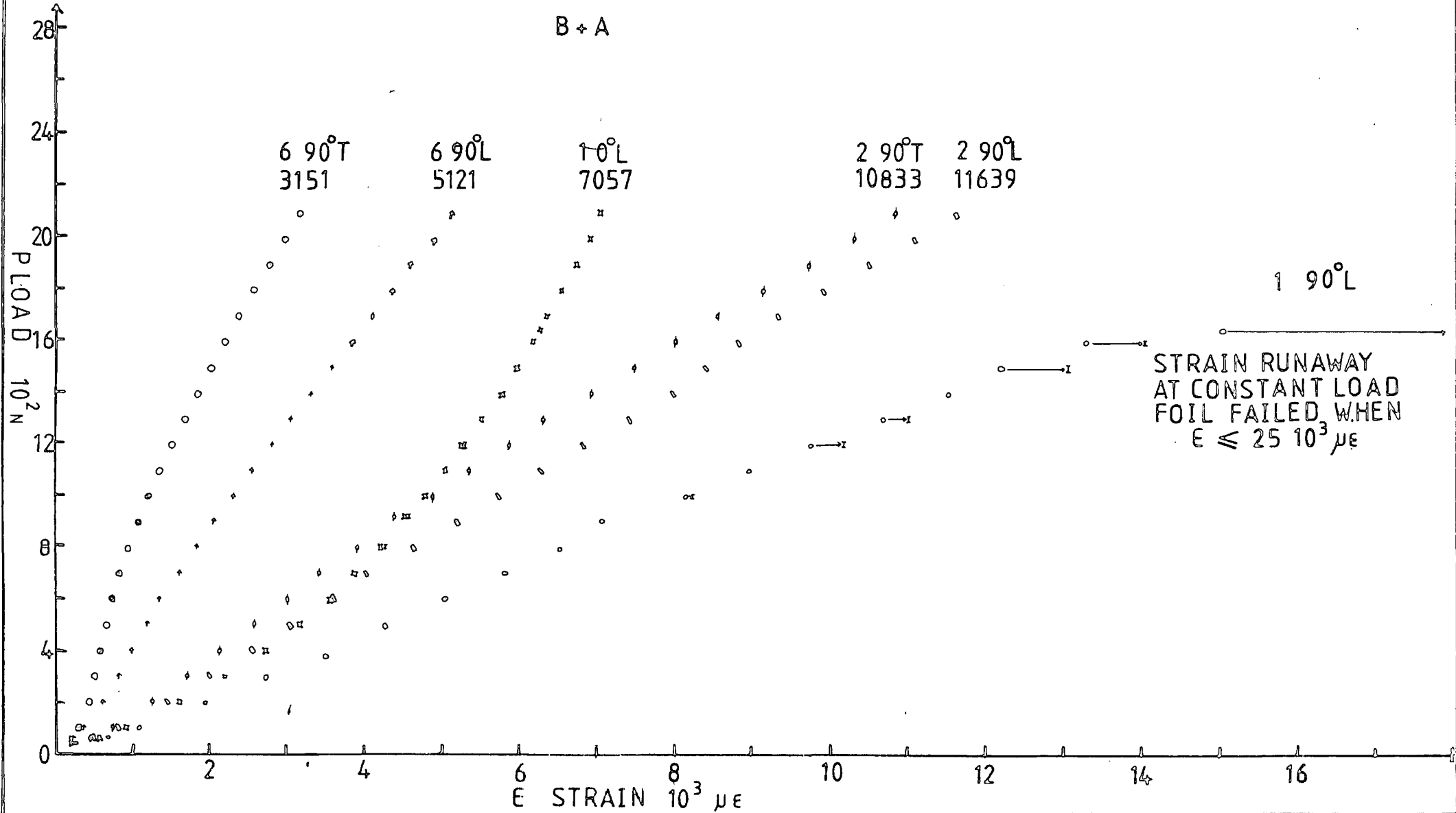
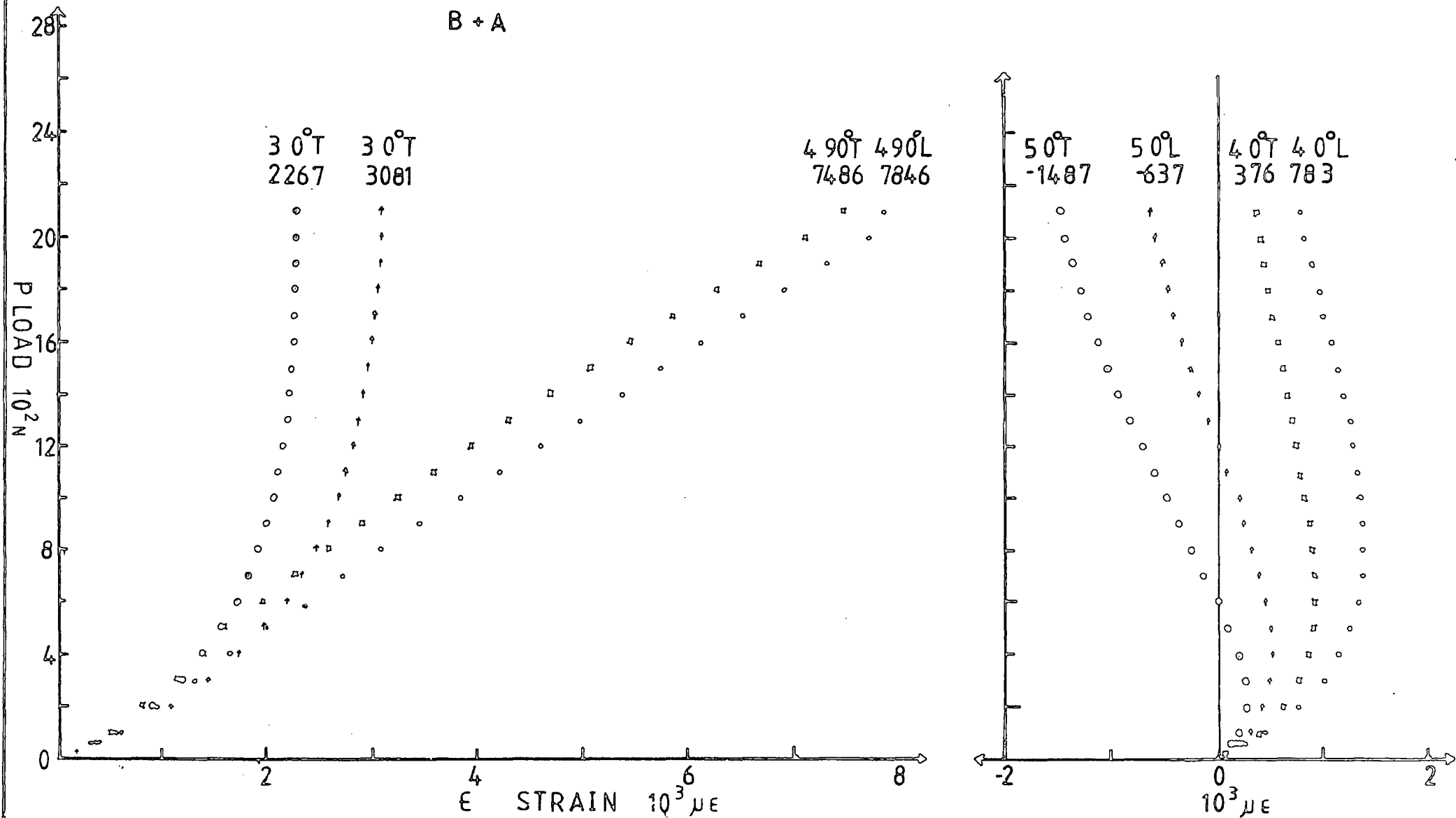


Figure 4.49 EXPERIMENT 8. STRAIN MEASUREMENTS TO FIRST FIBRE FAILURE



EXPERIMENT 9. NOTES AND OBSERVATIONS

Date of test : May 82

Plate dimensions

A = 0.202m B = 0.200m

h = 0.2032E-02m

A_S = 0.13m B_S = 0.13m

A_P = 0.01m B_P = 0.01m

Lay-up (+45°, 0°, +45°, 0°, -45°, 0°, -45°, 0°)_S

Ball bearings 0.3175E-01m

Central transverse displacement was increased at 0.5m/min in increments of 100N.

LOAD N	REMARKS
up to 400	At each increment of load there was a small amount of load relaxation (5N).
500	Large amount of load relaxation (45N) as the plate started to rotate in supports. This is illustrated in the diagram below and was the result of the large twisting stiffnesses.

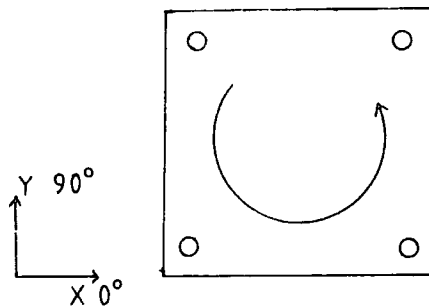


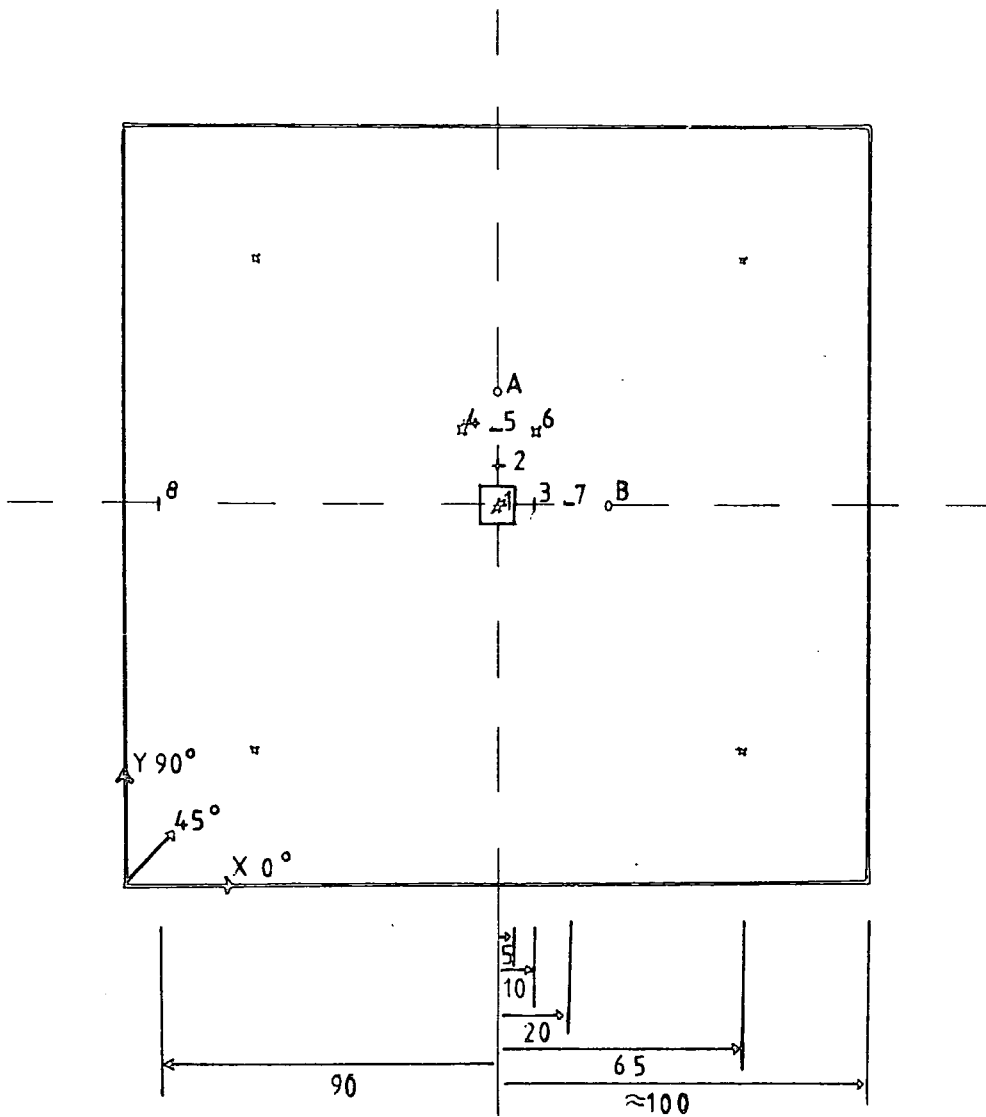
Figure 4.50 EXPERIMENT 9. STRAIN AND DIAL GAUGE ARRANGEMENT

16 LAYER $(0^{\circ}, +45^{\circ}, 0^{\circ}, +45^{\circ}, 0^{\circ}, -45^{\circ}, 0^{\circ}, -45^{\circ}, 0^{\circ})_s$

SCALE 1:4

strain gauges + CROSS-PLY TYPE FCA3-11 3MM
 - SINGLE-PLY TYPE FLA3-11 3MM

VIEW : FROM ABOVE



π POINT SUPPORT

□ PATCH LOAD

Figure 4.51: EXPERIMENT 9. TRANSVERSE DISPLACEMENTS

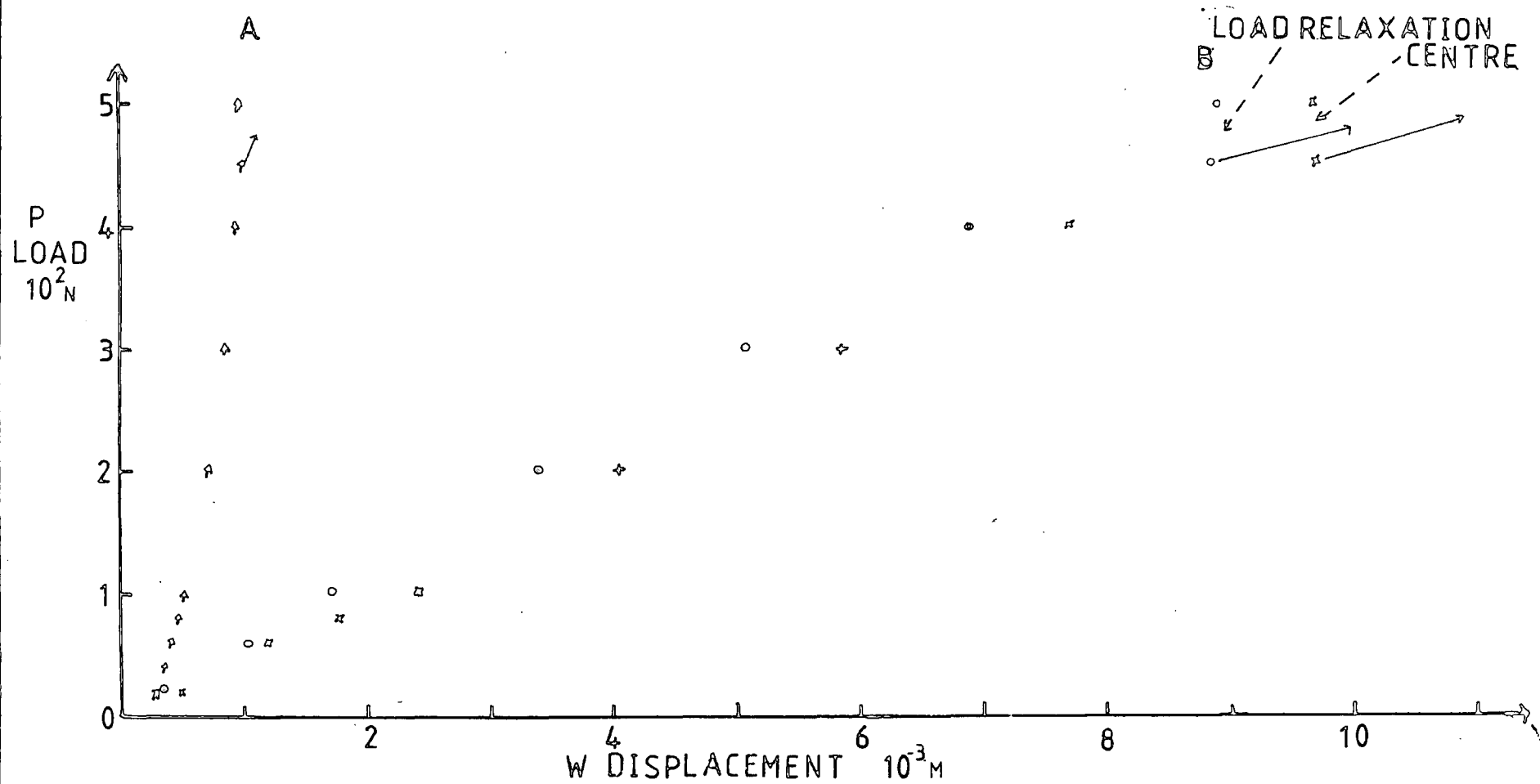


Figure 5.53 EXPERIMENT 9. STRAIN MEASUREMENTS

B+A

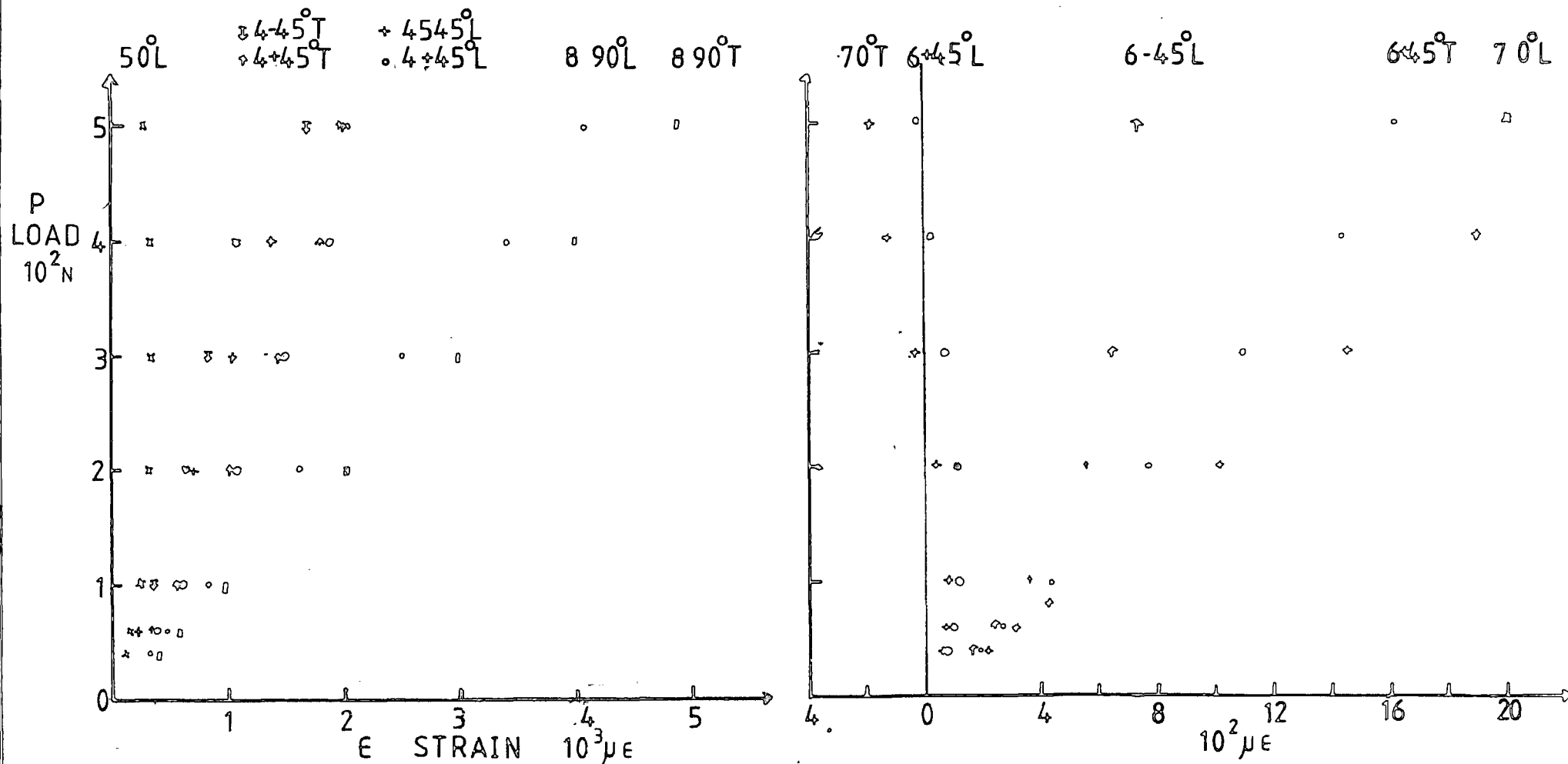


Table 4.10 Preferential bending

Exp. (Figs.)	Measured response by strain gauges during test to failure			Central transverse displ.	Centreline of preferential bending
	0° X	90° Y	±45°		
1 (4.11-4.12)	considerable stiffening	nearly linear	approx. linear after initial stiffening	linear	X
2 (4.13-4.26)	"	"	"	"	
3 and 4 (4.27-4.32)	little stiffening	little stiffening	stiffens	slight stiffening	Small amount Y
5 (4.33-4.36)	The responses noted only applied until the specimen just slipped through the supports -----			linear	Very large X
6 (4.37-4.40)	linear-weakens at high load	stiffens	nearly linear	linear	Small amount Y
7 (4.41-4.45)	nearly linear	stiffens	nearly linear	nearly linear-weakens at high loads	Small amount Y
8 (4.46-4.49)	slight stiffening	linear-weakens at high loads	-----	linear	X
9 (4.50-4.53)	The responses noted only applied until the specimen started to rotate about the supports			linear	Large amount X
	large stiffening	nearly linear	varied		

Table 4.11 Relevant information from those specimens which had first fibre failure in the test section

Exp.	Lay-up	Figure showing visible damage	Final load N	Final load after fibre failure N	Transverse central displ. $E-03$	Surface strains at the centre	Orien. of failed lamina
					μ	μE	
1	$(90^\circ, 0^\circ, 90^\circ, +45^\circ, 0^\circ, -45^\circ, 0^\circ, 0^\circ, -45^\circ, 0^\circ, +45^\circ, 0^\circ, 0^\circ, +45^\circ, 0^\circ, -45^\circ, 0^\circ)_S$	4.14	8200	-----	-----	15534 / 7844	outer tensile 90°
2		4.26	7960	1250	22	14426 6061	outer tensile 90°
4	$(+45^\circ, 90^\circ, -45^\circ, 0^\circ, 0^\circ, -45^\circ, 90^\circ, +45^\circ)_S$	4.32	13750	9000	16.9	11196 11573	outer tensile $+45^\circ$
6	$(+45^\circ, 0^\circ, -45^\circ, 90^\circ, 90^\circ, -45^\circ, 0^\circ, +45^\circ)_S$	Notes and Observations	2500	2375	22	7619 9084	compressive outer layer
7		Notes and Observations	2600	2420	17.5	13953 17624	outer tensile $+45^\circ$
8	$(0^\circ, 90^\circ, 0^\circ, 90^\circ, 0^\circ, 90^\circ, 0^\circ, 90^\circ)_S$	No visible fibre failure	2140	2060	16.5	7075 >25000	2 rd tensile 90°

Figure 4.54 BENDING DEFORMATION IN PLATE BENDING METHOD

Figure 4.54.1 SHORTENING OF SPAN DUE TO PREFERENTIAL BENDING

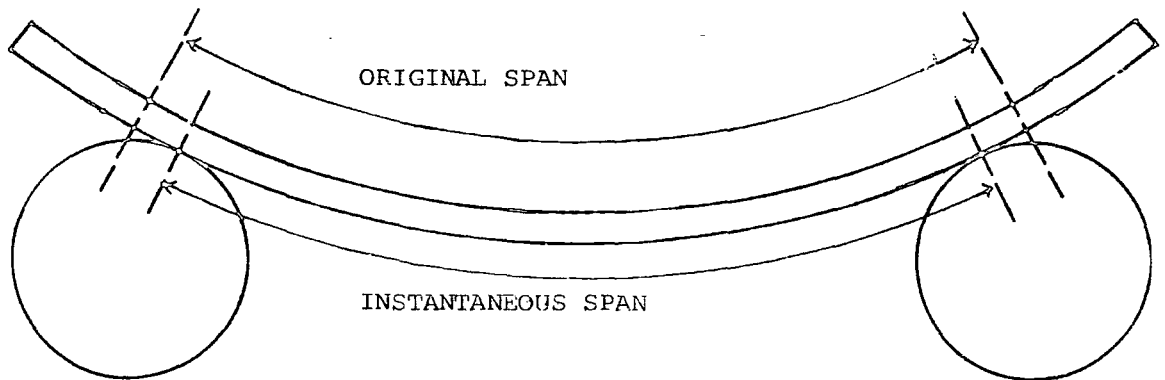
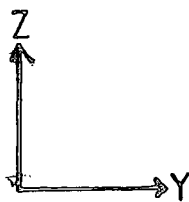


Figure 4.54.2 PROPOSED MATRIX FAILURE OF THE OUTER LAMINA AROUND THE CENTRE IN EXPERIMENT 8



CURVATURE HAS BEEN EXAGGERATED FOR CLARITY

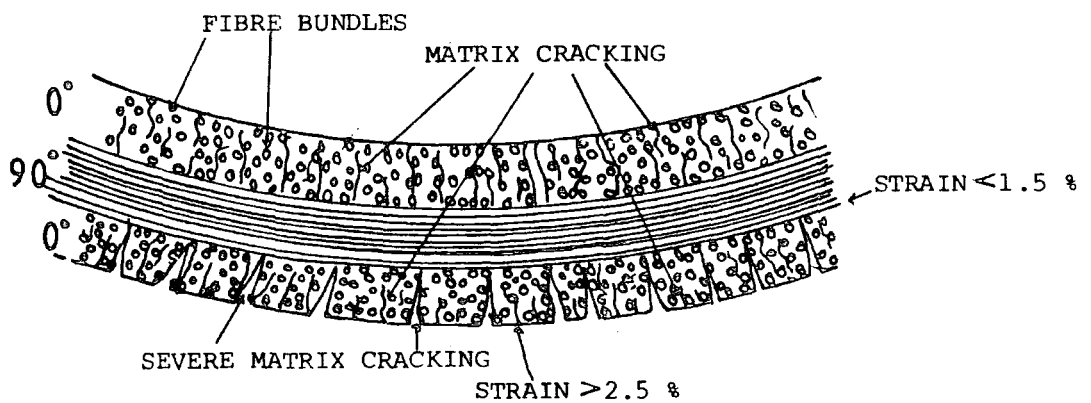


Table 5.1 Mesh constructions to analyses the experiments

Subscripts Q = Quarter plate model H = Half plate F = Full plate
 G = Graded mesh
 S = Square plate R = Rectangular
 E = Experiment

Mesh label . The first number refers to the order in which the meshes were employed in modelling the experiments. The last number gives the number of elements in the mesh.

Mesh label	Plate dimensions		Exps.	No. of eles. (along each side)		Size of elements along sides
	A	m B				
1SQGE36	.26	.26	1-4	36	(6)	0.03 *1, 0.025 *2, 0.02 *2, 0.01 * 1
1SQGE49	.26	.26	1-4	49	(7)	0.03 *2, 0.015 *4, 0.01 *1
1SQGE81	.26	.26	1-4	81	(9)	0.03 *1, 0.02 *1, 0.015 *2, 0.01 *5
1SQGE100	.26	.26	1-4	100	(10)	0.015 *6, 0.01 *4
1SHGE50	.26	.26	1-4	50	(5) (10)	0.03 *4, 0.01 *1 0.03 *4, 0.01 *2, 0.03 *4
1SHGE72	.26	.26	1-4	72	(6) (12)	0.03 *3, 0.02 *1, 0.01 *2 0.03 *3, 0.02 *1, 0.01 *4, 0.02 *1, 0.03 *3
1SFGE144	.26	.26	1-4	144	(12)	0.03 *1, 0.025 *2, 0.02 *2, 0.01 *2, 0.02 *2, 0.025 *2, 0.03 *1
2RQGE100	.205	.275	5-7	100	(10) (10)	0.014 *2, 0.015 *1, 0.01 *3, 0.005 *2 0.01875 *2, 0.02 *2, 0.015 *2, 0.01 *2, 0.005 *2
2RHGE126	.205	.275	5-7	126	(9) (14)	0.035 *1, 0.02 *2, 0.015 *2, 0.01 *2 0.005 *2 0.0275 *1, 0.02 *1, 0.025 *1, 0.01 *2, 0.005 *4, 0.01 *2, 0.025 *1, 0.02 *1,
2RFGE144	.205	.275	5	144	(12) (12)	0.0275 *1, 0.018 *3, 0.01 *4, 0.018 *3, 0.0275 *1 0.0375 *1, 0.027 *3, 0.01 *4, 0.027 *3, 0.0375 *1
3RFGE144	.205	.275	6+7	144	(12) (12)	0.0275 *1, 0.0217 *3, 0.005 *4, 0.0217 *3, 0.0275 *1 0.0525 *1, 0.025 *3, 0.005 *4, 0.025 *3, 0.0525 *1
4SQGE100	.205	.205	8+9	100	(10)	0.0175 *2, 0.015 *1, 0.01 *3, 0.005 *4
4SHGE72	.205	.205	8+9	72	(6) (12)	0.035 *1, 0.0183 *3, 0.005 *2 0.035 *1, 0.0183 *3, 0.005 *4, 0.0183 *3, 0.035 *1
4SFGE144	.205	.205	8+9	144	(12)	0.035 *1, 0.0183 *3, 0.005 *4, 0.0183 *3, 0.035 *1

Table 5.2 Linear deformation experimental v numerical using Exps. 1 and 2 to provide a standard set of definitions for the material properties (E11, E22, G12, t, ν 12)

Model	Mesh	Load Vector	t E-03 m	E11 E+12N/m ²	E22 E+10N/m ²	G12 E+10N/m ²	ν 12	Central transverse displacement w_c E-03m/100N	Central tensile surface strains X(0°) μ E/100N Y(90°)
1	1SHGE50	C.L.V	0.127	0.1396	1.155	0.5771	.3	0.272	140 168
2	"	V.L.O	"	"	"	"	"	0.270	124 143
3	"	C.L.V	"	"	0.2889	"	"	0.297	137 179
4	"	V.L.O	"	"	"	"	"	0.295	135 168
5	"	C.L.V	"	0.1485	"	"	"	0.281	138 170
6	"	V.L.O	"	"	"	"	"	0.279	122 158
7	"	C.L.V	0.1194	"	"	"	"	0.338	158 187
8	"	V.L.O	"	"	"	"	"	0.335	134 169
9	"	C.L.V	"	"	"	0.6300	"	0.337	146 182
10	"	C.L.V	"	"	"	0.5771	.25	0.338	145 187
11	"	C.L.V	"	"	0.0	"	.3	0.348	152 189
12	"	C.L.V	"	"	0.5778	"	"	0.329	139 174
EXPERIMENTS 1 and 2 (average values measured in linear (embedding) load range)								(0.33 - 0.4)	160 200

Table 5.3 Linear displacement experimental-numerical (ACM) comparison, modelling Exps. 1 and 2 with different mesh constructions

Plate dimensions used in the numerical models

$$A = 0.26\text{m}$$

$$B = 0.26\text{m}$$

$$h = 0.406\text{E-}02\text{m (average thickness of the specimen tested in Exp. 2)}$$

$$A_s = 0.2\text{m}$$

$$B_s = 0.2\text{m}$$

$$A_p = 0.02\text{m}$$

$$B_p = 0.02\text{m}$$

Central patch load 100N (C.L.V)

$$\text{Lay-up } (90^\circ, 0^\circ, 90^\circ, +45^\circ, 0^\circ, -45^\circ, 0^\circ, 0^\circ, -45^\circ, 0^\circ, +45^\circ, 0^\circ, 0^\circ, +45^\circ, 0^\circ, -45^\circ, 0^\circ)_s$$

Material properties (applying the set of standard definitions)

$$E_{11} = 0.1485\text{E}+12 \text{ N/m}^2 \quad E_{22} = 0.2889\text{E}+10 \text{ N/m}^2$$

$$G_{12} = 0.5771\text{E}+10 \text{ N/m}^2 \quad \nu_{12} = 0.3$$

$$t = 0.1194\text{E-}03 \text{ m}$$

Model	Mesh	Central transverse displacement E-03m w_c /100N	Central tensile surface bending strain $\mu\epsilon$ /100N X (0°) Y (90°)	Modelling cases for $\pm 45^\circ$ layers
1	1SQGE36	0.339	157 197	case 1
2	1SQGE36	0.336	145 183	case 2
3	1SQGE49	0.339	159 199	case 1
4	1SQGE49	0.337	146 185	case 2
5	1SQGE81	0.339	160 201	case 1
6	1SQGE81	0.338	148 186	case 2
7	1SQGE100	0.340	160 201	case 1
8	1SQGE100	0.339 0.337	154 148 186	av. cases 1+2 case 2
9	1SHGE50	0.338	158 187	cases 1 + 2
10	1SHGE72	0.338	158 193	cases 1 + 2
11	1SFGE144	0.338	152 191	cases 1 + 2

EXPERIMENTS 1 and 2 (average values measured in linear(embedding) load range)

$$0.33 - 0.4$$

$$160$$

$$200$$

Figure 5.1 MESH CONSTRUCTIONS FOR EXPERIMENTS 1 TO 4

SCALE 1:4

Figure 5.1.1 MESH 1SFGE144

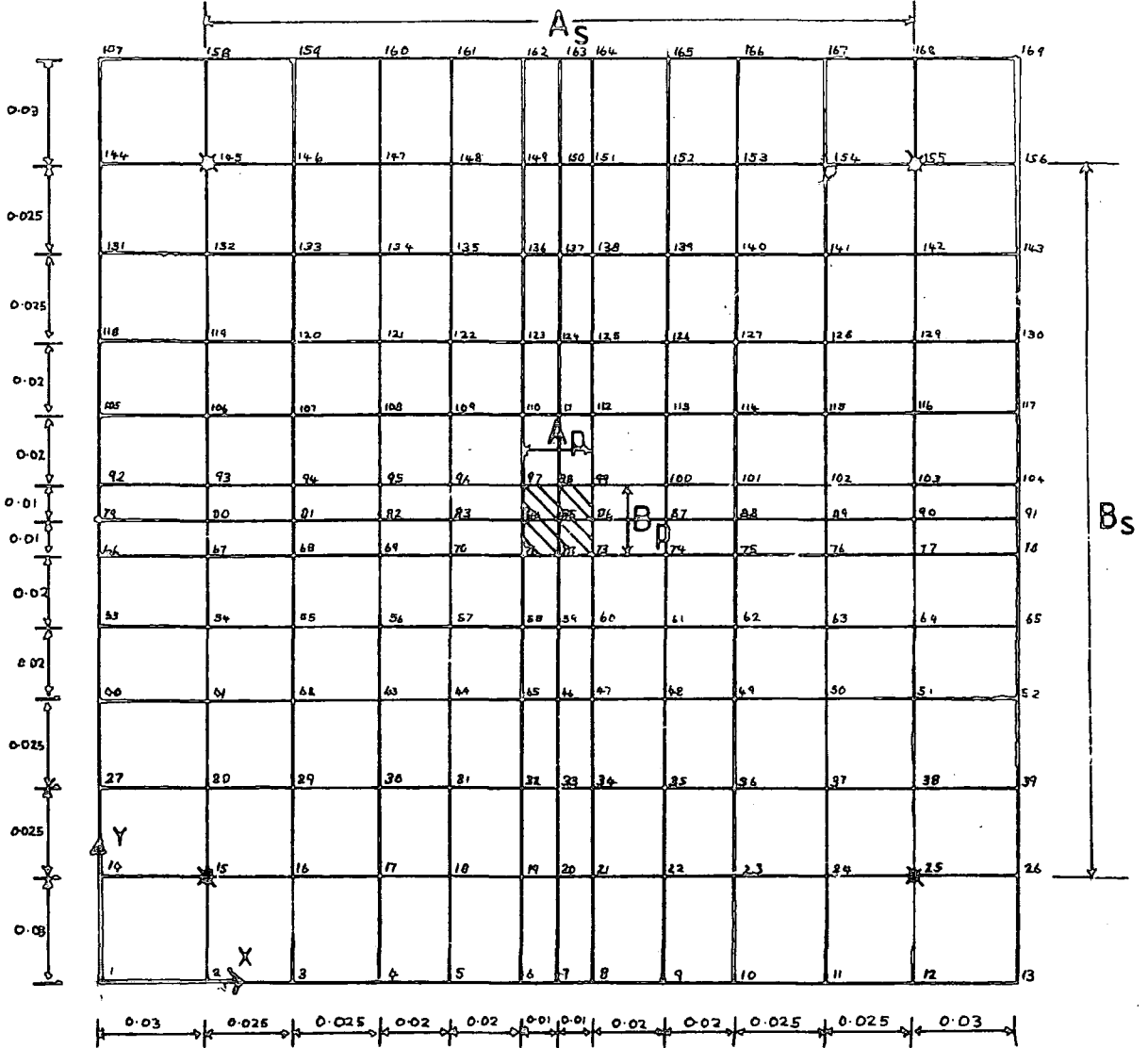


Figure 5.1.2 MESH 1SFGE36

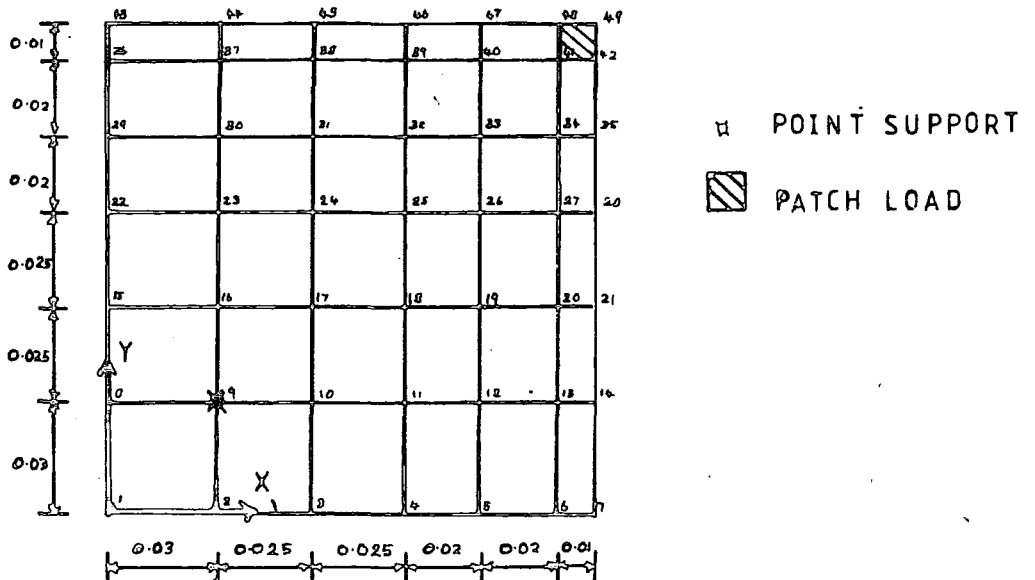


Figure 5.1 MESH CONSTRUCTIONS FOR EXPERIMENTS 1 TO 4

SCALE 1:2

Figure 5.1.3 MESH 1SHGE50

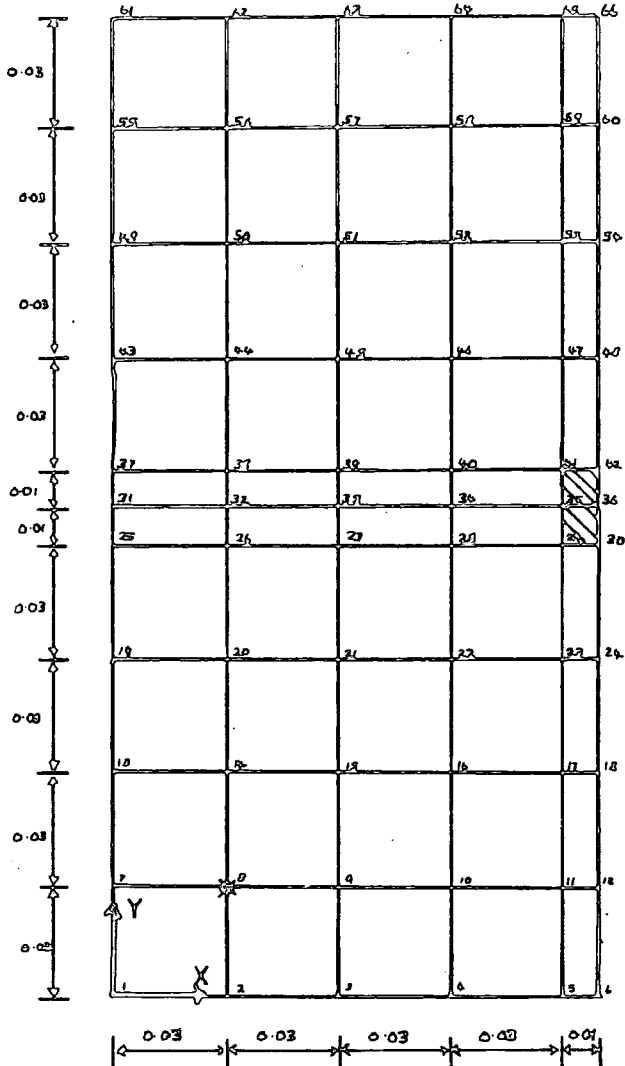


Figure 5.1.4 MESH 1SQGE100

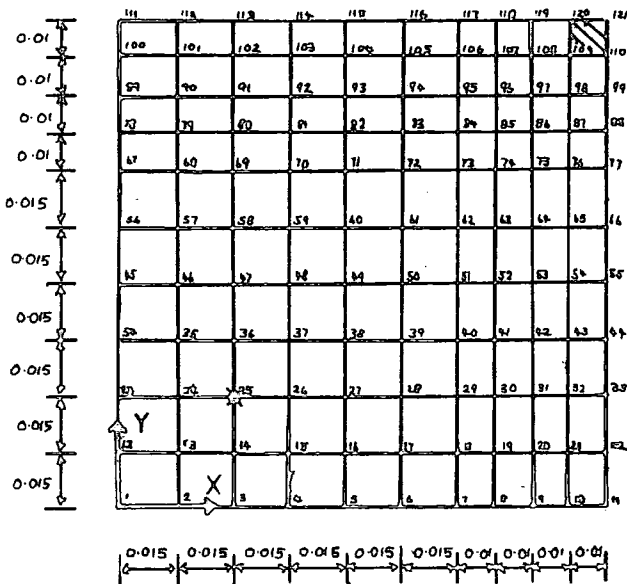


Table 5.4 Linear displacement experiment-numerical comparison: Overall modelling of Exp. 1 and 2

All data for the numerical models is given in Table 5.3

Mesh	Transverse displacements E-03m/100N						Tensile Surface strains centre µE/100N						Modelling cases
	Node	w _c	Node	w	Node	w	Node	ε _x 0°	ε _y 90°	Node	ε _x 0°	ε _y 90°	
1SQGE36 Fig 5.1.2	49	0.339	28	0.26	28	0.26	49	157	197	48	126 104	172	case 1 aver. 1 + 2 case 2
		0.338		0.26		0.26		151	197		115	176	
	49	0.336	28	0.26	28	0.26	49	145	183	48	103 125	173	
1SQGE100 Fig 5.1.4	121	0.340	66	0.25		0.25	121	161	201	120	129 108	181	case 1 aver. 1 + 2 case 2
		0.339		0.255		0.255		155	194		118	178	
	121	0.337	66	0.26		0.26	121	148	186	120	128 106	175	
1SHGE50 Fig 5.1.3	36	0.338					36	158	187	35	106	163	cases 1 + 2
1SFGE144 Fig 5.1.1	85	0.338	124	0.26	88	0.279	85	152	191	84	105 127 116	176 175 176	cases 1 + 2
EXP.	Pos.	w _c	Pos.	w	Pos.	w	Gauge	centre ε _x 0°	ε _y 90°	Gauge	ε _y 90°	Notes	
1 Fig 4.11 1	cen.	0.44					1	156	162			0-300n linear load range Initial gradient of failure test (1000N)	
							1	166	202				
2 Fig 4.15 2	cen	0.33	A	0.31	B	0.275	1	160	203		184	0-300N linear load range Initial gradient of failure test (1000N)	
							1	156	206		2		183

Table 5.4 (contd)

Mesh	Tensile Surface strains $\mu\text{E}/100\text{ N}$												Modelling cases
	Node	$E_x 0^\circ$	$E_y 90^\circ$	Node	$E_x 0^\circ$	$E_y 90^\circ$	Node	$E_x 0^\circ$	$E_y 90^\circ$	Node	$E_x 0^\circ$	$E_y 90^\circ$	
1SQGE36	'42'	137	161 133	41	109 106 140 151								case 1 aver. 1 + 2 case 2
		135	147		109	142							
	'42'	133	132 160	41	105 112 136 132								
1SQGE100	110	140	165 136	109	119 110 142 154	97	81	106	119	71	151		case 1 aver. 1 + 2 case 2
		138	150		113	146		80	105	71	150		
	110	136	164 135	109	115 106 137 150	97	79	104	119	70	149		
1SHGE36	42	132	141	29	108	146							cases 1 + 2
1SFGE144			162 133		106 114 137 149								cases 1 + 2
	98	135	148		110	143							

EXP.	Gauge	$E_x 0^\circ$	Gauge	$E_x 0^\circ$	$E_y 90^\circ$	Gauge	$E_x 0^\circ$	$E_y 90^\circ$	Gauge	$E_x 0^\circ$	$E_y 90^\circ$	Notes
1												0-300N linear load range
1						2+6	75B	100B	5+9	67B		Initial gradient of failure test
2	3	155	4	126	154	5+9		124	6	72	155	0-300N linear load range
2	3	143	4	118	156	5+9		114	6	70	150	Initial gradient of failure test

Table 5.4 (contd.)

Mesh	Tensile Surface strains $\mu\epsilon/100N$						Modelling cases
	Node	ϵ_{x0°	ϵ_{y90°	Node	ϵ_{x0°	ϵ_{y90°	
1SQGE36							case 1 aver. 1 + 2 case 2
				28	75	40	
					76	40	
1SQGE100				28	76	40	case 1 aver. 1 + 2 case 2
	99	112	94	97	81	106	
		111	94		80	105	
1SHGE50	99	110	93	97	79	104	case 1 aver. 1 + 2 case 2
1SFGE100					76 74	40 38	cases 1 + 2
				124	75	39	

EXP.	Gauge	ϵ_{y90°		Gauge	ϵ_{x0°		Gauge	ϵ_{x0°	Notes
		ϵ_{x0°	ϵ_{y90°		ϵ_{x0°	ϵ_{y90°			
1	3+7	99B	90B	-			11	71B	0-300N linear load range Initial gradient of failure test 0-300N linear load range Initial gradient of failure test
1	3+7	98B	90B	4+8	75	100			
2	8	116	112	7+10	78				
2	8	117	113	7+10	78				

Figure 5.2 CHANGE IN CENTRAL BIAXIAL STRESS RATIO $\frac{\sigma_y}{\sigma_x}$ WITH ALTERING POSITION OF SUPPORTS (MESH 1SQE100) UNDER A CONSTANT PATCH LOAD AREA $\frac{A_p}{B_p}$ FOR THE LAMINATION TESTED IN EXPERIMENTS 1 AND 2

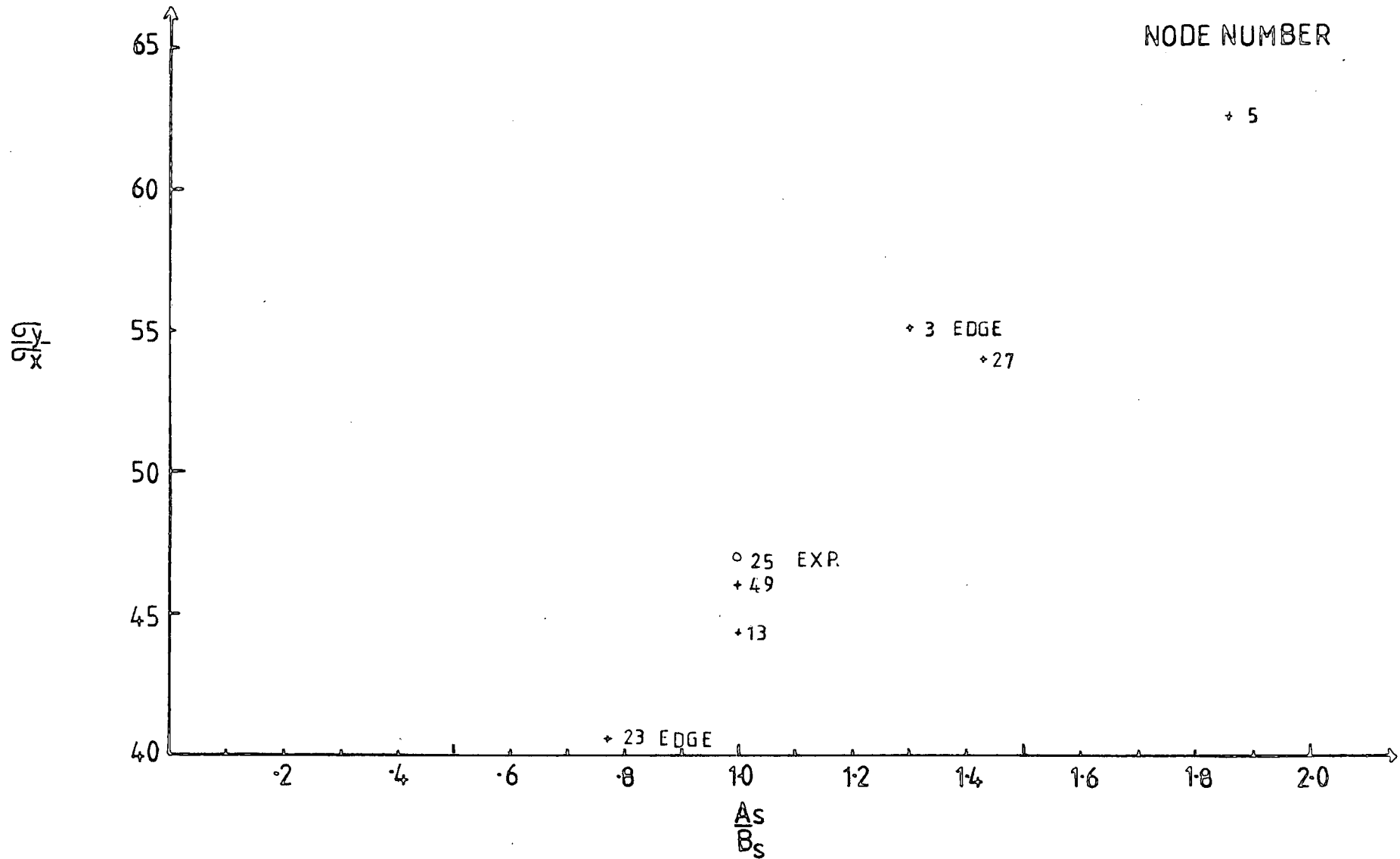


Figure 5.3 CHANGE IN CENTRAL BIAXIAL STRESS RATIO $\frac{\sigma_y}{\sigma_x}$ WITH ALTERING THE SIDE DIMENSIONS OF THE PLATE, X_s, Y_s (MESH 1SQE100) UNDER A CONSTANT PATCH LOAD $\frac{Ap}{B\bar{\sigma}} = 1$ FOR THE LAMINATION TESTED IN EXPERIMENTS 1 AND 2

515

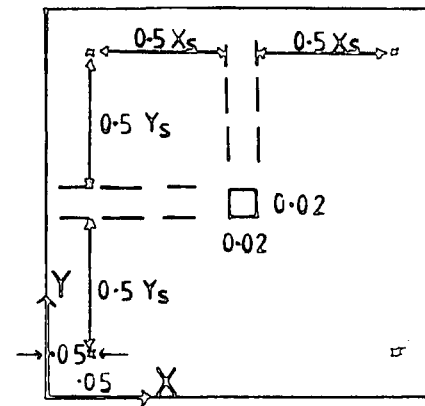
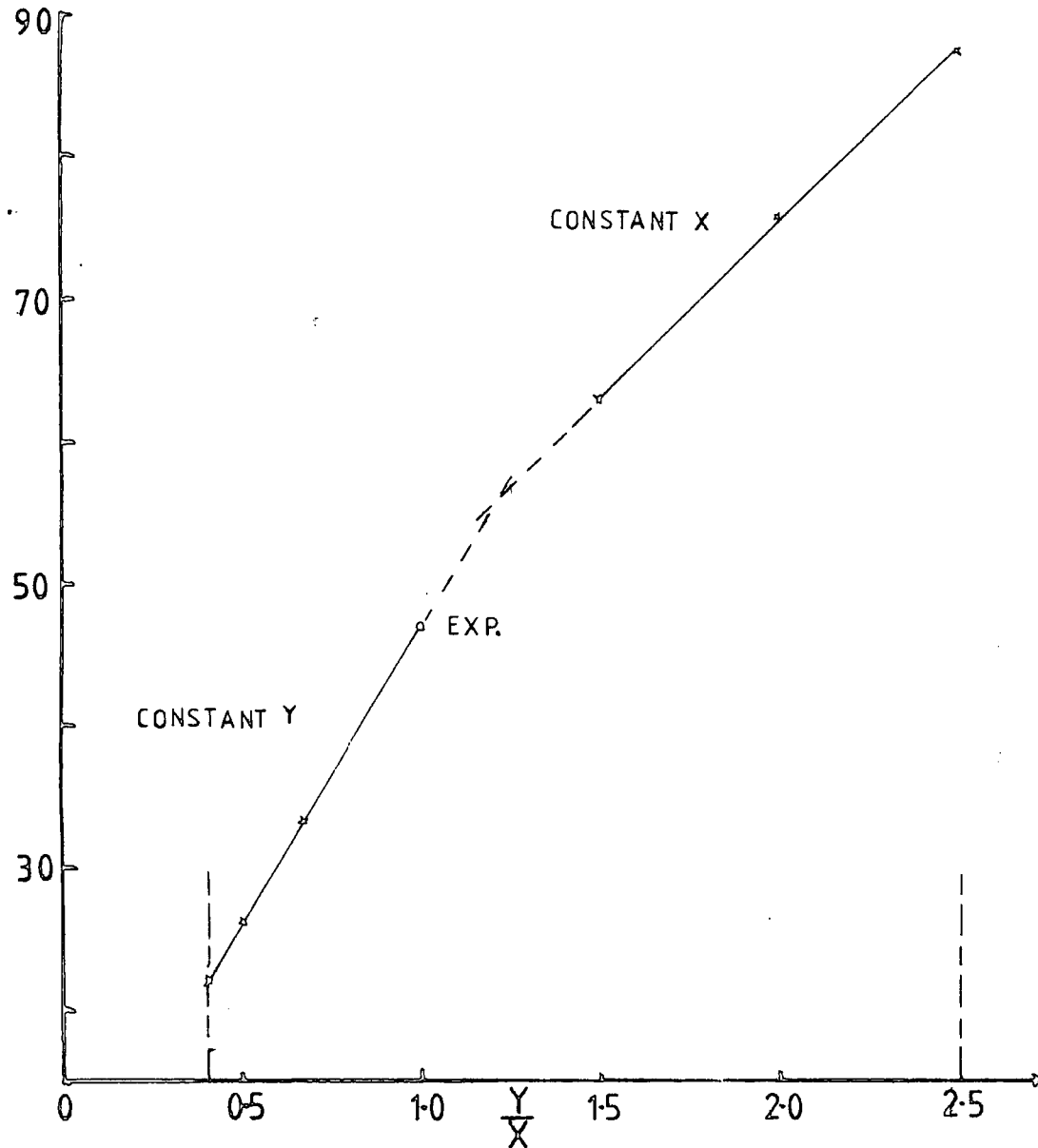


Table 5.5 Linear displacement experiment-numerical (ACM) comparison:
modelling Exps. 3 and 4 with different mesh constructions

Plate dimensions used in numerical models

$A = 0.26\text{m}$

$B = 0.26\text{m}$

$h = 0.552\text{E-}02\text{m}$ (includes protective layer)

$A_s = 0.2\text{m}$

$B_s = 0.2\text{m}$

$A_p = 0.02\text{m}$

$B_p = 0.02\text{m}$

Central patch load $P = 100\text{N}$ (C.L.V)

Material properties

$t = 0.127\text{E-}03\text{m}$ (the protective layer has not been taken into account)

$E_{11} = 0.1396\text{E+}12 \text{ N/m}^2$ $E_{22} = 0.2889\text{E+}10 \text{ N/m}^2$

$G_{12} = 0.5771\text{E+}10 \text{ N/m}^2$ $\nu_{12} = 0.3$

Lay-up $(+45^\circ, 90^\circ, -45^\circ, 0^\circ, 0^\circ, -45^\circ, 90^\circ, +45^\circ)_5$

Model	Mesh	Central transverse Displacement w_c E-03m/100N	Central surface tensile strains $\mu\text{E}/100\text{N}$			Modelling case
			X (0°)	Y (90°)	$\pm 45^\circ$	
1	1SQGE100	0.189	123	121	122	case 1
2	1SQGE100	0.188	115	112	114	case 2
3	1SHGE50	0.188	125	114	120	cases 1 + 2
4	1SHGE72	0.188	118	115	117	cases 1 + 2
5	1SFGE144	0.188	117	115	116	cases 1 + 2
6	1SHGE50*	0.159	105	103	104	cases 1 + 2
EXPERIMENTS 3 and 4 (average values from measurements in the linear (embedding) load range)						
		0.21	106	107	112	

* this model was performed to allow for the protective layer

$E_{11} = 0.1258\text{E+}12 \text{ N/m}$ $t = 0.138\text{E-}03\text{m}$

Table 5.6 Linear displacement experiment-numerical (ACM) comparison:
modelling Exp. 5 with different mesh constructions

Plate dimensions used in numerical models

A = 0.205m B = 0.275m

h = 0.191E-02m

A_S = 0.15m B_S = 0.20m

A_P = 0.02m B_P = 0.02m

Central patch load P = 100N (C.L.V)

Material properties

t = 0.1191E-03m

E11 = 0.1489E+12 N/m² E22 = 0.2889E+10 N/m²

G12 = 0.5771E+10 N/m² ν12 = 0.3

Lay-up (+45°,0°, -45°,90°,90°, -45°,0°, +45°)_S

Model	Mesh	Central transverse displacement w _c E-03m/100N	Central surface tensile strains μE/100N			Modelling case
			X (0°)	Y (90°)	±45°	
1	2RQGE100*	3.16	769	1220	995	case 1
average of Models 1 and 2			(547)	(983)	(764)	
2	2RQGE100*	3.06	325	746	532	case 2
3	2RHGE126+	3.12	530	960	710	cases 1 + 2
4	2RFGE144	3.2	553	1020	785	cases 1 + 2
EXPERIMENT 5		3.1		936	887	From linear load range with then
				1120	682	without rubber pad
				1100	750	Failure test

* 9 node patch load
+15 node patch load

Table 5.7 Linear displacement experiment-numerical (ACM) comparison:
modelling Exps. 6 and 7 with different mesh constructions

Plate dimensions used in the numerical models

$$A = 0.205\text{m} \quad B = 0.275\text{m}$$

$$h = 0.191\text{E}-02\text{m}$$

$$A_s = 0.15\text{m} \quad B_s = 0.12\text{m}$$

$$A_p = 0.01\text{m} \quad B_p = 0.01\text{m}$$

Central patch load $P = 100\text{N}$ (C.L.V.)

Material properties

$$t = 0.1191\text{E}-03\text{m}$$

$$E_{11} = 0.1489\text{E}+12 \text{ N/m}^2 \quad E_{22} = 0.2889\text{E}+10 \text{ N/m}^2$$

$$G_{12} = 0.5771\text{E}+10 \text{ N/m}^2 \quad \nu_{12} = 0.3$$

$$\text{Lay-up } (+45^\circ, 0^\circ, -45^\circ, 90^\circ, 90^\circ, -45^\circ, 0^\circ, +45^\circ)_s$$

Model	Mesh	Central transverse displacement w_c E-03m/100N	Central surface tensile strains $\mu\text{E}/100\text{N}$			Modelling case
			X (0°)	Y (90°)	$\pm 45^\circ$	
1	2RQGE100*	1.37	1022	1065	1045	case 1
	average of Models 1 and 2		(824)	(855)	(840)	
2	2RQGE100*	1.28	626	645	635	case 2
3	2RHGE126+	1.32	805	803	804	cases 1 + 2
4	3RFGE144	1.27	778	826	802	cases 1 + 2
EXPERIMENT 6 (the plate that was tested in Exp. 5)						
		1.5		900	748 ^{+45°}	
				816	614 ^{-45°}	
EXPERIMENT 7		1.39		841	1050 ^{+45°}	Linear load
				820	810 ^{-45°}	Failure test

* 4 node patch load

+ 6 node patch load

Table 5.8 Linear displacement experiment-numerical (ACM) comparison:
modelling Exp. 8 with different mesh constructions

Plate dimensions used in numerical models

$A = 0.2\text{m}$ $B = 0.2\text{m}$

$h = 0.188\text{E-}02\text{m}$

$A_s = 0.13\text{m}$ $B_s = 0.13\text{m}$

$A_p = 0.01\text{m}$ $B_p = 0.01\text{m}$

Central patch load $P = 100\text{N}$ (C.L.V.)

Material properties

$t = 0.118\text{E-}03\text{m}$

$E_{11} = 0.1509\text{E+}12 \text{ N/m}^2$ $E_{22} = 0.2889\text{E+}10 \text{ N/m}^2$

$G_{12} = 0.5771\text{E+}10 \text{ N/m}^2$ $\nu_{12} = 0.3$

Lay-up $(0^\circ, 90^\circ, 0^\circ, 90^\circ, 0^\circ, 90^\circ, 0^\circ, 90^\circ)_s$

Model	Mesh	Central transverse displacement w_c E-03m/100 N	Central surface tensile strains $\mu\text{E}/100 \text{ N}$		
			X (0°)	Y (90°)	
1	4SQGE100	1.27	774	972	
2	4SHGE72	1.27	759	956	
3	4SFGE144	1.27	760	956	
EXPERIMENT 8		1.53	880	1040	Linear load range

Table 5.9 Linear displacement experiment-numerical (ACM) comparison:
modelling Exp. 9 with different mesh constructions

Plate dimensions used in numerical models

$$A = 0.2\text{m} \quad B = 0.2\text{m}$$

$$h = 0.191\text{E}-02\text{m}$$

$$A_s = 0.13\text{m} \quad B_s = 0.13\text{m}$$

$$A_p = 0.01\text{m} \quad B_p = 0.01\text{m}$$

Central patch load $P = 100\text{N}$ (C.L.V.)

Material properties

$$t = 0.1191\text{E}-03\text{m}$$

$$E_{11} = 0.1487\text{E}+12 \text{ N/m}^2 \quad E_{22} = 0.2889\text{E}+10 \text{ N/m}^2$$

$$G_{12} = 0.5771\text{E}+10 \text{ N/m}^2 \quad \nu_{12} = 0.3$$

$$\text{Lay-up } (+45^\circ, 0^\circ, +45^\circ, 0^\circ, -45^\circ, 0^\circ, -45^\circ, 0^\circ)_s$$

Model	Mesh	Central transverse displacement w_c E-03m 100N	Central surface tensile strains $\mu\text{E}/100\text{N}$			Modelling case
			X (0°)	Y (90°)	$\pm 45^\circ$	
1	4SQGE100	2.30	1975	3908		case 1
average of Models 1 + 2			(1004)	(2239)	(1621)	
2	4SQGE100	1.82	13	570		case 2
3	4SHGE72	1.78	589	1453	1021	cases 1 + 2
4	4SFGE144	1.86	648	1684	1166	cases 1 + 2
5	4SFGE144	0.999	381	1724		with quarter plate B.C.
EXPERIMENT 9		2.3	605	1925	1165 ^{+45°}	Failure test (linear load range)

Table 5.10 Twisting stiffnesses for the specimens tested

Experiments	$\frac{D_{11}}{D_{16}}$	$\frac{D_{22}}{D_{26}}$	$\frac{D_{66}}{D_{16}}$
1 + 2	115.9	85.6	21.5
3 + 4	86.5	88.9	32.3
5 + 6 + 7	14.9	12.5	5.4
8	∞	∞	∞
9	8.9	1.6	1.6

Table 5.11 Linear displacement experiment-numerical comparison: Overall modelling of Exp. 7

All data for the numerical models is given in Table 5.7

Mesh	Transverse displacement E-03m/100N Node w_c		Tensile Surface strains UE/100N												Modelling cases
			centre												
			Node	ϵ_{x0°	ϵ_{y90°	$\epsilon_{\pm 45^\circ}$	Node	ϵ_{x0°	ϵ_{y90°	$\epsilon_{\pm 45^\circ}$	Node	ϵ_{x0°	ϵ_{y90°	$\epsilon_{\pm 45^\circ}$	
2RQGE100	121	1.27	121	626	646	636	119	402	620	511	99	593	396	495	case 2 aver. 1 + 2 case 1
				825	856	840		423	654	539		625	414	520	
				1023	1065	1044		443	688	566		657	432	544	
2RHGE100	80	1.32	80	805	859	832	100 60	438	605	523	78	650	421	535	cases 1 + 2
3RFGE144	85	1.27	85	778	826	802	83 87	395	641	520	59 111	595	397	496	cases 1 + 2

EXP.	Pos. w_c	Gauge	ϵ_{y90°	$\epsilon_{\pm 45^\circ}$	Gauge	ϵ_{x0°	ϵ_{y90°	$\epsilon_{\pm 45^\circ}$	Gauge	ϵ_{x0°	ϵ_{y90°	$\epsilon_{\pm 45^\circ}$	Notes
7 Fig 4.41	cen. 1.39	1	854	1054	2+4	450B	620B	630B	3+5	600	370	500B	0-50N linear load range -45° direction
				810				480B				660	
7	cen. ----	1	820	1000	2+4	390B	---	550B	3+5	---	---	---	Initial gradient of test to failure -45° direction
				750				480B				---	

Table 5.11 (contd.)

Mesh	Tensile Surface strains $\mu\text{E}/100\text{N}$												Modelling cases	
	Node	ϵ_{x0°	ϵ_{y90°	$\epsilon_{\pm 45^\circ}$	Node	ϵ_{x0°	ϵ_{y90°	Node	ϵ_x	ϵ_{y90°	Node	ϵ_{x0°		ϵ_{y90°
2RQGE100	118	268	499	359	88	480	250	111-112	-82	300	11-12	205	-73	case 2 aver. 1 + 2 case 1
		272	502	375		485	250		-72	267		183	-65	
	118	276	505	391	88	491	250	111-112	-62	234	11-12	162	-57	
2RHGE126								140-150	-70	320	8-23	193	-62	cases 1 + 2
3RFGE144								90-91	-64	281	50-163	170	-50	cases 1 + 2

EXP.	Gauge	ϵ_{x0°	ϵ_{y90°	$\epsilon_{\pm 45^\circ}$	Gauge	ϵ_{x0°	ϵ_{y90°	Gauge	ϵ_{x0°	ϵ_{y90°	Gauge	ϵ_{x0°	ϵ_{y90°	Notes
7	6+7	210B	440B	380B	8	406B	248B	9	-60	260	11	180	-52	0-50N linear load range
7	6+7			410B	8									Initial gradient of failure test

Table 5.12 Large (non-linear) displacement experimental - numerical (ACMBC) comparison using results from Experiments 1 and 2

Modelling data is defined in Table 5.3 . Mesh 1SQGE36 was employed and the comparison was made at the centre.

Load (N)	Central transverse displacement		Central tensile surface strains				Remarks
	Exps. w_c E-03m	ACMBC	Exps. X (0°)	ACMBC X (0°)	Exps. Y(90°)	ACMBC Y (90°)	
400	1.32 - 1.6	1.36(ACM)	640	572(ACM)	800	757(ACM)	Numerical results from ACM
	Exp. 2		Av. 1+2		Av. 1+2		No. of iterations
400	1.72	1.25	642	630 [B 618 , A 12]	826	868 [B 819 , A 49]	7
1200	4.20	2.86					6
2000	6.69	3.89	2380	2628 [B2480 , A148]	3850	3509 [B3012 , A497]	8
2800	8.70	4.68					9
3600	10.70	5.34	4405	4266 [B3962 , A304]	6543	5819 [B4832 , A996]	9
							Total C.P.U. time used was 970 s.

All results given are the combination of bending and axial components.
Strain measurements were made with Gauges 1 0° L B + A and 1 90° L B + A.

